ELECTROMAGNETIC FIELD INDUCED PERMEABILITY RESPONSE OF CELLS AND MEMBRANES

Submitted in total fulfilment of the requirements for the degree of

Doctor of Philosophy

By

Palalle G. Tharushi Perera

Faculty of Science, Engineering and Technology

Swinburne University of Technology

July 2020

Abstract

Effects of man-made electromagnetic fields (EMF) on living organisms potentially include transient and permanent changes in cell behaviour, physiology and morphology. At present, these EMF-induced effects are poorly defined, yet their understanding may provide important insights into consequences of uncontrolled (*e.g.*, environmental) as well as intentional (*e.g.*, therapeutic, or diagnostic) exposure of biota to EMFs. While super High frequency (SHF) EMFs have been widely used in many wireless communication devices, yet within the Terahertz (THz) range, their effects on biological systems are poorly understood.

In this work, for the first time, we comparatively studied the effects of SHF EMFs (18 GHz) and THz radiation on pheochromocytoma PC 12 neuron-like cells, a model cell line system, which is used for neurotoxicological and membrane transport studies, *Bacillus subtilis* spores that are remarkably resistant to extreme environmental conditions including UV radiation, and on a simple lipid membrane model, Giant Unilamellar Vesicles (GUVs) composed of 1,2-dioleoyl-sn-glycero-3-phosphocholine (DOPC).

Suspensions of the PC 12 cells were subjected to three consecutive cycles of 30s SHF EMF treatment with a specific absorption rate (SAR) of 1.17 kW kg^{-1}, with cells cooled between exposures to reduce bulk dielectric heating. The EMF exposure resulted in a transient increase in PC 12 cells permeability for 9 min in up to 90 % of the treated cells, as demonstrated by rapid internalisation of silica nanospheres (diameter $d \approx 23.5$ nm) and their clusters ($d \approx 63$ nm). Likewise, the GUVs exhibited permeability under the same conditions as evidenced by the translocation of silica nanospheres. In contrast, the PC 12 cells that received an equivalent bulk heat treatment behaved similar to the untreated controls, showing lack to minimal nanosphere uptake of approximately 1-2 %. Morphology and growth of the EMF treated cells were not altered, indicating that the PC 12 cells were able to remain viable after the EMF exposure.

Moving on from 18 GHz, in the next study we used electromagnetic radiation in the range of $0.3 – 19.5 \times 10^{12}$ Hz, generated by a synchrotron light source to investigate the response of PC 12 cells to THz irradiation. The PC 12 cells remained viable and physiologically healthy as confirmed by biochemical assays, however, exposure to THz radiation for 10 min was sufficient to induce a temporary permeability of the cell membrane. The length of exposure was increased with THz radiation given the low power of the beam which was in the range of

Microwatts. Analysis of Scanning Electron Microscopy (SEM) micrographs revealed the formation of atypical large (up to 1 μm) blebs on the surface of PC 12 cells exposed to THz radiation which was not observed in the PC 12 cells exposed to 18 GHz.

The analysis of the effect of prolonged exposures of 36 h of synchrotron sourced THz radiation of 0.3 – 19.5 × 10^{12} Hz to *Bacillus subtilis* spores, revealed a reduction in spore re-germination and changes to spore morphology as shown using SEM and Transmission Electron Microscopy (TEM) confirming the death of spores whereas exposures of 12 h did not result in any changes in spore morphology and re-germination. A comparative study was conducted where *B. subtilis* spores were Exposure of *B. subtilis* spores to three consecutive cycles of 30s SHF EMFs of 18 GHz with a specific absorption rate (SAR) of 1.43 kW kg^{-1}, did not affect spores viability, despite the spores morphology was temporarily altered. Nanosphere internalization into *B. subtilis* spores was not detected indicating that spores remained non-permeable following exposure of SHF EMFs or THz radiation.

Analysis of the data generated in due course of this project indicated that exposure to SHF EMFs (18 GHz) and THz radiation induced permeabilization of pheochromocytoma PC 12 neuron-like cells, It is believed that the cell permeability is likely to be electro-kinetic in nature due to the increased conductivity and mobility of ions across the cell membrane, with potential contribution from microthermal changes that cannot be easily captured at the macro level, as well as from the direct interaction of the EMF with water. However, the exact mechanism on how EMFs lead to membrane permeability remains unknown and requires further investigation.

The results of this work provide new insights into EMF-induced permeability effect in mammalian cells, suggesting a possible application of EMFs for facilitation of efficient transport of biomolecules, dyes and tracers, and genetic material across cell membrane in drug delivery and gene therapy, where permanent permeabilisation or cell death is undesirable.

Acknowledgements

Achieving this milestone would not have been real if not for my role model, Professor Elena Ivanova. I would like to express my deepest gratitude to her for the continuous guidance throughout my research career starting off as her summer intern back in 2013. The path she opened led me to achieve the biggest dream in life. I received tremendous mentoring from her in planning experimental work, conducting research and writing from day one of my PhD journey.

My heartiest gratitude to Professor Russel Crawford, Professor Rodney Croft, Professor Saulius Juodkazis for their support and academic guidance. Your expertise helped me complete the project.

I would like to offer my sincere thanks to the beamline scientists at the Australian Synchrotron; Far IR/THz beamline, Dr. Mark Tobin, Dr. Dominique Appadoo and Dr. Pimm Vongsvuit. Thank you for making the synchrotron sessions bearable day and night, the time spent at the beamline is one that I will cherish forever.

Similarly, I want to acknowledge Dr.Vi Khanh Truong, Dr.Vy Pham, Dr.Mohammad Al Kobaisi, Dr. Denver Linklater, Dr.Duy Nguyen, Jason Wandiyanto, Samuel Cheeseman for their constant support and friendship during the PhD journey. Dr. Rebecca Alfred, Ngan and Dr.Shanthi Joseph; I'm grateful for the technical support provided in the labs.

I was blessed with the best of friends who lifted me up; Tiara, Dr. Nadine, Dr.Sanjida, and Dr.Simon, thank you for the wonderful times spent together. Our coffee dates, chit chats about life was a motivation to wake up every day and make it to the lab.

Family, I would not have achieved anything in life if not for them. I would like to thank my aunt Sriyani Silva for providing me with shelter when I first arrived in Australia in 2012 for my higher studies. My cousins in Australia; Shanaka, Sahan, Induwarie, Chuti, Chamila, Nalin, Muditha and Padmi the memories we created will not be forgotten. Also, my extended family, aunty Nilangi, uncle Felician, Romina, Sachin, Ramon and Brittany; the support received from miles away lifted my spirits. I will also mention my relatives and cousins back at home as they are a big part in my life; Mohan, Rasanga, Duminda, Neranjala, Iresha, Shakila, Shanaka.

Lastly but most importantly, my dearest parents. Ammi and Thaththi, you have been my greatest support system throughout this journey. I owe everything to you. The unconditional

love received as a child till today is what drove me to achieve my goals. Roman, you have been my rock, the most supportive husband one can ask for, your dream was to see me walk up the stage and here we are today with our greatest blessing, our ‘son’shine, Kivain.

To you all, I dedicate this thesis….

I would like to dedicate the thesis with love to my dearest parents, Mr. Upali Perera, Mrs. Srikanthi Marasinghe, also to my beloved husband, Mr. Roman Withanage and to my bundle of joy, Kivain Withanage.

Declaration

I, Palalle Gamaarachchige Tharushi Perera, declare that the thesis is my original work and contains no material which has been submitted for the award of any other degree or diploma from another university.

To the best of my knowledge, I certify that this thesis contains no material previously published or written by another person except where due reference has been made. Wherever contributions of others were involved, every effort has been made to acknowledge contribution of the respective workers or authors.

Palalle G. Tharushi Perera

List of Publications

Peer-reviewed articles

- **Perera, P.G.T.,** Bazaka, O., Bazaka, K., Croft, R.J., Crawford R.J., Ivanova, E.P. Translocation of silica nanospheres through giant unilamellar vesicles (GUVs) induced by the high frequency electromagnetic field (18 GHz). *Biophysical Journal*. (Prepared for submission).

- **Perera, P.G.T.,** Linklater, D., Wandiyanto, J.V., Appadoo, D., Tobin, M.J., Vongsvivut, J., Truong, V.T., Dekiwadia, C., Crawford, R.J., Croft, R.J., Ivanova, E.P. Exposure of *Bacillus subtilis* spores to electromagnetic radiation: Gigahertz vs Terahertz. (Prepared for submission).

Publications presented in the thesis:

- **Perera, P.G.T.,** Appado, D., Cheeseman, S., Wandiyanto, J., Linklater, D., Dekiwadia**,** C., Truong, V., Tobin, M.J., Vongsvivut., Bazaka, O., Bazaka, K., Croft, R.J., Crawford, R.J., Ivanova, E.P. PC 12 pheochromocytoma cells response to super high frequency terahertz radiation from synchrotron source. *Cancers.* 2019. 11 (2). 162.

- **Perera, P.G.T.,** Bazaka, O., Bazaka, K., Croft, R.J., Crawford R.J., Ivanova, E.P. Pheochromocytoma (PC 12) as a model cell line for membrane permeabilization studies in the presence of electromagnetic fields (EMFs): Recent advances. *Journal of Neurology and Neuromedicine.* 2019. 4 (1). p. 35-40.

- **Perera, P.G.T.,** Nguyen, T.H.P., Dekiwadia**,** C., Wandiyanto, J., Sbarski, I., Bazaka, O., Bazaka, K., Crawford, R.J., Croft, R.J., Ivanova, E.P. Exposure to high frequency electromagnetic field triggers rapid uptake of large nanosphere clusters by pheochromocytoma cells. *International Journal of Nanomedicine.*2018. 13. p.8429-8442.
- Orlowska, A.; **Perera, P.T.**; Al Kobaisi, M.; Dias, A.; Nguyen, H.K.D.; Ghanaati, S.; Baulin, V.; Crawford, R.J.; Ivanova, E.P. The Effect of Coatings and Nerve Growth Factor on Attachment and Differentiation of Pheochromocytoma Cells. *Materials* 2017, *11*, 60.

Other Publications:

- Wandiyanto, J.V., Linklater, D.; **Perera, P.G.T**., Orlowska A., Truong, V.K., Thissen, H.; Ghanaati, S., Baulin, V., Crawford, R. J., Juodkazis, S., Ivanova, E.P., Pheochromocytoma (PC 12) Cell response on mechanobactericidal titanium surfaces. *Materials.*2018, *11, 605.*

Book chapters:

- Bhadra C.M., **Tharushi Perera P.G**., Truong V.K., Ponamoreva O.N., Crawford R.J., Ivanova E.P. (2018) Renewable bio-anodes for microbial fuel cells. In: Martínez L., Kharissova O., Kharisov B. (eds) Handbook of Ecomaterials. Springer, Cham.

Conferences and poster presentation

- **Perera, P.G.T,** Appado, D., Cheeseman, S., Wandiyanto, J., Linklater, D., Dekiwadia**,** C., Truong, V., Tobin, M.J., Vongsvivut., Bazaka, O., Bazaka, K., Croft, R.J., Crawford, R.J., Ivanova, E.P. 'Exposure to synchrotron terahertz (THz) radiation induces cell membrane permeability in pheochromocytoma (PC 12) cells. Synchrotron User Meeting, 22nd -23rd November 2018, Melbourne.

- **Perera, P.G.T,** Nguyen, T.H.P., Dekiwadia**,** C., Wandiyanto, J., Sbarski, I., Bazaka, O., Bazaka, K., Crawford, R.J., Croft, R.J., Ivanova, E.P. 'Response of pheochromocytoma (PC 12) cells following exposure to electromagnetic fields of 18 GHz'. Asian Biophysics Association Symposium, 2nd – 6th December 2018, Melbourne.

- Nguyen, T.H.P., **Perera, P.G.T**., Pham, T.H.V., Croft, R., Crawford, R.J., Ivanova, E.P. 'Super high frequency (18 GHz) electromagnetic field induced membrane permeability on erythrocytes and PC-12 neuronal cells'. Science and Wireless 2016 (SW2016) hosted by The Australian Centre for Electromagnetic Bioeffects Research (ACEBR), 22nd November 2016, Melbourne.

- Animal Ethics Seminar, 28th October 2016, RMIT University, Melbourne.

ANSTO Grants (THz/Far-IR beamline)

- Reference No: AS181/THz/13152

Proposal ID: 13152

Project Title: Investigating molecular effect of terahertz (THz) exposure upon neural cell lines (PC-12)

In-kind ANSTO Grant Value: $ AUD131,136.00

- Reference No: AS182/THz/13536

Proposal ID: 13536

Project Title: The influence of terahertz (THz) exposure upon neuronal pheochromocytoma cells of the rat adrenal medulla (PC-12)

In-kind ANSTO Grant Value: $ AUD196,704.00

- Reference No: AS183/THz/14112

Proposal ID: 14112

Project Title: Investigating influence of terahertz (THz) exposure upon neuronal pheochromocytoma cells of the rat adrenal medulla (PC-12)

In-kind ANSTO Grant Value: $ AUD229,488.00

- Reference No: AS191/THz/14522

Proposal ID: 14522

Project Title: The influence of terahertz (THz) exposure upon neuronal pheochromocytoma cells of the rat adrenal medulla (PC-12) and spores of Bacillus subtilis spores

In-kind ANSTO Grant Value: $ AUD196,704.00

- **International Synchrotron Access Program (ISAP)** funding to visit Alba (Synchrotron in Barcelona, Spain).

Table of Contents

Contents

Abstract 2
Acknowledgements 4
Declaration 7
List of Publications 8
ANSTO Grants (THz/Far-IR beamline) 10
Table of Contents 11
List of Abbreviations 15
List of Figures 16
List of Tables 22
Chapter 1. Introduction 23
Chapter 2. Literature Review 30
2.1. Overview 31
2.2. Nature of Electromagnetic Radiation 32
2.3. Microwave (MW) Radiation 37
2.4. Terahertz Radiation 39
2.5 EMF induced effects 41
2.5.1. Biological effects of RF and microwave radiation 41
2.5.2. Biological effects of THz radiation 51
2.6. Current approaches used to achieve cell permeabilization 55
2.6.1. Electroporation 56
2.6.2. Sonoporation 57
2.6.3. Photoporation (Laser irradiation) 58
2.7. Giant Unilamellar Vesicles 59
2.7.1. Composition of liposomes 62
2.7.2. Techniques of liposome preparation 63
2.7.3. Characterisation of liposomes 65
2.7.4. Permeability of GUVs 67
2.8. Pheochromocytoma (PC 12) cells 69
2.8.1. Characteristics of PC 12 cells 69
2.8.2. Cell membrane lipid composition 70
2.8.3. PC 12 cell differentiation 71
2.9. Bacillus subtilis spores 76
2.9.1. Structure and composition of spore coat 78

2.9.2. Heat resistance 81
2.9.3. Radiation resistance 81
Chapter 3. Materials and Methods 83
3.1. Overview 84
3.2. Materials 84
3.2.1. Lipids 84
3.2.2. Silica nanospheres 84
3.2.3. PVA-VP(poly(vinyl alcohol)- vinyl pyrrolidone) 84
3.2.4. Poly-L-lysine 85
3.2.5. Fibronectin 85
3.2.6. Laminin 85
3.2.7. Cultivation of *Bacillus subtilis and* spore sample preparation 85
3.2.8. PC 12 cell line 86
3.3. Construction of GUVS 87
3.4. EMF exposures of 18 GHz 88
3.4.1. EMF exposures of 18 GHz on GUVs 88
3.4.2. EMF exposures of 18 GHz on PC 12 cells 90
3.4.3. EMF exposures of 18 GHz on *B. subtilis* spores 92
3.4.4. Dosimetry 93
3.5. Control samples 93
3.5.1. Peltier heat treatment 93
3.5.2. Controls 93
3.6. EMF exposures in the range of THz radiation 94
3.6.1. EMF exposures of 0.3 – 19.5 THz on PC 12 cells 94
3.6.2. EMF exposures of 0.3 – 19.5 THz on *B. subtilis* spores 96
3.7. Detection of membrane permeability following exposure to EMFs 98
3.7.1. GUVs 98
3.7.2. PC 12 cells 98
3.7.3. Permeability coefficient of EMF treated PC 12 cells 98
3.8. Dynamic Light Scattering (DLS) of silica nanospheres distribution 99
3.9. Transmission Electron Microscopy (TEM) 99
3.10. Atomic Force Microscopy 100
3.10.1. Bacterial cells 100
3.11. Cellular morphology 100
3.12. Viability 100

3.12.1. PC 12 cells 100
3.12.2. Spore germination 101
3.13. Cell proliferation 101
3.14. Protein concentration 101
3.15. Cell integrity 102
3.16. PC 12 cell differentiation 102
3.17. Assessment of neurite outgrowth 102
3.18. Statistical analysis 103
Chapter 4. Exposure to EMFs of 18 GHz triggers rapid uptake of large nanosphere clusters by pheochromocytoma cells (PC 12) 104
4.1. Overview 105
4.2. Background 106
4.3. Results 109
4.3.1. EMF induced cell membrane permeability 109
4.3.2. EMF induced effects on cell morphology and viability 114
4.3.3. EMF induced effects on intra-cellular physiology 116
4.4. Discussion 120
4.5. Conclusion 122
Chapter 5. Pheochromocytoma cells (PC 12) response to synchrotron source THz frequencies of 0.3 – 19.5 123
5.1. Overview 124
5.2. Background 125
5.3. Results 128
5.3.1. THz induced cell membrane permeability 128
5.3.2. THz induced effects on cell morphology and viability 133
5.3.3. EMF induced effects on intra-cellular physiology 136
5.3.4. PC 12 cell differentiation in the presence of THz radiation 138
5.4. Discussion 140
5.5. Conclusion 142
Chapter 6. The effect of coatings and nerve growth factor on attachment and differentiation of PC 12 cells 143
6.1. Overview 144
6.2. Introduction 145
6.3. Results 147
6.3.1. Protein distribution on the substratum 147
6.3.2. PC 12 cell attachment and initial differentiation in the presence of NGF 149

6.3.3. PC 12 cells metabolic activity and proliferation 151
6.3.4. Neurite extension and outgrowth 153
6.4. Discussion 154
6.5. Conclusion 156
Chapter 7. Response of *Bacillus subtilis* spores to high frequency electromagnetic fields 157
7.1.Overview 158
7.2. Introduction 159
7.3. Results and Discussion 161
7.4. Conclusion 168
Chapter 8. Translocation of silica nanospheres through giant unilamellar vesicles (GUVs) induced by EMFs of 18 GHz 169
8.1. Overview 170
8.2. Background 171
8.3. Results and Discussion 173
8.4. Conclusion 181
Chapter 9. General Discussion 182
9.1 Overview 183
9.2. EMF induced reversible permeabilization in PC 12 cells 184
9.3. Response of spores to EMFs of 18 GHz and 0.3 to 19.5 THz 189
9.4. Significant outcomes of the research and future directions 190
10.References 192

List of Abbreviations

BCA	Bicinchoninic acid assay
B. subtilis	*Bacillus subtilis*
CLSM	Confocal laser scanning microscopy
E. coli	*Escherichia coli*
EMFs	Electromagnetic fields
FITC	Fluorescein isothiocyanate
GHz	Gigahertz
GUVs	Giant unilamellar vesicles
LDH	Lactate dehydrogenase
MHz	Megahertz
MTS	(3-(4,5-dimethylthiazol-2-yl)-5-(3-carboxymethoxyphenyl)-2-(4-sulfophenyl)-2H-tetrazolium)
MW	Microwave
PC 12	Pheochromocytoma cells
RF	Radiofrequencies
SAR	Specific absorption rate
SEM	Scanning electron microscopy
SHFs	Super high frequency
TEM	Transmission electron microscopy
THz	Terahertz
UV	Ultraviolet

List of Figures

Figure 2. 1. *E. coli* cells exposed to EMF. SEM images (a and b) of EMF exposed bacterial cells; (c and d) Untreated cells. Bacterial cells ten mins after EMF exposure (e and f); (g and h) Heat-treated cells (Peltier plate). Panel b shows cytosolic leakage. Adapted from (Shamis et al., 2011b, p. 3020). 42
Figure 2.2. Illustration of the possible effects on cells following EMF exposure. Changes in cellular proliferation rates, metabolic activity, morphology, viability and protein concentrations are some of the suggested possible effects. 47
Figure 2. 3. Current techniques used for cell membrane poration in delivering drugs and genes. Electroporation, sonoporation, photoporation and EMFs cause poration of cell membranes using different mechanisms. Electric pulses, ultrasound, lasers, electric, and magnetic fields are causing cell membrane alterations.....58
Figure 2. 4. **Critical components of a drug delivery system.** A delivery system has to be efficient when delivering drugs to a specific site not forgetting that the release of a drug depends on a certain stimuli (trigger based). 60
Figure 2.5. Structure of *B. subtilis* spore illustrating the various coats as visualised using Transmission Electron Microscopy. The spore coat consists of several different layers that play essential roles in the process of spore dormancy and germination. Scale bar 200 nm. ...78
Figure 3. 1.GUVs synthesis using the gel assisted method. A thin layer of hydrogel is spread on the ozone cleaned glass slide. Lipids will be placed on the hydrogel and placed under a vacuum. Placing the lipids inside the vacuum will help evaporate the solvent. The lipids were originally present in a solvent (chloroform). Addition of an aqueous solvent, 280 mM sucrose will help to hydrate the lipid film, generating liposomes as illustrated. 87
Figure 3. 2.**Experimental set up of GUVs being exposed to EMF. (A)** The microwave chamber used in EMF treatments. The micro petri dish (diameter = 65 mm, depth of suspension = 0.6 mm) containing the GUVs will be placed as depicted on the image..**(B)** Modelling of the microwave chamber showing absorbed power and electric field. The modelling was performed using CST Microwave Studio and 3D Electromagnetic Simulation software. **(C)**Schematic representation of the cycles of EMF exposure**.** The first stage of the EMF treatment increases the temperature of the GUVs to 40 °C. After the treatment (1 min), the GUVs in solution were allowed to cool down at 25° for 2 min before the next exposure. After the three EMF treatments, the GUVs were imaged after addition of the silica nanosphere.....89
Figure 3. 3. The experimental set up of EMF treatments of PC 12 cell suspensions. (A) The microwave chamber. The temperature probe was placed inside the PC 12 suspension, which was placed on the ceramic pedestal. Insets of PC 12 as visualized under phase contrast microscopy in preparation for EMF exposure. Cells appear to be floating in suspension in a group of few cells. **(B)** Absorbed power and electric field modelling performed using CST Microwave Studio and 3D Electromagnetic Simulation software, the image depicts the position of the tip of the temperature probe (side and top view), on the right is Peltier heating stage and the PC 12 cell suspension will be placed on (diameter = 65 mm, depth of suspension = 0.6 mm).**(C)Temperature rise in the suspension of PC 12 cells in the presence of EMF radiation.** The rise in temperature of the cells in suspension during EMF treatment was monitored every second for the first 60 s. EMF treatments were carried out only for 30 s to

prevent the overheating of cells. **(D) Heat profile in the suspension of PC 12 in the absence of EMF radiation.** In the Peltier heating graph, the temperature profile during EMF treatments was replicated and the cells were exposed to the same temperature but in the absence of EMF radiation. 91
Figure 3. 4. Assembling of the Diamond Liquid Cells (DLC) for the exposure of THz radiation. PC 12 cells were loaded into the DLC **(B)** and assembled as illustrated before exposure. After loading the sample, the DLC is viewed under a microscope to confirm the absence of air bubbles. 94
Figure 3. 5. Experimental set up of THz exposure. **(A)** Closed-loop pulse tube cryostat containing the DLC and the **(B)** Liquid Nitrogen Cryostat. **(C)** Sample holder to which the DLC are mounted on for exposure.....95
Figure 3. 6.Experimental setup of GHz (A-C) and THz (D-E) radiation on *B. subtilis* spores. (A) Spore suspension placed inside the microwave chamber on the ceramic pedestal with the temperature probe sitting inside the suspension. **(B)** Lambda Technologies Vari-Wave Model LT 1500**. (C)** Increase in temperature of the spore suspension within the first 30 s of GHz exposure. **(D)** Closed – loop pulse tube cryostat encompassing the DLC holder and the inset illustrates the path of the beam in red arrows. **(E)** DLC used for THz exposure.....97
Figure 4. 1. Internalisation of silica nanospheres by PC 12 cells following exposure to EMF radiation of 18 GHz. (A). CLSM micrographs depicting fluorescent silica nanospheres being internalisation by PC 12 cells after EMF exposure. The nanospheres as visualized tend to exist in clusters in working solution. Scale bar 5 μm. **(B).** Characterisation of silica nanospheres clusters in working solution. Dynamic light scattering (DLS) results for silica nanospheres after sonication (15 min) revealed that the nanospheres are present in clusters of 3- 4 as an effective diameter of 63.9 nm was recorded. 110
Figure 4. 2.Confocal micrographs illustrating the duration of PC 12 cell permeability following EMF exposure. CLSM images showing fluorescent silica nanospheres being internalisation by PC 12 cells, 3, 6 and 9 min after EMF exposure. No nanosphere uptake was visualised after 10 min. The results suggest that permeability lasted for 9 min. Scale bar 5 μm. The internalisation of silica nanospheres of 23.5 nm was further confirmed by TEM images (**Figure 4.3**). Nanospheres in working solutions was found to be in monodispersed and in clusters. It appeared that the EMF-treated PC 12 cells internalised the nanospheres (red circles) and their clusters (green insets) and were located inside the cell cytoplasm. No internalised nanospheres were detected on TEM images for the control or the heat-treated sample groups. 112
Figure 4. 3. TEM micrographs depicting Silica NS internalisation by EMF treated PC 12 cells. Typical TEM images showing PC 12 cells exposed to EMF of 18 GHz were able to internalise silica nanospheres (23.5 nm) and clusters (63.9 nm) as indicated by arrows. No nanosphere internalisation was detected in the heat treated and the control groups. Nanospheres were also seen to cluster around the radiated cells (red circles). 113
Figure 4. 4. Analysis and quantification of PC 12 cell morphology and viability. (A) Scanning electron micrographs (top row) of PC 12 cells after being exposed to EMF radiation. No significant changes in cell morphology were detected in the EMF treated groups in comparison to the heat-treated and the control samples. Scale bar 2μm. CLSM images (middle row) depict cell viability, PC 12 cells exposed to EMF, heat treatments and the control are all remained viable. Phase contrast (bottom-optical) images of the same field of view. Scale bar 5 μm. **(B) Quantification of viable PC 12 cells after EMF radiation.** The number of viable

cells in the EMF treated and the other control groups vary slightly, no significant changes (p>0.05) were detected. Data are means ± standard deviation (SD) and representative of 3 independent repeats.....115
Figure 4. 5.Analysis of intra-cellular morphology of PC 12 cells. (A) Metabolic activity (MTS) **(B)** Total protein concentration (BCA) of PC 12 cells. The metabolic activity of PC 12 cells in response to EMF radiation appeared to be slightly higher than the heat-treated and the control samples but there is no significant difference (p> 0.05), in the absorbance values recorded for the EMF and the control. No significant changes in protein concentration was detected in the EMF treated groups, the heat-treated and the control groups. **(C)** LDH release by PC 12 cells. The degree of LDH release of the EMF treated and the other groups did not display any significant differences. Data are means ± standard deviation and are representative of three independent experiments (p > 0.05). 117
Figure 4. 6. PC 12 cell differentiation following exposure to EMFs of 18 GHz. Phase contrast images captured of EMF treated cells, heat treated and controls. The cells were seeded at a density of 3 × 10^4 cells / mL. Cells were seeded in full serum medium allowing for attachment and partial change of medium was carried out every two days with a NGF concentration of 50 ng/ mL in low serum medium. No changes were visualised of the neurite outgrowth under the various conditions on days 2, 4 and 6. Scale bar 5 µm. 119
Figure 5. 1. Membrane permeabilization of PC 12 cells following exposure to PC 12 cells. Confocal laser scanning microscopy (CLSM; top row) images illustrate the uptake of silica nanospheres (FITC) by the THz treated cells whereas the untreated control does not exhibit any nanosphere uptake. No signal was detected in the FITC channel for the untreated cells. Scale bar 5µm.Thin sliced transmission electron microscopy (TEM) micrographs confirm silica nanospheres (NS) being internalised by the PC 12 cells (red arrow; bottom). Nanospheres are also seen lining the cell membrane whereas no nanosphere internalisation was observed in the untreated control cells. Scale bar 1µm. 130
Figure 5. 2. Assessment of membrane permeability of PC 12 cell after exposure to THz radiation. CLSM micrographs showing fluorescent silica nanospheres being internalised by PC 12 cells, after 5, 9,10,15 and 20 min following exposure. PC 12 cells were permeable for up to 20 min after being exposed to THz radiation. Scale bar 10 µm. 132
Figure 5. 3. Analysis of PC 12 cell morphology using SEM. Following exposure to THz radiation, morphology analysis revealed significant bleb formation on the PC 12 cells (circled in white) whereas blebs were not present on the untreated PC 12 cells. 134
Figure 5. 4. Assessment of PC 12 cell viability following 10 min exposure to THz radiation. (A) Confocal laser scanning images showing viable (green) PC 12 cells after being exposed to synchrotron source THz radiation for 10 min. **(B)** The untreated control cells. Scale bar 5µm. **(C)** Optical micrographs of PC 12 cells following exposure to THz radiation and the **(D)** untreated control. Scale bar 10 µm. **(E)**Quantification of viable PC 12 cells following exposure to THz radiation. No significant changes in cell viability were detected between the THz treated and the control group (p = 0.977). Data are presented as mean ± SD and are representative of the three independent repeats.....135
Figure 5. 5. Intra-cellular physiological analysis of PC 12 cells after THz exposure. (A) Metabolic status (MTS) over the duration of 7 days and following exposure. The metabolic activity of THz treated PC 12 cells were similar to the untreated control following exposure (p = 0.803) after day 1 and no significant changes were observed over the course of 7 days. **(B)** The total protein concentration of the THz treated sample after exposure and over a 7 day

period. The total protein content of the THz treated sample was relatively low in comparison to the control straight after exposure (p = 0.574) and over the course of 7 days. The statistical analysis of the results did not reveal a statistically significant difference (p>0.05). Data are means ± standard deviation (SD) and representative of 3 independent repeats. 137
Figure 5. 6. Investigation of PC 12 cell differentiation 7 days after exposure to THz radiation. The tissue culture plates were coated with 10 µg/ mL of collagen and PC 12 cells seeded at a density of 10^6 cells/mL. Cells were grown in low serum medium with NGF at concentration of 50 ng/mL. Partial refreshment of medium was carried out every two days**. (A)** The PC 12 cells were labelled with a lipophilic membrane stain, Dil (1,1'-Dioctadecyl-3,3,3',3'-Tetramethylindocarbocyanine Perchlorate. No changes were observed among the THz treated PC 12 cells and the untreated control. Scale bar 10 µm**.** The phase contrast images were captured on day 7 of PC 12 cell differentiation. Scale bar 10, µm. **(B) Quantification of axon outgrowth**. THz treated PC 12 cells and the untreated control was able to undergo neuronal differentiation extending neurites from 0 - > 40 µm in diameter with the THz treated sample and the control mainly having extensions from 0 -20 µm (p = 0.857) and 20 – 40 µm (p = 0.976). (**C) Quantification of neurite bearing cell population.** More than 80 % of the THz treated cell population exhibited 1-3 neurite bearings whereas 73% of the control cell population exhibited 1-3 neurite bearings (p = 0.855). Even though the THz treated sample demonstrated more neurite bearings in comparison to the control sample, the results were not statistically significant. 139
Figure 6. 1. (**A**) **Atomic force micrographs of surfaces with different coatings.** The AFM analysis show an even distribution of single and two-component coatings on the surfaces of the polystyrene substratum. **(B) Initial differentiation and attachment of PC 12 cells after two days of incubation in the presence and absence of NGF solution.** Cells were seeded at a density of 3 × 10^4 cells/mL on poly-L-lysine, laminin, fibronectin, poly-L-lysine/laminin, and poly-L-lysine/fibronectin-coated wells. The cells were grown in a medium that was supplemented with human recombinant NGF (50 ng/mL). The control wells did not contain any coating. In these experiments the PC 12 cells appeared to attach to the surface in clusters. Scale bar is 5 µm.....148
Figure 6. 2. Comparative analysis of differentiation of PC12 cells on substrata with single- and two-component coatings in the presence of NGF solution. The NGF concentrations used were 0, 25, 50, and 100 ng/mL. Cells were grown over a period of five days; fixed in 4% PFA for 15 min and stained with WGA-488 (membrane, green), DAPI (nuclei, blue). Significant neurite outgrowth was observed for cells grown on substrata with double coatings containing poly-L-lysine/laminin and poly-L-lysine/fibronectin. Substrata containing single coatings of poly-L-lysine and laminin exhibited poor cell differentiation. 150
Figure 6. 3. PC 12 cell proliferation on substrata with different coatings in the presence of NGF solution. PC 12 cells were grown over a period of 5 days in the presence of 0, 25, 50, or 100 ng/mL NGF. Incubation of PC 12 cells on substratum surfaces in the presence of 50 ng/mL NGF resulted in an increased amount of attachment on day (a) 1, (b) 3 and (c) 5 compared to the other NGF solutions. Results are presented as the mean ± standard deviation. Unless otherwise specified, statistically significant differences in cell proliferation grown on the different substrata are shown versus the absence of NGF solution. "*" indicates the degree of statistically significant differences.....152
Figure 6. 4. Quantification of neurite outgrowth on different coatings under the influence of various NGF concentrations. The PC 12 cells were grown on various coatings over a period of five days and in the presence of 0, 25, 50 and 100 ng/mL NGF. Over fifty fields of

view were analysed for each condition. The results indicated a two-fold greater neurite outgrowth occurring on substrata containing the dual-component coatings of poly-L-lysine/laminin and poly-L-lysine/fibronectin with increasing NGF concentrations. Results are presented as minimum, 1st quartile, median, 3rd quartile, and maximum. "*" indicates the degree of statistically significant differences. 153
Figure 6. 5. Schematic representation of the bio-interfaces of the PC 12 cells undergoing attachment onto different substratum samples. (A) possible chemical interactions between the polystyrene substratum and the coating materials. The aldehyde and ketone groups present on the surface of polystyrene undergo a Schiff base reaction and bind covalently with the amine groups. **(B)** negatively-charged fibronectin (pI 5.5–6.0) binding to the positively charged poly-L-lysine coating via electrostatic interactions. **(C)** laminin (pI 6.4) with a net negative charge also binds electrostatically to the poly-L-lysine layer. Laminin interacts with the PC12 cell surface receptors via the integrin binding domain. 155
Figure 7. 1. ***B. subtilis*** **spores' viability following GHz and THz exposure.** Viability of the spores were not affected following GHz exposure. The 12h THz treated sample and the untreated control did not exhibit a reduction in the viable counts. A statistically significant reduction was exhibited after 36 h of THz exposure in comparison to the control ($p = 0.041$). 163
Figure 7. 2. ***B. subtilis*** **spores' morphology following exposure to 18 GHz**. TEM micrographs revealed no changes in the internal structure of the spores after exposure to 18 GHz. Scale bar 200 nm. The morphology of the GHz treated spores appears to be different to the untreated control. Spore morphology changes following GHz exposures of 30 s, spores appear dehydrated but no changes in spore viability detected. Scale bar 2 µm. 164
Figure 7. 3. ***B. subtilis*** **spores' morphology following exposure to synchrotron THz radiation after 12 and 36 h.** TEM Slicing of the 12 h THz treated spores did not exhibit any changes in comparison to the untreated control, whereas the spores were disintegrated after 36 h in the presence of synchrotron THz radiation. The spore core and the layers forming the spore capsule appear to be affected in 36 h exposed sample. Scale bar 200 nm (top row) 0.5 µm (middle row). The SEM micrographs illustrate no changes in the morphology of the spores after 12 h of THz exposure, however the spores following 36 h treatment appears to be damaged in comparison to the untreated control group. Scale bar 2 µm. 166
Figure 8. 1. The stability and size distribution of the GUVs and the size distribution of the nanospheres' clusters. (A) Time lapse images of GUVs in suspension. Images were captured continuously for a period of 30 min at 0, 5, 10, 15, 20, 25, 30 min. The GUVs remained stable in solution before exposure to EMF radiation. Scale bar 5 µm. (B) The size distribution of GUVs. The diameter of the liposomes synthesised using the gel assisted method ranged from 5 – 20 µm. (C) Atomic force microscopy of the nanosphere clusters and water and corresponding cross-sectional profile (right) indicating the height and width of the nanosphere cluster. The nanospheres were vortexed for one min in order to keep the experimental conditions consistent. The nanospheres tend to exist in clusters of 10 or more nanospheres (200 – 1000 nm). 174
Figure 8. 2. EMF induced membrane permeability of GUVs. Confocal laser scanning micrographs showing the GUVs internalising nanospheres following EMF exposure. The original solution containing the nanospheres were sonicated before addition GUVs. The non - treated GUVs were used as the control, no nanosphere uptake was visualised, while the EMF treated GUVs (top row) were able to internalise nanospheres (existing as clumps). The presence

of the green signal (FITC) overlapping with the red signal (Dil) when merged confirms that the nanospheres are present bound to the GUVs. Membrane permeability was not detected in the untreated GUVs as there was no overlapping of the FITC and Dil channels. 176

List of Tables

Table 1. Different parameters in electromagnetic radiation. The field intensity, distance, frequency, surface power density and magnetic flux density are the main parameters that needs to be taken into consideration. 33
Table 2. Electromagnetic fields grouped according to their frequency and source. Electromagnetic fields are used in High frequencies of 100 KHz – 300 GHz are being used in most daily appliances. 36
Table 3. Nanosphere uptake by bacterial cells after EMF exposure. The loading capacity varied from one species to another and the highest loading capacity was seen with the 23.5 nm silica nanosphere. According to the table, internalisation was present upon exposure to EMFs. Adapted from (Nguyen et al., 2015a, p. 4). 44
Table 4. Liposomal lamellarity and sizes. Different liposomal preparation methods yield liposomes in different sizes and lamellarity as listed in the table. 65
Table 5. Various proteins used in PC 12 cell neuronal differentiation. Fibronectin, Laminin, Poly-L-lysine, Collagen and Albumin have shown to enhance cell attachment and differentiation. 71

Chapter 1. Introduction

1.1. Overview

A detailed background on the research conducted is presented in **Chapter 2,** the literature review provided discusses the nature of electromagnetic radiation, summarizing the various parameters, sources of non-ionizing electromagnetic radiation as grouped according to the European Commission depending on the frequencies. Detailed information on microwave radiation and terahertz (THz) radiation, focusing mainly on the EMF induced effects on these types of radiation is provided. Biological effects of radiofrequencies and microwave radiation in the range of 18 GHz have been listed where different bacterial strains have revealed reversible membrane permeability, changes in the cell morphology and viability in the presence of 18 GHz. Biological effects in response to THz radiation reported by scientists have been discussed and not many studies have been conducted using THz radiation to the scarce availability of THz radiation generating sources. Possible targets of EMFs (skin – being the first point of contact) and the mechanisms suggested in the literature have been included while there are no conclusive results as to what the possible targets and the methods of actions of EMFs on biological entities. The various techniques used to achieve membrane permeabilization is included and these techniques are electroporation utilizing electric pulses, sonoporation utilizing ultrasound, photoporation utilizing laser radiation. Moving on, detailed information is presented on Giant Unilamellar Vesicles (GUVs) including the composition of liposomes, the various methods used in the preparation of liposomes, characterization of liposomes and research conducted on GUVs permeability in response to magnetic fields and ultrasound radiation. In the present study GUVs were used to study membrane permeability in response to EMFs of 18 GHz. Following is a section on pheochromocytoma cells (PC 12) which is the eukaryotic cell line used in the current study to gain insights on induced membrane permeability in response to EMFs in the range of microwaves and THz radiation. The final section of the literature review includes detailed information on *Bacillus subtilis* spores given the complexity of its spore coat and extreme resistance to heat and various types of radiation. *B. subtilis* spores were used in the current research to study their response to EMFs of 18 GHz and synchrotron sourced THz radiation.

Description of the experimental set up of the project including the different materials used, construction of GUVs, EMF of 18 GHz exposures including the different parameters, dosimetry, controls used, synchrotron sourced THz exposures along with the controls is presented in **Chapter 3**. The two different types of exposures have been highlighted. EMFs of 18 GHz were in the range of 30 s whereas THz radiation lasted for 10 min given the low power

of the beam. The various techniques used to detect membrane permeability in PC 12 cells following exposures of 18 GHz and THz radiation, membrane permeability of GUVs was also investigated. These techniques include confocal scanning microscopy and transmission electron microscopy. Apart from membrane permeability, samples were collected, and the various bioassays used in testing cell viability (LIVE/DEAD assay), protein concentrations, proliferation, metabolic activity, membrane integrity and PC 12differentiation is listed in **Chapter 3**. Morphology of PC 12 cells and spores were studied using scanning electron microscopy. Information on spore germination including viable counts following exposures of 18 GHz and THz radiation is provided. Statistical analysis is carried out using the Statistical Package for Social Sciences (SPSS).

Experimental chapters will follow with **Chapter 4** being the exposure of PC 12 cells to EMFs of 18 GHz. PC 12 cell membrane permeability following exposures were confirmed by the internalization of silica nanospheres and its clusters as depicted using confocal and transmission electron micrographs. The intra-cellular physiology of PC 12 cells were assessed using the MTS assay to gain information on the metabolic activity of the PC 12 cells in comparison to the heat treated and the untreated control. Total protein content of the PC 12 cells using the BCA assay was investigated, membrane integrity of the PC 12 cells were analyzed using the LDH assay and a detailed explanation is reported in **Chapter 4**. Differentiation of PC 12 cells in the presence of EMF of 18 GHz were studied along with the heat treated and the untreated controls where no differences were recorded in the EMF treated, heat treated and the untreated controls.

The effect of PC 12 cells in the presence of synchrotron sourced THz radiation was studied in **Chapter 5** with the main focus being the cell membrane permeability in response to THz radiation. PC 12 cells were exposed to a radiation of 0.3 – 19.5 THz for 10 min in the presence of low power. PC 12 cell membrane permeability following exposures were confirmed by the internalization of silica nanospheres and its clusters as depicted using confocal and transmission electron micrographs. PC 12 cell morphology studied using scanning electron microscopy revealed the formation of blebs in the THz treated sample whereas the untreated control depicted no blebbing. MTS and BCA assays were employed to test PC 12 metabolic activity and protein concentrations, respectively. Intra-cellular physiology of PC 12 cells were examined over a period of 5 days. Differentiation of the PC 12 cells was assessed after THz exposure which included the extent of neurite outgrowth and neurite bearings.

The effect of different coatings and various concentrations of nerve growth factors on the attachment and differentiation of PC 12 cells was reported in **Chapter 6**. Cellular attachment plays a great role in the differentiation of PC 12 cells hence an appropriate coating and optimal conditions for PC 12 differentiation were investigated and reported. The effect of various parameters including the concentration of Nerve Growth Factor (NGF), various coatings including poly-L-lysine (PLL), fibronectin (Fn), laminin (Lam), double coatings composed of PLL/Lam and PLL/Fn on the differentiation process of PC 12 cells were studied. Cellular morphology as visualized using brightfield phase contrast microscopy, cellular metabolism and proliferation using the MTS assay was recorded. A detailed study of the neurite outgrowth and the generation of axons on the different coatings under various NGF concentrations were looked into in **Chapter 6.**

The effect of EMFs of 18 GHz and synchrotron sourced THz radiation on the robust spores of *B. subtilis* is reported in **Chapter 7**. Short exposures of 30 s were carried out in the presence of 18 GHz and prolonged exposures (12 h and 36 h) of 0.3 -19.5 THz were conducted on the spores. Spores were exposed to a fixed frequency of 18 GHz at a constant power of 17 W, whereas the synchrotron sourced THz radiation emitted was having a low power in the range of microwatts. Spore germination was studied using colony counts, morphology and the internal structure of spores were assessed using scanning electron microscopy and transmission electron microscopy, given the complexity of the spore structure and its extreme resistance to radiation and environmental conditions

The final experimental chapter deals with a model cell membrane referred to as GUVs. GUVs are considered as a model membrane system that is capable of mimicking live cell membrane conditions. GUVs constructed using simple phospholipids were exposed to EMFs of 18 GHz and the findings are given in **Chapter 8.** Characterization of the GUVs were carried out depending on the size and stability before exposing them to EMFs of 18 GHz. The response of phospholipids in the presence of EMFs of 18 GHz were analyzed using confocal laser scanning microscopy. The presence of only simple phospholipids helps eliminate certain targets of EMF radiation while helping to gain an understanding how EMFs interact with biomolecules.

The general discussion emphasizing on the reversible membrane permeabilization following EMFs (18 GHz) and synchrotron source THz radiation on pheochromocytoma PC 12 neuron-like cells while providing suggested reasoning as to why *B. subtilis* spores that are remarkably resistant to extreme environmental conditions including UV radiation exhibits deformities

upon exposure to low power THz radiation for long periods is provided in **Chapter 9**. GUVs help eliminate certain targets of EMFs including voltage gated channels. The possible targets and mechanisms of how EMFs of 18 GHz and synchrotron sourced THz radiation induced effects function is reported in **Chapter 9.**

1.2. Aims

The various bioeffects resulting from EMFs have been reported in the literature but no conclusive results of the specific targets of EMFs have been listed, the **main focus** of the project was investigating the membrane permeability and possible aftereffects from EMF exposures. Previous reports showed the ability of EMFs of 18 GHz induced a reversible increase in membrane permeability in different Gram-negative and Gram-positive bacterial species, including *Planococcusmaritimus* KMM 3738, *Staphylococcus aureus* CIP65.8^{T}, *S. aureus* ATCC 25923,*S. epidermidis* ATCC 14990^{T}, *Escherichia coli*; and yeast and red blood cells (Nguyen et al., 2015b, Shamis et al., 2011a). The present lack of understanding of the mechanisms that drive such rapid changes in membrane permeabilization, and the nature of the biomolecules affected by high frequency electromagnetic irradiation limits the use of 18 GHz EMFs in biomedical applications. In order to fill the gaps the current study will explore the bioeffects of EMFs on eukaryotic cells, bacterial spores and investigate whether the exposure of pheochromocytoma cells to such fields would affect membrane permeabilisation, proliferation rates and metabolic status. Different techniques including confocal laser scanning microscopy, transmission electron microscopy, scanning electron microscopy together with fluorescent markers were used in the study to gain insights to membrane permeabilization and morphology. Extremely resistant spores of *B. subtilis* were exposed to EMFs of 18 GHz and synchrotron sourced THz radiation to explore the effects arising from EM radiation. The hypothesis behind the present study is that at these EMFs, non-ionizing electromagnetic radiation encounters a polar molecule (water) and transfers a fraction of its energy to this molecule, driving it to oscillate which in turn has an effect on other cellular constituents. The effects arising from EMF exposures cannot be explained by the increase in bulk temperatures, given that the exposures are at controlled temperatures in the presence of EMFs of 18 GHz and synchrotron sourced THz radiation. Controls exposed to similar temperatures did not exhibit the same changes as EMF exposed sample groups. There is enormous complexity in gaining an insight to the underlying molecular mechanisms upon exposure to EMF. People have suggested possible biological targets of EMF and out of the these the cell plasma membrane, in particular ion channels; altering the rate of opening and closing or they can have a direct effect ion fluxes via the channels (Cagni et al., 2007). This was analysed by implementing a system of equations, the Poisson-Smoluchowski equation where the effect of an exogenous EMF in the radiofrequency range was applied on to the ion channel (Cagni et al., 2007). Moreover, there were a few differences observed in the response to EMF as a function of

orientation with respect to channel axis, such differences were observed mostly at increasing field intensities (Cagni et al., 2007). The project then focuses on the possible targets of EMF radiation and as to why EMFs are able to induce changes in biological entities, a simple phospholipid membrane (GUVs) used in the study helps to eliminate certain suggested targets.

Chapter 2. Literature Review

2.1. Overview

Existing literature available on the aspects covered in the PhD program is reported in the chapter. Definition of electromagnetic fields, characteristics of MW radiation, THz radiation, EMF induced effects on various cell lines emphasizing on the transient permeabilisation of the plasma membrane is reported in the chapter. The characterization of the biological models used and the methods currently in use to gain their permeabilization are also presented.

2.2. Nature of Electromagnetic Radiation

Non-ionizing electromagnetic fields (EMFs) have been used for functioning of power transmission, wireless and radio communication, devices in daily use such as tablets, portable computers and smartphones (Redlarski et al., 2015, Vijayalaxmi et al., 2014, Zeni et al., 2003).The increased use of electromagnetic radiation driven appliances also increases the exposure of humans and other organisms to EMFs (Redlarski et al., 2015, Lewczuk et al., 2014, Kim et al., 2017, Santini et al., 2018). It is of utmost importance to understand the effects that EMF possess on biological matter and the mechanisms that lead to the changes that occur due to the ongoing concerns of the public regarding the adverse effects on human health due to exposure (Vijayalaxmi et al., 2014). Researchers have been studying the extent of genetic damage in animal and human cells exposed both *in vivo* and *in vitro* to RF in the past decades as it is crucial to understand the DNA damage occurring in somatic cells, as such mutations will be passed onto subsequent generations (Vijayalaxmi et al., 2014) .

Non-ionising electromagnetic radiation or electromagnetic fields (EMF) consist of two independent components (Lewczuk et al., 2014, Artacho-Cordon et al., 2013):

- Electric - known as an electric field in which Coulomb forces act on electrically charged or non-moving (stationery) objects, represented by a state of space.
- Magnetic - known as a magnetic field where Lorenz forces act on electrically charged moving (non-stationary) objects, represented by a state of space.

In order to obtain a complete understanding of what electromagnetic radiation is they can be characterized depending on many physical parameters including (Lewczuk et al., 2014, Artacho-Cordon et al., 2013, Redlarski et al., 2015) **(Table 1)**.

Table 1. Different parameters in electromagnetic radiation. The field intensity, distance, frequency, surface power density and magnetic flux density are the main parameters that needs to be taken into consideration.

Parameter	Definition	References
Field Intensity	With regard to electric fields, its intensity E is given in volts per metre (V/m) while in the case of magnetic fields, its intensity *H* is given in amperes per metre (A/m)	(Artacho-Cordon et al., 2013, Lewczuk et al., 2014)
Distance (R)	from an object given in metres (m)	(Lewczuk et al., 2014)
Frequency (f)	measured in hertz (Hz) in time dependent fields whereas for time independent fields, f is said to be 0	(Lewczuk et al., 2014)
Surface power density	represents the intensity of power radiated including the area that power is being radiated to, measured in watts per square metre (W/m^2)	(Lewczuk et al., 2014)
The magnetic flux density	Represented using tesla (T) and exists only in the presence of a flow of a current	(Artacho-Cordon et al., 2013, Lewczuk et al., 2014)

The European Commission grouped the sources of non-ionising radiation depending on their source and frequency (Redlarski et al., 2015), namely:

(i) Radio frequency fields (RF),
(ii) Intermediate frequency fields (IF),
(iii) Extremely low frequency fields (ELF)
(iv) Static fields.

Power transmission lines or electrically powered devices consist of ELF fields ranging from 1Hz- 100 KHz (ICNIRP, 2020), mainly consisting of frequencies of 50 or 60 Hz that are quasi-stationery, the electric and magnetic fields can be analysed separately together with the effects on organisms (Lewczuk et al., 2014, Redlarski et al., 2015, Artacho-Cordon et al., 2013). ELFs are found to have a potential negative impact on organisms even though the mechanism of its action on biological entities is unknown (Lewczuk et al., 2014). On another aspect, electronic devices such as mobile phones, radio transmitters or television sets emit radiation ranging from 300 MHz – 300 GHz (Lewczuk et al., 2014) **(Table 2)**. Researchers have suggested that high frequency radiation may increase the temperature of organs and tissues causing harm to viable cells (Lewczuk et al., 2014, Redlarski et al., 2015). So far, there has been no clear results of negative influence on humans despite the fact that very low frequency EMF were classified as being carcinogenic by The international Agency for Research on Cancer in 2002 (IARC) (Lewczuk et al., 2014, Simko et al., 2001, Feng et al., 2016). Recent evidence have been provided that exposure to RF-EMF are capable of inducing beneficial effects *in vivo* and *in vitro* while protecting bio entities from damage arising from subsequent treatments with physical or chemical agents (Falone et al., 2018). Observations have suggested that pre-exposure to non-ionizing EMF is able to induce a phenomenon similar to that adaptive response (AR) (Vijayalaxmi et al., 2014).

Thereby our focus is towards understanding the effects of electromagnetic radiation in the super high frequency range (Gigahertz and Terahertz). At these high frequencies the electric and magnetic fields are tightly coupled and their effects cannot be evaluated separately (Artacho-Cordon et al., 2013). Microwave radiation is an important part of the electromagnetic spectrum consisting of frequencies from 300 MHz – 300 GHz and a corresponding wavelength in the range of 1 m – 1 mm (Banik et al., 2003, Lewczuk et al., 2014, Artacho-Cordon et al., 2013). EMFs in the Microwave region was at a single frequency of 18 GHz whereas the synchrotron sourced THz radiation is a broadband source emitting radiation with varying frequencies

(Choudhury, 2014). The effects resulting from 18 GHz is due to the exact frequency EM waves, on the other hand the effects due to THz radiation can be a result of EM waves in the range of 0.3 – 19.5 THz. The THz band consists of a wavelength that is situated in between microwave and infrared rays in the electromagnetic spectrum (Zhao et al., 2014b). Research has just begun on THz that has frequencies ranging from 0.1 mm – 1 mm (1 THz = 10^{12} Hz) which were referred to as far infra-red waves in the late 1980s (Zhao et al., 2014b, Wallace et al., 2006). The findings following the exposures of the single frequency in the MW region and the EM waves in the 0.3-19.5 THz is reported in the thesis.

Table 2. Electromagnetic fields grouped according to their frequency and source. Electromagnetic fields are used in High frequencies of 100 KHz – 300 GHz are being used in most daily appliances.

Type of EMF	Frequency	Uses	References
Radio frequencies (RF)	100 KHz - 300 GHz	Used in the operation of general appliances: television, smartphones, tablets, radio, microwave ovens Medical uses: Magnetic Resonance Imaging (MRI)	(Redlarski et al., 2015, Lewczuk et al., 2014)
Intermediate frequency fields (IM)	300 Hz – 100 KHz	Used in video screens, for antitheft devices in homes, shops and cars, welding appliances Medical uses: Magnetic Resonance Imaging (MRI)	(Redlarski et al., 2015, Lewczuk et al., 2014)
Extremely low frequency fields (ELF)	Less than 300 Hz	Electric trains and trams operate on very low frequencies, power transmission cables, electrically powered appliances	(Redlarski et al., 2015, Lewczuk et al., 2014, Artacho-Cordon et al., 2013)
Static fields	-	Presence in nature, electrolysis, video screens Medical uses: Magnetic Resonance Imaging (MRI)	(Redlarski et al., 2015, Lewczuk et al., 2014)

2.3. Microwave (MW) Radiation

Microwave radiation is an important part of the electromagnetic spectrum consisting of frequencies from 300 MHz – 300 GHz and a corresponding wavelength in the range of 1 m – 1 mm (Banik et al., 2003, Lewczuk et al., 2014, Artacho-Cordon et al., 2013). Microwave radiation does not exhibit ionising properties hence it is a type of non-ionising radiation. Microwaves are used extensively in many fields. Popular uses of microwave radiation in the food industry include drying, thawing, baking foods and also for sterilization purposes which includes the inactivation of microorganisms present in food (Woo et al., 2000). Many studies have reported a decrease in microorganisms present in beef, chicken, turkey, corn-soy milk, potatoes and frozen food after being exposed to microwave radiation (Woo et al., 2000). Microorganisms that have been killed upon exposure to microwaves include *Escherichi*a *coli, Staphylococcus aureus, Streptococcus faecalis, Salmonella, Listeria* spp. and *Clostridium perfringes* (Woo et al., 2000).

Microwaves upon interaction with biological materials tend to cause various biological effects and the extent of the effect depends on many factors including, field strength, frequency, modulation, waveforms and the length of exposure (Banik et al., 2003). Researchers have suggested that the heating effect of microwaves are mainly responsible for the changes caused (Woo et al., 2000) but some findings state the presence of non-thermal microwave effects depending on the amount of energy required to cause different types of molecular transformations (Banik et al., 2003). Microwave radiation has been employed as a modern technique for the purpose of sterilization in the food industry (Banik et al., 2003). There is to great conflict on how cell death is caused in microorganisms; the heating produced by microwave radiation is mainly responsible for cell death; death was caused due to microwave electric fields and not only heat (Banik et al., 2003, Woo et al., 2000). It has been observed that the destruction of microorganisms due to microwave radiation occur at temperatures that are well below than the thermal destruction point (Woo et al., 2000) adding to the fact that microwaves do possess non-thermal effects.

One of the many factors leading to the above conflict is the difficulty in maintaining a constant temperature during microwave irradiation (Banik et al., 2003). Apart from that, another source of inaccuracy is the uneven distribution of the electric field present inside the microwave chamber (Shamis et al., 2011a). It appears that there are numerous reflections occurring inside the enclosed cavity which leads to constructive interference patterns within the cavity creating

regions called ‘hot spots’(Shamis et al., 2011a). A hot spot can be defined as thermal irregularity that is caused due to non-linear dependence of electromagnetic and thermal properties of the material on temperature (Shamis et al., 2011a). The presence of hot spots lead to un uniform power absorption by the sample as the number of waves reaching different points vary causing non uniform heating and un even temperature distribution in the sample (Shamis et al., 2011a).

2.4. Terahertz Radiation

The terahertz (THz) band is of significant importance to many research institutions including the military bases for security applications (Zhao et al., 2014b, Wilmink and Grundt, 2011, Zeni et al., 2007) and also in medical and pharmaceutical applications (Anton et al., 2015). The THz band consists of a wavelength that is situated in between microwave and infrared rays in the electromagnetic spectrum (Zhao et al., 2014b).. The radiation can be described using other frequently used terms: wavelength (lambda sign = 30-3000 μm); wavenumber (k = 3.3-334 cm^{-1}); period (period sign = 0.1-10 picoseconds); temperature (T = 4.8-478 K); photon energy (E = 0.4-41 milli-electron volts) (Wilmink and Grundt, 2011).

The uses of THz radiation is widespread, sub-THz vibrational spectroscopy is an emerging technique that is used in bio-sensing and THz are presently being used at main airports for security screening procedures (Globus et al., 2013, Wilmink and Grundt, 2011). The technique is based on the interaction that occurs between the terahertz radiation and the internal molecular vibrations that possess low energy (Globus et al., 2013). Other instances where THz radiation has proved to be useful is its use in the diagnosis of cancer and burn at medical centers (Wallace et al., 2006), and at border protection checkpoints for the identification of concealed weapons, drugs and explosives (Wilmink and Grundt, 2011) . THz with a frequency greater than GHz, possess unique advantages, the THz pulse widths in the sub picosecond scale which allows the facile analysis of materials such as semiconductors, super conductors, liquids and biological samples using time-resolved transient spectroscopy (Zhao et al., 2014b). THz pulse imaging (TPI) (typically in the range of 0.1 THz to 10 THz; wavelength range of 3 mm to 30 μm)in reflection geometry have been used in the study of skin tissue and related cancers by (Woodward et al., 2002) both in vivo and vitro conditions. Interaction of this frequency range excites the vibrational modes of molecules yielding spectroscopic information and contrast (Woodward et al., 2002). The sensitivity of THz radiation to polar molecules (water) makes the technique suitable in investigating the hydration levels in the skin and help to determine the lateral spread of skin cancer given the increase of basal cell carcinoma (BCC) in white populations (Woodward et al., 2002). In the study by (Woodward et al., 2002) the authors were able to differentiate between the normal and diseased tissue (BCC) using the THz pulse shape in the time domain (Woodward et al., 2002). BCC tissue exhibited a *positive* THz contrast, inflammation and scar tissue whereas the normal tissue exhibited a *negative* THz contrast (Woodward et al., 2002). TPI was also used in studying human breast tumors by (Fitzgerald et

al., 2006), human breast tissue specimens with carcinoma excised from women. Two image parameters investigated were the minimum of the THz impulse function, the ratio of the minimum to the maximum of the THz impulse function (Fitzgerald et al., 2006).Investigation of the correlation coefficient of tumour areas and the shape of the tumour regions demonstrate the potential of THz pulsed imaging encouraging future studies to determine the specificity and sensitivity of the technique (Fitzgerald et al., 2006).THz pulsed spectroscopy (TPS) was employed by (Ashworth et al., 2009) in the range of 0.15 – 2.0 THz to measure the refractive indices of freshly excised healthy breast tissue from 20 patients. Apart from using histology in classifying the tissues as healthy fibrous, healthy adipose or breast cancers, the average complex refractive index determined for each group revealed that the samples containing cancer had a greater refractive index and an absorption coefficient (Ashworth et al., 2009). In another study by (Wallace et al., 2006) TPI was employed to differentiate normal tissue and regions of tumour in BCC. The absorption coefficient and refractive indices recorded were higher for BCC than normal tissues (Wallace et al., 2006). TPI was also used in generating 3dimensional images of tissue structures including teeth (Crawley et al., 2003). In a study by (Crawley et al., 2003), 14 samples of dental tissue were imaged using pulsed THz radiation and the enamel thickness was quantified accurately using this technique. The results from the work conducted using THz imaging indicated that both TPI and TPS can be used in differentiating between healthy tissue and cancerous tissue due to the differences present in the fundamental optical properties (Woodward et al., 2002, Ashworth et al., 2009, Wallace et al., 2006).The high coherent (strong spatial and strong temporal) property of THz helps to assist the absorption coefficients and refractive indices of samples and due to the THz photons possessing low energy, the radiation does not damage tissues and since there is no harmful ionization present THz are ideal for biopsy (Zhao et al., 2014b).

THz photons do not possess the energy to ionize biological samples hence the radiation is considered to be non-ionising (Wilmink and Grundt, 2011). Non-ionizing and ionizing radiation can have different impacts on biological tissues (Wilmink and Grundt, 2011). It is important to note that THz do not carry enough energy that can cause direct ionization effects to biomolecules and water (Wilmink and Grundt, 2011). Ionisation results in the formation of highly reactive free radicals that can cause indirect or secondary damage to biomolecules (Wilmink and Grundt, 2011) whereas THz do not generate free radicals but can cause thermal effects which cannot be distinguished from the effects that are caused due to bulk heating (Wilmink and Grundt, 2011).

2.5 EMF induced effects

Many of the studies evaluate the impact of EMF before, during, after or following exposure to standard genotoxic agents trying to mimic real life situations. Different after effects investigated includes single and double strand breaks (SB), micronuclei (MN), chromosomal aberration (CA), mutations (M) and sister chromatid exchanges (SCM) in response to a range of frequencies, specific absorption rates (SAR), modulations, exposure durations using different cell types (Vijayalaxmi et al., 2014).

2.5.1. Biological effects of RF and microwave radiation

Electromagnetic fields in the frequencies of microwave radiation are known to increase the conductivity and permeability of materials significantly (Bober et al., 1997) mainly due to enhanced mobility of ions (Challis, 2005) and diffusion (Antonio and Deam, 2007). One of the main differences between high frequency EMFs is that they have the ability to amplify kinetic process unlike low frequency EMFs (Shamis et al., 2011a). This is mainly due to the fact that mobility of ions depends on either diffusion or application of an electric field (Despa, 1995). The permeability of the cell membrane is low to external molecules (Towhidi et al., 2016).

The frequency of 18 GHz were used in most of the experiments as this frequency produced the shortest wavelength which is comparable to the bacterial cell diameter and therefore will have the maximum effect on cell kinetics (Shamis et al., 2011a, Nguyen et al., 2015b, Shamis et al., 2012a).The PC 12 cells on the other hand are comparatively large with a diameter of 10 μm (Nakazawa et al., 1991).

In a study conducted by (Shamis et al., 2011a), *Escherichia coli* cells were exposed to microwave radiation of 18 GHz. The cell density of the bacterial cells were adjusted to 10^8 CFU per mL optical density (OD_{600} recorded at 600 nm: 0.1) in phosphate saline buffer. The sample for EMF exposure comprised of 2 mL of working suspension in micro-petri dish. The sample was subjected to specified radiation of 18 GHz for 1 min where the temperature increased from 20°C to 40°C with 1 min cooling (on ice) in between. In order to maximize the EMF exposed on to the bacterial cell, there were 3 cycles of exposure employed. Various techniques (Scanning Electron Microscopy, Confocal Laser Scanning Microscopy) were used to determine cell morphology and viability after exposure. The SEM analysis revealed that the *E. coli* cells that were dried for 60 s after EMF exposure displayed a cell morphology that was

different to all other groups tested. Up to 98% ± 1% of the cells had a dehydrated appearance. Cell viability tests revealed that up to 87.7% ± 4% of EMF treated cells and 98% ± 1% of heat treated (Peltier plate) cells remained viable and were able to recover on nutrient agar. The results suggest that the specific MW effects were not bactericidal given the statistical data, which stated that there is no significant difference between the EMF treated and the Peltier plate treated control group. The small decrease in the cell number could be due to the thermal shock experienced by the cells. Previous research conducted by the same group (Shamis et al., 2008, Shamis et al., 2009) were able to achieve nearly complete bacterial inactivation after MW radiation at a temperature of 45 °C. The use of various experimental conditions such as osmolarity or temperature can give rise to various MW effects. There is evidence confirming that EMFs does have an effect on the bacterial cell membrane as the SEM images show cytosolic fluid leakage into the external environment (**Figure 2.1.**).

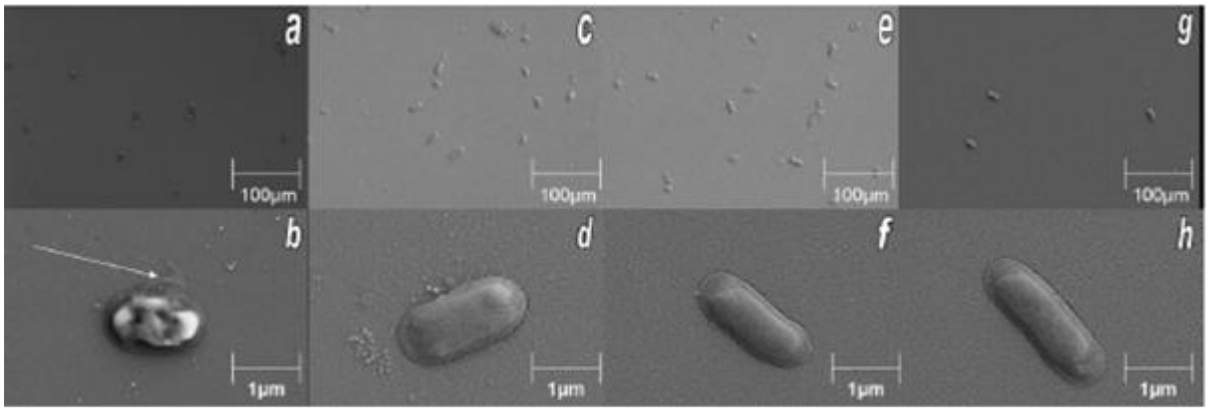

Figure 2. 1. *E. coli* cells exposed to EMF. SEM images (a and b) of EMF exposed bacterial cells; (c and d) Untreated cells. Bacterial cells ten mins after EMF exposure (e and f); (g and h) Heat-treated cells (Peltier plate). Panel b shows cytosolic leakage. Adapted from (Shamis et al., 2011a, p. 3020).

The cell membrane of the bacterial cell has to be altered in a certain way for the fluid to leak into the exterior. However, the affect only lasted for a short period of time as the cells appeared to have recovered their shape within 10 min after MW exposure. The reason can be the reabsorption of these fluids into the cell. There were no morphological changes detected in the heat-treated or the non-treated cells. Taking all the results into account, a mechanism for reversible leakage for cellular contents have been suggested. It is proposed that molecular transport produced by MW radiation is controlled by electro-kinetic mechanisms which help to increase the transport rates (membrane charging and discharging is responsible for molecular transport and electrical behaviour) (Shamis et al., 2011a).

In order to gain an idea on the membrane integrity and reversible poration occurring within the cell membrane, FITC fluorescent dextran probes (150-kDa) were used in the study. The high molecular mass dextran molecules do not carry any charge; therefore, they are not in any way affected by electric fields. The simple assay was implemented to determine if there is any pore formation and if any, to determine the pore size. The free-floating dextran molecules will penetrate the cell membrane during rehydration and remain trapped inside the cells. From the results obtained, 100% of the microwave (MW) exposed cells have ingested dextran, only 17% ± 3% of the untreated controls and 13% ± 4% of the heat-treated cells appeared to be fluorescent. The minor amount of fluorescence observed in the control groups could be a result of centrifugation that cells undergo. The size of a dextran probe was calculated to be 15.9 nm. Given the results, it can be concluded that the size of the pores formed in the bacterial cell membrane are 15.9 nm or bigger confirming membrane poration in *E. coli* cells upon exposure to EMF at 18 GHz (Shamis et al., 2012a, Shamis et al., 2011a, Shamis et al., 2012d).

Another study was conducted by (Nguyen et al., 2015b) to investigate EMF induced permeability effects of Gram positive cocci. The various bacterial cells that were exposed to EMFs were *Planococcus maritimus* KMM 3738, *Staphylococcus aureus* CIP65.8^{T}, *S. aureus* ATCC 25923 and *S. epidermidis* ATCC 14990^{T}. Transmission electron microscopy (TEM), uptake of silica nanoparticles, indirect propidium assay was employed to understand the state of the bacterial cells after exposure of EMF (Nguyen et al., 2015b). TEM images show that all the strains were able to internalize the nanospheres in varying degrees **(Table 3)** and no change in cellular morphology detected however the scanning electron micrographs depicted traces of cytosolic fluids leaked into the surroundings after exposure to EMF (Nguyen et al., 2015b).

Table 3. Nanosphere uptake by bacterial cells after EMF exposure. The loading capacity varied from one species to another and the highest loading capacity was seen with the 23.5 nm silica nanosphere. According to the table, internalisation was present upon exposure to EMFs. Adapted from (Nguyen et al., 2015b, p. 4).

	Silica nanospheres 23.5 nm		**46.5 nm**	
Bacterial strains	**Loading Capacity**	**Bacterial cells that internalised nanospheres (%)**	**Loading capacity**	**Bacterial cells that internalised nanospheres (%)**
P. maritimus KMM3738	172 ± 8	97 ± 5	75 ± 8	80 ± 9
S. aureus ATCC 25923	161 ± 8	99 ± 4	81 ± 8	40 ± 7
S. aureus CIP 65.8^T	261 ± 8	99 ± 3	114 ± 8	44 ± 7
S. epidermidis ATCC 14990^T	211 ± 8	99 ± 5	Not detected	Not applicable

The cell viability was analysed using direct counting of colony forming units and the results show that 84% of the strains studied were able to remain viable after EMF exposure. The Specific Absorption Rate (SAR) value was calculated to be 5.0 kW kg^{-1}, which induced cell permeability in all the strains. The propidium iodide (PI) assay was implemented as the main technique in confirming cell membrane electroporation. Propidium iodide is not able to pass through intact membranes, however upon disruption of a cell membrane, the propidium cation (Pr^{2+}) can penetrate through the cell membrane and bind with nucleic acids within the cell which will fluorescence (Pakhomova et al., 2011, Nesin et al., 2011). No internalisation of PI or nanospheres, were detected in the bacterial cells exposed to conventional heat treatment. From these results it can be deducted, that the permeability occurred not because of bulk heating hence it could be a EMF driven result due to the EMF interaction with the cell membranes or with its components present (*e.g.*, membrane proteins or phospholipids, etc.), or microthermal changes at the macro level that is not easily detectable. In another study *Staphylococcus aureus* was exposed to microwaves of 2.45 GHz at a temperature of 46ºC, changes in a range of enzymatic activity was detected including cytochrome-c oxidase, malate dehydrogenase and ketoglutarate (Drefuss and Chipley, 1980).Membrane permeability was not recorded. ELFs of 50 Hz magnetic fields was used in a study conducted by (Feng et al., 2016) where human amniotic epithelial cells were radiated for 60 min. Increased Cytochrome-c release and mitochondrial permeability transition (MPT) with no significant effect on

mitochondrial membrane potential was detected (Feng et al., 2016). Effects of mobile phone radio frequency EMFs of 918 MHz was tested on human and rat primary astrocytes by (Tsoy et al., 2019). The data revealed that the EMF treatment was able to reduce amyloid beta peptide (Aβ), as the accumulation of (Aβ) in the brain leads to neuro-inflammation, mitochondrial dysfunction , oxidative stress and neuronal death causing Alzheimer's disease (AD) (Tsoy et al., 2019). The authors believe that the technique can be utilized in future as a therapeutic potential for the treatment of AD. In a study conducted by (Kim et al., 2017) the effects of RF-EMFs of 835 MHz on the cerebral cortex of mice were assessed. The RF-EMF delivered had a SAR of 4.0 W/kg for a period of 5 hours a day for 12 weeks, important findings include the induction of autophagy, damage of myelin sheath activity and the mice exhibited hyperactivity-like behaviour (Kim et al., 2017).

Recent studies have shown that many medical appliances use electromagnetic waves in various ways to heal wounds on the skin, help restore bone fractures and to reduce pain and swelling for different postsurgical needs (Artacho-Cordon et al., 2013). There is enormous complexity in gaining an insight to the underlying molecular mechanisms upon exposure to electromagnetic waves. People have suggested possible biological targets of electromagnetic waves and out of the these the cell plasma membrane, in particular ion channels; altering the rate of opening and closing or they can have a direct effect ion fluxes via the channels (Cagni et al., 2007). This was analysed by implementing a system of equations, the Poisson-Smoluchowski equation where the effect of an exogenous electromagnetic waves in the radiofrequency range was applied on to the ion channel (Cagni et al., 2007). No non-thermal effects were observed as there were no signal amplifications observed confirming the absence of gating mechanisms and complete stiffness of channel walls (Cagni et al., 2007). Moreover, there were a few differences observed in the response to electromagnetic waves as a function of orientation with respect to channel axis, such differences were observed mostly at increasing field intensities (Cagni et al., 2007).Over the years, various electromagnetic waves have been utilized and various mechanisms suggested to as how they interact with cells (Artacho-Cordon et al., 2013). The presence of numerous 'frequency windows' for biological action; frequencies where a biological response is detected and the presence of carrier frequencies, mixtures of modulated frequencies adds to the difficulty in dealing with EMF (Funk et al., 2009). Taking all into account researchers have thus focused on the thermal effects that radiation cause at a tissue-specific absorption rate known as SAR (Funk et al., 2009).

(Artacho-Cordon et al., 2013) has come up with a possible explanation on the reactions that can occur inside a cell upon exposure to EMF. The diagram given below summarizes the possible pathways (**Figure 2.2.)**. EMFs change the membrane structure and penetrability of small molecules (Ca^{2+}) which leads to changes in temperature or local pH and also involves in the re organization of cytoskeleton components. It was suggested that the microtubule polymerization maybe disturbed by IMF (100-300 KHz) (Artacho-Cordon et al., 2013). The alterations of cell-signalling pathways that are EMF driven could be initiated by the changes in melatonin, secondary messengers (Ca^{2+}, AMPc) or by the alterations that occur in ions. It is also suggested that EMF has effects on gene expression which leads to DNA damage and formation of free radicals that in turn affects DNA structure resulting in chromosomal aberrations (micronucleus formation) (Santoro et al., 1997). Free radicals are short lived molecules with unpaired electrons, an important characteristic of free radicals is that they can react with non-radicals resulting in the formation of new radicals hence initiating chain reactions (Dreher and A.F., 1996). There is no direct interaction of EMF with DNA because the energy present in EMF is insufficient to break the chemical bonds present in DNA (Simko et al., 2001). The indirect link of EMF on DNA is via the free radicals that are formed which interacts with DNA and other cellular components leading to free radical mediated effects (Simko et al., 2001). Considering the health effects that EMFs possess on reproductive organs numerous studies illustrated that the detrimental effects due to EMFs from laptops, mobile phones, and other electric devices on sperm quality provide evidence for heavy electron leakage from the electron transport chain present in the mitochondria as the main cause of EMF damage (Santini et al., 2018). Similarly, evidence of mitochondrial origin reactive oxygen species (ROS) production and the contribution of oxidative stress are the main causes of damage to female reproductive health following exposure to EMFs (Santini et al., 2018).

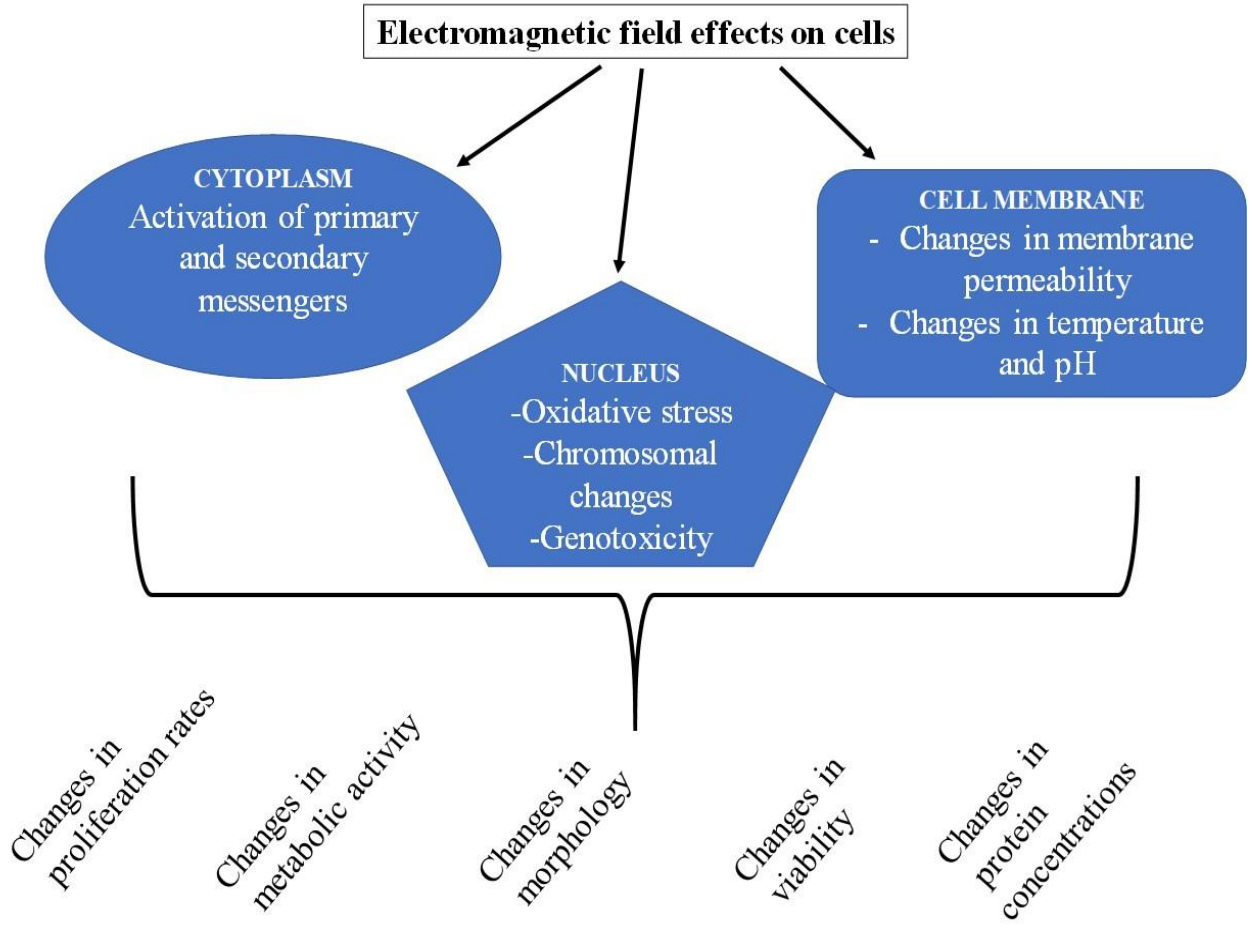

Figure 2.2. Illustration of the possible effects on cells following EMF exposure. Changes in cellular proliferation rates, metabolic activity, morphology, viability and protein concentrations are some of the suggested possible effects.

.

Protective effects from EMF have been investigated by various researchers (Falone et al., 2018, Vijayalaxmi et al., 2014, Zeni et al., 2003). Recent evidence have been provided that exposure to RF-EMF are capable of inducing beneficial effects *in vivo* and *in vitro* while protecting bio entities from damage arising from subsequent treatments with physical or chemical agents (Falone et al., 2018). Observations have suggested that pre-exposure to non-ionizing EMF is able to induce a phenomenon similar to that adaptive response (AR) (Vijayalaxmi et al., 2014). AR is a phenomenon in which cells were pre-exposed to extremely low, non-toxic doses of certain genotoxic agents that became resistant to the damage caused by subsequent exposure to higher and toxic dose of the same, similar or another genotoxic agent (Vijayalaxmi et al., 2014). (Samson and Cairns, 1977) were the first to report AR in *E. coli,* bacteria that was grown on in low and non-toxic dose of an alkylating mutagen (N-methyl-N-nitro-nitrosoguanidine, MNNG 1µg/mL) showed increased resistant to both mutation and cell killing by the subsequent exposure to a higher dose of MNNG 100 µg/mL (Samson and Cairns, 1977). The low dose is generally termed as adaptation dose (AD) whereas the high dose is referred to as the challenge dose (CD) (Vijayalaxmi et al., 2014). The induction of AR was demonstrated in many different organisms including various mammalian cell lines pre-exposed to non-ionising EMFs following subsequent exposures to chemical mutagens.

In a study conducted by human neuroblastoma cells (SH-SY5Y) were exposed to RF of 1950 MHz for 20 h with a SAR of 0.3 or 1.25 W/kg and 3 h following the exposure, the cells were treated with a chemical agent inducing DNA damage (menadione) (Falone et al., 2018). No differences were detected among the sham and RF exposed samples and analysis of gene expression revealed that the pre-exposure to 1950 MHz almost inhibited the dramatic loss of glutathione peroxidase based antioxidant scavenging efficiency that was induced by menadione (Falone et al., 2018). The study reported that cells pre-exposed with RF exhibited decreased menadione dependent DNA oxidative damage while enhancing antioxidant scavenging efficiency and restoring DNA repairing capabilities (Falone et al., 2018).

Another study reported that ELFs of 60 Hz with a field strength of 0.8 mT exposed onto human lymphocytes is capable of interacting with cellular system indirectly, probably as an initiator or as a co carcinogen (Cho, 2003).The effects of ELFs (50 Hz, 2 mT) on brain proteins in mice were evaluated in a study, the results revealed that exposure did have an effect on the level of protein expression following a 4 day exposure (Strasak et al., 2009).

These suggested changes inside a cell can influence the rate at which it proliferates, cell cycle and the apoptosis cascade (Artacho-Cordon et al., 2013). Up to date, no such mechanism has been proved in theory.

Mammals contain an array of cells that exist in various shapes and sizes sharing similar characteristics with cell morphologies that appear to be oval and round under the microscope (Wilmink and Grundt, 2011, Radoicic et al., 2014). The plasma membrane encloses the cellular contents, providing a selective barrier between what enters and leaves the cell (Wilmink and Grundt, 2011, Geng and Lu, 2013, Radoicic et al., 2014). There is great debate as to if EMFs penetrate the cell membrane, it is generally thought that EMFs have a great difficulty in passing the cell plasma membrane (Funk et al., 2009). The plasma membrane comprises of a phospholipid bilayer, which contains lipids including cholesterol (50%), and proteins (50%) integrated into it (Wilmink and Grundt, 2011, Radoicic et al., 2014). The phospholipid bilayer present consists of a hydrophilic polar head attached to hydrophobic carbon chains (Wilmink and Grundt, 2011, Radoicic et al., 2014). The fluidity and the structure of the hydrocarbon tails is determined by the degree of saturation (Wilmink and Grundt, 2011). Saturated hydrocarbon tails do not contain C=C, whereas unsaturated hydrocarbon tails do contain C=C and are less restricted than saturated hydrocarbon tails (Wilmink and Grundt, 2011). The membrane permeability can be increased transiently by the application of electric fields and the impulse can be transmitted chemically (Artacho-Cordon et al., 2013). Temperature or pH changes are known to be caused by electrical simulation (Funk et al., 2009) which leads to membrane destabilization. The findings in cellular biology now can be explained by ion dynamics (H^+, Ca^{2+} , voltage sensors and ion related pumps) and by the way they act on small signalling molecules. Various insightful studies (Adams et al., 2007) demonstrated that there is a clear link between EMF and cell biology. Direct current electric fields (DC EF) were employed in the study and the findings show that DC EF produced by H^+ , Ca^{2+}, K^+ ion channels provide signals that specifically affects the cell behaviour during normal tissue turnover, embryonic development and regenerative repair (Adams et al., 2007). In future, there are attempts to link EMF research to quantum physics and thermodynamics in order to gain an understanding on cellular biology (Funk et al., 2009).

The physiology of the cell cytoskeleton is important as living cells depend on it as an anchor for various internal processes including cell migration, proliferation, differentiation and extra cellular transportation (Gupta et al., 2015, Artacho-Cordon et al., 2013, Wilmink and Grundt, 2011). Some researchers have reported that there is no influence of EMF detected on motor

proteins in murine macrophages or the cytoskeleton (Artacho-Cordon et al., 2013). Previous research conducted has shown that the components of cytoskeleton seem to have reorganised (Santoro et al., 1997) after exposure to EMFs.

A cell is made up of two separate regions known as the cytosol and the cytoplasm (Wilmink and Grundt, 2011). The cytosol covers a large area of the cell consisting mainly of water and organic, inorganic ions (potassium, magnesium, sodium, phosphate, calcium and chloride). The cytoplasm has a pH of ~7.1 – 7.2 and contains a thick alkaline liquid. It is believed that the changes occurring in signalling pathways due to EMF interactions on the cell membrane impose an effect on the cytoplasm (Artacho-Cordon et al., 2013).

2.5.2. Biological effects of THz radiation

The THz exposure parameters (power, frequency exposure duration) and the properties or the composition of the biological sample (scattering properties, absorption properties and the index of refraction) are the two major factors that influence THz-induced biological effects (Wilmink and Grundt, 2011). The review focuses on the effects of THz radiation on eukaryotic and prokaryotic cells. Not many studies were conducted on the effects that THz had on biological samples due to the scarce availability of THz generating sources and sensitive detectors (Zhao et al., 2014b, Wilmink and Grundt, 2011, Zeni et al., 2007) whereas the effects of electromagnetic waves (microwaves) in the frequency of Gigahertz (GHz) on certain various biological entities have been studied (Nguyen et al., 2015b, Shamis et al., 2011a, Nguyen et al., 2016, Shamis et al., 2012d).

EMFs have been studied and the results indicate that these electric and magnetic waves in varying degrees act on biological targets including cell growth and proliferation, differentiation, enzyme activities, genetic make-up of cells and out of which the cell membrane has gathered most of the attention.

A study conducted by (Zeni et al., 2007) explored if THz radiation was able to induce genotoxic effects in human peripheral blood leukocytes. The study used human blood samples from healthy donors and were exposed to THz radiation for 20 min. Frequencies of 120 and 130 GHz radiation with SAR values of 0.4 mW g^{-1}, 0.24, 1.4 and 2 mW g^{-1} were tested (Zeni et al., 2007). It was found that the THz exposures with varying SAR values did not induce genotoxicity or alterations of the cell cycle kinetics using the alkaline comet assay straight after exposure (Zeni et al., 2007).(Clothier and Bourne, 2003) investigated the effects of THz radiation on human skin cells. Human skin is the first point of contact with EMFs, thereby its important in understanding how the skin responds to EM radiation. Human keratinocytes were exposed to 1-3 THz at up to 0.45 Jcm^{-1} for 10, 20 or 30 min at room temperature (rtp), the results exhibited no changes in differentiation, no donor-specific inhibition or changes in cell cycle in comparison to the untreated sample (Clothier and Bourne, 2003).In another study human dermal fibroblasts exposed to continuous THz radiation from an optically pumped molecular gas THz laser source (2.52 THz, 227 mW/cm^2) for up to 80 min were shown to be 90 % viable (Am et al., 2004, Subramanian et al., 1997, Hoop et al., 2017). When exposed to the narrow-band THz radiation (2.3 THz, 1.4 W/cm^2), human embryonic stem cells (hESCs) showed no structural chromosomal aberrations or difference in cell morphology when

compared to the untreated control, and only some minor upregulations of mitochondria-related genes were reported (Bogomazova et al., 2015). (Hintzsche et al., 2011) utilised a human-hamster cell line in order to investigate and quantify spindle disturbances following exposure to THz radiation. Monolayer cultures were exposed to THz radiation of 0.106 THz for 30 min with power densities that ranged from 0.043 mW/cm^2 to 4.3 mW/cm^2 (Hintzsche et al., 2011).After analyzing 6,365 mitotic cells, the results suggested that 0.106 THz radiation can be a spindle acting agent as indicated by the appearance of spindle disturbances at anaphase and telophase of cellular divisions (Hintzsche et al., 2011).

Fröhlich concluded that the interactions of THz radiation with cells may arise as mediated by the excitation of biological macromolecules (Fröhlich, 1968) or nonlinear/linear resonance mechanisms (Bogomazova et al., 2015). Fröhlich also predicted that biological systems are able to support coherent excitations which fall in the range $10^9 – 10^{12}$ Hz (Weightman, 2012, Fröhlich, 1968). The ability of vibrational modes within protein molecules to order and condense into a lowest-frequency vibrational mode in a process similar to Bose-Einstein condensation was demonstrated experimentally using egg white-derived lysozyme, where exposure to 0.4 THz electromagnetic radiation resulted in a local increase of electron density in a long α-helix motif linked to a slight longitudinal compression of the protein helix (Lundholm et al., 2015) The possible explanations that researchers have come up with on how low frequency EMFs act on cells suggest that changes occur in cell membrane pathways or in the ions present. It is also stated these waves damage DNA via the formation of free radicals. The project aims in evaluating the effects that high frequency EMFs have on artificial cell membranes and also mammalian cells. The different bioassays will provide information on the reactions that occur inside the cells, the gene expression of the eukaryotic cell lines will be tested as they will provide evidence if any DNA damage is done on exposure to high frequency EMFs.

2.5.2.1. Human skin – the first point of contact with radiation

C is considered to be the largest primary biological target for THz radiation, the human cornea is also another target that has gathered considerable attention in regard to THz radiation (Wilmink and Grundt, 2011).The skin is the body's most extensive organ as it acts as the first line of defence protecting the organism from potential microbial assault, excessive loss of water and toxic agents (Lemfack et al., 2016, Grice and Segre, 2011, Chiller et al., 2001). The skin is in permanent contact with the outside environment hence heavily colonised by a diverse range of microorganisms, collectively referred to as the skin microbiota, which includes bacteria, fungi and viruses (Grice and Segre, 2011, Lemfack et al., 2016). The skin also acts as an eco-system with its abundance folds, topographically specialized niches and invaginations (Grice and Segre, 2011, Grice et al., 2009), harbouring the growth of commensal bacteria which provides protection to the host from pathogenic bacteria (Chiller et al., 2001) hence the skin microbiota is mainly responsible in health and disease (Lemfack et al., 2016). Bacteria out of the other entities are generally dominant based on the gene expression (16S rRNA) analysis (Lemfack et al., 2016). The results indicate that there are approximately 1000 species of bacteria residing on the human skin (Lemfack et al., 2016, Grice and Segre, 2011, Grice et al., 2009).

The function of the skin microbiome is being studied in great deal over the past few decades in order to gain an insight on the microbial involvement in skin disorders and to develop therapeutic approaches in humans (Grice and Segre, 2011, Lemfack et al., 2016, Cogen et al., 2008). A wide range of the skin niches are occupied by symbiotic microorganisms that provide protection to harmful or pathogenic organisms (Grice and Segre, 2011). A few ways that this is done includes the production of toxic metabolites, depletion of essential nutrients, inhibition of translocation and breakdown of toxins (Chiller et al., 2001). These microorganisms may also play an important role in educating the vast number of T cells present in the skin, preparing them to respond accordingly to marked pathogenic cells (Grice and Segre, 2011). Commensals release species-specific antibiotic substances called bacteriocins, bacteriocins have the ability to inhibit other virulent organisms (Chiller et al., 2001). Colonizing bacteria can also induce the host to increase antibody production while stimulating phagocytosis and cytokine production which helps to clear pathogens (Chiller et al., 2001).

Characterizing the microbiota can advance the understanding of the vital balance that exists between the host and the microorganism (Grice and Segre, 2011). Disrupting the balance on

any one side of the equation leads to skin infections or disorders (Grice and Segre, 2011). Antibiotic exposure, life style changes, modified hygienic practices, host genotype and host physiology may alter the skin microbiome leading to disturbances in the balance (Grice and Segre, 2011, Grice et al., 2009). Genomic approaches have revealed a greater diversity of bacterial species than culture based methods (Grice and Segre, 2011). In a study conducted to characterize the presence of different bacterial species, 16S ribosomal RNA gene sequences were obtained from 20 skin sites of humans (Grice et al., 2009). Nineteen bacterial phyla were detected whereas the highest number of sequences were assigned to four phyla (Grice et al., 2009, Grice and Segre, 2011, Lemfack et al., 2016).

Basal cell carcinoma (BCC) is the most common form of skin cancer worldwide especially in white populations, cases of over one million per annum were reported in the US by the American Cancer Society in 2001 (Woodward et al., 2002) thereby developing techniques that are able to differentiate between cancerous and normal tissue is crucial (Wallace et al., 2006, Woodward et al., 2002).

To date, the various studies conducted have concluded that the EMF effects in the RF range may not enhance or decrease the damage induced by genotoxic agents as the currently available data is not sufficient in providing a final conclusion (Vijayalaxmi et al., 2014).

2.6. Current approaches used to achieve cell permeabilization

Experiments conducted in unveiling the human genome has opened up new fields of genomics, proteomics and transcriptomics (Towhidi et al., 2016, Duscher et al., 2016, Stegle et al., 2015, Taher et al., 2015, Wes et al., 2016). Gene therapy was introduced in the 1990s in the field of erectile dysfunction (ED) with different therapeutic genes (Song et al., 2015). Research on these fields have provided an insight to understanding the pathogenicity of diseases, nowadays increasingly defined by gene networks and gene signatures (Duscher et al., 2016, Stegle et al., 2015, Taher et al., 2015, Wes et al., 2016). Gene networks consist of many hundreds of genes that are interconnected. The manipulation of these genes via inhibition or activation is necessary in understanding these complex interactions. Since the cell membrane is impermeable to DNA and RNA (Dorsett and Tuschl, 2004, Wu et al., 2002, Xiang and Chen, 2000) and in order to overcome this barrier, various transfection methods such as viral transduction, lipofection and electroporation have been employed (Ramamoorth and Narvekar, 2015, Silva et al., 2015). Viral transduction is when the molecule to be transferred is encapsulated in viral vectors; viral vectors used are adenovirus or lentivirus (Silva et al., 2015, Ramamoorth and Narvekar, 2015, Peng et al., 2012). Viral vectors have safety concerns connected with toxicity, immunogenicity and oncogenesis (Zu et al., 2015). Lipofection is a lipid-mediated method, a liposome is incorporated with the desired product and it will merge easily with the cell membrane in delivering the product (Silva et al., 2015, Ramamoorth and Narvekar, 2015). Sonoporation is another technique used in delivering genes and drugs into cells (Yu and Xu, 2014, Wells et al., 2010, Delalande et al., 2013). Few examples of the different technique used in gene transfer include microinjection, impalefection, biolistic gene transfer, magnetofection, hydroporation, photoporation (Das et al., 2015).

2.6.1. Electroporation

Electroporation also known, as electropermeabilization, is powerful yet a simple technique that has been used in breaching the cell membrane barrier (Geng and Lu, 2013, Towhidi et al., 2016) which results in increasing cell membrane permeability (Hansen et al., 2015). Electroporation can be applied to release nucleic acids, intracellular proteins and other metabolites out of the cell for analysis purposes (Geng and Lu, 2013). On another aspect, electroporation is used in delivering drugs, genes and nanoparticles into a cell for cellular manipulation or therapeutic purposes (chemotherapeutic drugs for cancer treatment) (Geng and Lu, 2013, Hansen et al., 2015, Romeo et al., 2018). Over the past years, electroporation has been a successful technique in introducing DNA into drosophila, zebrafish, insects and chicken embryos (Peng et al., 2012).

The mechanism behind electroporation is the increase in transmembrane potential (TMP) of a cell above 0.2 – 1 V (Geng and Lu, 2013), irrespective of the cell type leading to reversible pore formation, these electro-pores allow DNA or large molecules to enter the cell (Garcia et al., 2014, Towhidi et al., 2016, Hansen et al., 2015, Joergensen et al., 2011, Zu et al., 2015, Geng and Lu, 2013) by the application of external pulsed electric fields (PEFs) (Romeo et al., 2018). The method uses pulsed electric field to cause permeability of cell membranes (Geng and Lu, 2013). The application of an external pulsed electric field (PEF) of adequate strength and duration helps to obtain the threshold (Garcia et al., 2014). Therapies based on electroporation involved placing electrodes around or within a target tissue while delivering a series of 8 – 100 short (~ 100 μs) electric pulses of high voltage (~1000-3000 V) (Garcia et al., 2014). In the presence of optimised pulse parameters, the membrane can return to its intact state once after pulse withdrawal (Bonetta, 2005, Towhidi et al., 2016, Geng and Lu, 2013). Optimal electroporation conditions also depend on the cell type and the molecule being transfected (Joergensen et al., 2011). Conventional electroporation uses electrodes fabricated out of graphite, aluminum and stainless steel, in the case of bacterial electroporation; the electrodes are separated by 1, 2 or 4 mm (Geng and Lu, 2013, Garcia et al., 2016). High voltage pulses are normally generated using a pulse generator that has a special capacitor discharge equipment (Geng and Lu, 2013). The cells are first detached from the substrate in conventional electroporation and then exposed to electric pulses in a suspension containing desired extra cellular molecules (Towhidi et al., 2016). Drawbacks of this method are mainly because the cells in suspension can have negative effect on normal cellular functions and cell viability (Zu et al., 2015). Since the cells are floating in suspension, there is no control over the area of electroporation (Towhidi et al., 2016).

2.6.2. Sonoporation

Sonoporation is a technique that increases cell membrane permeability by exposure to ultrasound leading to the formation of transient pores, which facilitates the transport of substances such as DNA and other molecules (peptides and proteins) (Sadiq et al., 2015, Yu and Xu, 2014, Ohta et al., 2008, Lentacker et al., 2014). Ultrasound radiation has a wide range of applications that include imaging, physiotherapy, flow analysis, kidney stone shattering, tumour and fibroid ablation (Schroeder et al., 2009). The frequencies used are greater than 20 KHz hence termed as ultrasonic (Sheikh et al., 2011, Koneru et al., 2012). Ultrasonic waves are generated using piezoelectric crystal transducer made up of barium titanate or lead-zirconate-titanium (Sheikh et al., 2011). The production of a wave occurs in response to an electrical stimulus or impulse in the piezoelectric crystal, with the conversion of electric energy into vibrational or mechanical energy (Sheikh et al., 2011). The ultrasound radiation may be pulsed or continuously applied for a period of time (30 s – 5 min) with pore sizes ranging from 1 – 100 micrometres (Sheikh et al., 2011). The transient membrane alteration leaves the compound trapped inside (Deepik et al., 2014).

The difference between electroporation and sonoporation is that the cells are being exposed to ultrasonic sound waves instead of electric pulses (Sadiq et al., 2015). Sonoporation is used in gene transduction along with microbubbles in the presence of ultrasound (Ohta et al., 2008). In general, cavitation in tissues are created by high ultrasound intensities in the absence of microbubbles, this leads to mechanical damage of tissues due to the temperature increase (Ohta et al., 2008, Das et al., 2015). Cavitation is the formation of gas-filled bubbles in an area being exposed to ultrasound (Das et al., 2015). However, the microbubble present in solution can help reduce the required ultrasound intensity necessary to generate cavitation upon ultrasound exposure in target cells (Ohta et al., 2008). Ultrasound, as a non-invasive technique has the capability of encouraging the drug or gene transfer into the cell with the possibility of limiting is effect onto a desired area in a desired time period (Yu and Xu, 2014). Advantages of sonoporation is that the technique can be used on any cell type including fungi, bacteria, mammalian a(Deepik et al., 2014) and plant cells (Das et al., 2015). There is no physical contact involved since it is a non- invasive method and it does not require any ion free media hence sonoporation can be applied human fluid or cells growing in natural media (Das et al., 2015). A drawback on the technique is that efficiency of transfection *in vitro* and *in vivo* conditions were found to be low (Das et al., 2015).

2.6.3. Photoporation (Laser irradiation)

Lasers have the ability to efficiently introduce foreign DNA into cells in culture (Das et al., 2015). The change in cell membrane permeability occurs upon laser irradiation resulting in the formation of pores at the site of contact (Das et al., 2015). The method of how the cell membrane opens up temporary due to exposed wavelengths is not known but it is suggested that this can occur due to various effects including heating, photochemical effects, absorption or the creation of ROS (Das et al., 2015). A favourable aspect in laser irradiation is that the poration of an individual cell or a group of cells can be viewed under the microscope, using the same objective for laser delivery and imaging (Das et al., 2015). A drawback on this method is the relatively low transfection rate and high impulses on cells can cause cell death (Das et al., 2015).

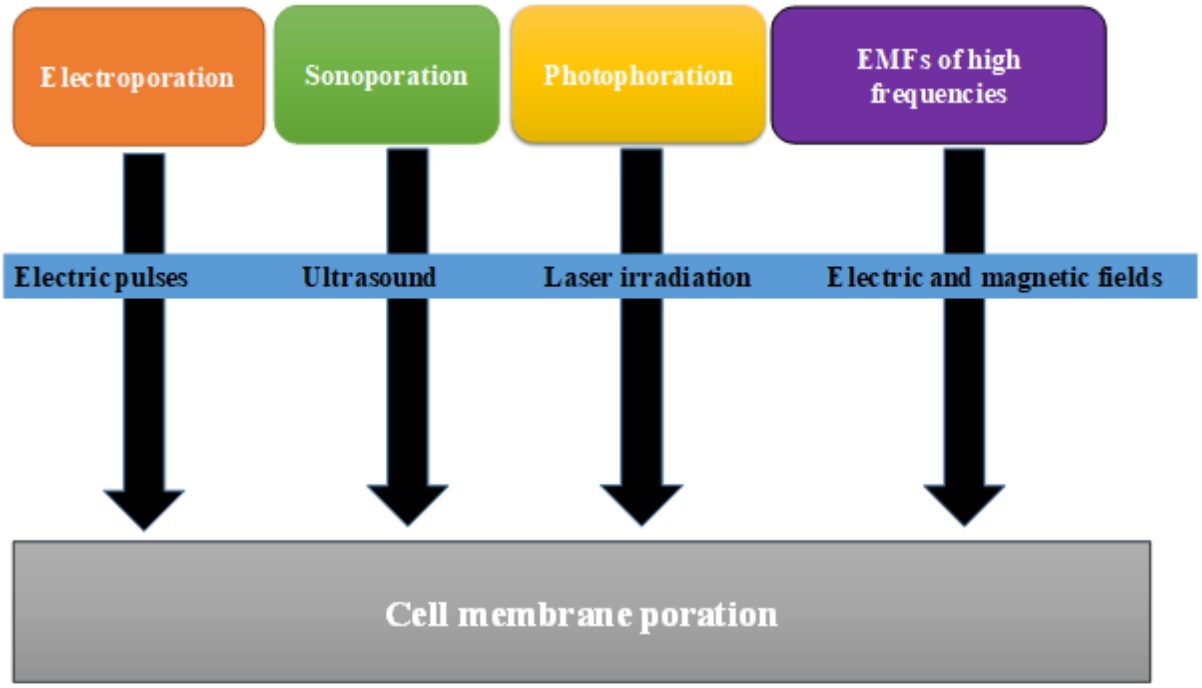

Figure 2. 3. Current techniques used for cell membrane poration in delivering drugs and genes. Electroporation, sonoporation, photoporation and EMFs cause poration of cell membranes using different mechanisms. Electric pulses, ultrasound, lasers, electric, and magnetic fields are causing cell membrane alterations.

2.7. Giant Unilamellar Vesicles

Recent advances in biotechnology, medicine and chemical engineering have led to the discovery of highly potent drug delivery systems (Yu and Xu, 2014, Safari and Zarnegar, 2014, Lewandowska-Lancucka et al., 2016, Mozaferi, 2005, Grull and Langereis, 2012, Çağdaş et al., 2014). Active drug compounds were known as the only treatment for diabetes, cardiac problems, cancer, asthma, osteoporosis and other diseases (Langer and Peppas, 2003, Heller, 2005). Much attention in the past decade was on the materials and the construction strategies of drug delivery and gene therapy (Yu and Xu, 2014)using solvent-activated formulations and diffusion controlled drug delivery systems (Liechty et al., 2010). Polymers, hydrogels, liposomes, proteins and nanoparticles are examples of biomaterials that act as vectors in drug delivery systems (Liechty et al., 2010, Langer and Peppas, 2003, Yu and Xu, 2014, Safari and Zarnegar, 2014, Pattni et al., 2015).

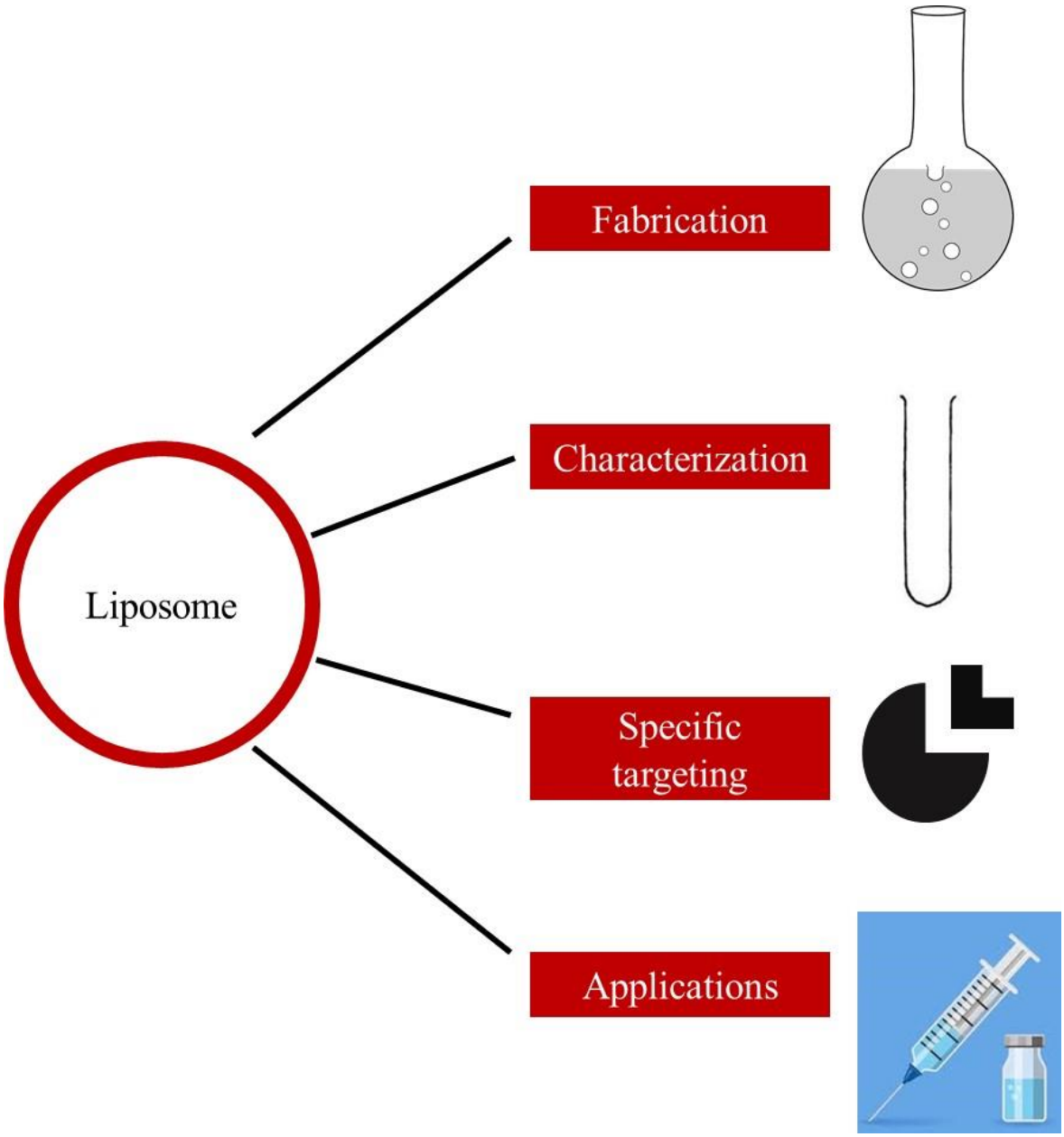

Figure 2. 4. **Critical components of a drug delivery system.** A delivery system has to be efficient when delivering drugs to a specific site not forgetting that the release of a drug depends on a certain stimuli (trigger based).

An efficient drug delivery system must address target specificity, biocompatibility, intracellular transport, drug stability while being responsive to physiological environments and providing accurate feedback control (Liechty et al., 2010, Li et al., 2016, Bunker et al., 2016). Another important aspect is the need of a stimuli-responsive delivery system capable of releasing the encapsulated gene or drug upon arrival at the target site (Yu and Xu, 2014, Safari and Zarnegar, 2014, Bunker et al., 2016).

Liposomal drug delivery has become a promising tool due to its various advantages (Lewandowska-Lancucka et al., 2016, Mozaferi, 2005, Schroeder et al., 2009, Huang, 2008). These include improved solubility of encapsulated drugs, prevention of biological and chemical degradation under storage conditions of various agents, reduced toxicity and the non-specific side effects of the encapsulated drug and increased compatibility with nontoxic and biodegradable material (Pattni et al., 2015, Paini et al., 2015, Bunker et al., 2016, Mozaferi, 2005). Another important feature of liposomes is the feasibility to visualise them under normal conditions Liposomes once formed can be observed under bright field illumination is the or phase contrast however the membranes can be visualised best under dark field illumination (Mueller and Chien, 1983).

2.7.1. Composition of liposomes

Liposomes can function well as they are composed of phospholipids that self enclose in forming spherical lipid bilayers with and aqueous core within the bilayers (Pattni et al., 2015, Paini et al., 2015, Kubiak et al., 2011, Weinberger et al., 2013). The polar heads of the phospholipids favour aqueous environments whereas the hydrophobic tails self-organise in a desirable manner. Due to the presence of a hydrophilic core and hydrophobic bi layer, liposomes can incorporate molecules that are hydrophilic as well as lipophilic (Pattni et al., 2015, Paini et al., 2015, Alavi et al., 2017). Liposomes can be made up of phospholipids that occur naturally or synthetic phospholipids including phosphatidylethanolamine (PE), phophatidylcholine (PC), phosphatidylglycerol and phosphatidylserine (Pattni et al., 2015, Alavi et al., 2017). Liposomes have been constructed using bovine brain lipid extracts, purified egg-lecithin, azolectin, synthetic dipalmitoyllecithin (DPL), mixtures of these, in the presence of tocopherol and cholesterol (Mueller and Chien, 1983). The size of the liposomes can range from 20 nm to 100 micrometres (Kuribayashi et al., 2006, Hishida et al., 2018) with a membrane thickness of 4 – 6 nm (Sabin et al., 2006) or 10 nm in GUVS (Kuribayashi et al., 2006).

2.7.2. Techniques of liposome preparation

2.7.2.1. Gentle lipid film hydration

The conventional lipid film hydration method involves spontaneous swelling of dried lipid films in various aqueous solutions (Kuribayashi et al., 2006) originally developed by Reeves and Dowben (Walde et al., 2010, Bagatolli et al., 2000). Lipids (dry) will be deposited on a solid surface and hydrated using an aqueous solution (Walde et al., 2010). The hydration of the lipid bilayer has to be carried out in the liquid-disordered state at a temperature above the main phase transition temperature of the lipids ($T_{m)}$ which corresponds to the solid-ordered (S_o)/ liquid-disordered (I_d) or the gel/liquid-crystalline phase (Walde et al., 2010). The lipid mixture will be dried completely using nitrogen gas, to which the aqueous solution will be added gently (Mueller and Chien, 1983).

Recent AFM studies have found a correlation existing between the physical state of the lipid bilayer and the ability to generate giant vesicles: successful formation of giant vesicles were observed when smooth, flat layers in the liquid-disordered phase was hydrated whereas the hydration of solid-ordered phase lipids did not lead to the formation of giant vesicles (Hishida et al., 2018). The study used DOPC (disordered liquid crystalline phase) and DPPC (ordered gel-phase) for the synthesis of GUVs at room temperature (Hishida et al., 2018). Similar morphologies of GUVs were observed even in dry films, whereas the differences in morphology originated due to the phase of the phospholipid (Hishida et al., 2018).

2.7.2.2. Electroformation

Electroformation is a well-known energy driven method used in the formation of GUVs (Micheletto et al., 2016) developed by (Angelova and Dimitrov, 1988). In the process of electroformation an alternating electric field is applied onto a hydrated lipid stack which will induce oscillating motion of the entire lipid stack as a result of the electro-osmotic behaviour of the aqueous medium (Micheletto et al., 2016). Due to this, a decrease in both the surface and line tensions of the swollen lipid bilayers increases the bilayer separation and bending (Micheletto et al., 2016) which will give rise to GUVs with a relatively narrow distribution (Kuribayashi et al., 2006). The formation of GUVs using electroformation possess certain advantages over the spontaneous method, which includes higher yields of giant vesicles, higher unilamellarity and less membrane defects (Micheletto et al., 2016).

2.7.2.3. Rapid solvent exchange method

The technique based on organic solvent, the Rapid Solvent Exchange (RSE) method is designed specifically to form homogenous suspensions by instant precipitation of a lipid mixture present in an aqueous buffer (Buboltz and Feigenson, 1999, Bagatolli et al., 2000). This involves rapidly exchanging lipids between two environments, an organic solvent to an aqueous environment (Buboltz and Feigenson, 1999). New membrane structures will be formed in water without the lipid mixture being passed through an intermediary solid state (Buboltz and Feigenson, 1999). Suspensions consisting of phospholipid and cholesterol have proven to be free of crystal artifactual when constructed using the rapid solvent exchange method (Buboltz and Feigenson, 1999).

In summary the preparation of liposomes factors including the ionic strength, lipid composition, pH, substrate used in drying the lipid film and the addition of sugars and their molarity seem to be critical in obtaining giant vesicles (Bagatolli et al., 2000). Given the conditions, there is no one or unique conditions in preparing giant vesicles. There are instances where the vesicles were successfully prepared at low ionic strength (less than 10 mM) (Mueller and Chien, 1983).As a general rule, the most important conditions required in constructing GUVs include: (i) the temperature at which the vesicles are being prepared must be greater than the phase transition temperature of the lipids being synthesised to form GUVs (Bagatolli et al., 2000). This condition also influences the lamellarity (small unilamellar, large unilamellar and multilamellar) of the vesicles performed. (ii) Agitation during vesicle formation should be prevented in order to form large structures (Bagatolli et al., 2000). However, given the possible mechanisms and proposed models, the exact mechanism of GUV formation is not known (Bagatolli et al., 2000). (Angelova and Dimitrov, 1988) pointed that vesicle formation requires separation of the layers and bending. In the initial stage of vesicle formation, the normal forces that cause repulsion between the lipid layers, the tangential forces that help bend the lipid layers are crucial in lipid formation (Bagatolli et al., 2000). (Angelova and Dimitrov, 1988) suggested that the influence of external electric fields act strongly on the normal forces and that the electric fields can prevent or induce vesicle formation. Electroosmotic fields come into play in the presence of alternating current (Bagatolli et al., 2000). The electric field will induce a mechanical stress on the bilayer which will generate rupture of the bilayers leading to formation of different sized pieces and these pieces are able to bend and form thin-walled liposomes.

2.7.3. Characterisation of liposomes

2.7.3.1. Size and Lamellarity

Different techniques involved in liposome production leads to liposomes with different lamellarity and sizes. (Table 1.6.3.1.). The size of the liposomes constructed are measured using various techniques including size exclusion chromatography (SEC), dynamic light scattering (DLS), nuclear magnetic resonance (NMR) and other microscopic techniques include atomic force microscopy (AFM), transmission electron microscopy (TEM) and cryogenic-TEM (Pattni et al., 2015).

Table 4. Liposomal lamellarity and sizes. Different liposomal preparation methods yield liposomes in different sizes and lamellarity as listed in the table.

Lamellarity	Size	References
Small unilamellar vesicles (SUV)	20 – 100 nm	(Alavi et al., 2017, Buboltz and Feigenson, 1999)
Large unilamellar vesicles (LUV)	➢ 100 nm	(Alavi et al., 2017, Mozafari, 2005)
Giant unilamellar vesicles (GUV)	➢ 1000 nm	(Dimova et al., 2006, Alavi et al., 2017, Rodriguez et al., 2005)
Oligolamellar vesicles (OLV)	➢ 100 – 1000 nm	(Kuribayashi et al., 2006)
Multilamellar vesicles (MLV)	➢ 500 nm	(Alavi et al., 2017, Mozafari, 2005)

2.7.3.2. Encapsulation Efficiency (EE)

EE of liposomes is measured by unloading the drug from the liposome by replacing the media with an aqueous media containing an organic phase (ethanol, methanol, acetonitrile and Triton X -100) (Pattni et al., 2015, Edwards and Baeumner, 2006, Ong et al., 2016). Removal of the drug from the formulation is carried out using dialysis, ultracentrifugation and dialysis (Pattni et al., 2015). The concentration of the loaded media is then estimated using several techniques including fluorescence and or UV spectroscopy, gel electrophoresis, protein or enzyme-based assays (Pattni et al., 2015). Other techniques that measure EE require the use of instruments such as ultra-performance liquid chromatography (UPLC), high performance liquid chromatography (HPLC), liquid chromatography-mass spectrometry (LC -MS) (Edwards and Baeumner, 2006). EE of the liposomes vary depending on the size, in a study conducted by (Ong et al., 2016) revealed that size of liposomes affected the extent of the bioavailability of the drug. Also the amount of drug encapsulated possess a significant impact on the systematic absorption, larger amount led to increased oral bioavailability (Ong et al., 2016).

2.7.4. Permeability of GUVs

The ease of observing GUVs using optical microscopy and its membrane dynamics with lipid packing arrangements helps in understanding the bio-nano interface which can be employed in nanotechnology, medicinal applications in treatment and diagnosis of diseases (Fixler et al., 2018). GUVs possess the ability to respond to various external stimuli including light, magnetic fields with alternating frequencies and ultrasound radiation (Pattni et al., 2015, Nappini et al., 2011, Podaru et al., 2014, Silverstein and Williamson, 2019).

2.7.4.1. Magnetic Field Induced Permeability

GUVs, the standard model used so far in permeabilization studies was used by (Nappini et al., 2011) to investigate its response in the presence of magnetic fields. For this study, GUVs were loaded with a fluorescent dye and core/shell cobalt ferrite nanoparticles that have been coated with rhodamine B isothiocyanate were prepared and adsorbed onto the membrane of the GUVs (Nappini et al., 2011). Confocal Laser Scanning Microscopy (CLSM) revealed that in the presence of low frequency alternating magnetic fields (LF-AMF) led to the release of fluorescent dye which was induced by magnetic nanoparticle energy along with mechanical vibrations that perturbed the GUV membrane while keeping its rigidity (Nappini et al., 2011).

2.7.4.2. Ultrasound Induced Permeability

In the recent years, the use of liposomes to entrap drugs and gas for ultrasound controlled drug release and enhanced ultrasound controlled drug delivery have increased.(Huang, 2008),. Presently, significant applications of liposomal ultrasound based drug and gene delivery *in vivo* conditions are seen in cardiac disease, tumour and stroke therapy (Huang, 2008). As mentioned enhanced permeability as well as uptake in liposomes is crucial in understanding how these membrane like structures function.

Previous studies have been conducted where ultrasound waves have been used to trigger the release of drugs from liposomes that are nano sterically stabilized (nSSL)(Schroeder et al., 2009, Grull and Langereis, 2012). Pre-clinical trials have demonstrated that Magnetic Resonance Imaging (MRI) combined with high intensity focused ultrasound (HIFS) is capable of establishing hyperthermia (40 – 45 ºC) enhancing the drug release of temperature sensitive liposomes (TSLs) in tumour tissues over time (Grull and Langereis, 2012).(Schroeder et al., 2007) utilized low frequency ultrasound (LFUS) to release drugs encapsulated inside liposomes with three different liposomal formulations with similar lipid bilayer compositions ranging around 100 nm. Cisplatin, doxorubicin, and methylprednisolone hemi succinate were the drugs

used and all three formulations were exposed to LFUS for less than 3 min, interestingly 80% of drug release was seen in all the formulations (Schroeder et al., 2007). Furthermore, no differences were observed in liposome size distribution, chemical properties of the liposomes or the drugs released in response to LFUS (Schroeder et al., 2007). In a similar study conducted by (Schroeder et al., 2009) nSSL were loaded with an anti-cancer chemotherapeutic agent cisplatin was administered intraperitoneally to mice with well-developed murine lymphoma tumors in peritoneal cavity. LFUS was applied to the abdominal wall externally for 120 s, following the exposure the release of the drug was monitored and quantified (Schroeder et al., 2009). The results revealed that nearly 70% of the liposomes loaded with cisplatin released it in tumors that were exposed to LFUS whereas less than 3% released their cargo in the absence of LFUS (Schroeder et al., 2009).

The findings suggest that LFUS radiation helps to achieve increased membrane permeability in liposomes, hence it is important to investigate the permeability of liposomes at 18 GHz.

Apart from cell membrane like lipid structures, permeability of eukaryotic cell lines in response to EMFs of 18 GHz and synchrotron sourced THz radiation was studied using Pheochromocytoma cells.

2.8. Pheochromocytoma (PC 12) cells

2.8.1. Characteristics of PC 12 cells

Different neuronal cell models have been used for mechanistic studies and for the detection of potential neurotoxicants (Das et al., 2004). Clonal cell lines that can express neuronal properties can be used as a model for studying of the nervous system (Greene and Tischler, 1976b, Westerink and Ewing, 2008a). Pheochromocytoma (PC 12) cell line was isolated from a tumour arising from chromaffin cells of the adrenal medulla of a rat in 1976 by Greene & Tischler (Greene and Tischler, 1976b, Vaudry et al., 2002). PC 12 cells can be used as a valuable model in studying cell signalling, main reasons being that the cell line is able to not respond to a few growth factors, hormones and neurotrophins (Vaudry et al., 2002). Most importantly, PC 12 cells exhibit distinct responses to differentiation, cellular proliferation and survival which can be assessed independently (Vaudry et al., 2002). PC 12 cell line has been used widely to study the neuroprotective effects from drugs and for components present in TCM with MPP^+ or models injured due to H_2O_2 (Zhang et al., 2018). PC 12 cells are referred to as having neuron like properties due to their ability to respond to nerve growth factor (NGF) by differentiating into sympathetic ganglion neurons (Das et al., 2004) and they can be sub cultured indefinitely (Westerink and Ewing, 2008a). Upon treatment with NGF, PC 12 cells cease proliferation, initiate the process of differentiation by extending neurites while becoming electrically excitable (Das et al., 2004). Most studies that address the mechanism of PC 12 cell differentiation in response to NGF, monitors its effect in an exponentially growing cell population (Rudkin et al., 1989) assuming that every cell present in the population responds in an identical manner (Rudkin et al., 1989).

2.8.2. Cell membrane lipid composition

The project focuses on the membrane permeability following EMFs hence the lipid composition of the cell lines being studied is important. Membrane fatty acid compositions, cholesterol contents and phospholipid compositions are generally modified in different kinds of mammalian cells (Spector and Yorek, 1985).Modifications leading to intact mammalian cell membranes can cause changes to membrane fluidity, cellular functions that includes carrier mediated transport, properties of membrane bound enzymes that bind to opiate and insulin receptors, endocytosis, phagocytosis, depolarization-dependent exocytosis, prostaglandin production, chemotherapeutic cytotoxicity and cell growth (Spector and Yorek, 1985). Lipid composition of PC 12 cells have been studied in the presence and absence of NGF. Acidic and neutral lipid fractions have been isolated by column chromatography and analyzed using high performance thin layer chromatography (HPTLC). In a study conducted by (Ariga et al., 1988) it was found that the total lipid concentration was approximately 220 µg/mg of protein while the concentration of neutral glycolipids was in the range of 1.6 -1.8 µg/ mg of protein for both cells in the presence and absence of NGF. The major component present in the neutral glycolipid fraction accounted for approximately 80% of the total was characterized as a globoside using HPTLC mobility, fast atom bombardment mass spectrometry, carbohydrate analysis and mild acid hydrolysis (Ariga et al., 1988). Major fatty acids of globoside were C16:0, C18:0, C22:0, C24:1 and C24:0 where C18 sphingenine was present in almost all of the long chain bases (Ariga et al., 1988). Various other glycolipids identified includes glucosylceramide (15%), globotriosylceramide (4.5%), lactosylceramide (4%) (Ariga et al., 1988).

2.8.3. PC 12 cell differentiation

2.8.3.1. PC 12 cell attachment on substratum

It has been found that the various factors that can influence PC 12 axonal outgrowth in vivo conditions are chemotactic and, or trophic factors including NGF and various concentrations (Orlowska et al., 2017, Fuji et al., 1982b) contact guidance (Roufa et al., 1983) and the physicochemical interaction of actively differentiating nerve fibers with the different types of substrata encountered through the elongation process (Orlowska et al., 2017, Wandiyanto et al., 2018, Roufa et al., 1983, Fuji et al., 1982b). The physical and chemical properties of the substratum used in PC 12 cell adhesion plays a critical role in determining the growth pattern of neurons by supporting them (Roufa et al., 1983). Cellular growth and differentiation requires the presence of a structured environment that cells can interact (Attiah et al., 2003b). It was suggested by (Harrison, 1910) that the neuronal growth cone tends to select the path that offers least resistance and migrate in spaces or 'groves', this suggestion was further supported by various studies. A study by (Orlowska et al., 2017) investigated the effect of five types of coating including Laminin (Lam), poly-l-lysine (PLL), fibronectin (Fn) and combinations of these coatings on PC 12 attachment and differentiation. The results revealed that over a period of five days, increased attachment of PC 12 cells were observed on substrata containing Lam and combinations of PLL/ Fn (Orlowska et al., 2017). The results displayed various extents of neurite outgrowth on the different substrata tested, substrata possessing dual coatings (PLL/Lam and PLL/Fn) exhibited the highest extension of neurites (Orlowska et al., 2017). A study by (Wandiyanto et al., 2018) reported that bactericidal nanostructured surfaces on titanium are able to enhance the attachment of PC 12 cells. In addition, PC 12 cell differentiation was exhibited on the nanostructured titanium whereas the non-structured surface did not support PC 12 cell adhesion or differentiation (Wandiyanto et al., 2018).

Table 5. Various proteins used in PC 12 cell neuronal differentiation. Fibronectin, Laminin, Poly-L-lysine, Collagen and Albumin have shown to enhance cell attachment and differentiation.

Protein coating	NGF concentration (ng/mL)	Differentiation period	Marker assessed	References
Poly-L-lysine	100	3 - 4 days	Assessing intermittent hypoxia (IH) effects on PC 12 proliferation and differentiation	(Chen et al., 2014b)
	50	Assessed for pit formation 60 min after treatment with NGF	Changes in surface morphology and coated pit formation of PC 12 cells in response to NGF	(Connolly et al., 1984a)
	50	8 days	Role of miR-200 in regulation neuronal proliferation and differentiation	(Pandey et al., 2015a)
	50 (EGF & bFGF)	Assessed every 6 hours under continuous stimulation for 3 ays	Investigation the underlying mechanisms of the timing dependent requirement for NGF for cell differentiation	(Chung et al., 2010)
Poly-D-lysine	100	7 days	Analyse the morphological changes in neurite growth and altered protein expression of GAP-43 and MAP2 in the presence of senegenin	(Jesky and Chen, 2016b)
Fibronectin	20 (bFGF)	5 days	Manipulation of focal adhesion of neural stem cells	(Yang et al., 2013)
Fibronectin Laminin Poly-L-lysine Albumin conA	20	5 - 7 days	Determining the effect of Glyscosaminoglycans on PC 12. Adhesion and neurite formation	(Akeson and Warren, 1986a)
Collagen (Type I rat tail)			Gene expression pattern in PC 12 cells with reduced PMCA2 and PMCA3	(Boczek et al., 2012b)
Collagen	50	5 days	Detecting differentiation in a mixed population of differentiating and proliferating cells	(Weber et al., 2013)
Collagen Laminin Entactin	20 (EGF) 40 (FGF)	7 days	Modelling PC 12 differentiation on micro-patterned substrates with neural matrix components	(Garcia-Parra et al., 2012)
Collagen Polyorinithine Poly-L-lysine	50 – 200 (2.5 S)	4 -14 days	To gain an insight of to PC 12 receptors and ion channels	(Shafer and Atchison, 1991b)
	50	90 min after stimulation	Importance of MAP kinase cascade for PC 12 differentiation	(Traverse et al., 1992)

50	14 days	Effect of chit oligosaccharide on PC 12 differentiation	(Yang et al., 2009)
50	3 days	Determining if ribosomal protein genes can act as a reference gene for neuronal differentiation	(Zhou et al., 2010)
100	1-3 days	Neurite length, neurite alignment and straightness	(Tonazzini et al., 2013)

2.8.3.1. PC 12 cell response to NGF

Given the current assumption that all PC 12 cells in a population respond to NGF in a similar manner (Rudkin et al., 1989), it was found that the majority of the population is multiplying while only a minority of the cells start extending neurites in the first days of NGF exposure (Greene and Tischler, 1976b, Greene, 1978). Hence it was suggested that PC 12 cells do not respond in an identical manner but on the contrary the response appears to be differential (Rudkin et al., 1989), depending on the status of cell and the parameter being investigated. In a study conducted revealed that the addition of NGF alone to serum free PC 12 cells does not cause a detectable increase in the cell number but stimulates neurite outgrowth at a rapid rate than when added to cultures that are growing exponentially in full serum medium(Greene, 1978).. In an attempt to exploit a system in order to elucidate the mechanism of NGF action, a set of experiments were designed by (Rudkin et al., 1989) to test the possibility that if serum starvation resulted in cell synchronization and to illustrate the cellular response to serum and NGF using selected markers that involve proliferation (DNA synthesis, cell number) and differentiation (neurite extension, appearance of the binding sites of saxitoxin, down regulation of the epidermal growth factor (EGF) receptor). Long term differentiation (more than 14 days) of PC 12 cells by the addition of NGF has displayed an increase in electrical excitability, which is presumably due to an increase in the amount of voltage-sensitive Na^+ channels as measured by saxitoxin binding (Rudkin et al., 1989).The findings revealed that serum starvation led to the accumulation of cells in the G_1 phase of the cell cycle and NGF action on the cells accumulated in the G_1 phase was more robust in comparison to an exponentially growing culture of cells, where only a certain number of cells were in the G_1 phase (Rudkin et al., 1989). In light of these findings, it can be stated that PC 12 cells respond to NGF in a cell cycle-specific manner (Rudkin et al., 1989). In the study conducted by (Orlowska et al., 2017), different concentrations of NGF (0,25,50 and 100 ng/mL) were added to low serum medium and the results showed that enhanced neurite extension was in the presence of a NGF concentration of 50 ng/mL confirming that PC 12 cells respond differently to various concentrations of NGF. The study by (Orlowska et al., 2017) supports the findings by (Rudkin et al., 1989) confirming that the differentiation of PC 12 cells into neuron like structures was accompanied by an arrest of the PC 12 cells in the post-mitotic G0 stage of the cell cycle, the cell proliferation was assessed using MTS assay. PC 12 cell response to NGF following EMF exposures was investigated in the current study.

2.8.3.2. Expression of proteins related to PC 12 differentiation

The extent of PC 12 differentiation is assessed using quantitative or semiquantitative morphological methods which includes, determination of the cell size, no of cells displaying neurite processes and the neurite length (Das et al., 2004, Orlowska et al., 2017). Expression of specific proteins during the process of differentiation can be used as a marker for neurochemical measurement (Das et al., 2004). Neurotypic proteins that have been associated with PC 12 differentiation and axonal elongation including the growth associated protein 43 (GAP- 43), synapsin and synaptophysin are presynaptic membrane associated proteins (Das et al., 2004). PC 12 differentiation in response to NGF is induced via its actions at the receptor tyrosine kinase (RTK), TrkA (Chao and Hempstead, 1995) which will then initiate several signalling cascades (Vaudry et al., 2002, Greene and Tischler, 1976b) that includes the Raf/MEK/MAPK (mitogen-activated protein kinase) pathway and also the PLCλ/PKC pathway (Das et al., 2004). The contradictory finding that *ras* and *src* oncogene products improved rather than blocking NGF induced differentiation led to the identification of signalling pathways that involve both Ras and Src as a part of the signalling cascade that responds to NGF (Vaudry et al., 2002). The responses of both NGF and the epidermal growth factor (EGF), require extra cellular regulated kinases (ERK) and MAPK. I In addition, the neurotransmitter, pituitary adenylate cyclase-activating polypeptide (PACAP) stimulates neurite outgrowth through ERK activation in a process that is comparable to but distinct from NGF signalling (Vaudry et al., 2002). The very different outcomes due to EGF and NGF stimulation could arise from the duration of signalling through ERKs (Vaudry et al., 2002). Rapid and transient Ras- and Rap1- dependent ERK phosphorylation is induced in response to EGF stimulation whereas NGF stimulation of ERK is both rapid and continuous, with sustained activation that is dependent on signalling to ERK via Rap1 (Vaudry et al., 2002).

The expression of GAP 43, an endogenous substrate for PKC is stimulated in the presence of NGF in PC 12 cells, and the up regulation of GAP – 43 mRNA and the GAP-43 protein is linked with the PC 12 cells differentiating into neuronal like cells (Das et al., 2004). Localisation of synaptophysin and synapsin will occur in the presynaptic membrane regulating the synaptic vesicle fusion and release of neurotransmitters (Das et al., 2004). Thereby actively differentiating PC 12 cells will exhibit an increase of these proteins in culture. A study by (Das et al., 2004) assessed the expression of GAP -43 and synapsin I in differentiating PC 12 cells. It was found that the expression of GAP – 43 was low on day 0 and increased to maximum levels on day 05 whereas the expression of synapsin I increased relatively slowly on days 0 – 4 and rapidly on days 5 – 7 (Das et al., 2004).

2.9. Bacillus subtilis spores

Bacterial endospores are considered to be the most resilient form of life on earth given the fundamental resistance to extreme environments and antimicrobial treatments (Berendsen et al., 2016, Errington, 2003). Spore formation in *B. subtilis* is initiated when vegetative cells are exposed to harsh environmental conditions and nutrient deprivation (Yen Shin et al., 2015, Grossman and Losick, 1988, Dittmann et al., 2015, Moeller et al., 2009) leading to a metabolically dormant and close to indestructible cell (Driks, 2002, Kaieda et al., 2013). Spores are highly resistant to a variety of harsh conditions including extreme temperatures, chemicals, UV (Ultra-violet) and ionising radiation because of their unique structure (Rao et al., 2016, Setlow et al., 2016, Dittmann et al., 2015, Moeller et al., 2009). Metabolically dormant spores do not contain little or no high energy compounds like ATP or NADH (Setlow, 2006). In its dormant state, damage done to the DNA or macromolecules cannot be repaired due to their lack of enzyme activity (Setlow, 2006). Repair of DNA damage can occur in process of germination when the spore returns to life resuming metabolic activity, in the case of accumulated damage during dormancy the chances of repair on germination is less leading to the death of germinated spore (Setlow, 2006). However, spores are capable of surviving for many years, there are reports suggesting that spores may even live for million years (Setlow, 2006). Consequently, spores have developed a multitude of mechanisms to protect macromolecules from damage during extended periods of dormancy and these mechanisms that has evolved with time also protect spores from damages that can arise from acute treatments (Setlow, 2006).

As the spore formation initiates, the cell will first create an internal protoplast containing a copy of its own chromosome (Driks, 2002). Afterwards, development will continue as proteins start being synthesized within the protoplast and the surrounding cell cytoplasm will merge into the numerous complex structures that make up the spore (Driks, 2002). These events lead to a metabolically dormant and close to indestructible cell (Driks, 2002). During the process of spore formation, asymmetrical division occurs in a single rod shaped cell which will generate two genetically identical daughter cells with morphologically distinct compartments (Tan and Ramamurthi, 2014, Driks, 2002) consisting of a larger cell which is referred to as a ‘mother cell’ and a smaller ‘forespore’ (Tan and Ramamurthi, 2014, Sharp and Pogliano, 1999). The membranes of the larger mother cell will migrate around engulfing the forespore (Sharp and Pogliano, 1999). Towards the completion of this process the leading edges of the migrating membranes encounter and fuse which will then release the forespore into the large mother cell cytoplasm (Sharp and Pogliano, 1999). Spore forming species have broad biotechnological

applications in gut health promotion (probiotics), fermentation, protection of crops helping to increase the crop yield, foreign carriers for vaccine antigens and also in the production of a range of useful enzymes, chemicals and fuels (Berendsen et al., 2016). However, there are species which are pathogenic, and their spores play a major role in spread of infection, different strains include *Bacillus antharacis, Clostridium botulinium, Clostridium difficile, Clostridium perfringens* and *Clostridium tetani* (Berendsen et al., 2016, Setlow, 2006). In the USA alone, pathogenic forespores are estimated to cause over one million cases of foodborne illness (Berendsen et al., 2016). Furthermore, non-pathogenic bacterial spores are one of the main causes of financial losses to the food industry due to the ability of spores to thrive high temperature processes such as pasteurization, sterilization which leads to reduced shelf life and food spoilage (den Besten et al., 2018).

2.9.1. Structure and composition of spore coat

Resistance of spores can arise from the spore structure and the chemical composition of the spore coats (Setlow, 2006).

The *Bacillus* spore structure consists of a an inner spore core surrounded by an inner forespore membrane, a cortex, outer forespore membrane and an exterior spore coat consisting of different layers and a surface layer or the exosporium (Figure 2.8.1) (Plomp et al., 2005, Setlow, 2006).

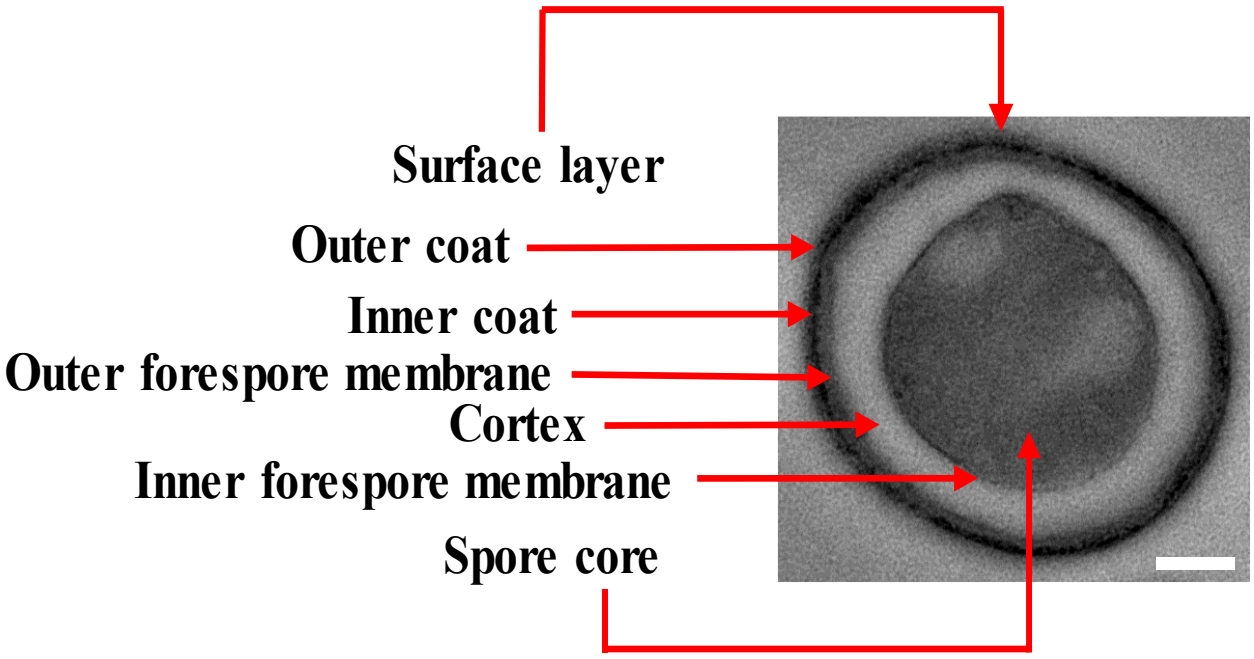

Figure 2.5. Structure of *B. subtilis* spore illustrating the various coats as visualised using Transmission Electron Microscopy. The spore coat consists of several different layers that play essential roles in the process of spore dormancy and germination. Scale bar 200 nm.

The surface layer or exosporium is a bulky loosely fitting structure found mainly in the spores of *Bacillus cereus* group whereas the spores of *B. subtilis* possess an exosporium which is greatly reduced in size (Setlow, 2006) and this layer can be considered as an expanded version of the outermost coat layer consisting of glycoproteins.

The multilayer spore coat is made up of carbohydrates and structural proteins and it plays an important role in the protection and germination of spores (Plomp et al., 2005, Kaieda et al., 2013). The remarkable resistance of the bacterial spore coat with a diameter of ~ 1 μm consisting of approximately 70 different proteins protects it from environmental insults (Wu et al., 2015, Henriques and Moran, 2007, McKenney et al., 2013, Driks, 1999). The function of many individual coat proteins are unknown up to date. Apart from providing resistance to exogenous lytic enzymes that can degrade the cortex and predation by protozoa, the spore coat does not play a major role in resistance against heat, chemicals and radiation (Setlow, 2006). The exact function of the outer fore-spore membrane that lies under the spore coat is unknown, but it has been reported that this structure is essential in the formation of spores.
The spore cortex consisting of a cross-linked thick layer of modified peptidoglycan helps to preserve resistance to heat and maintain dormancy (Yen Shin et al., 2015, Plomp et al., 2005, Setlow, 2006). The cortex is said to maintain a lower water activity in the spore core (Kaieda et al., 2013, Setlow, 2006). The core contains less water than the cortex and the water content of the core is inversely related to the spores heat resistance (Kaieda et al., 2013). However it has not yet been reported how the spore cortex accomplishes the reduction of water content of the spore core (Setlow, 2006). In the process of germination, the cortex starts to degrade which is essential for expansion of the spore core following outgrowth (Setlow, 2006).

The germ cell wall lying under the cortex is also composed of peptidoglycans, with a structure that is similar to peptidoglycan in a vegetative cell. The germ cell wall does not play a role in spore resistance but converts into the cell wall of an outgrowing spore (Setlow, 2006).

The inner fore spore membrane acts as a strong permeability barrier in providing spore resistance to various substances especially those that are capable of crossing the membrane causing damage to spore DNA in comparison to the outer membrane (Setlow, 2006). In the dormant state of the spore, the inner membrane appears compressed but starts to increase in the first minutes of spore germination. Studies have reported that the lipid molecules in the inner membranes are largely immobile from analysis using lipid fluorescence probes, whereas the lipid probes become fully mobile on spore germination (Cowan et al., 2004).

DNA or the genetic material, ribosomes, tRNAs and DPA associated with Calcium ions is present in the spore core surrounded by an inner membrane with low permeability to small solutes, ions and water (Plomp et al., 2005, Kaieda et al., 2013, Setlow, 2006). There are two small molecules present in the spore core that is important in spore resistance. One of the two being water, water comprises close to 70- 80% of the wet weight in a in the protoplast of a growing cell but makes up only 27 -55 % of the wet weight of a spore depending on the species (Setlow, 2006). The quantity of free water that is present in the spore core is extremely low such that the macromolecular movement is significantly restricted (Cowan et al., 2003). The low core water content is considered to be the one of the main factors responsible for the enzymatic dormancy of spores and is important in determining the resistance of spores to wet heat. However, the mechanism in which the reduction of spore core water content occurs during sporulation remains a mystery (Cowan et al., 2003, Setlow, 2006). During the first minutes of spore germination, the spore core starts to take up water rapidly restoring enzymatic activity and macromolecular motion (Setlow, 2003, Cowan et al., 2003). The second core small molecule that is important in providing resistance is pyridine-2,6-dicarboxylic acid (dipicolinic acid, DPA).

DPA located in the core consists of 5-15 % of the dry weight recorded for spores in both species of *Bacillus* and *Clostridium* (Setlow, 2006), DPA is mostly chelated with divalent cations such as Ca^{2+}. Synthesis of DPA occurs in the mother cell compartment of a cell that is sporulating while being taken up into the forespore and afterwards excreted within the first minutes of spore germination and the mechanisms leading to this has not yet been found. The quantity of DPA present in the spore core exceeds its solubility, whether chelated or not, however the exact state that DPA exists in the spore core is not known. Previous findings have reported that the spore core exists as a glass structure, but this hasn't been proved by any means. It has been suggested that the accumulation of DPA in the spore core plays a significant role in the reduction of water content during sporulation and UV photochemistry of spore DNA (Setlow, 2006).

A group of small, acid-soluble spore proteins (SASP) belonging to the α/β - type is said to be important in providing resistance in spores (Moeller et al., 2009). The synthesis of α/β -type SASP occurs only in the developing forespore, prior to DPA uptake (Setlow, 2006). SASPs make up to about 3-6 % of the total spore protein (Setlow, 2006).

In a study conducted by (Dittmann et al., 2015) it was presented that dormant *Bacillus* spores retain a highly ordered crystalline core structure that contains the genetic material, DNA but only in the presence of small acid soluble proteins (SASPs) which are capable of protecting spore DNA (Moeller et al., 2009). The α/β – type SASP are found exclusively in the spore core where they saturate the spore DNA. The binding of SASPs alters the structure and property of DNA dramatically while being important factors in providing spore resistance to UV radiation

and many chemicals (Setlow, 2006). Genomic instability due to long exposures to THz radiation was also reported by (Korenstein-Ilan et al., 2008) in lymphocytes and the authors suggest that THz radiation at a frequency of 0.1 THz is able to excite low-frequency collective vibrational modes of biomolecules (Korenstein-Ilan et al., 2008). However, in the case of spore outgrowth, α/β - type SASP are broken down in the early stages, if not their presence will interfere significantly with development of the spore by blocking of DNA transcription (Setlow, 2006).

2.9.2. Heat resistance

A signature property of bacterial spores is their resistance to heat when suspended in aqueous environments termed as wet heat resistance (Setlow, 2006). Spores in general exhibit resistance to temperatures of 40 °C or higher than growing cells of the same strain. The core water content determines the spore wet heat resistance (Setlow, 2006). Spores of different species of *Bacillus* contain 27–55% of core wet weight in the form of water, the level of core water is inversely proportional to the spore resistance towards wet heat (lower the core water content; higher the resistance) (Setlow, 2006).

The heat load necessary to inactivate microorganisms depends on the degree of heat resistance and the level of reduction required (den Besten et al., 2018). Inactivation of bacterial spores requires higher heat loads as (den Besten et al., 2018)

2.9.3. Radiation resistance

In comparison to growing cells, spores are more resistant to ionizing radiation even though the reasons for elevated spore resistance to ionizing radiation is not yet confirmed (Nicholson et al., 2000). One factor that might be responsible for the elevated resistance to ionising radiation may be the low core water content that probably reduces the ability of ionising radiation to generate hydroxyl radicals that damage the spore (Setlow, 2006). However, to date no systematic study has shown the has proven the relationship between core water content and the degree of ionising radiation. There is also no information on the possible role of α/β – type SASP and DPA in spore resistance to ionizing radiation (Nicholson et al., 2000). Previous research conducted using EMFs in the range of UV light with a wavelength of 254 nm have demonstrated that the spores of *B. subtilis* exhibit a higher degree of resistance (10 to 50 times) in comparison to vegetative cells (Moeller et al., 2009, Nicholson et al., 2000). It was reported that α/β-type SASP play a major role in spore resistance to 254 nm, dry heat, wet heat and oxidizing agents but not SASP-γ (Moeller et al., 2009). In the case of longer wavelengths. The response of spores and growing cells are similar with spores being slightly more resistant than the growing cells. One factor that may be involved in spore UV resistance is

the shielding of UV sensitive spore components such as DNA by pigments located in the outer layer of spores (Nicholson et al., 2005).

Chapter 3. Materials and Methods

3.1. Overview

The chapter focuses on the materials and the methods that was employed in investigating the effects arising from EMFs of 18 GHz and super high frequencies in the range of THz radiation. The different materials used in constructing simple lipid membrane models, eukaryotic and prokaryotic cell lines have been listed in this chapter. Experimental setups, critical parameters of exposure including frequencies, power, temperature and durations of exposure is described in detail.

3.2. Materials

3.2.1. Lipids

The lipids were purchased from Avanti Polar Lipids (Alabaster, AL) in the liquid form, dissolved in chloroform. The lipid solutions were stored at -20°C when not in use. DOPC **(**1,2-dioleoyl-*sn*-glycero-3-phosphocholine) was used with a fluorescent marker 1,2-dioleoyl-sn-glycero-3-phosphoethanolamine-N-(lissamine rhodamine B sulfonyl) (rhodamine-DOPE) in a 0.2 mol % mixture.

3.2.2. Silica nanospheres

Fluorescent silica nanospheres with a diameter of 23.5 ± 0.2 nm (FITC) (Corpuscular, Cold Spring, NY, USA) was used to investigate the membrane permeability of the samples that were exposed to EMF treatment.

3.2.3. PVA-VP (poly(vinyl alcohol)- vinyl pyrrolidone)

The mesoporous hydrogels were synthesised through the free radical polymerisation of linear poly(vinyl alcohol) (PVA) using the cross linker n-vinyl pyrrolidone(VP). High molecular weight 125 kDa (abbreviated as H-PVA) was used in synthesising the gel. Ceric ammonium nitrate (CAN) was used to initiate the chain reaction leading to the formation of more free radicals. Aqueous PVA solution (5 wt. %) was prepared by dissolving PVA in H_2O at 70°C under constant magnetic stirring. The solution was then subsequently cooled down to room temperature. An appropriate weight of n-vinyl pyrrolidone (VP) monomer (0.1 ml) was added into the PVA solution under magnetic stirring at a maintained temperature of 40 °C. Ceric ammonium nitrate (CAN) was added as an initiator (0.8 ml) of the free-radicle polymerization reaction. The entire system was purged continuously with N_2 gas for 3hours to remove the

presence of any oxygen bubbles. The resulting homogenous polymer solutions formed were casted on a glass side (76mm× 26mm× 1mm) for the synthesis of GUVs.

3.2.4. Poly-L-lysine

Sterile-filtered poly-L-lysine (PLL) (molecular weight 150,000–300,000 Da) was purchased from Sigma-Aldrich (Sydney, Australia) and used at the recommended concentration of 0.01% w/v in water. The sterile filtered solution was stored at 4°C until required.

3.2.5. Fibronectin

Fibronectin (Fn) was purchased from Sigma-Aldrich (Sydney, Australia) in lyophilized powder form. An aqueous working solution of 40 μg/mL concentration was prepared and stored at −20 °C until required.

3.2.6. Laminin

Laminin (Lam) derived from a mouse Engelbreth-Holm-Swarm (EHS) sarcoma was purchased from Sigma-Aldrich (Sydney, Australia). An aqueous working solution of 10 μg/mL concentration was prepared and stored at −20 °C until required.

3.2.7. Cultivation of *Bacillus subtilis and* spore sample preparation

Bacillus subtilis ATCC6051 was purchased from the American Type Culture Collection (ATCC, Manassas, VA, USA). *B. subtilis* was cultured on nutrient agar (NA, Oxoid, Basingstoke, England) for one week in order to induce sporulation. The collection of spores were conducted by washing them in 2 mL of sterile H_2O. The spore suspension was centrifuged at 4,500 × g for 10 min and washed twice with sterile H_2O. The final debris free spore pellet was resuspended in 2 mL of sterile H2O and exposed to 80 °C for 20 min to kill all the vegetative cells. The final spore suspension was stored at 4°C until further use. A spore staining, followed by microscopic observation was carried out to confirm the presence and purity (>95%) of spores. After a serial dilution, the number of viable spores were quantified using a plate count.

3.2.8. PC 12 cell line

Pheochromocytoma cells are derived from the rat adrenal medulla(Greene and Tischler, 1976a). The PC 12 cell line used in this study was purchased from the American Type Culture Collection (ATCC, USA). The PC 12 cells were cultured in a complete Gibco™ RPMI medium (Thermo Fisher Scientific, Australia)supplemented with 10% Gibco™ horse serum (Thermo Fisher Scientific, Australia, HS), 5% Gibco™ foetal bovine serum (Thermo Fisher Scientific, Australia, FBS) and 1% Gibco™ penicillin/streptomycin (Thermo Fisher Scientific, Australia, PS). The cells were maintained at 37 °C with 5% CO_2 in a 95% humidified incubator. The medium was changed every two days and passaged accordingly when the confluence reached 90%. Stock solutions of the PC 12 cells were prepared in a medium containing 90% FBS and 10 % DMSO and stored in liquid nitrogen. Supplements were stored as aliquots at -20ºC.

.

3.3. Construction of GUVS

The GUVs were constructed using the gel assisted method as described elsewhere (Weinberger et al., 2013). In brief, the glass slides (25 mm × 75 mm × 1 mm) were cleaned with chloroform, toluene, acetone and 100% ethanol. After the final wash of ethanol, the glass slides were dried using an ozone cleaner for 60 min. A thin layer of high molecular weight PVA-VP was created on the glass slide using 50 µL of the hydrogel, the PVA film was dried at 80 °C for 30 min. On to the dry PVA film, 50 µL of the stained lipid in chloroform was added and kept under a vacuum for 30 min. The O-rings used in the process were cleaned using toluene, acetone and 100% ethanol. After evaporation of chloroform, the O-ring was placed on the glass slide covering the area containing the stained lipid. Into the O-ring, 1mL of 280 mM sucrose was added and kept for 15 min. From the mixture, 0.5 mL of the sucrose and the lipid were transferred into an Eppendorf tube. Another 0.5 mL of 280 mM glucose was added, and the volume adjusted to 1 mL.

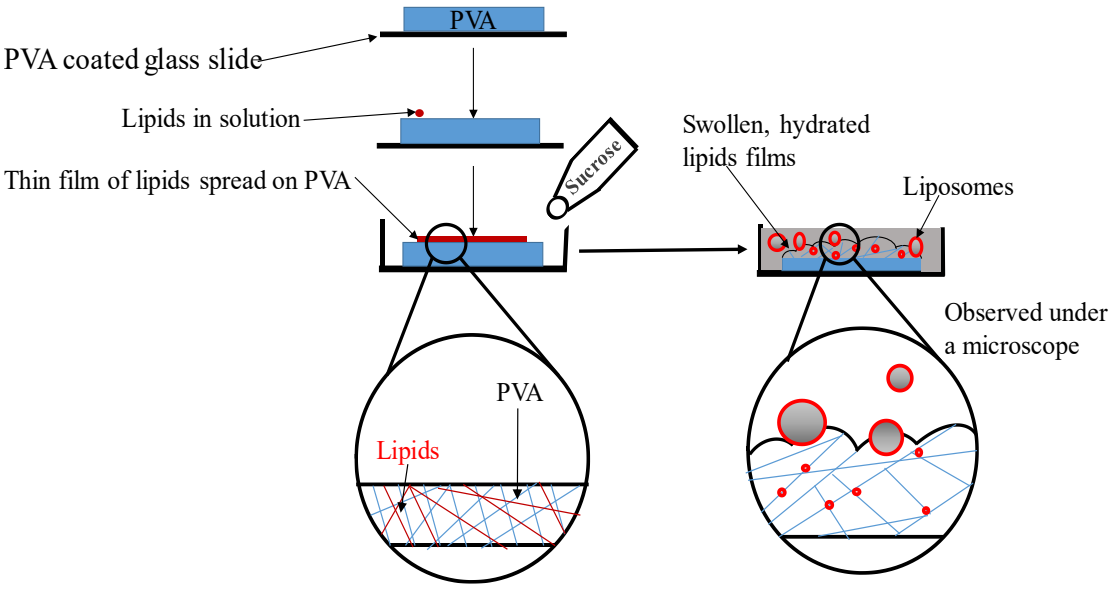

Figure 3. 1.GUVs synthesis using the gel assisted method. A thin layer of hydrogel is spread on the ozone cleaned glass slide. Lipids will be placed on the hydrogel and placed under a vacuum. Placing the lipids inside the vacuum will help evaporate the solvent. The lipids were originally present in a solvent (chloroform). Addition of an aqueous solvent, 280 mM sucrose will help to hydrate the lipid film, generating liposomes as illustrated.

3.4. EMF exposures of 18 GHz

3.4.1. EMF exposures of 18 GHz on GUVs

The microwave exposure of the GUVs were carried out according to the previously developed procedure as described elsewhere (Nguyen et al., 2016, Nguyen et al., 2015b). The increase in temperature was monitored in the presence of EMF radiation for 60 s. GUVs prepared in an 280 mM aqueous sugar solution was exposed to EMFs in 60 s-long cycles, which allowed for the temperature to be maintained below 40°C. The MW apparatus (Lambda Technologies Vari-Wave Model LT 1500) used in the study has an option of varying the frequency range from 5 – 18 GHz. The frequency was adjusted to a fixed frequency of 18 GHz at a power of 17 W, as described elsewhere (Shamis et al., 2011a, Nguyen et al., 2015b). The LT 1500 instrument is capable of delivering controlled EMF as the frequency and the power can be adjusted accordingly. The frequency delivered by the LT 1500 is well above a household microwave which is 2.45 GHz. The micro Petri dish (35 mm diameter, Griener Bio One, Frickenhausen, Germany) with the sample was placed on the ceramic pedestal (Pacific Ceramics, Sunnyvale, CA, USA, ε' , = 160, loss tangent < 10^{-3}) on the hotspot free location, identified by electric field modelling using CST Microwave Studio 3D Electromagnetic Simulation Software (CST MWS) (CST of Americ, Framingham, MA, USA) and experimental temperature measurements. GUVs were exposed to EMF for a duration of 60 s. The temperature rise in the GUVs suspension was monitored using a built-in temperature probe, a LuxtronFiber Optic Temperature Unit (LFOTU) (LumaSense Technologies, Santa Clara, CA, USA). After the MW treatment, the sample was cooled down to 25°C for 2 min. The microwave chamber was cooled using ice packs to bring the temperature to 25 °C. The sample was exposed to three cycles (60 s; 2 min cooling) of MW radiation while keeping all the other environmental factors constant.

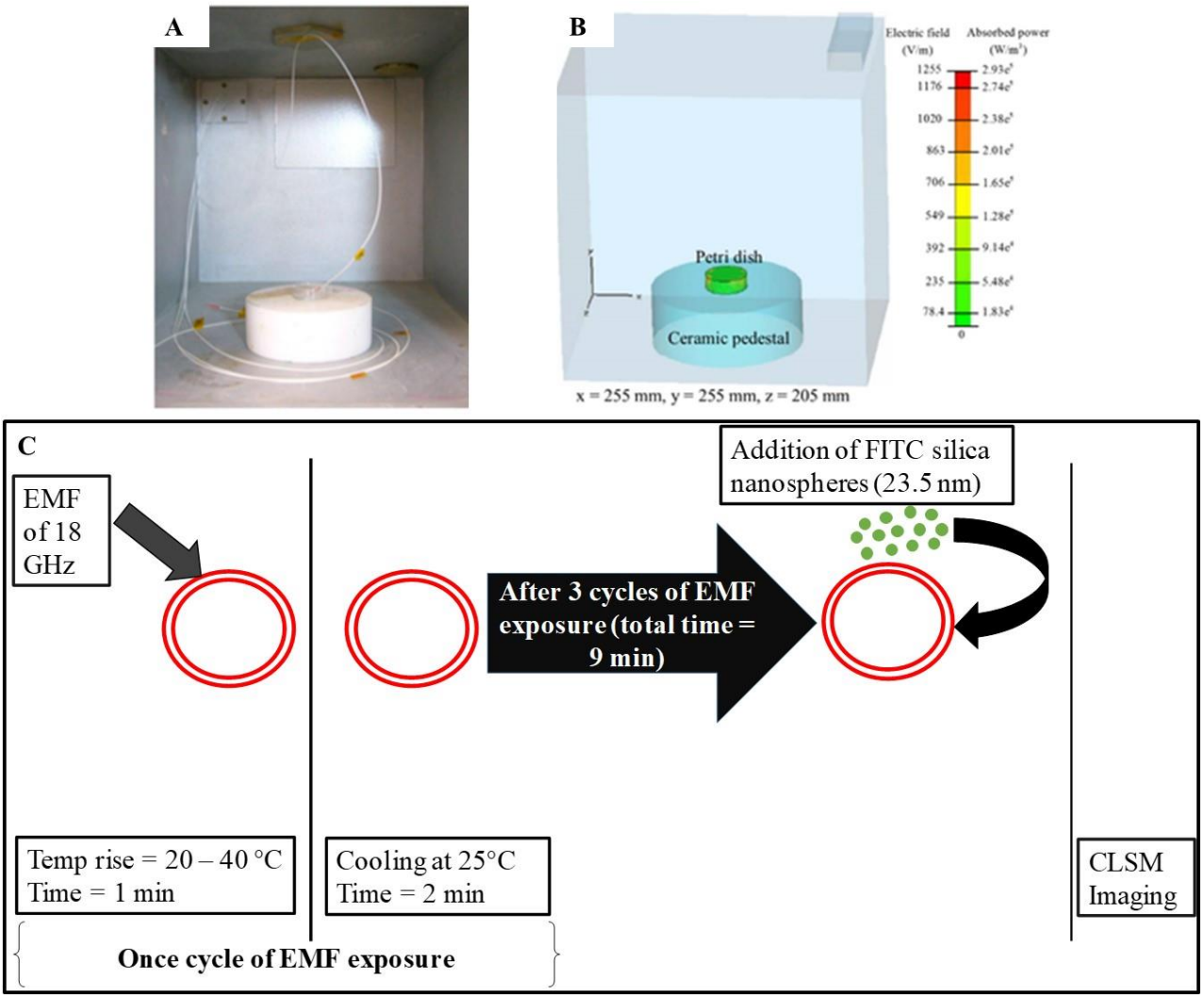

Figure 3. 2.Experimental set up of GUVs being exposed to EMF. (A) The microwave chamber used in EMF treatments. The micro petri dish (diameter = 65 mm, depth of suspension = 0.6 mm) containing the GUVs will be placed as depicted on the image..**(B)** Modelling of the microwave chamber showing absorbed power and electric field. The modelling was performed using CST Microwave Studio and 3D Electromagnetic Simulation software. **(C)**Schematic representation of the cycles of EMF exposure**.** The first stage of the EMF treatment increases the temperature of the GUVs to 40 °C. After the treatment (1 min), the GUVs in solution were allowed to cool down at 25° for 2 min before the next exposure. After the three EMF treatments, the GUVs were imaged after addition of the silica nanosphere.

3.4.2. EMF exposures of 18 GHz on PC 12 cells

The EMF treatments of the PC 12 cells were carried out according to the previously developed procedure as described elsewhere (Nguyen et al., 2016, Nguyen et al., 2015b).The increase in temperature was monitored in the presence of EMF radiation for 60 s. The cells were exposed to EMFs in 30 s-long cycles, which allowed for the temperature to be maintained below 37 °C **(Figure 3.3C).** The MW apparatus (Lambda Technologies Vari-Wave Model LT 1500) used in the study has an option of varying the frequency range from 5 – 18 GHz. The frequency was adjusted to a fixed frequency of 18 GHz and the power ranged from 17 W, as described elsewhere (Shamis et al., 2011a, Nguyen et al., 2015b). In brief, the micro Petri dish (35 mm diameter, Griener Bio One, Frickenhausen, Germany) with the sample was placed on the ceramic pedestal (Pacific Ceramics, Sunnyvale, CA, USA, $\varepsilon' = 160$, loss tangent $< 10^{-3}$) on the hotspot free location, identified by electric field modelling using CST Microwave Studio 3D Electromagnetic Simulation Software (CST MWS) (CST of America, Framingham, MA, USA) and experimental temperature measurements. The cell density of PC 12 used for EMF exposure was adjusted to 6×10^4 cells/ mL in phosphate buffered saline (PBS) using a hemocytometer (Paul Marienfeld GmbH&Co.KG Lauda-Konigshofen, Germany). The PC 12 cell suspensions were exposed to EMF for a duration of 30 s. The temperature rise in the cell suspension was monitored using a built-in temperature probe, a LuxtronFiber Optic Temperature Unit (LFOTU) (LumaSense Technologies, Santa Clara, CA, USA). After the MW treatment, the sample was cooled down to 25°C for 2 min. The microwave chamber was cooled using ice packs to bring the temperature to 25 °C. The sample was exposed to three cycles (30 s; 2 min cooling) of MW radiation while keeping all the other environmental factors constant.

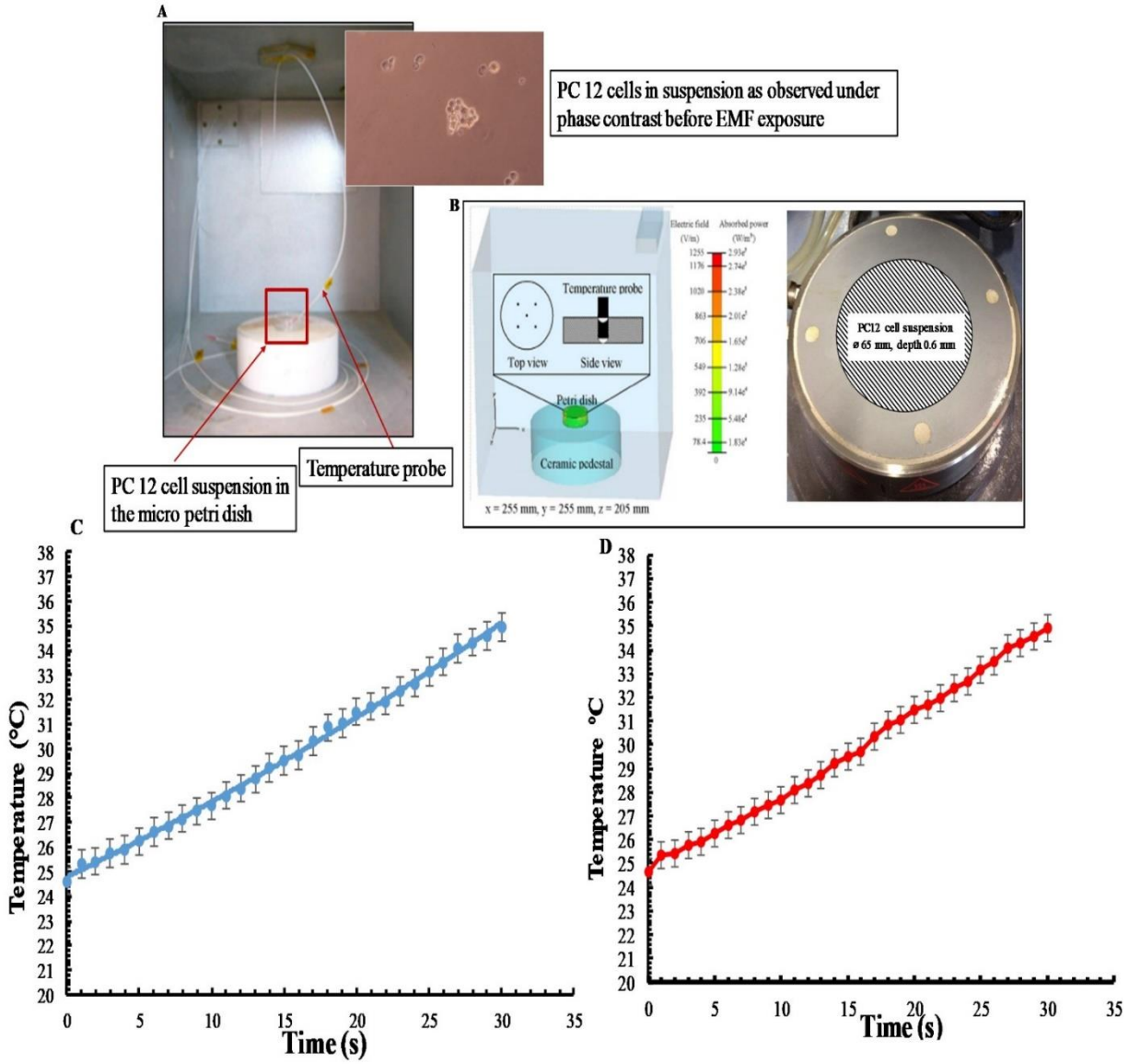

Figure 3. 3. The experimental set up of EMF treatments of PC 12 cell suspensions. (A) The microwave chamber. The temperature probe was placed inside the PC 12 suspension, which was placed on the ceramic pedestal. Insets of PC 12 as visualized under phase contrast microscopy in preparation for EMF exposure. Cells appear to be floating in suspension in a group of few cells. **(B)** Absorbed power and electric field modelling performed using CST Microwave Studio and 3D Electromagnetic Simulation software, the image depicts the position of the tip of the temperature probe (side and top view), on the right is Peltier heating stage and the PC 12 cell suspension will be placed on (diameter = 65 mm, depth of suspension = 0.6 mm).**(C)Temperature rise in the suspension of PC 12 cells in the presence of EMF radiation.** The rise in temperature of the cells in suspension during EMF treatment was monitored every second for the first 60 s. EMF treatments were carried out only for 30 s to prevent the overheating of cells. **(D) Heat profile in the suspension of PC 12 in the absence of EMF radiation.** In the Peltier heating graph, the temperature profile during EMF treatments was replicated and the cells were exposed to the same temperature but in the absence of EMF radiation.

3.4.3. EMF exposures of 18 GHz on *B. subtilis* spores

EMF radiation on *B. subtilis* spores were carried out according to the previously developed procedure as described elsewhere (Nguyen et al., 2016, Nguyen et al., 2015b). The concentration of the spore sample was adjusted to 10^5 CFU/mL in milliQ water. The increase in temperature was monitored in the presence of EMF radiation for 60 s. The cells were exposed to EMFs in 30 s-long cycles, which allowed for the temperature to be maintained below 37 °C. The MW apparatus (Lambda Technologies Vari-Wave Model LT 1500) used in the study has an option of varying the frequency range from 5 – 18 GHz. The frequency was adjusted to a fixed frequency of 18 GHz and the power ranged from 17 W, as described elsewhere (Shamis et al., 2011a, Nguyen et al., 2015b). In brief, the micro Petri dish (35 mm diameter, Griener Bio One, Frickenhausen, Germany) with the sample was placed on the ceramic pedestal (Pacific Ceramics, Sunnyvale, CA, USA, $\varepsilon' = 160$, loss tangent < 10^{-3}) on the hotspot free location, identified by electric field modelling using CST Microwave Studio 3D Electromagnetic Simulation Software (CST MWS) (CST of America, Framingham, MA, USA) and experimental temperature measurements. The spore suspensions were exposed to EMF for a duration of 30 s. The temperature rise in the cell suspension was monitored using a built-in temperature probe, a LuxtronFiber Optic Temperature Unit (LFOTU) (LumaSense Technologies, Santa Clara, CA, USA). After the MW treatment, the sample was cooled down to 25°C for 2 min. The microwave chamber was cooled using ice packs to bring the temperature to 25 °C. The sample was exposed to three cycles (30 s; 2 min cooling) of MW radiation while keeping all the other environmental factors constant.

3.4.4. Dosimetry

The specific absorption rate (SAR) was calculated assuming that the dielectric loss tangent describing the energy dissipation was the same as water at 25 °C and 18 GHz as described elsewhere (Panagopoulos et al., 2013) .

$$SAR = c \times \left.\frac{\partial T}{\partial t}\right|_{t=0} \qquad (1)$$

SAR is calculated using equation (1), where *c*, the specific heat capacity of the medium was similar to that of water, which is 4.18 $kJkg^{-1}°C^{-1}$, and $\left.\frac{\partial T}{\partial t}\right|_{t=0}$ is the time derivative of the temperature determined at t = 0 s ($°C\ s^{-1}$). It was essential to determine the SAR value as it is considered as an accurate measure of energy absorbed by a biological material (Haemmerich et al., 2005, Panagopoulos et al., 2013). Five different locations on the petri dish were used to gather temperature measurements and spatial averaging was used in determining SAR using 150 measurements. The experiment was designed to prevent overheating of the PC 12 cells by avoiding hot spots while maintaining adiabatic conditions.

3.5. Control samples

3.5.1. Peltier heat treatment

The temperature profile during the EMF exposure was replicated using bulk heat treatment. The Peltier plate heating/cooling system (TA Instruments, New Castle, DE, USA).A 2 mL aliquot of PC 12 cell suspension was spread on the Peltier stage (Figure 5.1B) and was subjected to heating from 25 °C to37 °C for a period of 30 s, which was followed by cooling to 25 °C for 2 min before the application of the next heat treatment to replicate the changes in the temperature conditions experienced by EMF-treated cells. A portable infrared/ thermal monitoring camera (Cyclope 330 S, Minolta, Osaka, Japan) was used to detect the temperature rise and fall during the cycle. The peltier treated PC 12 cells were used as the heat-treated control group.

3.5.2. Controls

PC 12 cells grown in full serum medium was used as the untreated control group. This control group was not exposed to any kind of treatment.

3.6. EMF exposures in the range of THz radiation

3.6.1. EMF exposures of 0.3 – 19.5 THz on PC 12 cells

For THz exposure, a pair of custom made diamond liquid cells (DLC) were used to contain the PC 12 samples; the DLC were labeled 'A' and 'B' where 'A' was the control and 'B' the exposed sample). Each DLC consists of three stainless steel components (**Figure 3.4**): a 6 mm diameter carbon vapour deposited (CVD) window, 400 µm thick with a 0.5° wedge is glued to 2 of them, and the third component is a spacer (5 - 300 µm) that can be changed according to the application; in this application, the 300 µm spacer was used, yielding a volume of 22.4 µL.
PC 12 cells prepared in growth media were injected into the DLC's which were then loaded on a Janis ST100 cryostat multi-sample holder (**Figure 3.5**).DLC B was mounted in the middle position of the cryostat where the beam was located while DLC A (the control) was mounted on the top position, and thus the PC 12 cells in this DLC were not exposed to any radiation but were in the same environment as those in DLC B; in this configuration the PC 12 cells in DLC B were exposed for a period of 10 min to the synchrotron THz radiation.

The Bruker IFS125 spectrometer located at the THz beamline of the Australian Synchrotron was used to expose the PC 12 cells to synchrotron THz radiation; the spectrometer was equipped with a 6 µm Mylar beam splitter. The synchrotron is a broadband source that emits radiation ranging from the THz to hard X-rays, however the light-energy reaching the sample is limited to 10 - 650 cm^{-1} (0.3 – 19.5 THz, $\lambda \sim 15.38$ - 1000 µm) by the beam splitter. The cell density of the PC 12 cells used for THz exposure was adjusted to 3×10^4 cells per 22.4 µL.

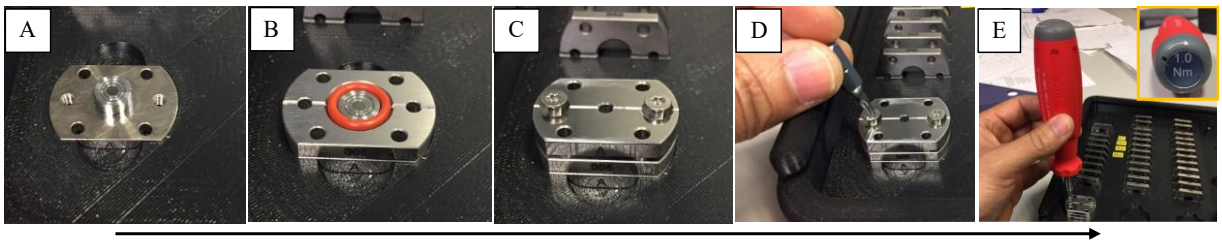

Figure 3. 4. Assembling of the Diamond Liquid Cells (DLC) for the exposure of THz radiation. PC 12 cells were loaded into the DLC **(B)** and assembled as illustrated before exposure. After loading the sample, the DLC is viewed under a microscope to confirm the absence of air bubbles.

The temperature of the DLC during exposure was recorded repeatedly using an IR-gun (Fluke, Infrared thermometers, Everett, WA, USA) before and at the end of exposure. After the exposure, the DLC was disassembled and the cells were collected for experimental assays.

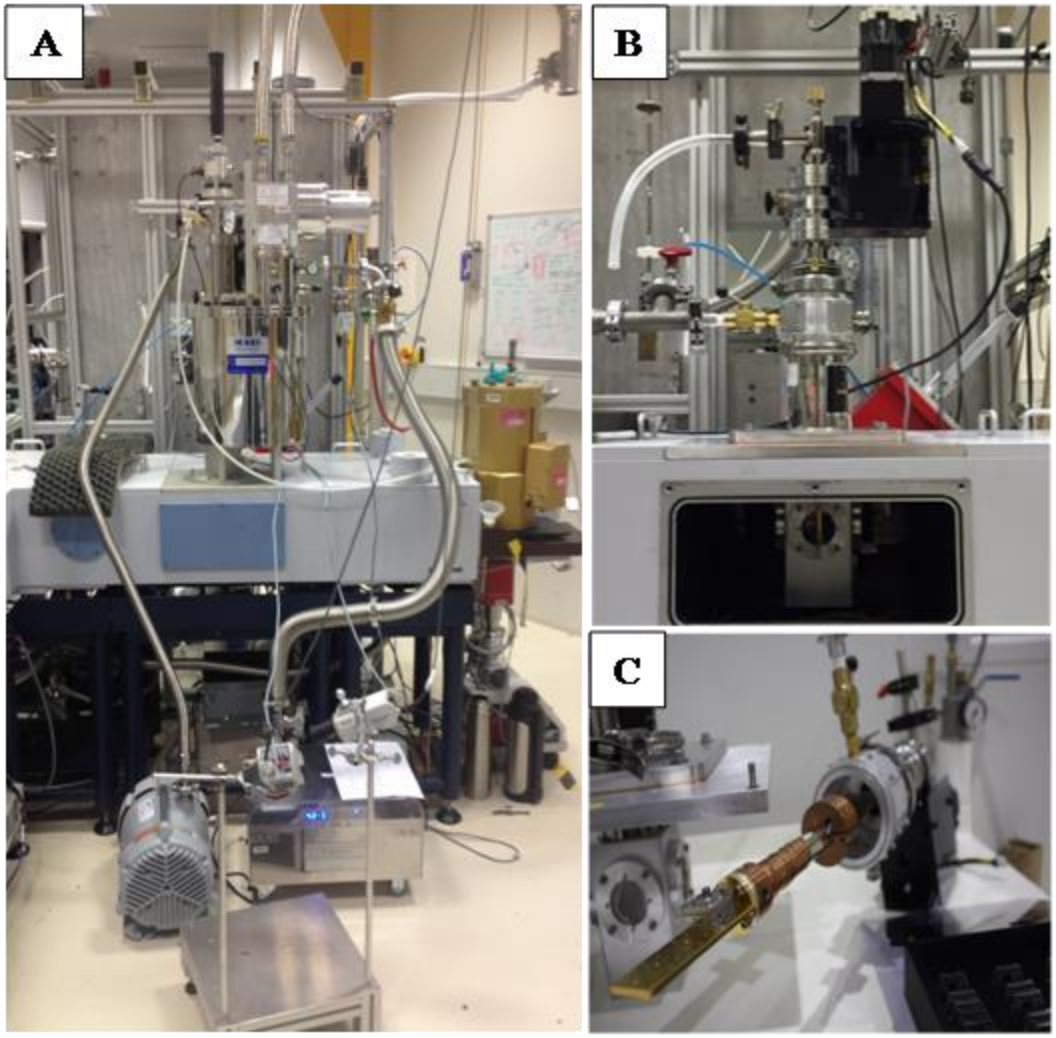

Figure 3. 5. Experimental set up of THz exposure. **(A)** Closed-loop pulse tube cryostat containing the DLC and the **(B)** Liquid Nitrogen Cryostat. **(C)** Sample holder to which the DLC are mounted on for exposure.

3.6.2. EMF exposures of 0.3 – 19.5 THz on *B. subtilis* spores

For THz exposure, a pair of custom made diamond liquid cells (DLC) were used to contain the *B. subtilis* spore samples; (the DLC were labelled 'A' and 'B' where 'A' was the control and 'B' the exposed sample). Each DLC consists of three stainless steel components (Figure 1E): a 6 mm diameter carbon vapour deposited (CVD) window, 400 µm thick with a 0.5° wedge is glued to 2 of them, and the third component is a spacer (5 - 300 µm) that can be changed according to the application; in this application, the 300 µm spacer was used, yielding a volume of 22.4 µL. *B. subtilis* spores prepared in sterile H_2O were injected into the DLC's which were then loaded on a Janis ST100 cryostat multi-sample holder. DLC B was mounted in the middle position of the cryostat where the beam was located while DLC A (the control) was mounted on the top position, and thus the *B. subtilis* spores in this DLC were not exposed to any radiation but were in the same environment as those in DLC B; in this configuration the *B. subtilis* spores in DLC B were exposed for 12 and 36 h of synchrotron THz radiation.

The Bruker IFS125 spectrometer located at the THz beamline of the Australian Synchrotron was used to expose the *B. subtilis* spores to synchrotron THz radiation; the spectrometer was equipped with a 6 µm Mylar beam splitter. The synchrotron is a broadband source that emits radiation ranging from the THz to hard X-rays, however the light-energy reaching the sample is limited to 10 - 650 cm^{-1} (0.3 – 19.5 THz, $\lambda \sim 15.38$ - 1000 µm) by the beam splitter. The spore density used for THz exposure was adjusted to 10^5 CFU/mL per 22.4 µL. The temperature of the DLC during exposure was recorded repeatedly using an IR-gun (Fluke, Infrared thermometers, Everett, WA, USA) before and at the end of exposure. After the exposure, the DLC was disassembled and the cells were collected for experimental assays.

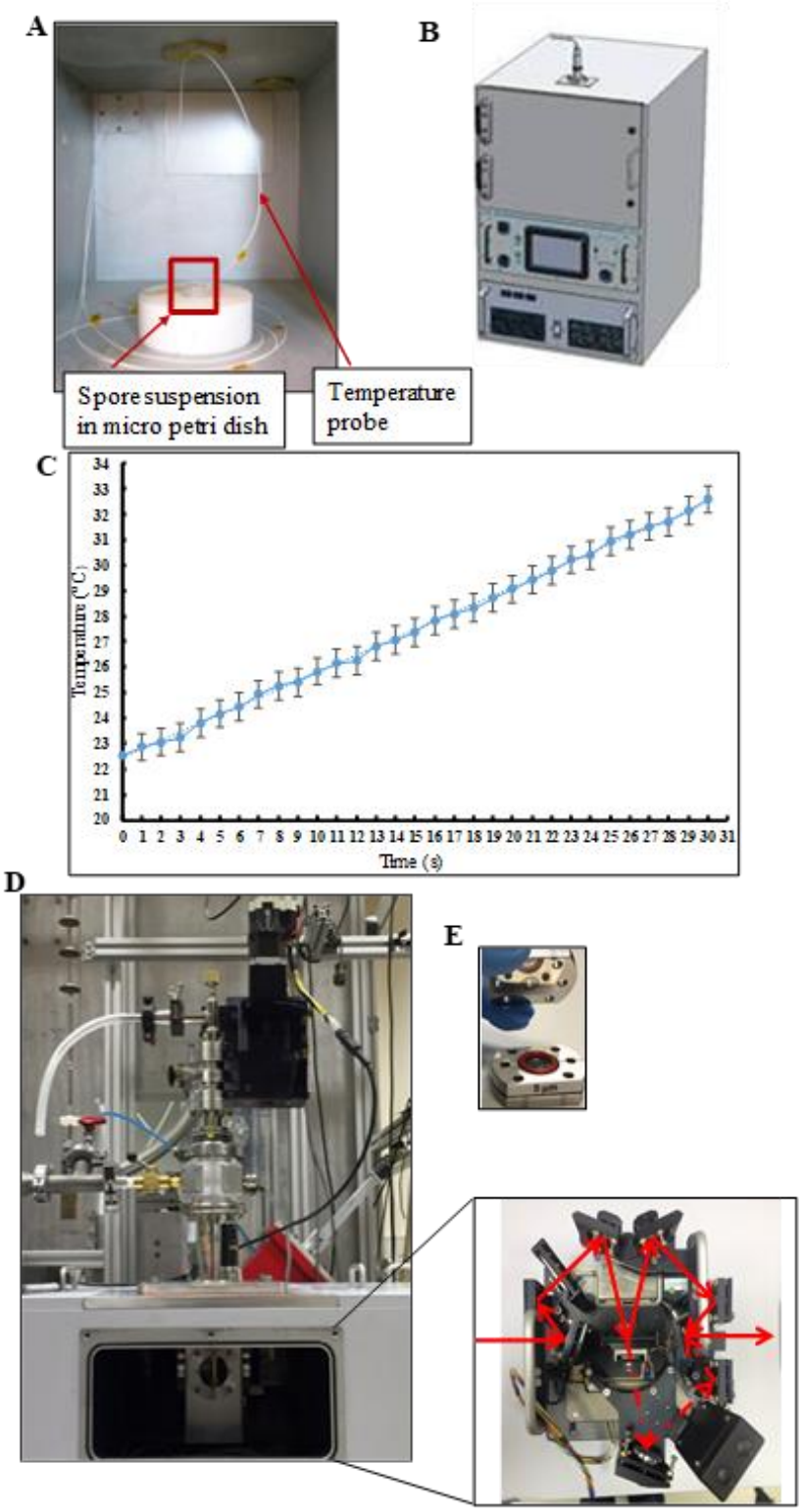

Figure 3. 6.Experimental setup of GHz (A-C) and THz (D-E) radiation on *B. subtilis* spores. (A) Spore suspension placed inside the microwave chamber on the ceramic pedestal with the temperature probe sitting inside the suspension. **(B)** Lambda Technologies Vari-Wave Model LT 1500**. (C)** Increase in temperature of the spore suspension within the first 30 s of GHz exposure. **(D)** Closed – loop pulse tube cryostat encompassing the DLC holder and the inset illustrates the path of the beam in red arrows. **(E)** DLC used for THz exposure

3.7. Detection of membrane permeability following exposure to EMFs

3.7.1. GUVs

Green fluorescent (FITC), hydrophilic and neutrally charged silica nanospheres (23.5 nm ± 0.2 nm) (Corpuscular, Cold Spring, NY, USA) were used to detect changes in the cell membrane permeability. The reason for using these nanospheres is that it rarely translocates through the hydrophobic lipid bilayer (Pogodin et al., 2012), the absence of any charge on the surface of the nanospheres prevents any non-specific interactions with the membrane (Verma and Stellacci, 2010). After the final treatment of the cell suspensions, 10 µL of the nanospheres were added to 2 mL of the EMF treated samples in solution and incubated for 5 min.

3.7.2. PC 12 cells

Fluorescent silica nanospheres with a diameter of 23.5 ± 0.2 nm (FITC)(Corpuscular, Cold Spring, NY, USA) were used to study the permeability of PC 12 cells. The membrane phospholipids were stained using carbocyanine DIL (1,1'-dioctadecyl-3,3,3',3'-tetramethylindocarbocyanine perchlorate) dye (ThermoFisher Scientific, Australia). Immediately following the EMF exposure, the nanospheres were added into the cell suspension at a concentration of 10 µg/mL. After 5 min of incubation, the samples were washed twice using PBS and centrifuged at 1300 rpm for 5 min at 25 °C. The procedure was repeated for the heat-treated cells and the untreated controls, where the cell samples were mixed with 10 µL of FITC nanosphere solution. A 150 µL aliquot of the sample was visualised using a Flouview FV10i-W inverted microscope (Olympus, Tokyo, Japan).

3.7.3. Permeability coefficient of EMF treated PC 12 cells

The nanosphere uptake following EMF exposure was quantified according to the fluorescence intensity generated from the silica nanospheres internalised by the PC 12 cells using a FLUOstar Omega microplate reader (BMG LABTECH, Cary, NC, USA), a method that was used previously.(Nguyen et al., 2016)The mass m of a silica nanosphere was determined from the density of silica ρ and the volume of a silica nanosphere V, related to the radius r as $V = \frac{4}{3}\pi r^3$. The average radius of a green nanosphere was 11.75×10^{-7} cm (Corpuscular), and hence the volume was estimated to be 6.8×10^{-18} cm^3, and mass 1.8×10^{-17} g. The mass of a single nanosphere was used to calculate the number of internalized nanospheres. The sample preparation was done according to the method used for CLSM analysis. The correlation of the nanosphere concentration and the fluorescence intensity was established using a calibration curve. Standards of nanosphere concentrations were prepared (0.5, 1, 2, 4, 6, 8, 10, 12 µg/mL).

Confocal laser scanning images were used in quantifying nanosphere uptake by counting the number of cells emitting the green flourescence in parallel with the cells that are not permeabilized. Ten different fields of view were analysed. The transient increase in permeability is expressed as a percentage.

3.8. Dynamic Light Scattering (DLS) of silica nanospheres distribution

The particle distribution of silica nanospheres were performed using DLS (Zetasizer Nano ZS ZEN3600, Malvern, UK). For DLS experiments, a 1 mL aliquot of the nanosphere stock solution was sonicated for 15 min. After sonication, 10 µL were withdrawn and diluted in 2 mL of sterile milliQ water. The mean effective diameter of the nanospheres and their clusters was measured.

3.9. Transmission Electron Microscopy (TEM)

After 5 min of incubation in the presence of nanospheres following EMF exposure, cell suspensions were pelleted by centrifugation at 1300 rpm for 5 min at 25 °C. The cells were then washed twice with phosphate buffer saline (PBS, 10 mM, pH 7.4) in order to remove any unbound nanospheres. The cell pellet was conditioned with 0.1M sodium cacodylate buffer (pH 7.4) The cell pellet was then re-suspended in primary fixative of 4 % paraformaldehyde and 2.5% glutarldehyde in 0.1M sodium cacodylate buffer for overnight at 4 degrees and washed thrice in cacodylate buffer for 10 minutes each. The cells were post-fixed in 1% osmium tetroxide and potassium ferrocyanide for an hour followed by three washes in distilled water for 10 mins each. The cells were dehydrated through a graded ethanol series (50%, 70%, and 90%) for 15 min. The cells were further dehydrated by passing through 100% ethanol series twice followed by 100% acetone series for 30 minutes at room temperature. The cells were further infiltrated with 1:1 ratio of acetone: Spurr's resin mixture for overnight. After that the cells were completely exchanged in 100% Spurr's resin twice for 3 hrs each. The resin samples were further polymerised at 70 degrees for 48 hours. The final block was trimmed, then cut into ultrathin sections (90 nm thickness) using a Leica Ultracut Ultramicrotome (Leica Microsystems, Wetzlar, Germany) with a diamond knife (Diatome, Pennsylvania, USA). Sections were placed onto 200 mesh copper grids and examined using a JEM 1010 instrument (JEOL). Approximately 40 TEM images were taken at ×5000 and ×10000 magnifications for sample analysis.

3.10. Atomic Force Microscopy

An Innova® atomic force microscope (AFM) (Bruker, USA). The tapping mode of analysis was employed for all samples, and all experiments were conducted under ambient temperature conditions using a phosphorus doped silicon probe (MPP-31120-10, Bruker, USA). AFM scans obtained from 5 µm × 5 µm surface areas were processed using Gwyddion software (available at www.gwyddion.net) (Nečas and Klapetek, 2012).

The solution containing the nanospheres was diluted (1:1000). After diluting, the sample was vortexed for 1 min and a small drop was placed on the silicon wafer. The droplet was dried for 30 mins and analysed using atomic force microscopy.

3.10.1. Bacterial cells

After EMF treatments, 10 µL was placed on the silicon wafer. The droplet was dried for 30 mins and analyzed using atomic force microscopy. A control sample that has not been exposed to EMF was used alongside for comparison purposes.

3.11. Cellular morphology

The scanning electron microscope FeSEM SUPRA 40VP (Carl Zeiss, Jena, Germany) with a primary beam energy of 3kV was used. A 100 µL aliquot of cells in PBS were placed on a glass cover slip (ProSciTech, Kirwan, Australia) in duplicate. The glass cover slips were then washed with nanopure H_2O (resistivity of 18.2 MW cm^{-1}) and dried with 99.99% purity nitrogen gas. The PC 12 cells exposed to EMF of 18 GHz were fixed in a cocktail of 4.0 % paraformaldehyde and 2.5 % glutaraldehyde for 30 min. The cells were then dehydrated by passing through a graded ethanol series (20%, 40%, 60%, 80% and 100%) for 15 min. Before imaging, the fixed cells were subjected to gold sputtering (6nm thick) using a NeoCoater MP-19020NCTR (JEOL, Tokyo, Japan). The same procedure was applied to non-treated and heat treated PC 12 cells. SEM images (10) of different magnification were captured and analysed.

3.12. Viability

3.12.1. PC 12 cells

The viability of PC 12 cells was determined using the LIVE/DEAD Viability/Cytotoxicity Kit (Invitrogen). The viability of the EMF-treated cells and the controls was monitored immediately after the treatment and confirmed through three technical replicates. CLSM was used in

assessing the number of viable cells; approximately 10 fields of view were analysed per sample type.

3.12.2. Spore germination

Spore recovery was tested using viable plate count, 100 µL of the spore samples retrieved from EMF and THz exposures was mixed with 900 µL of sterile milliQ water to create 1:10 dilution suspension. A series of dilutions were then performed using the same method until 10 dilutions were created. After the dilution series, 100 µL from each dilution were plated on nutrient agar (NA, Oxoid, Basingstoke, England) and incubated at 37 °C overnight with the appropriate controls. Colony forming units (CFUs) were counted after 24 h incubation according to the equation listed below.

$$\text{CFU} = \frac{\text{colony count} \times \text{dilution factor}}{\text{Volume plated (mL)}}$$

The CFU/mL was then expressed as percentage viability.

3.13. Cell proliferation

Cell proliferation was determined using the CellTiter 96® AQ_{ueous} One Solution Cell Proliferation Assay (Promega, Australia). The assay was performed by adding tetrazolium compound to the EMF treated PC 12 cell culture at a 10% ratio of the final volume. This allowed for the reduction of MTS (3-(4,5-dimethylthiazol-2-yl)-5-(3-carboxymethoxyphenyl)-2-(4-sulfophenyl)-2H-tetrazolium) to formazan, which resulted in the formation of a purple-coloured precipitate. After incubation for 90 min at 37 °C, the absorbance was recorded at a wavelength of 490 nm using a FLUOstar Omega microplate reader (BMG LABTECH, Cary, NC, USA).

3.14. Protein concentration

The total protein content present in the EMF treated cells and the non-treated cells was determined using the Bicinchoninic Acid Protein (BCA) Assay (Sigma-Aldrich, NSW, Australia). The PC 12 cells were lysed with 150 µL of protein lysis reagent (Sigma-Aldrich, NSW, Australia) and incubated for 15 min at 25 °C. After incubation, the cells were spun at 1300 rpm for 5 min at 25 °C. Then, 25 µL of the supernatant was placed onto a 96 well plate (Sarstedt, Germany) and 200 µL of BCA reagent (Bicinchoninic acid solution and Copper (II) Sulphate Pentahydrate 4%) was added. The sample was then incubated for 30 min at 37 °C and the absorbance was recorded at 562 nm using the FLUOstar Omega micro plate reader (BMG LABTECH, Cary, NC, USA).

3.15. Cell integrity

The release of lactate dehydrogenase (LDH) by the EMF treated PC 12 cells was tested using The CytoTox 96® Non-Radioactive Cytotoxicity Assay. From the PC 12 cell suspensions that were exposed to EMF radiation, 25 µL were withdrawn onto a 96 well plate (Sarstedt, Germany) and 25 µL of LDH Mix added. The samples were incubated for 30 min at 25 °C away from light. Afterwards, 25 µL of the LDH stopping solution was added and the absorbance read at 490 nm using the FLUOstar Omega micro plate reader (BMG LABTECH). The percentage release of LDH was then analysed.

3.16. PC 12 cell differentiation

PC 12 cells at a density of 10^5 cells per mL in Gibco™ 1640 Roswell Park Memorial Institute (RPMI) medium (10% HS, 5% FBS and 1% Pen/Strep) were seeded onto a 10 µg/mL collagen-coated 12-well polystyrene (PS) tissue culture plate according to the manufacturer's recommended procedure. One day after plating, the full serum culture medium was replaced with a low serum medium supplemented with 50 ng/mL Nerve Growth Factor (mouse recombinant NGF 7S, Sigma-Aldrich, Sydney, Australia). The culture medium was partially refreshed every two days.

3.17. Assessment of neurite outgrowth

A phase contrast brightfield inverted Olympus microscope (CKX41, Olympus, Tokyo, Japan) fitted with a Panasonic camera (DMC-GH3) was used to capture images of the differentiating PC 12 cells over a period of 7 days. CLSM was used to record PC 12 differentiation after 7 days. The cell membrane phospholipids were stained using carbocyanine DIL (1,1'-dioctadecyl-3,3,3',3'-tetramethylindocarbocyanine perchlorate) dye (Thermo Fisher Scientific, Australia).
The quantification of the occurrences of neurite extension was carried out using the Neuron J software (Image J plugin; NIH, Bethesda, MD, USA) by manually tracing the length of the neurites in 10 different fields of view.
The number of neurites per cell were quantified manually in 5 - 10 different fields of view and the results expressed as a percentage.

3.18. Statistical analysis

Statistical data processing was conducted using the Statistical Package for the Social Sciences, SPSS 24.0 (SPSS, Chicago, IL, USA). Statistically significant differences ($p<0.05$, $p<0.01$) among the various groups were calculated using a one-way ANOVA analysis followed by a Post HocTukey's multiple comparison test.

Chapter 4. Exposure to EMFs of 18 GHz triggers rapid uptake of large nanosphere clusters by pheochromocytoma cells (PC 12)

4.1. Overview

Effects of man-made electromagnetic fields (EMF) on living organisms potentially include transient and permanent changes in cell behaviour, physiology and morphology. At present, these EMF-induced effects are poorly defined, yet their understanding may provide important insights into consequences of uncontrolled (*e.g.*, environmental) as well as intentional (*e.g.*, therapeutic or diagnostic) exposure of biota to EMFs. In this work, for the first time, we study mechanisms by which a high frequency (18 GHz) EMF radiation affects the physiology of membrane transport in pheochromocytoma PC 12, a convenient model system for neurotoxicological and membrane transport studies. Suspensions of the PC 12 cells were subjected to three consecutive cycles of 30s EMF treatment with a specific absorption rate (SAR)of 1.17 kW kg^{-1}, with cells cooled between exposures to reduce bulk dielectric heating. The EMF exposure resulted in a transient increase in membrane permeability for 9 min in upto 90% of the treated cells, as demonstrated by rapid internalisation of silica nanospheres (diameter $d \approx 23.5$ nm) and their clusters ($d \approx 63$ nm). In contrast the PC12 cells that received an equivalent bulk heat treatment behaved similar to the untreated controls, showing lack to minimal nanosphere uptake of approximately 1-2 %.Morphology and growth of the EMF treated cells were not altered, indicating that the PC 12 cells were able to remain viable after the EMF exposure. The metabolic activity of EMF treated PC 12 cells was similar to that of the heat treated and control samples, with no difference in the total protein concentration and lactate dehydrogenase (LDH) release between these groups. These results provide new insights into the mechanisms of EMF-induced biological activity in mammalian cells, suggesting a possible use of EMFs to facilitate efficient transport of biomolecules, dyes and tracers, and genetic material across cell membrane in drug delivery and gene therapy, where permanent permeabilisation or cell death is undesirable.

4.2. Background

Life appeared and developed within the multitude of natural electromagnetic fields, but this natural environment has drastically changed with the introduction of the ever-growing spectrum of man-made electromagnetic fields (EMFs). Effects on biological matter exposed to the artificial EMFs have been a focus of research investigation since the 18th century,(Banik et al., 2003) with research effort becoming more intense now due to the growing prevalence of power transmission devices and consumer goods (e.g. microwave ovens) that rely on electromagnetic radiation to perform their functions.(Redlarski et al., 2015, Oliveira and Santos, 2016, Sokolovic et al., 2008). In recent years, a rapid growth in mobile communication systems, wireless and radio communications (Salford et al., 1997, Deshmukh et al., 2016) and the associated surge in usage of personal communication devices like tablets, portable computers, wifi-enabled 'smart' phones, televisions and cameras has significantly increased the likelihood of environmental exposure of humans and other organisms to EMFs (Redlarski et al., 2015, Lewczuk et al., 2014) and to the microwave radiation (MW) in particular. It is of utmost importance to explore and understand the effects arising from the interaction of electromagnetic fields with living entities at the micro and nano scale.

Microwave radiation is a part of the electromagnetic spectrum consisting of frequencies from 300 MHz to 300 GHz (Sokolovic et al., 2008, Banik et al., 2003),with a corresponding wavelength in the range of 1 m – 1 mm (Banik et al., 2003, Zuo et al., 2014). Early studies based on modelling efforts regarded such EMFs to be not sufficiently strong to induce significant biophysical or biochemical changes in living systems and affect their physiological functions. Recent findings, however, revealed evidence that depending on the amount of energy delivered into the system, MW radiation may induce a variety of molecular transformations that may in turn lead to modulation of chemical events that take place on cell surface (Banik et al., 2003, Shamis et al., 2012a) including molecular binding, signalling and trans-membrane transport. Previous reports stated that a treatment using EMF of 18 GHz was able to induce a reversible increase in membrane permeability in different Gram-negative and Gram-positive bacterial species, including *Planococcusmaritimus*KMM 3738, *Staphylococcus aureus* CIP65.8^{T}, *S. aureus* ATCC 25923, *S. epidermidis* ATCC 14990^{T}, *Escherichia coli*; and yeast and red blood cells (Nguyen et al., 2015b, Shamis et al., 2011a). Although permeabilisation was observed in all cell types, thereby suggesting a similar mechanism of induction, the differences in cell membrane fatty acid and phospholipid composition, such as the presence of pentadecanoic fatty acid or phosphatidyl-glycerol, determined the specific dose of 18 GHz EMF exposure required to induce permeabilisation and the size and number of nanoparticles that could be internalised by thus-treated cells (Nguyen et al., 2016). This phenomenon presents a motivating opportunity

as an alternative method for rapidly inducing a transient increase in membrane permeability as a means to attain a more efficient uptake of biomolecules, dyes and tracers, and genetic material by cells in drug delivery and gene therapy applications. This approach may be particularly useful for applications where permanent membrane damage or cell death are not desired, since the aforementioned treatment did not negatively affect cell viability regardless of the microorganism species being treated (Nguyen et al., 2016, Shamis et al., 2012c, Woo et al., 2000). However, in order to facilitate the translation of this phenomenon into real-life applications, more effort is needed to understand the mechanisms by which EMFs modulate key cellular processes and affect cell viability, particularly in mammalian cells.

The aim of this study was to explore the bioeffects of 18 GHz EMFs on eukaryotic cells and investigate whether the exposure of pheochromocytoma cells to such fields would affect membrane permeabilisation, proliferation rates and metabolic status. The present study focuses on the possible effect of electromagnetic fields at 18 GHz with short exposures of 30 s at a power of 17 W on a mammalian cell line (PC 12). The hypothesis behind the present study is that at this fixed frequency of 18 GHz, non-ionizing electromagnetic radiation encounters a polar molecule (water) and transfers a fraction of its energy to this molecule, driving it to oscillate which in turn has an effect on other cellular constituents. This research is significant because:

i) Just as man-made electromagnetic radiation, nanoparticles are becoming increasingly ubiquitous, being used in a very wide range of medical and cosmetic applications, as well as being released into the environment by many industries. Nanoparticle toxicity is closely related to their uptake and accumulation by cells. Therefore, it is important to understand how nanoparticle uptake is affected by even a brief exposure of human cells to electromagnetic field of low intensity.

ii) Closely related to (i) nanoparticles are increasingly being used for medical visualisation, cancer treatment and delivery of drugs and biomolecules. The efficacy of some of these applications is inherently linked to the ability of nanoparticles to cross the cellular membrane to deliver the treatment intracellularly. Thus, it is the aim of this research to test whether 18 GHz EMF can be applied to cells with the aim to induce a very specific set of outcomes, *i.e.*, a temporary increase in membrane permeability and nanoparticle uptake, while minimizing other biological effects, *e.g.*, changes in metabolic activity, of such an exposure.

The pheochromocytoma PC 12 cell line was selected as a model as it is easy to culture and because there is a large amount of background knowledge available on its proliferation and differentiation in response to pharmacological manipulation or exposure to other types of treatment (Jesky and Chen, 2016b, Westerink and Ewing, 2008a).

4.3. Results

The EMF treatments of the PC 12 cells were carried out according to the previously developed procedure as described elsewhere,(Nguyen et al., 2016, Nguyen et al., 2015b) and depicted in **Figure 3.3**. The increase in temperature was monitored in the presence of EMF radiation for 60 s. The cells were exposed to EMFs in 30 s-long cycles, which allowed for the temperature to be maintained below 37 °C **(Figure 3.1.C).**

4.3.1. EMF induced cell membrane permeability

The dosimetry results confirmed that PC 12 cells in suspension exposed to EMF of 18 GHz had a specific absorption rate (SAR) value of 1.17kW kg^{-1}, assuming no heat loss to the surrounding solution. Some heat loss to the medium can be neglected as the constituents are similar to that of water with a specific heat capacity of 4.18 $kJkg^{-1}°C^{-1}$. The rate of change of temperature was 0.28° per second **(Figure 3.3C)** during the first 30 s of exposure. The time of exposure was reduced to maintain the temperature below 37°C. The average temperature of the cell suspension after one 30 s cycle was recorded as 34.94 ± 1.73°C. To investigate the likely contribution of dielectric heating resulting from the absorption of MW radiation by the molecules to the observed changes in nanosphere uptake and cell metabolism, the temperature conditions experienced by the cells during EMF treatment were approximated by subjecting cells to the Peltier heating/cooling where the temperature profile in the absence of EMF was replicated, outlined in the Peltier heating/cooling diagram **(Figure 3.3D)** .

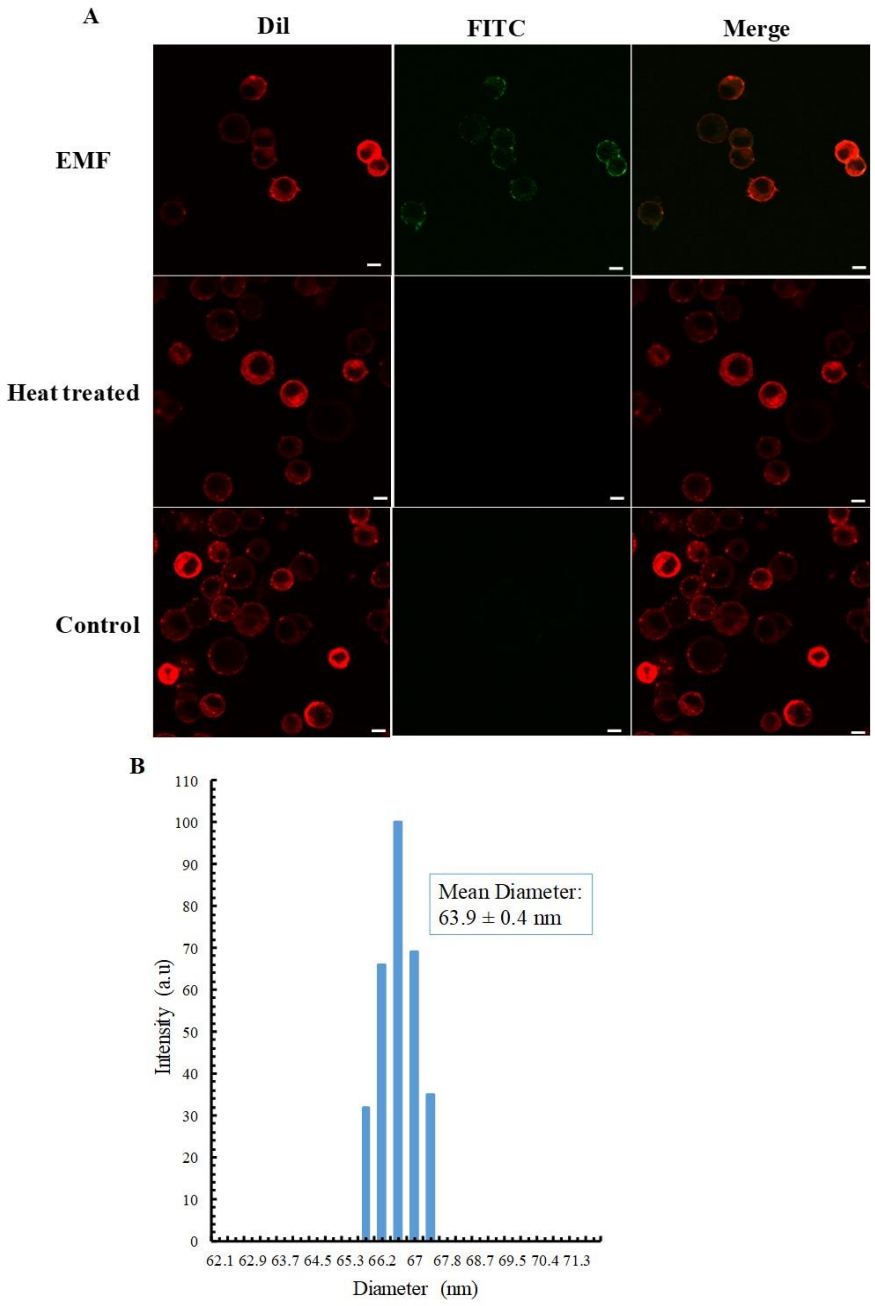

Figure 4. 1. Internalisation of silica nanospheres by PC 12 cells following exposure to EMF radiation of 18 GHz. (A). CLSM micrographs depicting fluorescent silica nanospheres being internalisation by PC 12 cells after EMF exposure. The nanospheres as visualized tend to exist in clusters in working solution. Scale bar 5 µm. **(B).** Characterisation of silica nanospheres clusters in working solution. Dynamic light scattering (DLS) results for silica nanospheres after sonication (15 min) revealed that the nanospheres are present in clusters of 3- 4 as an effective diameter of 63.9 nm was recorded.

Exposure to EMFs of 18 GHz triggered a transient increase in membrane permeability in the PC 12 cells,as confirmed by rapid internalisation of silica nanospheres(*d*=23.5 nm) evident in CLSM and TEM images**(Figure 4.1A and 4.3)**. It was confirmed by DLS that in the working solution, the nanospheres appeared in clusters of 3 to 4 nanospheres, with the average size of the majority of the clusters being ~63.9 nm **(Figure 4.1B)**. Approximately 90% of the PC12 cell population was able to uptake the nanospheres after EMF exposure, while the nanosphere uptake by the heat-treated and the untreated PC 12 cells was negligible, at 1-2%.

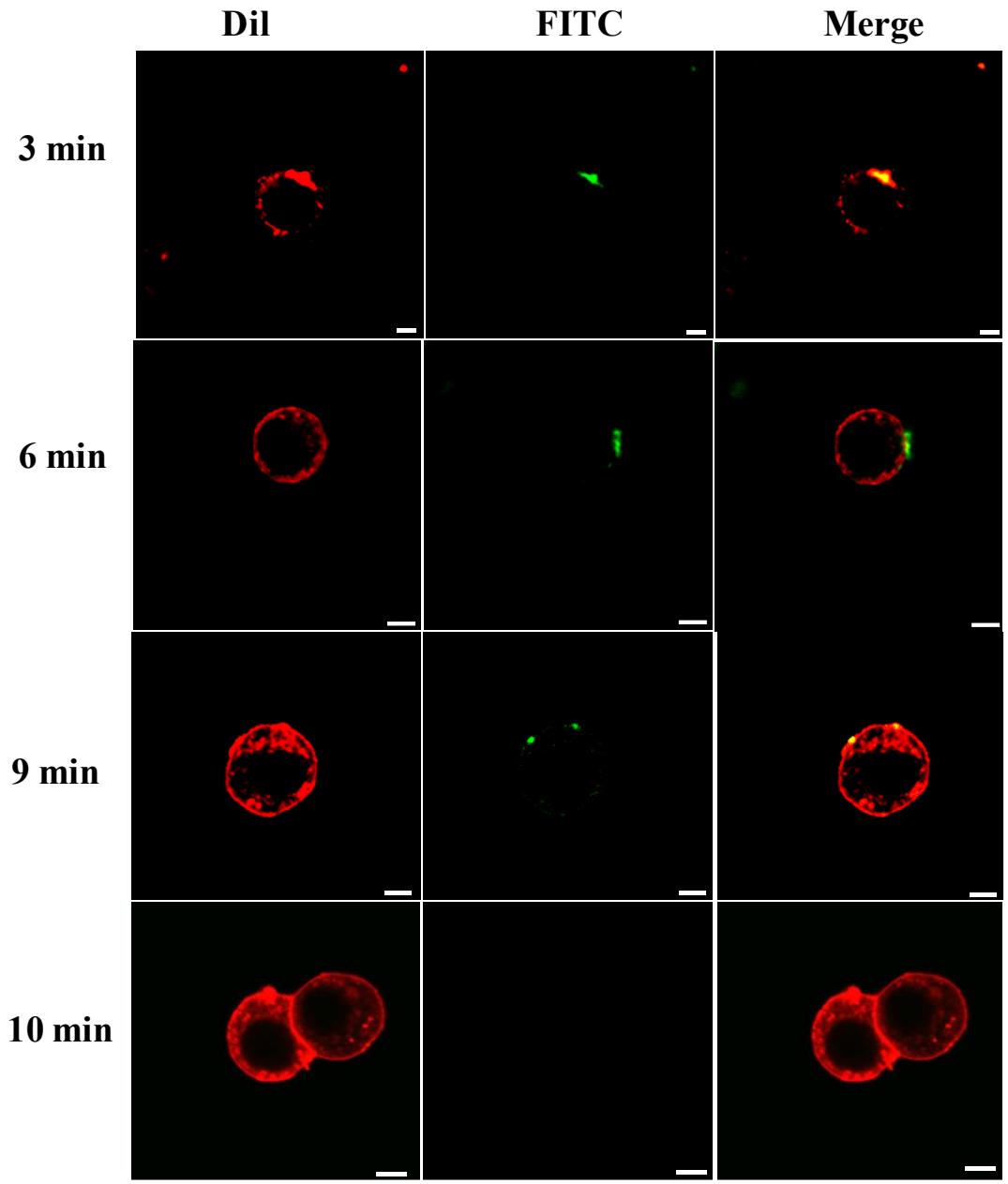

.

Figure 4. 2.Confocal micrographs illustrating the duration of PC 12 cell permeability following EMF exposure. CLSM images showing fluorescent silica nanospheres being internalisation by PC 12 cells, 3, 6 and 9 min after EMF exposure. No nanosphere uptake was visualised after 10 min. The results suggest that permeability lasted for 9 min. Scale bar 5 µm. The internalisation of silica nanospheres of 23.5 nm was further confirmed by TEM images (**Figure 4.3**). Nanospheres in working solutions was found to be in monodispersed and in clusters. It appeared that the EMF-treated PC 12 cells internalised the nanospheres (red circles) and their clusters (green insets) and were located inside the cell cytoplasm. No internalised nanospheres were detected on TEM images for the control or the heat-treated sample groups.

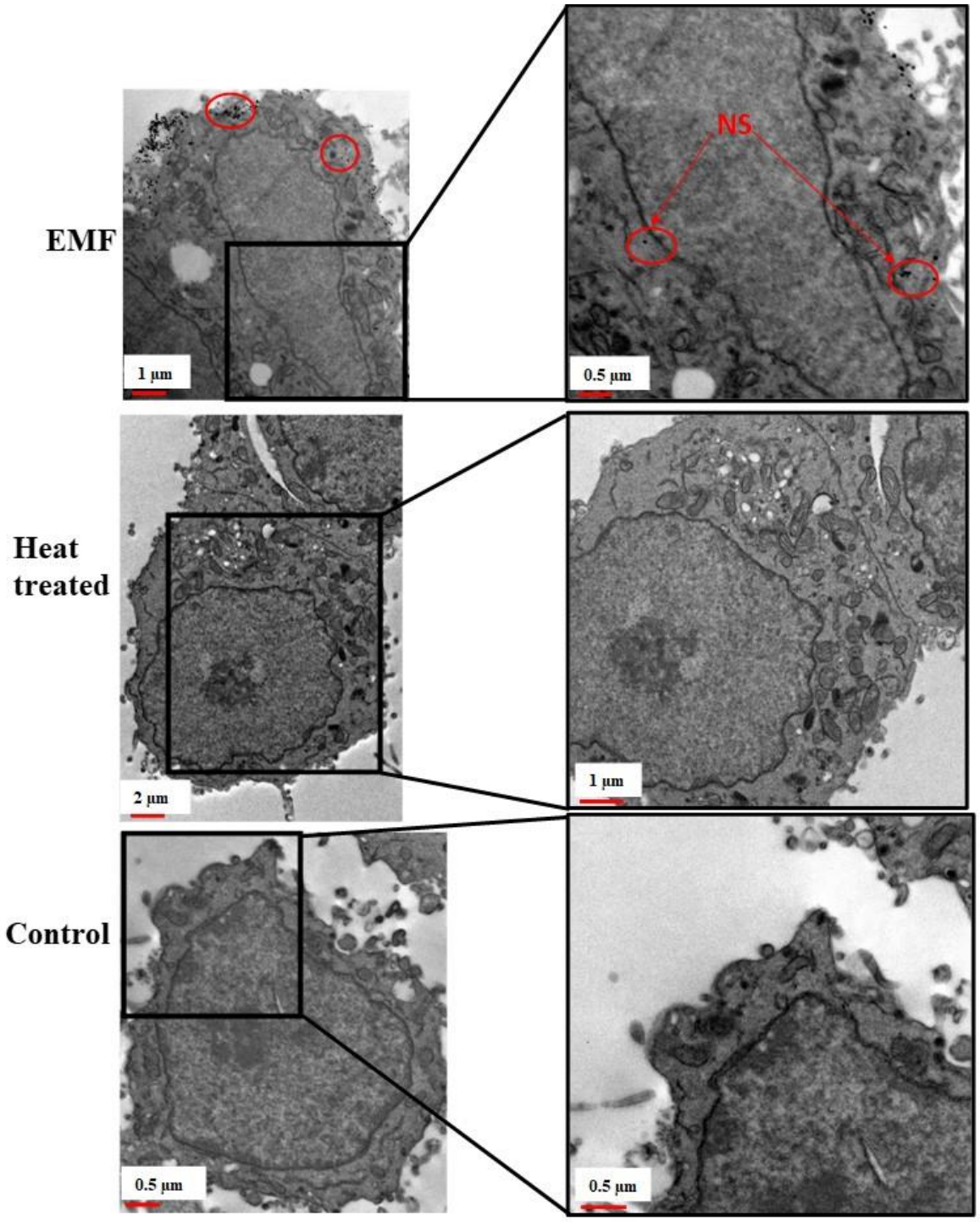

Figure 4. 3. TEM micrographs depicting Silica NS internalisation by EMF treated PC 12 cells. Typical TEM images showing PC 12 cells exposed to EMF of 18 GHz were able to internalise silica nanospheres (23.5 nm) and clusters (63.9 nm) as indicated by arrows. No nanosphere internalisation was detected in the heat treated and the control groups. Nanospheres were also seen to cluster around the radiated cells (red circles).

It can be concluded that EMF induced cell membrane permeability in PC 12 cells lasted for 9 min following exposure (**Figure 4.2.**). The PC 12 cells were not permeable after 10 min following exposure and the permeability was tested at four different time points (3, 6, 9 and 10 min) (**Figure 4.2**). Previous results established that the internalisation of silica nanospheres by bacterial cells continued up to 9 min after initial exposure and no uptake of the nanospheres were detected when the nanospheres were added 10 min after the initial exposure (Nguyen et al., 2015b) which was similar to the results obtained after exposing EMF treated PC 12 cells to nanospheres.

The concentration of the nanospheres in the EMF-exposed suspension was calculated to be 0.0031 μg mL^{-1}. By dividing the mass of a single nanosphere, the number of internalized nanospheres was estimated to be 1.7×10^{11} nanospheres. Since the cell concentration was 60,000 cells per mL, the number of internalized nanospheres per PC12 cell was calculated to be 2.8×10^{6} nanospheres. This was 100 times more than the number of nanospheres internalized by *Saccharomyces cerevisiae* cells in a previous study, which estimated to be 2.8×10^{4} nanospheres per cell (Nguyen et al., 2016). It should be noted that the yeast cells have a mean diameter of 5.5-5.9 μm (Srinorakutara, 1998) whereas PC 12 cells have a diameter of approximately 10-12 μm(Sagi et al., 2009)which is twice the size of a single yeast cell.

4.3.2. EMF induced effects on cell morphology and viability

Analysis of cell morphology using SEM revealed no significant differences between cells in EMF-treated, heat-treated and control groups (**Figure 4.4**; top row). No leakage of cytosol was observed in the EMF-treated samples.

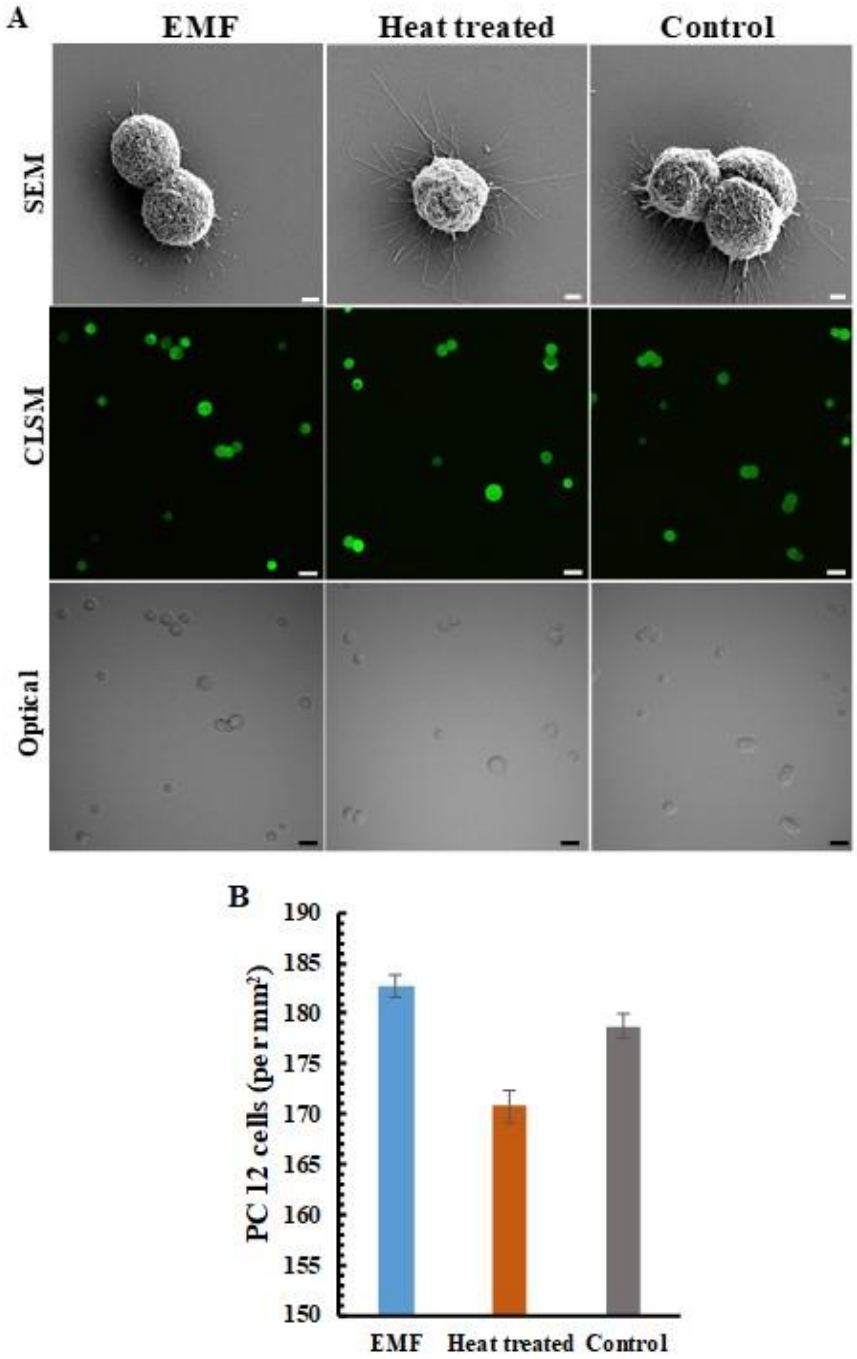

Figure 4. 4. Analysis and quantification of PC 12 cell morphology and viability. (A) Scanning electron micrographs (top row) of PC 12 cells after being exposed to EMF radiation. No significant changes in cell morphology were detected in the EMF treated groups in comparison to the heat-treated and the control samples. Scale bar 2µm. CLSM images (middle row) depict cell viability, PC 12 cells exposed to EMF, heat treatments and the control are all remained viable. Phase contrast (bottom-optical) images of the same field of view. Scale bar 5 µm. **(B) Quantification of viable PC 12 cells after EMF radiation.** The number of viable cells in the EMF treated and the other control groups vary slightly, no significant changes (p>0.05) were detected. Data are means ± standard deviation (SD) and representative of 3 independent repeats.

Viability of PC 12 cells after their exposure to the EMF radiation was investigated using CLSM. Visual examination of the fluorescence micrographs showed that the cells remained viable after EMF treatment (**Figure 4.4**; middle row), indicating that the exposure to the EMF of 18 GHz did not affect cell viability. A statistical analysis of the data did not reveal a statistically significant difference between the viability of the EMF-treated and the Peltier heated cells (p> 0.05), EMF-treated cells and the untreated control (p> 0.05), or Peltier treated cells and the untreated control (p> 0.05) (**Figure 4.4B**). This finding is in agreement with previously reported data showing that a 24 h exposure of human neuroblastoma cells (SH-SY5Y) to MW radiation at a lower frequency (900 MHz)and exposure level (2 W/kg) did not lead to cell death or increased rates of apoptosis (Joubert et al., 2006). This finding has a potentially important implication for the use of high frequency EMF treatment as a physical means to achieve a temporary increase in membrane permeability for, *e.g*., drug or genetic material delivery, where cell death is undesirable.

4.3.3. EMF induced effects on intra-cellular physiology

The relative metabolic activity of the cells was analysed using MTS assay. Increased metabolic activity was detected in the EMF-exposed PC 12 cells (**Figure 4.5A**). The absorbance recorded at 490 nm was directly proportional to the cell metabolic activity, as mitochondrial activity of metabolically active cells results in the conversion of MTS (salt) into a soluble formazan (Malich et al., 1997). The reduction of MTS mainly occurs in the mitochondria, hence providing a measure of mitochondrial function. The latter is an important indicator of cell health, since mitochondrial injury is considered to be an early step in apoptotic cell death (Lobner, 2000). Previously it was shown that EMF of 2.8 GHz with an average power of 30 mW/cm² used to treat PC12 for 5 and 15 min triggered some key apoptotic events as a result of the treatment, including the loss of mitochondria membrane potential and DNA fragmentation (Zuo et al., 2014).

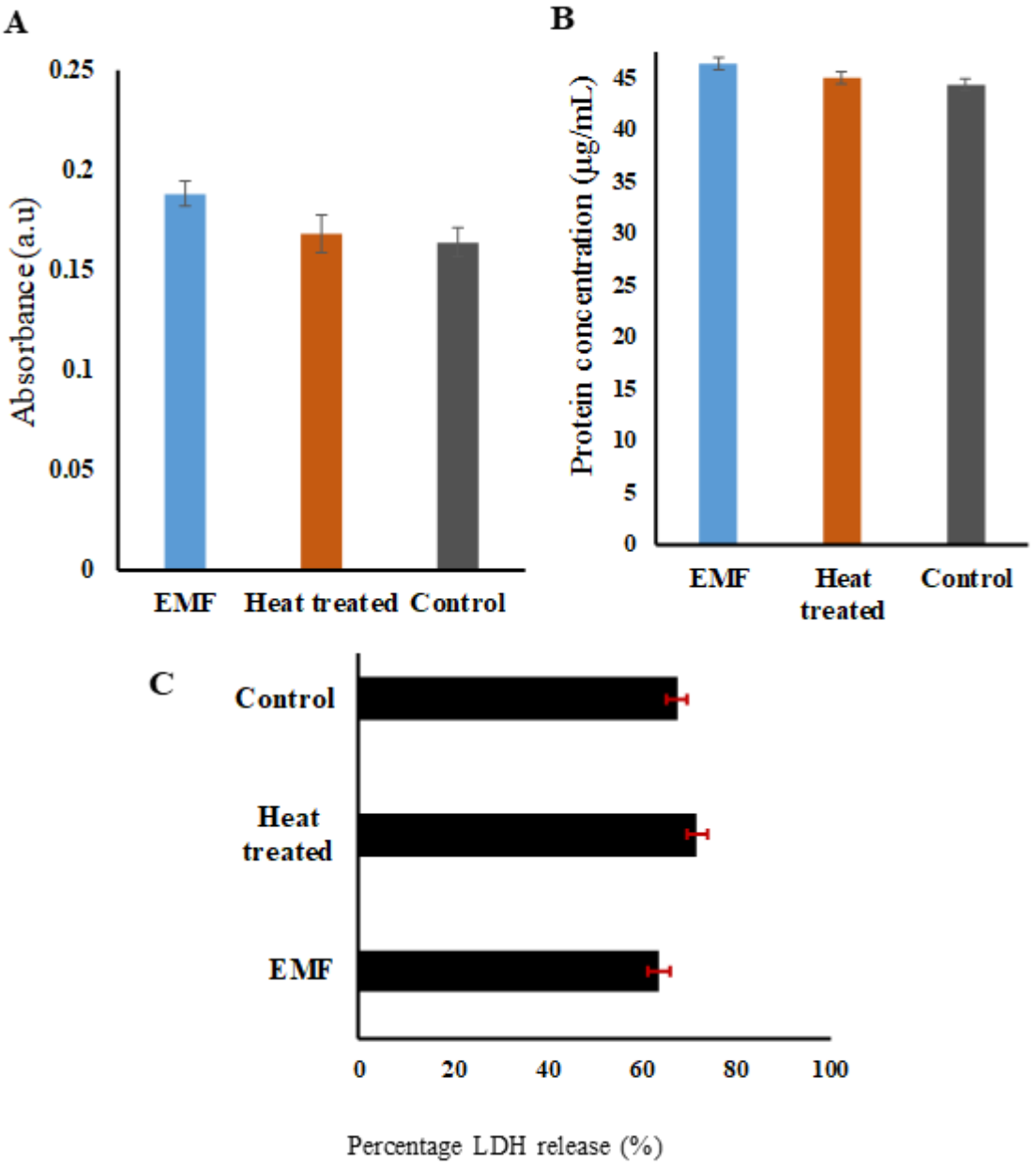

Figure 4. 5.Analysis of intra-cellular morphology of PC 12 cells. (A) Metabolic activity (MTS) **(B)** Total protein concentration (BCA) of PC 12 cells. The metabolic activity of PC 12 cells in response to EMF radiation appeared to be slightly higher than the heat-treated and the control samples but there is no significant difference (p> 0.05), in the absorbance values recorded for the EMF and the control. No significant changes in protein concentration was detected in the EMF treated groups, the heat-treated and the control groups. **(C)** LDH release by PC 12 cells. The degree of LDH release of the EMF treated and the other groups did not display any significant differences. Data are means ± standard deviation and are representative of three independent experiments (p > 0.05).

The 18 GHz EMF-treated cells exhibited a slightly higher metabolic activity in comparison to the heat-treated cells and the untreated control. Even though a higher absorbance was recorded, statistical analysis showed no statistically significant differences among EMF-treated and the Peltier heated cells(p> 0.05), EMF-treated and the untreated control cells (p> 0.05), or Peltier treated cells and the untreated control (p> 0.05) (**Figure 4.5A**).In another study, where the enzymatic activity of acetylcholinesterase (AChE) in PC 12 cells was investigated by exposing the cells to 1.8 GHz 217 GSM (Global System for Mobile Communication) for 24 h,(Valbonesi et al., 2016) it was found that subsequent to the treatment, the enzymatic activity increased 1.4 fold in comparison to the untreated control groups (Valbonesi et al., 2016).

The total protein content of the PC 12 cells was assessed using the BCA assay (**Figure 4.5B)**. The method employs the reduction of Cu^{+2} by proteins into a purple complex that can be quantified at 562 nm.(Smith et al., 1985)The total protein concentration of EMF-treated cells was found to be 46.4 ± 0.0092 µg/mL, whereas heat treated samples had a total protein concentration of 45.0 ± 0.02 µg/mL and the untreated controls had a protein content of 44.4 ± 0.02 µg/mL. A statistical analysis did not indicate any statistically significant difference in the protein concentration between EMF-treated, heat-treated and non-treated cells (p = 0.636) (**Figure 4.5B)**.

The lactate dehydrogenase release from the cells was analysed in order to assess the integrity of the plasma membrane following the EMF exposure (**Figure 4.5C**). The lactate dehydrogenase is a stable enzyme present in the cell cytoplasm in all types of cells. Cells typically release LDH into the cell culture medium when their plasma membranes are damaged, and the assay relies on measuring the LDH activity, where NADH is reduced to β-nicotinamide adenine dinucleotide(Han et al., 2011). The percentage of the LDH release was calculated after obtaining the maximum level of LDH released after a complete cell lysis. The level of release of LDH in the case of the EMF-treated sample and the control group was similar, however this can be attributed to the baseline LDH that is typically present in the serum-enriched medium used for cell growth (Hiebl et al., 2017). The already present LDH would thus contribute to the background LDH absorbance. In the heat-treated samples, however, a higher level of release of LDH when compared to that in the EMF-treated and the untreated control groups was noted. A statistical analysis revealed no statistically significant difference among all the groups, *i.e.*, EMF-treated and the Peltier heated cells (p> 0.05), EMF-treated cells and the untreated control (p> 0.05), Peltier-treated cells and the untreated control (p> 0.05) (**Figure 4.5C**).

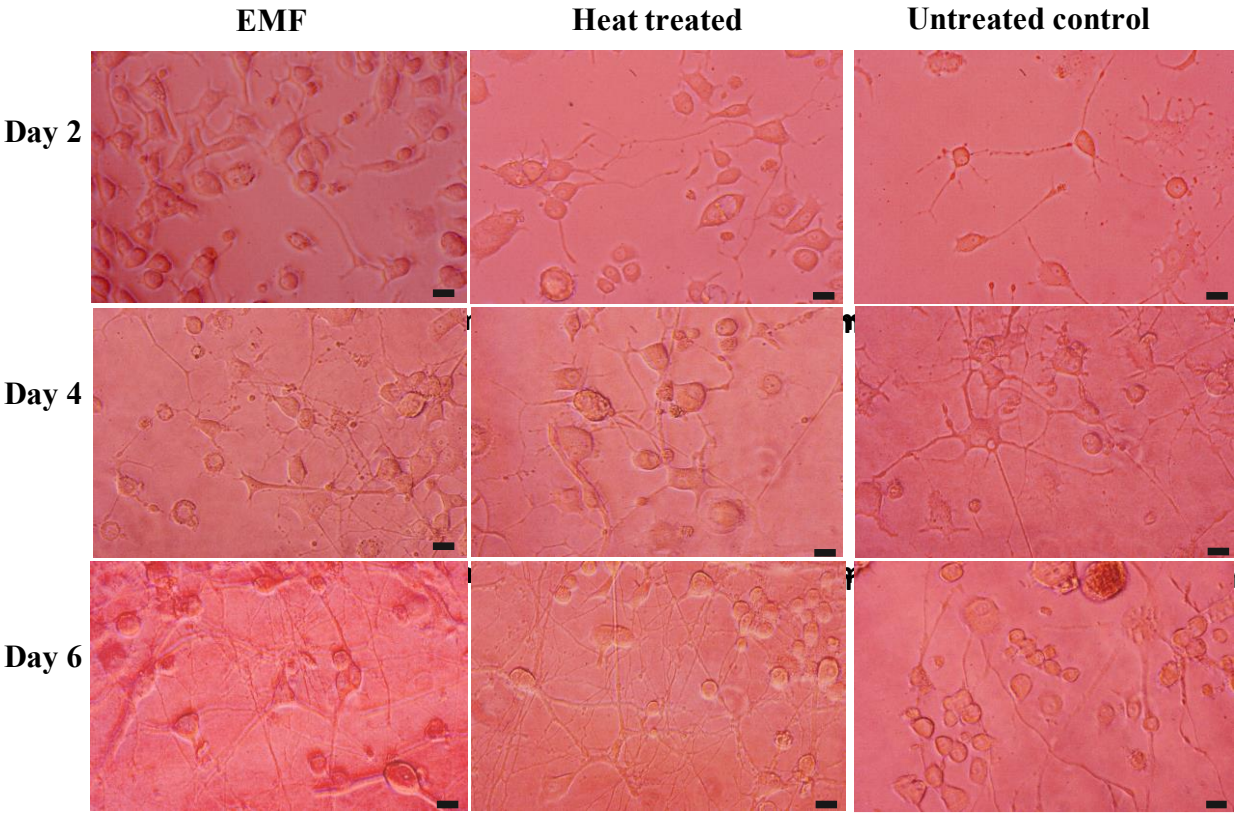

Figure 4. 6. PC 12 cell differentiation following exposure to EMFs of 18 GHz. Phase contrast images captured of EMF treated cells, heat treated and controls. The cells were seeded at a density of 3×10^4 cells / mL. Cells were seeded in full serum medium allowing for attachment and partial change of medium was carried out every two days with a NGF concentration of 50 ng/ mL in low serum medium. No changes were visualised of the neurite outgrowth under the various conditions on days 2, 4 and 6. Scale bar 5 µm.

EMFs of 18 GHz did not induce changes in PC 12 cell attachment and differentiation, approximately 90% of the cellular populations exhibited differentiation following attachment onto collagen coated surfaces in all the experimental samples. PC 12 cells in the presence of NGF concentrations of 50 ng/mL exhibits axonal outgrowth and the extent of neurite formation increased with time. Day 6 displays maximal differentiation and there are no significant differences among the samples (**Figure 4.6**).

4.4. Discussion

Thus, the results obtained in this study provided evidence that the exposure of PC 12 cells to EMFs of 18 GHz induced a significant increase in membrane permeability without compromising morphology, viability or metabolic activity of the treated cells. These results are in good agreement with that from the previous reports that showed the ability of EMF of 18 GHz induced a reversible increase in membrane permeability in different Gram-negative and Gram-positive bacterial species, including *Planococcusmaritimus*KMM 3738, *Staphylococcus aureus* CIP65.8^{T}, *S. aureus* ATCC 25923,*S. epidermidis* ATCC 14990^{T}, *Escherichia coli*; and yeast and red blood cells (Nguyen et al., 2015b, Shamis et al., 2011a).

In light of this body of evidence, it can be suggested that the phenomenon of cell membrane permeabilisation as a result of the exposure of cells to the EMF of 18 GHz is different from other cell poration phenomena achieved using a variety of techniques, including mechanical stress, sonoporation, electroporation and photoporation (Hansen et al., 2015, Zu et al., 2015, Sadiq et al., 2015). For instance, the sonoporation techniques cause permeabilization by means of ultrasound (frequency of 20 kHz with an intensity of 5 -55 W/cm^2) continuously applied to cells for 30 s – 5 min, with the resulting pore sizes of 1 – 100 micrometers (Sheikh et al., 2011). Therapies based on electroporation involve placing electrodes around or within a target tissue while delivering a series of 8 – 100 short (~ 100 μs) electric pulses of high voltage (~1000-3000 V)(Garcia et al., 2014). Photoporation delivers foreign material into cells using light generated by laser diodes operating at 450 nm at 0.3 mW for 40 ms (Paterson et al., 2005).

Similar to other cell poration techniques, the exposure to EMFs of 18 GHz could be used as a means to facilitate a more effective delivery of drugs, genes and nanoparticles into a cell for the purpose of cellular manipulation or therapy, e.g. by enhancing the uptake of chemotherapeutic drugs for cancer treatment (Geng and Lu, 2013, Hansen et al., 2015). The 18 GHz EMF may act as external stimuli, which can initiate membrane depolarization leading to permeability. Exposure of an artificial axon model to the 53.37 GHz EMF (SAR 1.1-1.6 GHz) has been shown to increase both the transmembrane K+ efflux from lipid vesicles and the transport of these ions across the lipid membrane by promoting the activity of the K+ carrier valinomycin, thereby affecting the amplitude of electrical signals that propagate through electrically excitable cells (D'Agostino et al., 2018). Furthermore, a review of 23 studies has suggested that voltage-gated calcium channels maybe activated upon exposure to EMFs, with downstream responses mediated through Ca^{2+}/calmodulin stimulation of nitric oxide synthesis and subsequent stimulation of the NO-cGMP-protein kinase G and NO-$ONOO^{-}$-oxidative stress pathways, where the former can have therapeutic and the latter have pathophysiological bioeffects, as well

as responses mediated by other processes regulated by Ca^{2+}(Pall, 2013). Evidence of EMF-induced oxidative stress in cells has been observed after repeated subject exposure to 9 GHz EMFs (SAR 0.4 W/kg),(Garaj-Vrhovac et al., 2011) with oxidative damage such as single-strand DNA breaks shown in tissues exposed to 2.45 and 16.5 GHz EMFs (SAR 1.0 and 2.01 W/kg, respectively) (Paulraj and Behari, 2006).The EMF-induced formation of reactive oxygen species, such as peroxynitrite, may result in lipid peroxidation and oxidation of proteins within the cellular membrane, thereby changing membrane fluidity, and affecting pore formation and resealing, and cell metabolism and viability (Bruno and Justin, 1994).

However, a similar nature of pore formation across multiple cell types that contain different levels of voltage-gated channels treated with 18 GHz EMFs indicates that in this case, the formation of pores may take place at the level of lipid bilayer, independently of the voltage-gated channels (Dermol-Černe et al., 2018). Furthermore, in this study, the viability, metabolic activity and membrane functional integrity of cells treated with 18 GHz EMF were not affected by the exposure.

4.5. Conclusion

Based on the results from this and previous studies that have used 18 GHz EMFs, it is clearly evident that the EMF-induced increase in permeability is not likely to originate from bulk heating of the suspension since exposure of cells to similar temperatures in the absence of MW radiation failed to induce cell permeabilisation. This leads us to believe that the observed effect is likely to be electro-kinetic in nature due to the increased conductivity and mobility of ions across the cell membrane, with potential contribution from microthermal changes that cannot be easily captured at the macro level, as well as from the direct interaction of the EMF with cell membranes and/or their structural and functional components (*e.g.*, phospholipids) (Nguyen et al., 2015b, Nguyen et al., 2016, Shamis et al., 2012c). Indeed, it is well known that when a polarized, non-ionizing electromagnetic oscillation encounters a polar or charged molecule, it transfers a fraction of its energy to this molecule, driving it to oscillate. The degree of thus-induced oscillation is greatest for unbound electrically charged particles, such as free ions that abound human tissues (Panagopoulos et al., 2013). Additional energy will be absorbed by the water dipoles, as well as by larger polar or charged molecules, including such biological macromolecules as nucleic acids, lipids, and proteins. These interactions will also result in oscillations due to the applied EMFs, however the magnitude of such energy absorption or oscillation are more difficult to estimate due to the bound nature of many such molecules. Yet, they may play an important role in the development of EMF-induced membrane permeability. Furthermore, the application of an EMF may also induce a local elastic tension through Maxwell's tensor, forcing the membrane to which the field is applied to prolate or oblate, with the result dependent on the properties of the EMF and the mechanical properties of the membrane (Portet et al., 2012, Goldberg et al., 2018).In summary, in this work we have explored the potential of 18 GHz EMF treatment to induce transient permeabilisation of cell membrane in a mammalian cell model without any detrimental effect to cell viability or metabolism, thereby providing a potential alternative to conventional poration techniques in drug delivery application.

Chapter 5. Pheochromocytoma cells (PC 12) response to synchrotron source THz frequencies of 0.3 – 19.5

5.1. Overview

High frequency (HF) electromagnetic fields (EMFs) have been widely used in many wireless communication devices, yet within the Terahertz (THz) range, their effects on biological systems are poorly understood. In this study, electromagnetic radiation in the range of 0.3 – 19.5 × 10^{12} Hz, generated by a synchrotron light source was used to investigate the response of PC 12 neuron-like pheochromocytoma cells to THz irradiation. The PC 12 cells remained viable and physiologically healthy, as confirmed by a panel of biological assays, however, exposure to THz radiation for 10 min at 25.2 ± 0.4 °C was sufficient to induce a temporary increase in their cell membrane permeability. High resolution Transmission Electron Microscopy (TEM) confirmed cell membrane permeabilization by visualisation of the translocation of silica nanospheres (d = 23.5 ± 0.2 nm) and their clusters (d = 63 nm) into the PC 12 cells. Analysis of Scanning Electron Microscopy (SEM) micrographs revealed the formation of atypical large (up to 1 μm) blebs on the surface of PC 12 cells exposed to THz radiation. Long term analysis showed no substantial differences in metabolic activity between the PC 12 cells exposed to THz radiation and untreated cells, however, a higher population of the THz treated PC 12 cells responded to the nerve growth factor (NGF) by extending longer neurites (up to 0 - 20 μm) compared to the untreated PC 12 cells (up to 20 μm). These findings present implications for the development of nanoparticle-mediated drug delivery and gene therapy strategies, since THz irradiation can promote nanoparticle uptake by cells without causing apoptosis, necrosis or physiological damage, as well as provide a deeper fundamental insight into the biological effects of environmental exposure of cells to electromagnetic radiation of super high frequencies.

5.2. Background

There has been recent growing interest, across a broad range of scientific fields, in the use of continuous-wave and pulsed electromagnetic radiation in the terahertz (THz) frequency range due to their potential for use in detection, imaging and communications technologies. The THz frequency range covers the portion of the electromagnetic spectrum that falls between microwaves and the infrared domains and is generally defined to include frequencies between 0.3 - 10 THz (Bogomazova et al., 2015). THz photons are not sufficiently energetic to break chemical bonds or cause ionisation of atoms or molecules (Zhao et al., 2014a). The ability of THz radiation to penetrate a wide variety of non-conducting materials, *e.g.,* clothing, cardboard and plastic, while being strongly attenuated in metals or water, presents a number of unique advantages for applications such as non-destructive imaging in biomedical applications, non-invasive national security and packaged goods inspection, and remote environmental sensing (Huang et al., 2018, Fan et al., 2014, Smye et al., 2001). THz radiation is also used for the time-resolved spectroscopic investigation of multibody systems and difficult-to-probe materials, such as complex nanostructures and foams, to reveal their fundamental properties including chemical composition, density, defect locations, and their technological potential (Zhao et al., 2014a). Upon interaction with molecules in a material, THz waves can induce low-energy excitations such as phonon, electronic interband, impurity-related and intraexcitonic transitions, and inter sub band excitations in solids, as well as intermolecular vibrations and translations in liquids (Michael et al., 2013). These excitations modulate the intensity and phase of the THz wave. The nature of these weak material bond vibrations and deformations correspond to specific chemical and physical properties of the material. The high coherent characteristics (*i.e.*, high spatial and strong temporal properties) of THz radiation also enhance absorption coefficients and refractive indices of samples (Weightman, 2012).

An important application of THz time-domain spectroscopy (THz-TDS) and imaging is the accurate detection and diagnosis of skin, breast, colon and liver cancer both *in vivo* and *ex vivo*(Huang et al., 2018). For example, when used on freshly excised tissues, THz-TDS operated in reflection mode was able to successfully differentiate between regions of cancerous, normal and pathologically changed tissue, with clearly distinguishable waveforms of reflected signals (Goryachuk et al., 2017). Similar results have been obtained on excised paraffin-embedded human breast tissue using THz transmission and reflection imaging, with the reflection mode providing better resolution and sharper margins between cancerous, fibro glandular, and fatty tissue regions, and the absorption mode being less sensitive to variations in tissue thickness (Bowman et al., 2016).

The viability of *in vivo* applications of THz imaging for detection of tissue hydration, corneal pathologies, skin burns and cancers depends upon the principle that terahertz photons are not energetic enough to cause lasting perturbations in biological materials, or to cause DNA damage (Wilmink et al., 2011). Whether this is indeed the case, however, remains a subject of debate as studies are limited by the scarcity of efficient THz generating sources and sensitive detectors (Weightman, 2012). For example, human dermal fibroblasts exposed to continuous THz radiation from an optically pumped molecular gas THz laser source (2.52 THz, 227 mW/cm^2) for up to 80 min were shown to be 90 % viable (Am et al., 2004, Subramanian et al., 1997, Hoop et al., 2017). When exposed to the narrow-band THz radiation (2.3 THz, 1.4 W/cm^2), human embryonic stem cells (hESCs) showed no structural chromosomal aberrations or difference in cell morphology when compared to the untreated control, and only some minor upregulations of mitochondria-related genes were reported (Bogomazova et al., 2015). Similarly, primary human keratinocytes exposed to THz radiation (0.2 to 3.0 THz, 0.45 J/cm^2) for 30 min showed only minor donor specific inhibition or stimulation of cell activity. Other groups, however, have suggested that THz radiation and thus generated electric fields may affect complex molecular processes involved in gene expression and DNA replication by inducing a large dipole moment in DNA (Smye et al., 2001), by producing vibrational modes in the hydrogen bonds in nucleobases (Fischer et al., 2002) and causing spatially localized unbinding of the strands in DNA helices (Alexandrov et al., 2010). Using mouse mesenchymal stem cells, heterogenic changes in gene expression were shown to be both irradiation and cell specific, *i.e.,* the activation and repression of genes were found to be dependent on duration and type of THz source (e.g. pulsed 10 THz vs continuous wave 2.52 THz, 1 to 3 mW/cm^2), as well as on the stage of stem cell differentiation (Bock et al., 2011).

In addition to modulating gene expression, THz exposure was also suggested to affect the cell membrane. It was previously reported that protrusions of the membrane on the cell surfaces and a decrease in the membrane potential was detected in 12 − 15% mollusc neuron cells irradiated at 30 mW/cm^2 for 1 min (Ol'shevskaia et al., 2009). Nevertheless, little is known about the specific effects of THz radiation on cell membrane and intracellular metabolic activity.

This study aims to fill this significant knowledge gap by investigating the possible effects of THz radiation (0.3 – 19.5 THz), generated by a synchrotron light source, on a model mammalian cell line, PC 12 pheochromocytoma cells. PC12 cell lines are derived from a pheochromocytoma of the rat adrenal medulla, a mixture of neuroblastic cells and eosinophilic cells (Lindenbaum et al., 1988, Refolo et al., 1989).Pheochromocytoma was chosen as a model cell line due to the large amount of background knowledge with respect to its proliferation and differentiation. The results of this study aim to provide a deeper fundamental insight into the biological effects of environmental exposure of cells to electromagnetic radiation as well as to

investigate whether THz radiation can induce transient cell membrane permeabilisation and promote nanoparticle uptake by cells without causing apoptosis, necrosis or physiological damage. The significance of the research is that it highlights the possibility of using THz irradiation of mammalian cells as a strategy to enhance nanoparticle-mediated drug delivery in the treatment of cancers(Avedisian et al., 2009)and gene therapy (Selvi et al., 2008), similar to 18 GHz radiation (Perera et al., 2018).The research investigates the efficiency of the technique in the context of delivering nanospheres into the cell and the ability of nanospheres to pass the cell membrane. The use of EMFs in delivering nanospheres can be promising in the case of metastatic pheochromocytoma. It is critical to study the specific outcomes including PC 12 cell proliferation and differentiation in the presence and after THz radiation for clinical applications.

5.3. Results

The THz treatments of the PC 12 cells were carried out according to the previously developed procedure (Section 3.6.1) and the loading of samples along with the experimental setup is depicted in **Figure 3.4 and 3.5**.

The PC 12 cells were exposed to THz radiation at frequencies ranging from 0.3 to 19.5 THz at for a period of 10 min. During the THz radiation exposure, the average temperature of the sample was recorded as 25.24 ± 0.37 °C. Assuming no power loss to the surrounding medium, the PC 12 cells were considered to absorb all the energy delivered to the sample. The increase in temperature measured in five different locations of the sample was in the range of only ± 0.37 °C due to the low power of the THz beam.

5.3.1. THz induced cell membrane permeability

Here, exposure to electromagnetic fields in the THz range triggered an increase in cell membrane permeability of PC 12 cells. Increased permeability was evidenced by an increased internalisation of silica nanospheres (d= 23.5 nm) and their clusters of ~ 63.9 nm by the cells, as compared to the untreated control cells **(Figure 5.2).** The uptake of the FITC-labelled silica nanospheres, which can be seen embedded in the cellular membrane was confirmed using Confocal Laser Scanning Microscopy (CLSM) and TEM **(Figure 5.1).** Visual examination of TEM images indicated that nanospheres were observed to line the cell membrane, as well as clusters being present in the cytoplasm, external to intracellular vesicles **(Figure 5.1).** Approximately 95% of the treated PC 12 cells were able to uptake the nanospheres following THz radiation exposure, while the nanosphere uptake by untreated PC 12 cells was negligible (4-5%). Silica nanospheres have an innate propensity to form clusters in working solution. In our recent work, we confirmed that the majority of the nanospheres in working solution appeared to be in clusters of 3-4 nanospheres with the average size of the majority of clusters being 63.9 nm (Perera et al., 2018). Single nanospheres represent less than 10 % in the working solution. The results of this study showed that subsequent to THz radiation exposure, PC 12 cells were able to internalise both individual nanospheres (red insets) and their clusters (green insets), which were then located inside the cell cytoplasm **(Figure 5.1).** The quantification of the nanospheres uptake by a single cell revealed that THz treated PC 12 cell was able to internalize 73 ± 9.8 clusters of the nanospheres, and approximately 5 ± 3.0 single nanospheres. The untreated control cells did not demonstrate any internalisation of nanospheres. Similar results were observed using electromagnetic radiation at a frequency of 18 GHz where a reversible increase in membrane permeability was observed in PC 12 cells (Perera et al., 2018) as well as

in different Gram-negative and Gram-positive bacterial species; *Planococcus maritimus* KMM 3738, *Staphylococcus aureus* CIP65.8^{T}, *S. aureus* ATCC 25923, *S. epidermidis* ATCC 14990^{T}, *Escherichia coli,* yeast and red blood cells (Nguyen et al., 2015b, Shamis et al., 2011a).

The internalization of the nanospheres by the cells was also quantified using the permeability co-efficient (Nguyen et al., 2016, Perera et al., 2018)depending on the fluorescence intensity detected from the fluorescent silica nanospheres. The concentration of the nanospheres in the THz radiation-exposed suspension was calculated to be 0.05 μg/mL, which is corresponding to 4.6×10^{7} nanospheres. By dividing the mass of a single nanosphere, the number of internalized nanospheres was 2.7×10^{12}. Since the cell concentration was adjusted to 60,000 cells/mL, the number of internalized nanospheres per PC 12 cell Notably, exposure of PC 12 cells to 18 GHz EME allowed the internalization of 2.8×10^{6} nanospheres (Perera et al., 2018). The greater number of nanospheres that could be internalised by the THz radiation-exposed PC 12 cells could be due to the longer time of exposure (10 min) compared to that of the GHz radiation exposure (30 s) (Perera et al., 2018).

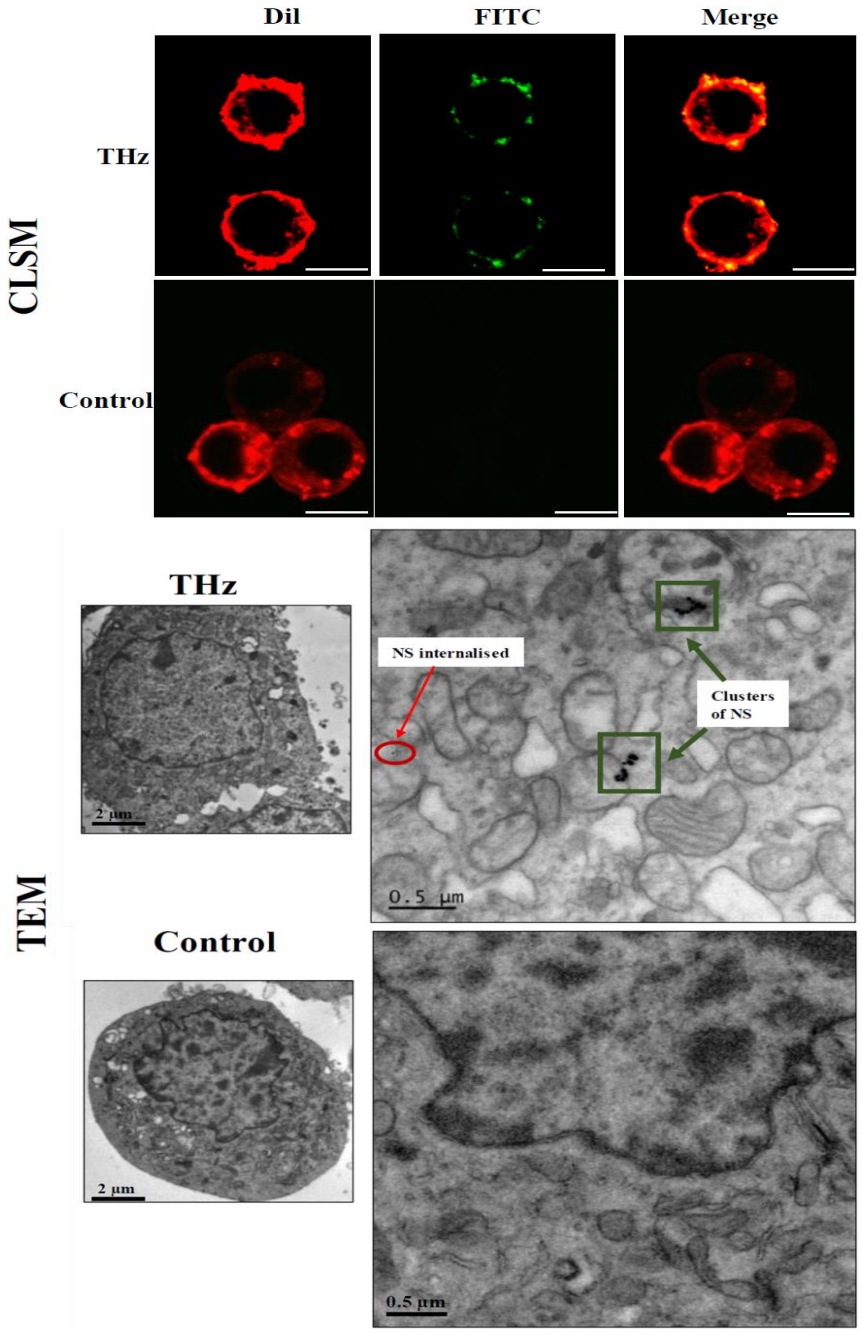

Figure 5. 1. Membrane permeabilization of PC 12 cells following exposure to PC 12 cells. Confocal laser scanning microscopy (CLSM; top row) images illustrate the uptake of silica nanospheres (FITC) by the THz treated cells whereas the untreated control does not exhibit any nanosphere uptake. No signal was detected in the FITC channel for the untreated cells. Scale bar 5µm.Thin sliced transmission electron microscopy (TEM) micrographs confirm silica nanospheres (NS) being internalised by the PC 12 cells (red arrow; bottom). Nanospheres are also seen lining the cell membrane whereas no nanosphere internalisation was observed in the untreated control cells. Scale bar 1µm.

To understand the temporal change in cell permeability, the degree of nanosphere internalisation was evaluated at time points of 5, 9, 10, 15 and 20 min following THz irradiation, and our results suggest that it was possible for THz radiation-induced permeability in PC 12 cells to last for up to 20 min **(Figure 5.2).** This is considerably longer than that achieved using electromagnetic radiation at a frequency of 18 GHz (Perera et al., 2018). The induced membrane permeability could be due to the strong dipole moments of the water molecules being induced as a result of the THz radiation exposure. It has been previously suggested that water molecules in the medium will heavily absorb the THz radiation, a process which would induce molecular vibrations that, in turn, lead to highly localised increases in temperature that may affect biological systems (Bogomazova et al., 2015, Weightman, 2012).

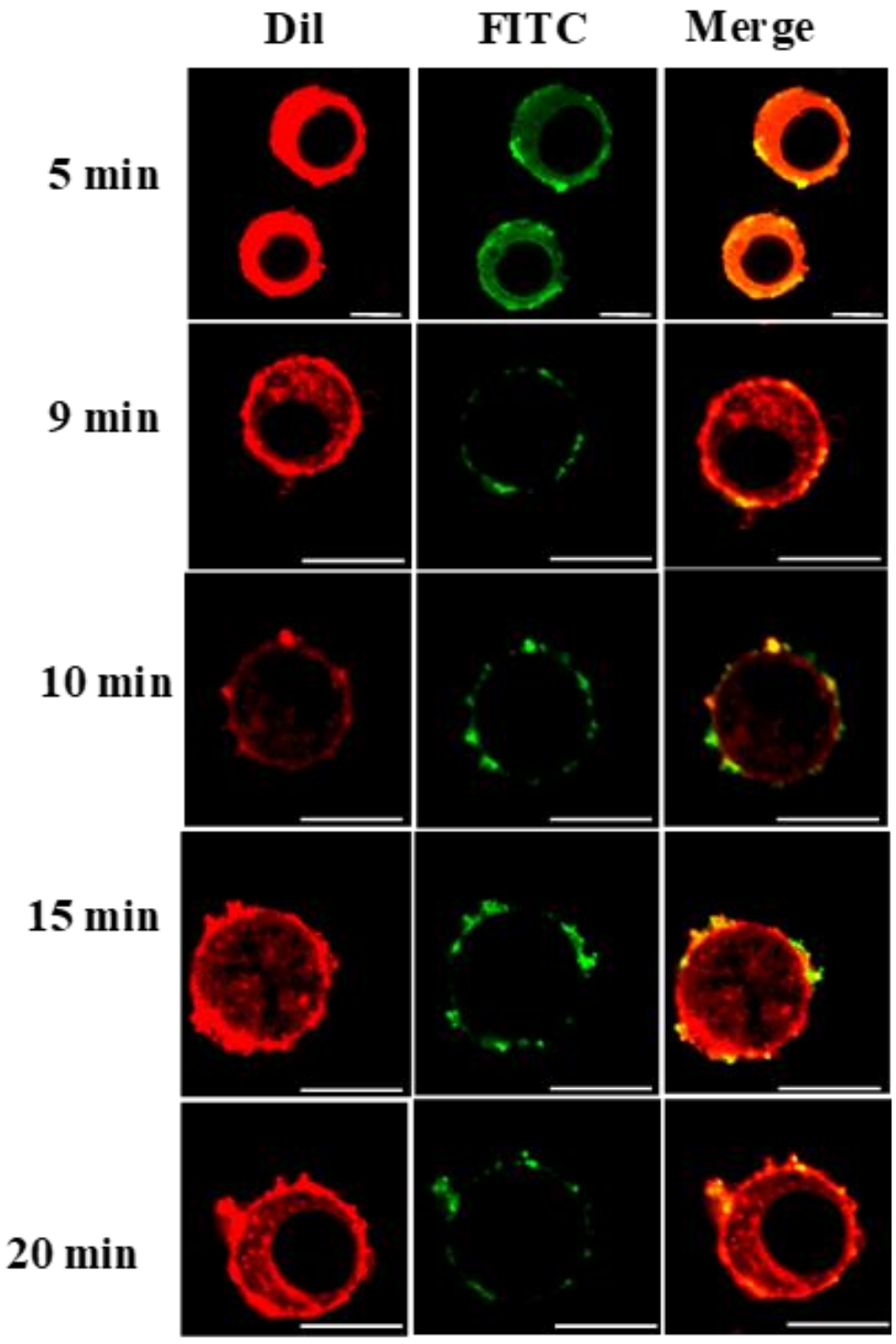

Figure 5. 2. Assessment of membrane permeability of PC 12 cell after exposure to THz radiation. CLSM micrographs showing fluorescent silica nanospheres being internalised by PC 12 cells, after 5, 9,10,15 and 20 min following exposure. PC 12 cells were permeable for up to 20 min after being exposed to THz radiation. Scale bar 10 μm.

5.3.2. THz induced effects on cell morphology and viability

In addition to changes in membrane permeability, analysis of the PC 12 cell morphology using SEM revealed the formation of large (1 – 2 μm) bleb-like structures, or spherical membrane protrusions, on the surfaces of PC 12 cells exposed to THz radiation **(Figure 5.3).** Non-treated cell exhibited typical cell morphology with small blebs of 0.3 – 0.5 μm in size. Bleb formation is observed mainly during cell migration, cytokinesis, apoptosis or cell spreading (Tinevez et al., 2009, Paluch and Raz, 2013). The formation of blebs is initiated by the contractile actomysin cortex, which creates hydrostatic pressure in the cytoplasm, thus leading to herniation of the plasma membrane (Tinevez et al., 2009). The cellular cortex consists of a thin meshwork of myosin, actin filaments and other proteins, and is able to exert pressure on the cell cytoplasm (Tinevez et al., 2009). It is possible that electromagnetic fields with frequencies in the THz range may cause deformation of the cell membrane as a result of the pressure exerted on the cell cytoplasm. It is interesting to note that no bleb formation was detected in PC 12 cells following exposure to electromagnetic fields at a frequency of18 GHz (Perera et al., 2018). In a study conducted using microwave radiation, cytoplasmic leakage was observed in *E. coli* following EMF exposure (Shamis et al., 2011a). No cytoplasmic leakage was observed in THz radiation-treated PC 12 cells, suggesting that PC 12 cells may form blebs in an effort to minimise intracellular changes induced by the THz radiation.

The viability of the PC 12 cells was investigated using CLSM and light micrographs. These studies revealed that treated cells exhibited a similar viability to that of the untreated control cells following THz radiation exposure for a period of 10 min **(Figure 5.4 A and B).** The cell number per $mm^2$was quantified and a subsequent statistical analysis did not reveal a statistically significant difference between the viability of cells in the THz-treated and control groups ($p>$ 0.05). In a study performed by Antonopoulos et al. (Antonopoulos et al., 1997), human lymphocytes were incubated in the presence of high frequency electromagnetic fields. No difference in the cell cycle progression was observed between the treated and control culture groups. Similarly, PC 12 cells exposed to 18 GHz EMFs did not show any changes in cell viability compared to that of the untreated control group, suggesting that the cells were able to remain viable after short-term exposure to EMFs of these types.

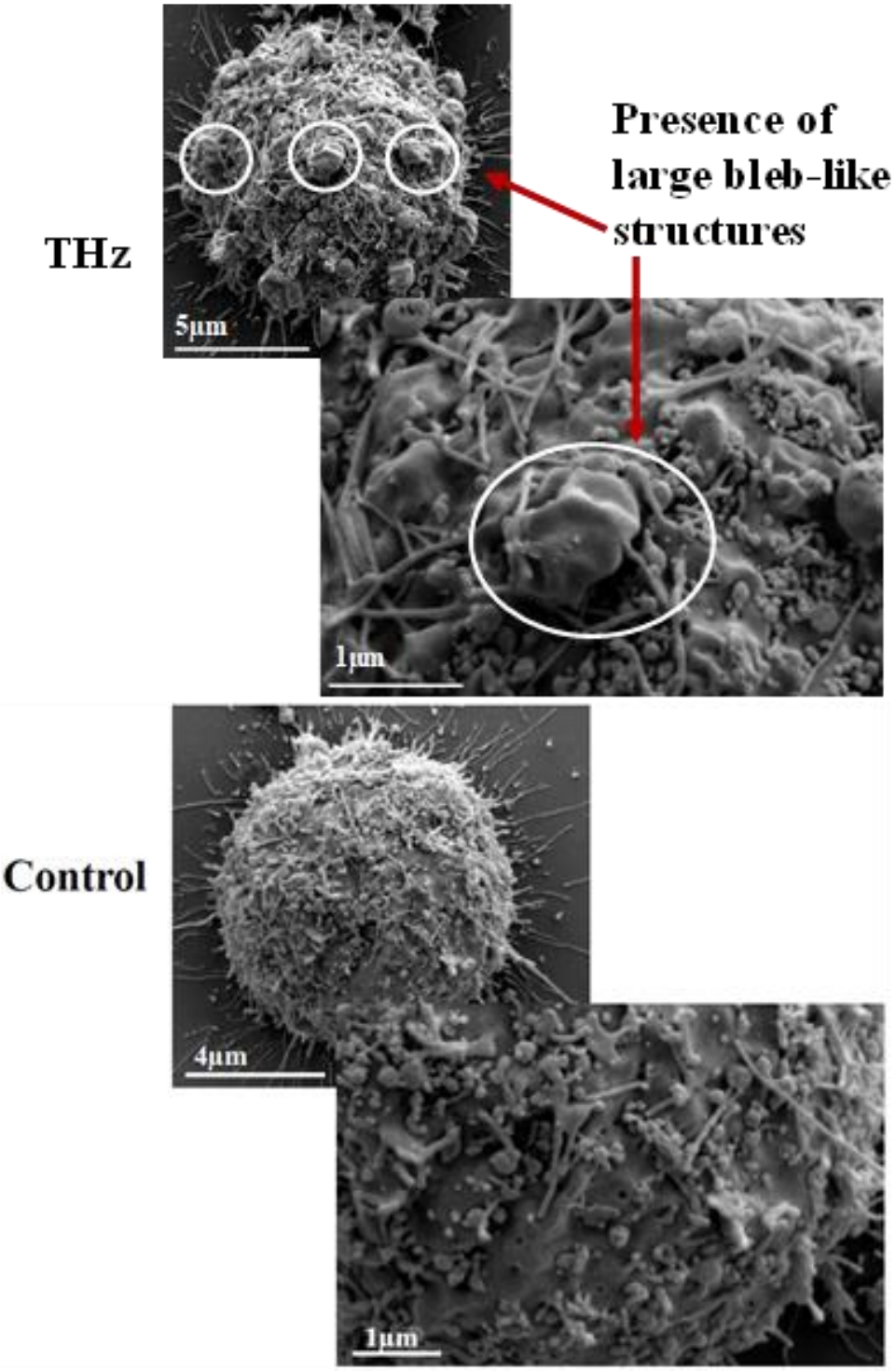

Figure 5. 3. Analysis of PC 12 cell morphology using SEM. Following exposure to THz radiation, morphology analysis revealed significant bleb formation on the PC 12 cells (circled in white) whereas blebs were not present on the untreated PC 12 cells.

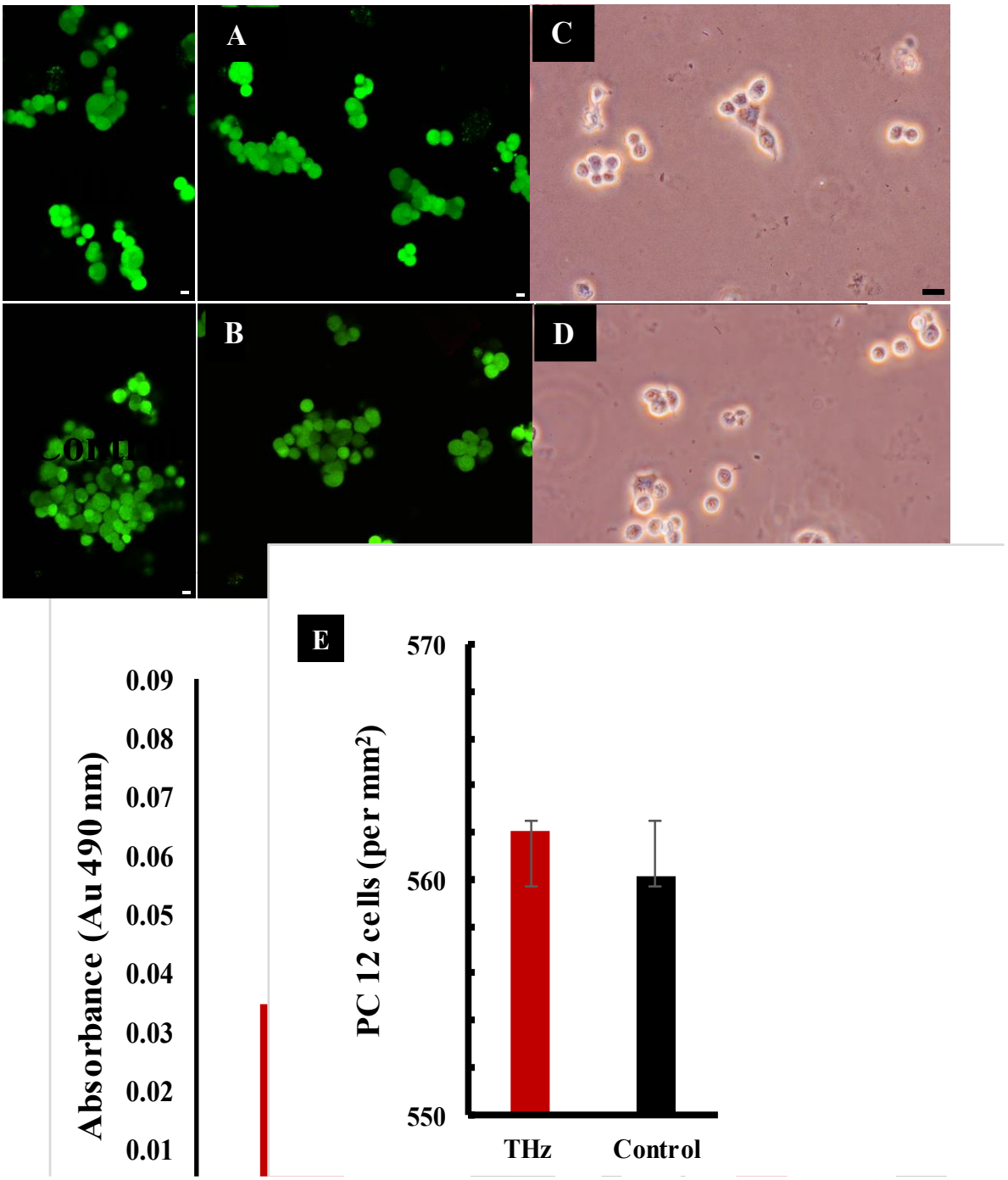

Figure 5. 4. Assessment of PC 12 cell viability following 10 min exposure to THz radiation. (A) Confocal laser scanning images showing viable (green) PC 12 cells after being exposed to synchrotron source THz radiation for 10 min. **(B)** The untreated control cells. Scale bar 5µm. **(C)** Optical micrographs of PC 12 cells following exposure to THz radiation and the **(D)** untreated control. Scale bar 10 µm. **(E)**Quantification of viable PC 12 cells following exposure to THz radiation. No significant changes in cell viability were detected between the THz treated and the control group ($p = 0.977$). Data are presented as mean ± SD and are representative of the three independent repeats.

5.3.3. EMF induced effects on intra-cellular physiology

The metabolic activity of cells was analysed immediately after 10 min of exposure to THz radiation. Increased metabolic activity was detected in PC 12 cells exposed to THz radiation in comparison to the untreated control (p = 0.803) **(Figure 5.5A).** The mitochondrial activity of metabolically active cells resulted in the conversion of tetrazolium dyeMTS (3-(4,5-dimethylthiazol-2-yl)-5-(3-carboxymethoxyphenyl)-2-(4-sulfophenyl)-2H-tetrazolium (salt) into a soluble purple formazan (Malich et al., 1997). The absorbance of formazan, recorded at 490 nm, is directly proportional to the cell metabolic activity. The reduction of MTS mainly takes place in the mitochondria, hence providing a measure of mitochondrial function (Lobner, 2000). Previous studies have shown that exposure of PC 12 cells to 18 GHz EMFs causes increased metabolic activity when compared to that of the untreated control cells (Perera et al., 2018). An increased level of enzymatic activity of acetylcholinesterase (AChE) and a higher lactate dehydrogenase (LDH) enzyme activity in *E.coli*(Shamis et al., 2012c)was also reported in PC 12 cells exposed to 1.8 GHz radiation (Valbonesi et al., 2016) . The metabolic activity of PC 12 cells was monitored every 2 days over a period of 7 days **(Figure 5.5A)** as PC 12 cells double every 36 – 48 h (Nishiki et al., 1990). At day 1, the metabolic activity of the THz treated PC 12 cells and the untreated control cells exhibited a similar metabolic activity, and this trend remained constant over the 7-day observation period **(Figure 5.5A)** (the difference in respective absorbance values was found to be not statistically significant between the two experimental groups). These results suggest that super high frequency THz radiation exposure does cause an initial short-term effect on the PC 12 cells but over a period of time, the metabolic activity of the cells returned to normal.

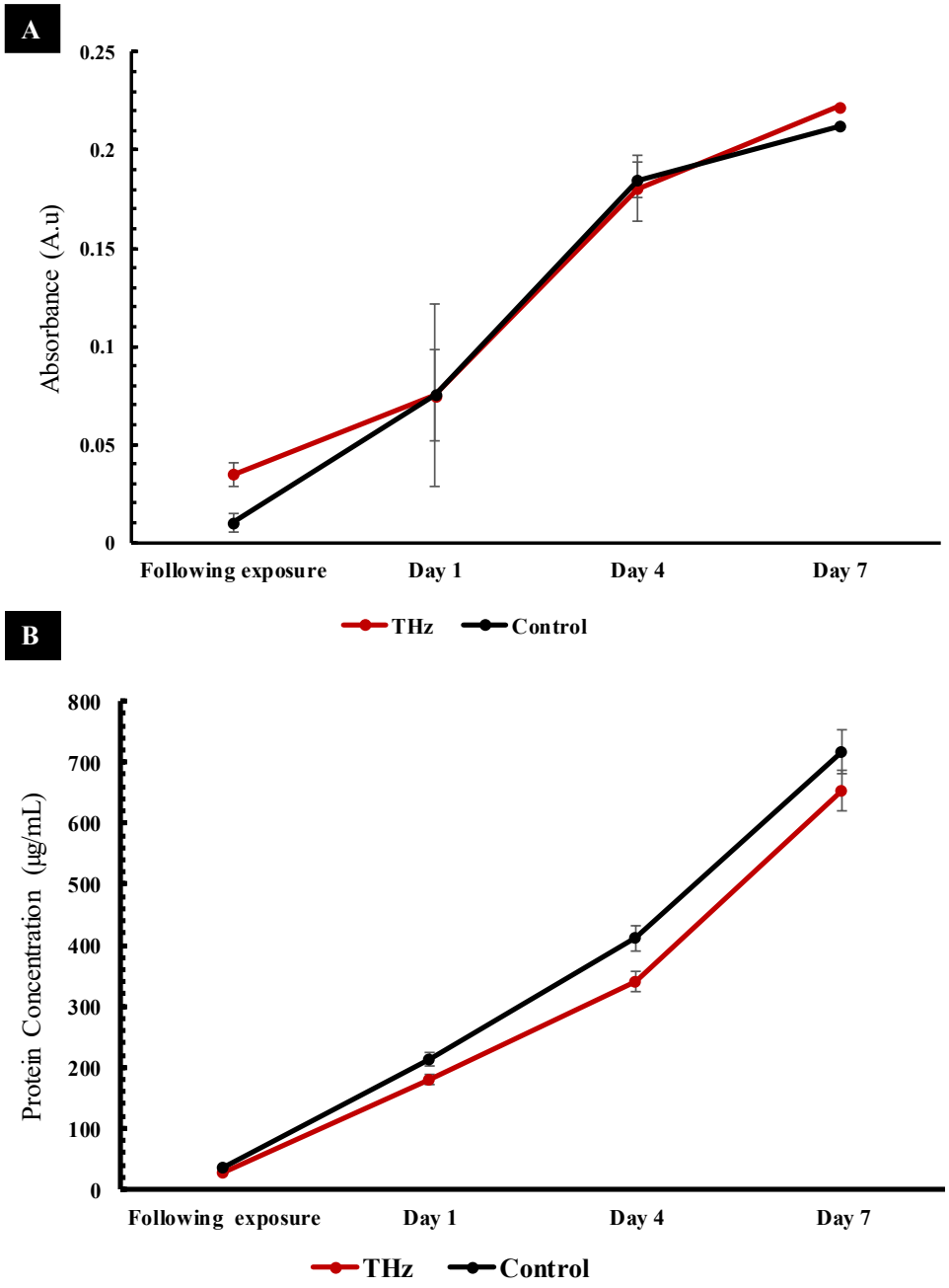

Figure 5. 5. Intra-cellular physiological analysis of PC 12 cells after THz exposure. (A) Metabolic status (MTS) over the duration of 7 days and following exposure. The metabolic activity of THz treated PC 12 cells were similar to the untreated control following exposure (p = 0.803) after day 1 and no significant changes were observed over the course of 7 days. **(B)** The total protein concentration of the THz treated sample after exposure and over a 7 day period. The total protein content of the THz treated sample was relatively low in comparison to the control straight after exposure (p = 0.574) and over the course of 7 days. The statistical analysis of the results did not reveal a statistically significant difference (p>0.05). Data are means ± standard deviation (SD) and representative of 3 independent repeats.

A bicinchoninic acid (BCA) assay was used to evaluate the total protein content of the PC 12 cells following exposure to THz radiation **(Figure 5.5B).** The technique focuses on the reduction of Cu^{2+} by proteins into a purple complex that can be spectrophotometrically quantified by measuring the absorbance at 562 nm (Smith et al., 1985). The total protein concentration of THz treated cells was found to be 28.95 ± 0.06 µg/mL. In comparison, the untreated controls had a relatively higher total protein concentration of 35.02 ± 0.01 µg/mL. Regardless, a statistical analysis did not indicate any statistically significant difference in the protein concentration between the THz-treated cells and the untreated control cells ($p = 0.574$) straight after exposure **(Figure 5.5B)**. Interestingly, the total protein concentration of the untreated PC 12 cells **(Figure 5.5B)** remained higher than that of the THz treated cells over the entire observation period of 7 days. The total protein concentrations were, however, found to be not statistically significant between the two experimental groups when tested on the appropriate days.

5.3.4. PC 12 cell differentiation in the presence of THz radiation

PC 12 cells can respond to nerve growth factor (NGF) in serum free or low serum medium by extending neurites and ceasing multiplication (Greene, 1978, Wandiyanto et al., 2018, Orlowska et al., 2017). The effect of THz radiation exposure on PC 12 cell differentiation was further investigated by treating the PC 12 cells with NGF and monitoring the neurite outgrowth for up to 7 days **(Figure 5.6).** THz-treated PC 12 cells underwent neuronal differentiation, with 86.17 ± 4.06% of the population extending neurites from 0 – 20 µm in length, while 14.90 ± 4.88% of the cell population extended neurites of 20 – 40 µm in length. The untreated control sample consisted of a population of 65.91 ± 5.04% with neurite lengths in the range of 0 – 20 µm, while 23.86 ± 3.48% had neurites in the length of 20 – 40 µm. In comparison to the control, the THz-treated cells demonstrated more neurites in the 0 – 20 µm range on day 7 and less in the range of 20 – 40 µm.

When analysing the neurite outgrowth, more than 80% ± 2.30 of the THz treated cell population exhibited 1-3 neurite bearings and 73% ± 5.13 of the control cell population exhibited 1-3 neurite bearings. Even though the THz treated sample demonstrated more neurite bearings in comparison to the control sample, the results were not statistically significant ($p = 0.855$).

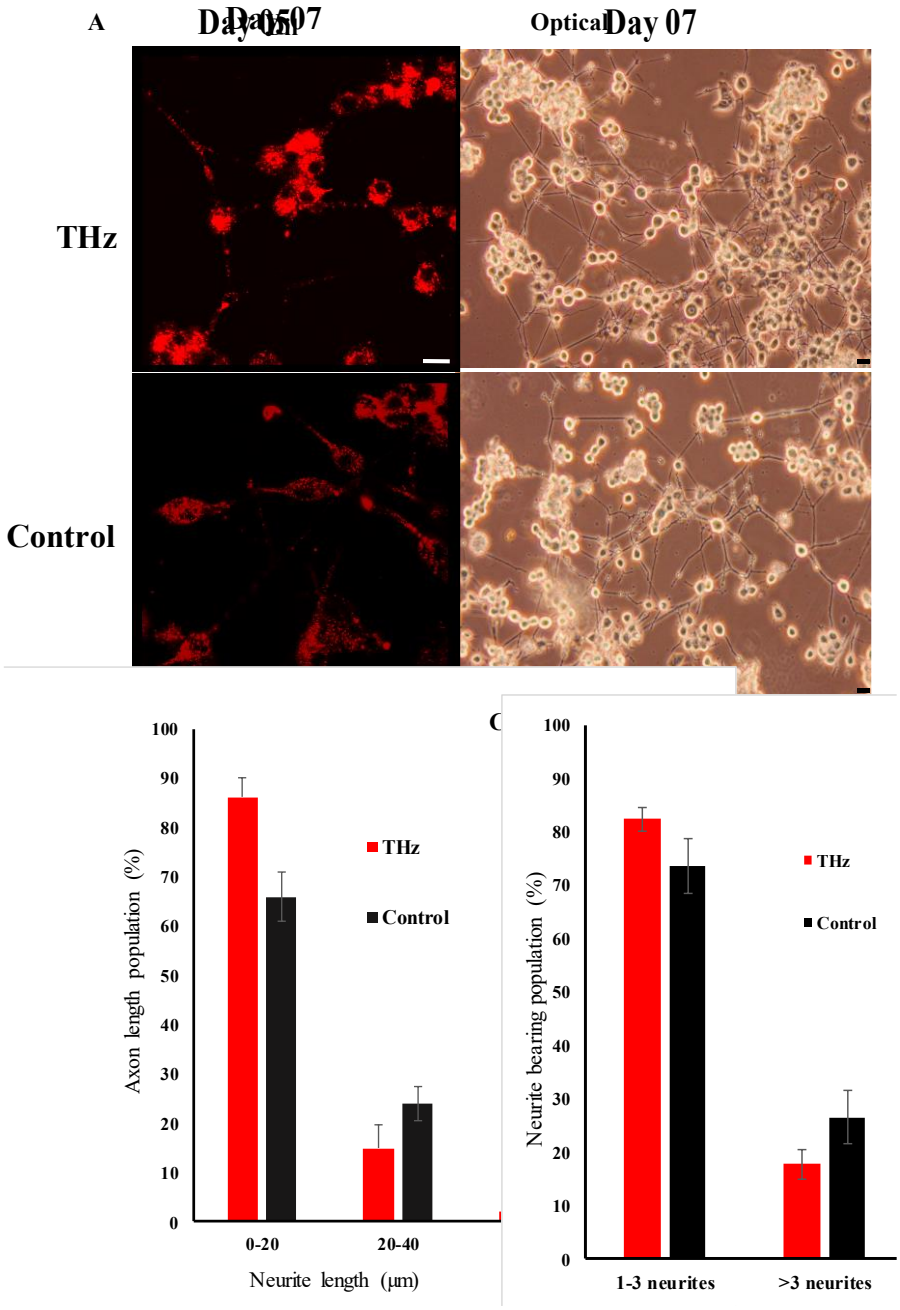

Figure 5. 6. Investigation of PC 12 cell differentiation 7 days after exposure to THz radiation. The tissue culture plates were coated with 10 µg/ mL of collagen and PC 12 cells seeded at a density of 10^6 cells/mL. Cells were grown in low serum medium with NGF at concentration of 50 ng/mL. Partial refreshment of medium was carried out every two days**. (A)** The PC 12 cells were labelled with a lipophilic membrane stain, Dil (1,1'-Dioctadecyl-3,3,3',3'- Tetramethylindocarbocyanine Perchlorate. No changes were observed among the THz treated PC 12 cells and the untreated control. Scale bar 10 µm**.** The phase contrast images were captured on day 7 of PC 12 cell differentiation. Scale bar 10, µm. **(B) Quantification of axon outgrowth**. THz treated PC 12 cells and the untreated control was able to undergo neuronal differentiation extending neurites from 0 - > 40 µm in diameter with the THz treated sample and the control mainly having extensions from 0 -20 µm ($p = 0.857$) and 20 – 40 µm ($p = 0.976$). **(C) Quantification of neurite bearing cell population.** More than 80 % of the THz treated cell population exhibited 1-3 neurite bearings whereas 73% of the control cell population exhibited 1-3 neurite bearings ($p = 0.855$). Even though the THz treated sample demonstrated more neurite bearings in comparison to the control sample, the results were not statistically significant.

5.4. Discussion

Considering the findings in this study, and those in the literature, it can be suggested that EMFs of super high frequencies in the THz range induce cell membrane permeabilisation following short exposure times (10 min). These results are in general agreement with those obtained by Fröhlich(Fröhlich, 1968), who concluded that the interactions of THz radiation with cells may arise as mediated by the excitation of biological macromolecules or nonlinear/linear resonance mechanisms (Bogomazova et al., 2015). Fröhlich also predicted that biological systems are able to support coherent excitations which fall in the range 10^9 – 10^{12} Hz (Weightman, 2012, Fröhlich, 1968). The ability of vibrational modes within protein molecules to order and condense into a lowest-frequency vibrational mode in a process similar to Bose-Einstein condensation was demonstrated experimentally using egg white-derived lysozyme, where exposure to 0.4 THz electromagnetic radiation resulted in a local increase of electron density in a long α-helix motif linked to a slight longitudinal compression of the protein helix (Lundholm et al., 2015).
A primary keratinocyte cell line exposed to THz radiation of 1-3 THz illustrated no significant difference among the control and the exposed cells (Clothier and Bourne, 2003). No signs of induced stress were observed with the exposed cells and the non-treated control cells (Clothier and Bourne, 2003). In a study conducted by (Alexandrov et al., 2013), a single frequency THz radiation of 2.52 was used to irradiate mouse mesenchymal stem cells (mMSCs) which resulted in an increase in the initiation of differentiation. The results obtained suggests that THz radiation affects gene expression leading the mMSCs towards differentiation (Alexandrov et al., 2013).

Furthermore, the existing body of literature suggests that the main targets of super high frequency EMF waves in cells are likely to be water molecules, membrane-associated proteins, *e.g.* proton F_0F_1-ATPase bioenergetic enzyme in bacterial cells, and genetic material (Soghomonyan et al., 2016). When bacterial cells were treated with either low intensity millimeter waves or electromagnetic fields of extremely high frequencies, strong effects in aqueous suspensions were seen at 50.3, 51.8, 65.5, 64.5, 95 and 105 GHz, and observed biological effects were at least in part attributed to radiation-induced changes in the structure of water molecules present in the surrounding medium (Soghomonyan et al., 2016). Since water is the main constituent in all biological systems, the energy absorbed might initiate water cluster structuring and subsequent changes (increased or decreased) in chemical activity or the level of hydration in intracellular structures and components, such as membrane-associated proteins (Soghomonyan et al., 2016, Weightman, 2012). Normal functioning of many proteins relies on changes in their conformation, often involving rotational and vibrational frequencies in the THz

region. Thus, it is likely that application of external stimulation at THz frequencies will induce transient conformational changes and temporary changes in the function and level of enzymatic activity of membrane-associated proteins, increasing conductivity and mobility of ions across cell membranes. As such, it is also likely that the mechanism of cell membrane permeabilisation in PC 12 cells is electro-kinetic in nature and is associated with the THz radiation-induced changes in membrane conductivity and ion transport (Nguyen et al., 2015b, Perera et al., 2018).

5.5. Conclusion

In summary, our findings contribute to a more in-depth understanding of how electromagnetic fields of low-energetic intensity operating within microwave and terahertz frequencies interact with cells in the context of environmental exposure *e.g.* when these waves are used for communication, remote sensing devices, and imagining. Furthermore, our findings suggest that EMFs in the range of THz radiation could be used as a powerful tool to enable a more efficient delivery of genes, nanoparticles and therapeutic drugs, where THz radiation could act as an external stimulus for rapid permeabilisation of the cell membrane while inducing negligible damage due to bulk heating. There is a strong interest in the development of effective yet safe permeabilisation strategies, with currently used techniques including electroporation using an electrical field pulse (Sadiq et al., 2015), sonoporation with ultrasound waves (Yu and Xu, 2014, Ohta et al., 2008), and photoporation using laser pulses (Banavath et al., 2018).

Chapter 6. The effect of coatings and nerve growth factor on attachment and differentiation of PC 12 cells

6.1. Overview

Cellular attachment plays a vital role in the differentiation of pheochromocytoma (PC12) cells. PC12 cells are noradrenergic clonal cells isolated from the adrenal medulla of *Rattus norvegicus* and studied extensively as they have the ability to differentiate into sympathetic neuron-like cells. The effect of several experimental parameters including (i) the concentration of nerve growth factor (NGF); (ii) substratum coatings, such as poly-L-lysine (PLL), fibronectin (Fn), and laminin (Lam); and (iii) double coatings composed of PLL/Lam and PLL/Fn on the differentiation process of PC12 cells were studied. Cell morphology was visualised using brightfield phase contrast microscopy, cellular metabolism and proliferation were quantified using a 3-(4,5-dimethylthiazol-2-yl)-5-(3-carboxymethoxyphenyl)-2-(4-sulfophenyl)-2H-tetrazolium (MTS) assay, and the neurite outgrowth and axonal generation of the PC12 cells were evaluated using wide field fluorescence microscopy. It was found that double coatings of PLL/Lam and PLL/Fn supported robust adhesion and a two-fold enhanced neurite outgrowth of PC12 cells when treated with 100 ng/mL of NGF while exhibiting stable metabolic activity, leading to the accelerated generation of axons.

6.2. Introduction

Pheochromocytoma (PC 12) cell line is commonly used in *in vitro* studies to examine neuronal differentiation and neurotoxicity implicated in neurodegenerative disease (Jesky and Chen, 2016a, Westerink and Ewing, 2008b). PC 12 cells are noradrenergic clonal cells originated from *Rattus norvegicus* transplantable pheochromocytoma (Jesky and Chen, 2016a), exhibiting reversible response to nerve growth factor (NGF). After NGF exposure, PC 12 acquire characteristic phenotypic properties associated with sympathetic neuronal like cells, which includes the inhibition of proliferation, outgrowth of neurites, and the possibility to be electrically excitable (Jesky and Chen, 2016a, Westerink and Ewing, 2008b, Gordon et al., 2013b). Upon differentiation, the neuronal like PC 12 cells start to express various integral proteins that are responsible for neurite growth (Jesky and Chen, 2016a) and can transmit signals along axons (Fuji et al., 1982a, Akeson and Warren, 1986b).

In laboratory conditions, PC 12 cells attach poorly to polystyrene tissue culture surfaces (Attiah et al., 2003a, Fuji et al., 1982a) where they grow mostly as floating cell aggregates (Attiah et al., 2003a). This poor adhesion ultimately results in insufficient neurite outgrowth (Fuji et al., 1982a). Functionalization of the surface can improve the attachment of PC 12 cells. Previously it was shown that the pre-treatment of the substrate surface with proteins, especially extracellular matrix components, enhanced not only cell adhesion but also their growth, morphology, migration, differentiation, and life-span (Kleinman et al., 1987).

Various substrate surface coatings used in PC 12 neuronal process formation have been reported, *e.g.*, glycoproteins, collagen (type IV from human placenta, type I) (Ergin et al., 2015, Ogra et al., 2016, Boczek et al., 2012a, Marino et al., 2013), laminin (Cowley et al., 1994) and fibronectin (Gordon et al., 2013b). In addition, it was shown that polyornithine (Shafer and Atchison, 1991a, Chen et al., 2014a, Pandey et al., 2015b, Connolly et al., 1984b, Gordon et al., 2013b), poly-D-lysine, and poly-L-lysine can be used to enhance PC12 cells attachment (Ergin et al., 2015, Ogra et al., 2016, Boczek et al., 2012a, Marino et al., 2013). Although Tomaselli *et al.* (Tomaselli et al., 1988) have shown that laminin and collagen type IV coated surfaces promoted PC 12 adhesion to a greater degree than fibronectin, there is a lack of systematic assessment of suitability of various coatings that would enhance attachment and differentiation of PC 12 cells.

Therefore, the aim of our study was to investigate the effect of five types of coatings including laminin, fibronectin, poly-l-lysine and their combinations on PC 12 cells attachment, proliferation and differentiation. The extent of PC 12 cells differentiation using different coatings and concentration of NGF was monitored by a set of parameters related to cellular

functions. The cell proliferation and metabolic activity were analysed by direct cell counting and MTS assay, respectively. Cell morphology and neuronal-like characteristics were analysed by using bright field phase contrast microscopy and wide field fluorescence microscopy.

6.3. Results

Single and two-component coatings were investigated in this study. The glycoproteins, such as Lam and Fn, are typical components of the extracellular matrix (Freire et al., 2002, Akeson and Warren, 1986b, Tomaselli et al., 1988, Rogers et al., 1983), and therefore both were selected. It was also reported that Lam and Fn positively influenced outgrowth of neurons, axonal guidance, differentiation and cell proliferation. Since PLL was reported to facilitate cell attachment and improve differentiation of PC12 cells (Mazia et al., 1975a), PLL was also selected. In addition to single component coating, the combinations of PLL/Lam and PLL/Fn were also studied.

6.3.1. Protein distribution on the substratum

An AFM analysis confirmed that an even distribution of the coatings was present on the plastic surfaces of the cell culture wells (Figure1A). The S_a of the control (2.2 ± 0.2 nm) was found to be similar to that present on the substrata with a single coating, namely, Fn (1.8 ± 0.1 nm) and PLL (2.1 ± 0.7 nm). The Lam coating exhibited a higher S_a of 2.9 ± 0.4 nm. The PLL/Fn and PLL/Lam dual component coatings were found to have S_a of 3.4 ± 0.4 nm and 5.8 ± 1.2 nm, respectively.

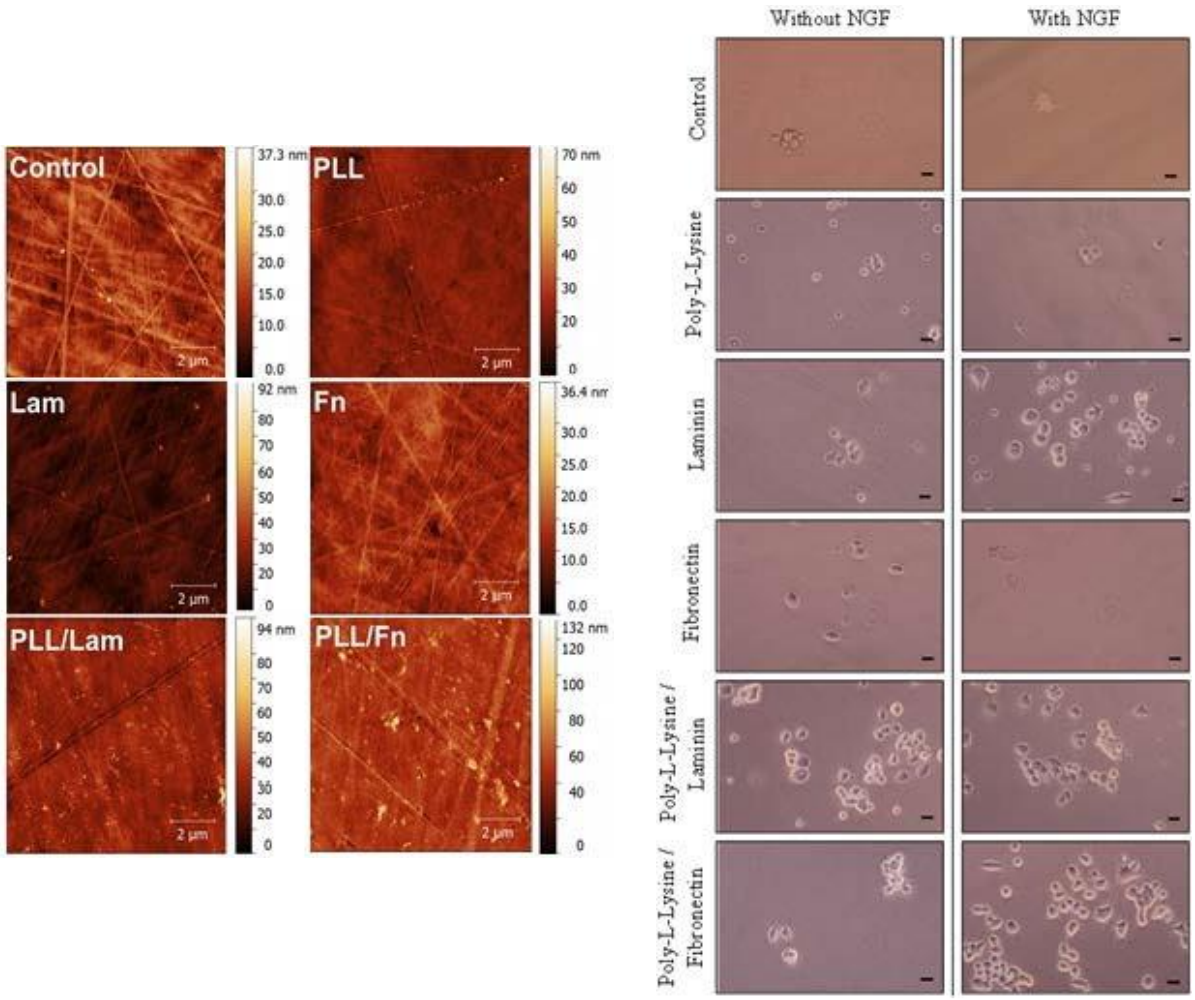

Figure 6. 1. (A) Atomic force micrographs of surfaces with different coatings. The AFM analysis show an even distribution of single and two-component coatings on the surfaces of the polystyrene substratum. **(B) Initial differentiation and attachment of PC 12 cells after two days of incubation in the presence and absence of NGF solution.** Cells were seeded at a density of 3×10^4 cells/mL on poly-L-lysine, laminin, fibronectin, poly-L-lysine/laminin, and poly-L-lysine/fibronectin-coated wells. The cells were grown in a medium that was supplemented with human recombinant NGF (50 ng/mL). The control wells did not contain any coating. In these experiments the PC 12 cells appeared to attach to the surface in clusters. Scale bar is 5 µm.

6.3.2. PC 12 cell attachment and initial differentiation in the presence of NGF

The extent of growth of the PC 12 cells on substrata containing the five different coating types, together with various concentrations of NGF, was investigated in order to identify the most suitable growth conditions for the stimulated attachment and differentiation of PC 12 cells into neuron-like cells. Cell attachment, growth, and differentiation patterns were monitored over a five-day period **(Figures 6.1B and 6.2**). The initial differentiation and attachment propensity of the PC12 cells after 48 h (day 2) was studied using phase-contrast brightfield microscopy (**Figure 6.1B**).

The densities of attached cells on the substrata possessing a single Lam coating and dual-component coatings were found to be comparable, whereas isolated, spherically shaped cells were observed without protrusions on substrata containing the PLL and Fn coatings. Enhanced levels of cell attachment were detected on substrata containing the PLL/Fn and Lam coatings in the presence of 50 ng/mL NGF **(Figure 6.1B**). In the absence of 50 ng/mL NGF, only a few cells were observed to have attached to these surfaces. These results confirmed that the presence of a coating is essential for robust cell attachment to be supported, whereas it was apparent that NGF could act as a co-factor for achieving enhanced levels of cell attachment.

In order to compare and confirm the cell differentiation processes on the various substrata being investigated, PC 12 cells were stained with a membrane specific protein and imaged using wide field fluorescence microscopy (**Figure 6.2**). Analysis of the fluorescence micrographs indicated that the dual component PLL/Fn and PLL/Lam coatings supported enhanced levels of PC 12 cell differentiation, as evidenced by the presence of neurite outgrowth. In contrast, on PLL- and Lam-coated surfaces, the PC 12 cells exhibited a lower degree of differentiation, with no or just a few non-differentiated cells being observed on the Fn- and non-coated surfaces.

PC 12 cells incubated on Fn- or non-coated surfaces exhibited little to no attachment propensity in both the presence and absence of NGF. These results are consistent with previously reported data that suggested that NGF acted as a co-factor in enhancing the attachment and differentiation of cells, however, the surface coating itself was found to be the main factor determining the extent to which cells would attach to surfaces.

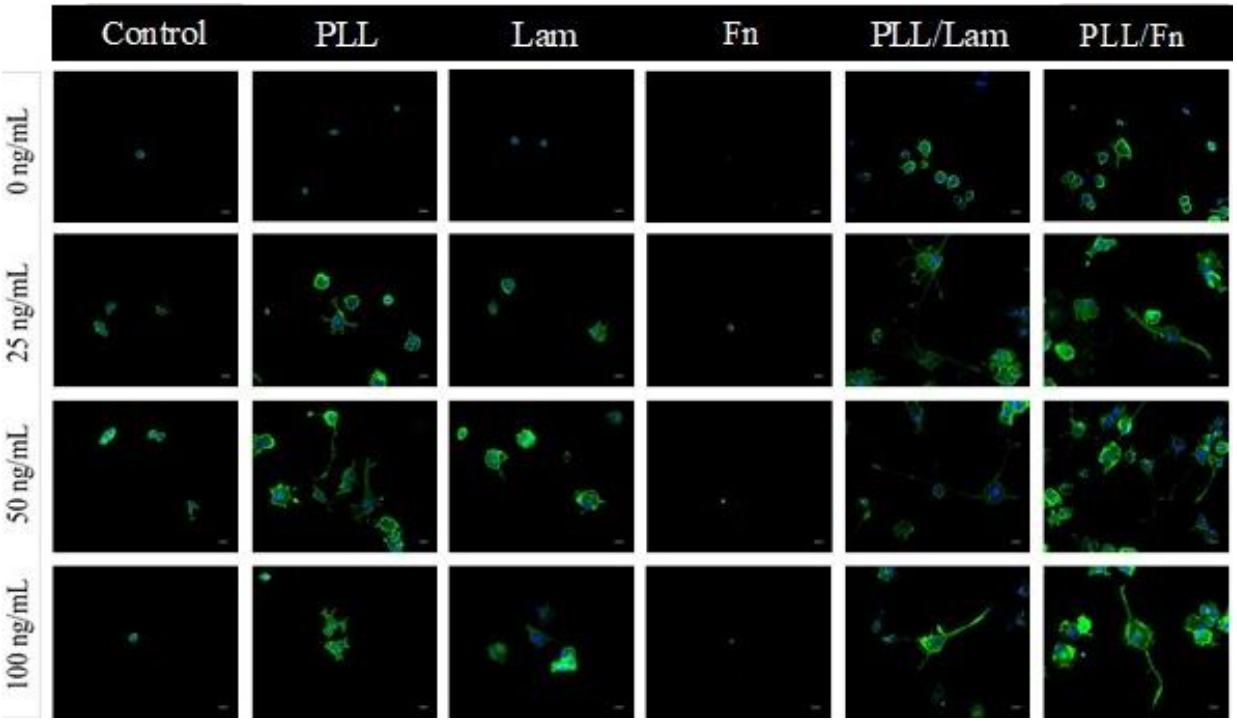

Figure 6. 2. Comparative analysis of differentiation of PC12 cells on substrata with single- and two-component coatings in the presence of NGF solution. The NGF concentrations used were 0, 25, 50, and 100 ng/mL. Cells were grown over a period of five days; fixed in 4% PFA for 15 min and stained with WGA-488 (membrane, green), DAPI (nuclei, blue). Significant neurite outgrowth was observed for cells grown on substrata with double coatings containing poly-L-lysine/laminin and poly-L-lysine/fibronectin. Substrata containing single coatings of poly-L-lysine and laminin exhibited poor cell differentiation.

6.3.3. PC 12 cells metabolic activity and proliferation

The differentiation of PC 12 cells into neuron-like cells has been found to be accompanied by an arrest in the post-mitotic G0 stage in the cell cycle, which in turn decreased their potential to proliferate (Jesky and Chen, 2016b, Westerink and Ewing, 2008a, Gordon et al., 2013a). A commonly used method for the evaluation of proliferation activity is through monitoring cell metabolic activity via an MTS assay (Berridge and Tan, 1993). In this work, an MTS assay was employed to study the metabolic activity of the PC 12 cells while attached to the different substratum surfaces. PC 12 cells grown on PLL-coated substrata exhibited an increased growth after five days when both 25 and 50 ng/mL NGF was present, compared to growth in the absence of NGF **(Figure 6.3).** At a concentration of 100 ng/mL NGF, however, a decrease in cell growth was observed. This decrease is likely to be associated with a progression of the cells into an arrested G0 stage, which is characteristic of PC 12 cells that have undergone a differentiation to form neuron-like cells. Analysis of the metabolic activity of the PC 12 cells 24 h after seeding (day 1) indicated that the metabolic activity of the cells increased in the presence of NGF, however, when cells were incubated on a PLL-coated substratum, an increase in metabolic activity was not observed. After the third day of growth, a similar metabolic activity was observed for all cells attached to all surfaces.

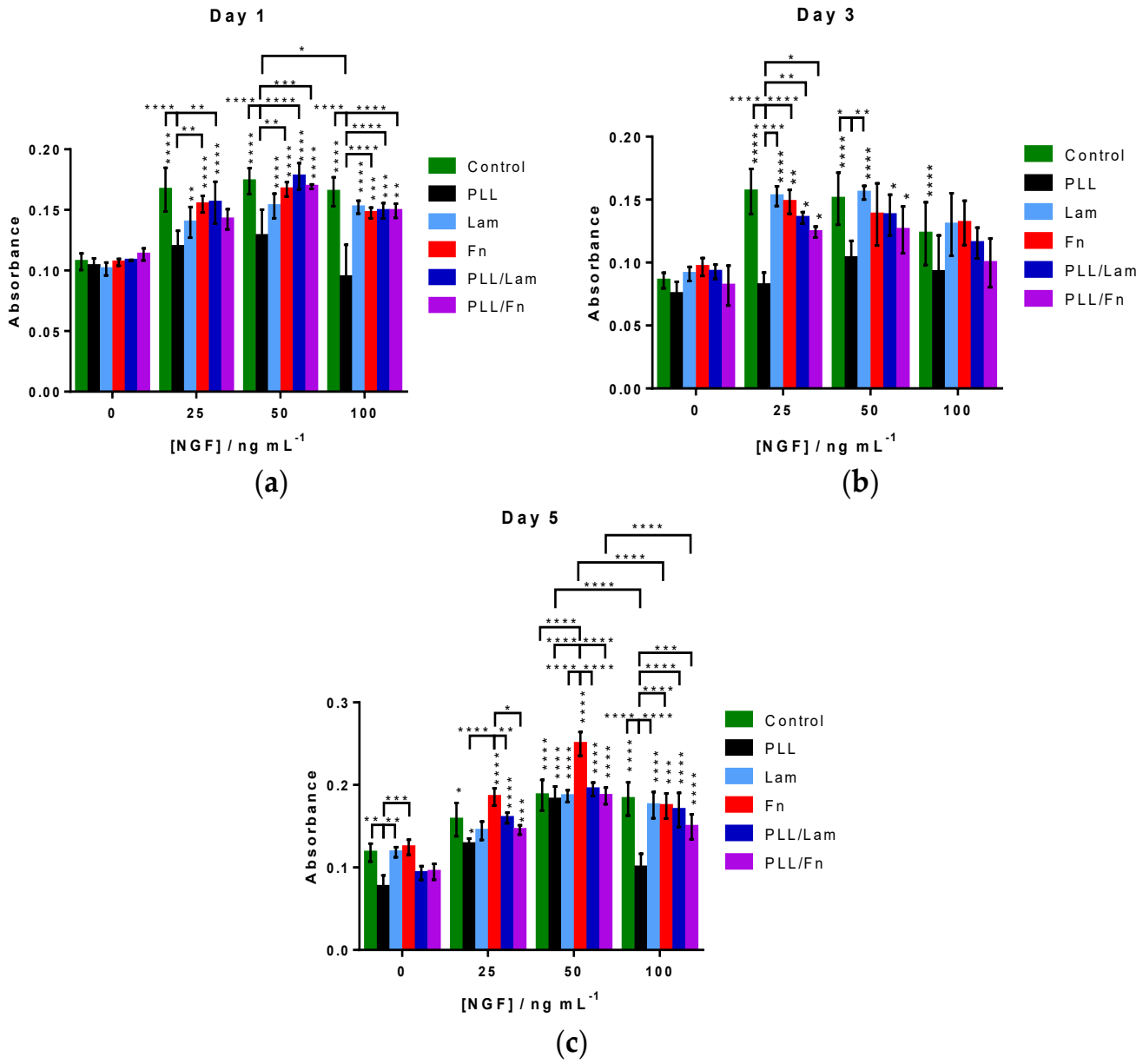

Figure 6. 3. PC 12 cell proliferation on substrata with different coatings in the presence of NGF solution. PC 12 cells were grown over a period of 5 days in the presence of 0, 25, 50, or 100 ng/mL NGF. Incubation of PC 12 cells on substratum surfaces in the presence of 50 ng/mL NGF resulted in an increased amount of attachment on day (a) 1, (b) 3 and (c) 5 compared to the other NGF solutions. Results are presented as the mean ± standard deviation. Unless otherwise specified, statistically significant differences in cell proliferation grown on the different substrata are shown versus the absence of NGF solution. "*" indicates the degree of statistically significant differences.

After the 5th day, cell proliferation was found to increase with increasing NGF concentration for all substrata. Cells incubated in the presence of substrata coated with PLL, Fn and PLL/Fn and 100 ng/mL NGF exhibited a statistically significant decrease in proliferation compared to that observed in the presence of 50 ng/mL NGF.

6.3.4. Neurite extension and outgrowth

The neurite outgrowth was evaluated for individual cells, grown under different experimental conditions. The results are presented in **Figure 6.4.** A comparative analysis of these data indicated that increases in NGF concentration stimulated the outgrowth of neurites, despite the metabolic activity of the cells being greater at 50 ng/mL (**Figure 6.3**). It was also found that substrata with two-component coatings stimulated the outgrowth of neurites in the presence of a 100 ng/mL NGF solution (**Figure 6.4**). PC 12 cells incubated in the presence of substrata with or without a single coating showed reduced levels or no outgrowth of neurites, most likely because of low cell attachment occurring on these surfaces. The substrata possessing dual component coatings stimulated the differentiation of neurites **(Figure 6.4)** after cell proliferation had been arrested (in the presence of 100 ng/mL NGF) after the 5th day of incubation (**Figure 6.3**).

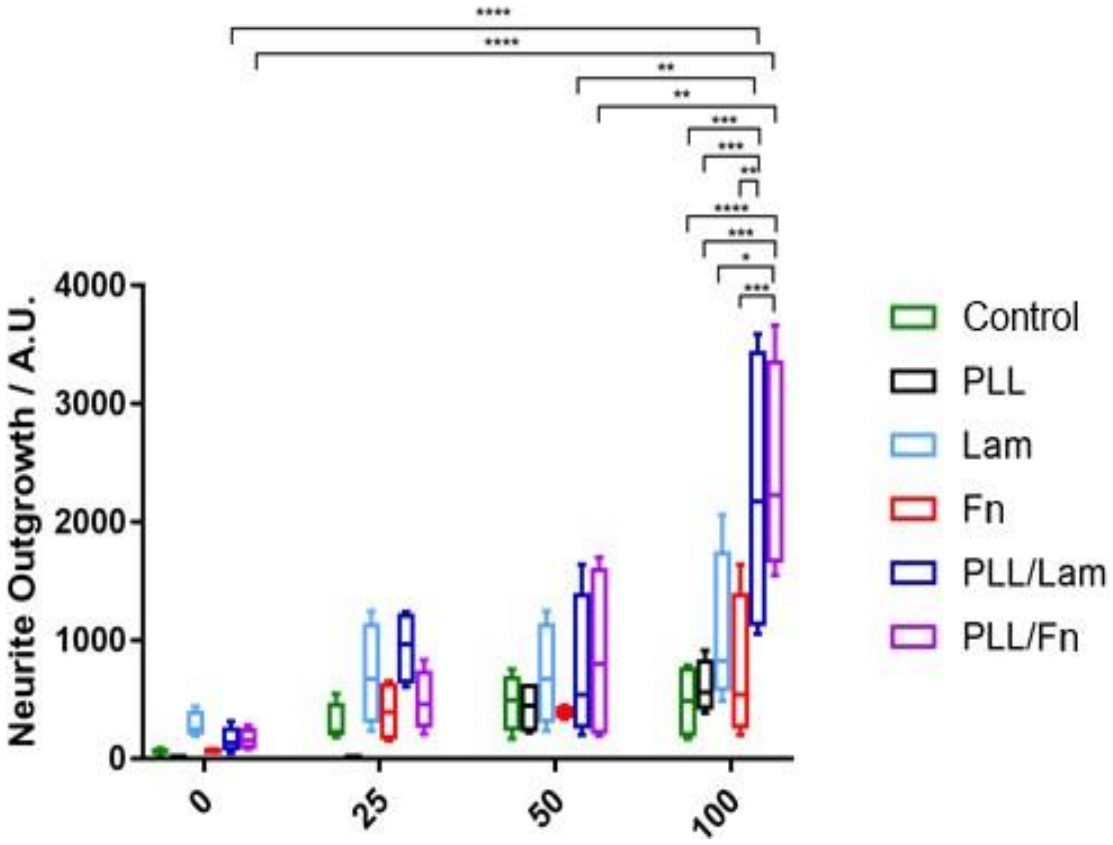

Figure 6. 4. Quantification of neurite outgrowth on different coatings under the influence of various NGF concentrations. The PC 12 cells were grown on various coatings over a period of five days and in the presence of 0, 25, 50 and 100 ng/mL NGF. Over fifty fields of view were analysed for each condition. The results indicated a two-fold greater neurite outgrowth occurring on substrata containing the dual-component coatings of poly-L-lysine/laminin and poly-L-lysine/fibronectin with increasing NGF concentrations. Results are presented as minimum, 1st quartile, median, 3rd quartile, and maximum. "*" indicates the degree of statistically significant differences.

6.4. Discussion

The results of this study have demonstrated that PC 12 cells incubated in the presence of substrata with dual-component coatings composed of PLL/Lam or PLL/Fn exhibited enhanced attachment, proliferation, and outgrowth of neurites. It is likely that this enhancement has occurred because PLL offers an increased number of cationic sites that can bind to the ionic sites present on the polystyrene surfaces of the tissue culture wells via hydrogen bonding or electrostatic interactions (**Figure 6.5A**). The glycoproteins, while effectively binding to PLL via electrostatic interactions (Fn and Lam isoelectric point of 5.5–6.0 (Vartio, 1982) and 6.4 (Paulsson et al., 1985), respectively (**Figure 6.5B,C**), also provided specific binding sites for the PC12 cells, allowing greater levels of cell attachment to take place (Pierschbacher and Ruoslahti, 1984), because cell surface receptors that promote cellular adhesion to extracellular matrices (Hynes, 1992) are known to facilitate adherence the PC12 cells (Hynes, 1992). It was also demonstrated that the cell attachment domain of Fn consists of potential chains, of β-turns, which form the most hydrophilic region for cell attachment (Pierschbacher and Ruoslahti, 1984). The integrin binding domain present on Lam (Vartio, 1982) can bind with the integrin receptors present on the surface of PC 12 cells (**Figure 6.5C**), resulting in adhesion and the initiation of cell differentiation. The PC 12 cells strongly attached to the substrata containing a PLL coating due to the negatively-charged cell membrane and nonspecific electrostatic interactions with the highly positively-charged PLL surface (**Figure 6.5A**) (Mazia et al., 1975b). The single-component coatings composed of only glycoproteins were most likely not able to support a robust attachment onto the surfaces of the tissue culture wells because of the weak binding affinity of this protein to the well surface. As a result, the PC12 cells would not have been able to withstand the washing procedures taking place during the incubation period.

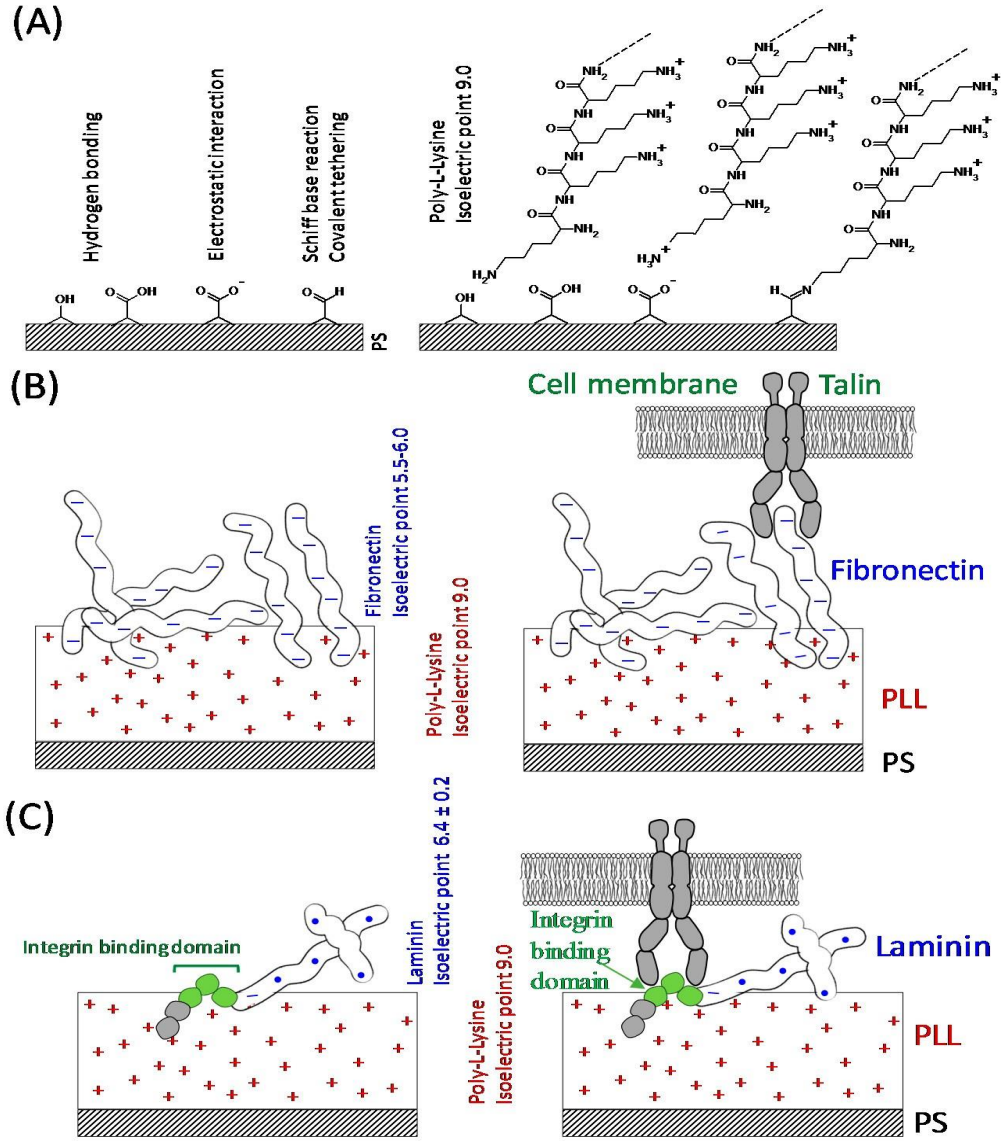

Figure 6. 5. Schematic representation of the bio-interfaces of the PC 12 cells undergoing attachment onto different substratum samples. (A) possible chemical interactions between the polystyrene substratum and the coating materials. The aldehyde and ketone groups present on the surface of polystyrene undergo a Schiff base reaction and bind covalently with the amine groups. **(B)** negatively-charged fibronectin (pI 5.5–6.0) binding to the positively charged poly-L-lysine coating via electrostatic interactions. **(C)** laminin (pI 6.4) with a net negative charge also binds electrostatically to the poly-L-lysine layer. Laminin interacts with the PC12 cell surface receptors via the integrin binding domain.

6.5. Conclusion

In summary, substrata containing the two-component coatings of PLL/Lam and PLL/Fn in the presence of 100 ng/mL NGF solution were found to result in the greatest levels of attachment of PC12 cells followed by early stimulation of cell differentiation and neurite outgrowth.

Chapter 7. Response of *Bacillus subtilis* spores to high frequency electromagnetic fields

7.1. Overview

In this chapter the effects of EMFs of 18 GHz and 0.3 – 19.5 THz on the *B. subtilis* spores have been investigated. Since the spores of *B. subtilis* are capable of withstanding extreme environmental conditions, EMFs of 18 GHz with a power of 17 W delivered a SAR of 1.38 kW kg^{-1}, however, maintaining the temperature of approximately 40 °C. Exposure of spores to THz radiation of 0.3 to 19.5 THz for 12 and 36 h after exposure was conducted at the temperatures between 22.8 °C ± 0.47 °C and 23.2 °C ± 0.3 °C, the rise in temperature was in the range of only 0.47 °C with the power being in the range of microwatts. Following 30 s exposures to EMFs of 18 GHz, spores remained unaffected as confirmed using direct plate counting techniques to monitor the spores' germination rates, SEM and TEM image analyses. It was found that after 12 h exposure at 0.3 – 19.5 THz, no changes in spores' morphology and viability have occurred, while after 36 h exposure the spores appeared disintegrated as revealed through the examination of SEM and TEM images. A four-fold reduction in spore germination has been also observed. The mechanism of the effects of SHF EMF remains unclear at this stage.

7.2. Introduction

The emission of electromagnetic radiation from mobile phones, smart meters and as cosmic background radiation leads to concerns as their exposure ranges from single biomolecules to cells and to whole organisms (Sitnikov et al., 2019, Sherrard et al., 2018, Perera et al., 2019). The outcome of the interaction of electromagnetic fields (EMFs) with biological entities is still a matter of controversy requiring further study (Sitnikov et al., 2019, Perera et al., 2019).

Previously it was reported that SHF EMF of 18 GHz was able to induce a reversible membrane permeability in different Gram-negative and Gram-positive bacterial species, including *Planococcus maritimus* KMM 3738, *Staphylococcus aureus* CIP65.8^{T}, *S. aureus* ATCC 25923, *S. epidermidis* ATCC 14990^{T}, *Escherichia coli*; and yeast and red blood cells (Nguyen et al., 2015b, Shamis et al., 2011a). It was also reported that EMFs using eukaryotic cell lines have shown enhanced osteogenesis in mesenchymal stem cells (Bloise et al., 2018) increased reversible membrane permeability and differentiation in pheochromocytoma cells (PC 12) (Perera et al., 2018, Perera et al., 2019) at 18 GHz and 0.3 – 19.5 THz. Pulsed weak EMFs have also shown to stimulate rapid accumulation of reactive oxygen species (ROS) (Sherrard et al., 2018) whereas the exposure of human neuroblastoma in the frequency of MHz have exhibited reduced menadione-dependent DNA oxidative damage (Falone et al., 2018).

In this study, the interaction of SHF EMFs (GHz and THz) with the dormant *B. subtilis* spores was investigated for the first time as the initial step in understanding the effect of electromagnetic radiation on bacterial spores using the spores of *B. subtilis.* Heterotrophic, non-pathogenic, spore-forming *B. subtilis* bacteria are commonly found in soil (Driks, 1999, Yen Shin et al., 2015, Plomp et al., 2005) vegetative cells are exposed to harsh environmental conditions and nutrient deprivation (Yen Shin et al., 2015, Grossman and Losick, 1988, Dittmann et al., 2015, Moeller et al., 2009) leading to a metabolically dormant and close to indestructible cell (Driks, 2002, Kaieda et al., 2013). Spores are highly resistant to an extreme temperature, chemicals, UV (Ultra-violet) and ionising radiation because of the unique structure of the spore coat (Rao et al., 2016, Setlow et al., 2016, Dittmann et al., 2015, Moeller et al., 2009). The remarkable resistance of the bacterial spore is due to its coat (approximately 1 μm in diameter) consisting of approximately 70 different proteins that protect the spore from environmental

insults (Wu et al., 2015, Henriques and Moran, 2007, McKenney et al., 2013, Driks, 1999). The proteins are extensively cross-linked via a modified peptidoglycan spore cortex; the core contains water enriched with calcium chelate of dipicolinic acid (DPA) and small acid - soluble proteins (α/β-type SASPs) (Moeller et al., 2009). The complex spore structure is recalcitrant to biochemical analysis hence the molecular details of this structure remains largely unknown (Wu et al., 2015). As the spore formation initiates, the cell will first create an internal protoplast containing a copy of its own chromosome (Driks, 2002). During the process of spore formation, asymmetrical division occurs in a single rod shaped cell which will generate two genetically identical daughter cells with morphologically distinct compartments (Tan and Ramamurthi, 2014, Driks, 2002) consisting of a larger cell which is referred to as a 'mother cell' and a smaller 'forespore' (Tan and Ramamurthi, 2014, Sharp and Pogliano, 1999). The membranes of the larger mother cell will migrate around engulfing the forespore (Sharp and Pogliano, 1999). Towards the completion of this process the leading edges of the migrating membranes encounter and fuse which will then release the forespore into the large mother cell cytoplasm (Sharp and Pogliano, 1999).

7.3. Results and Discussion

Upon exposure of the spores to EMFs of 18 GHz, the a SAR value was estimated being1.38 kW kg^{-1} assuming minimal or no heat loss to the surrounding medium, which was water with a specific heat capacity of 4.18 kJ kg^{-1} C^{-1}. The rate of temperature was 0.33 °C for the first 30 s of exposure, the average increase of temperature was recorded to be32.58 °C ± 2.07 °C (Figure 3.6C). Exposure of spores to THz radiation of 0.3 to 19.5 THz for 12 and 36 h after exposure was conducted at temperatures between 22.85 °C ± 0.47 °C and 23.25 °C ± 0.3 °C. The rise in temperatures in the sample following exposures measured in four independent experiments was in the range of only > ± 0.47 °C due to the low power of the beam in the range of microwatts.

Analysis of the rates of spores' germination after exposures revealed that the EMFs in the range of GHz didnot cause changes in the rates of spore germination following a 30 s exposure. Spore viability after 12 h of THz exposure was similar to that of the untreated control samples, whereas statistically significant changes were observed after 36 h long exposures **(Figure 7.1)** in the percentage of germination (p = 0.041).

In order to understand the possible cause leading to changes in germination, a thorough understanding of the spore structure is necessary. The *Bacillus* spore structure (Figure 4; untreated control) consists of an inner spore core surrounded by an inner forespore membrane, a cortex, outer forespore membrane and an exterior spore coat consisting of different layers (Plomp et al., 2005). DNA or the genetic material and DPA associated with calcium ions are present in the spore core surrounded by an inner membrane with low permeability to small solutes, ions and water (Plomp et al., 2005, Kaieda et al., 2013). The spore cortex consisting of a cross-linked with proteins thick layer of modified peptidoglycan, which helps to preserve resistance to heat and maintain dormancy (Yen Shin et al., 2015, Plomp et al., 2005). The cortex is said to maintain a lower water activity in the spore core (Kaieda et al., 2013). The core contains less water than the cortex and the water content of the core is inversely related to the spores heat resistance (Kaieda et al., 2013). The multilayer spore coat is made up of carbohydrates and structural proteins and it plays an important role in the protection and germination of spores (Plomp et al., 2005, Kaieda et al., 2013).

Examination of the internal structure of *B. subtilis* spores using transmission electron microscopy following exposure to EMFs of 18 GHz revealed no changes in the internal structure of the spores in comparison to the untreated control (**Figure 7.2**). SEM micrographs, however, revealed that following exposure to EMFs of 18 GHz, the spores appear to have a dehydrated structure as seen on Figure 3 whereas no change was observed in the untreated control sample. Previously, similar effect was observed in *E. coli* cells that were exposed to EMFs of 18 GHz. The cells exhibited dehydrated appearance similar to that observed with the spores (Shamis et al., 2011b). (Shamis et al., 2011b) also reported in the same study that the cell viability of *E. coli* was not affected and the EMF treatment was not bactericidal.

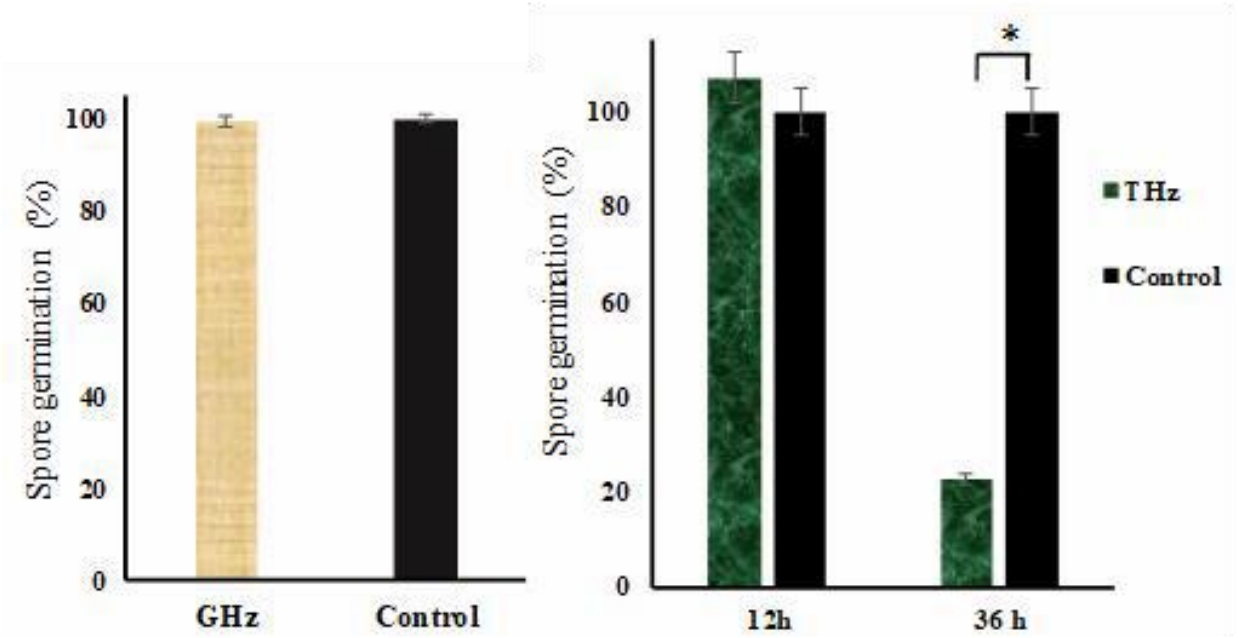

Figure 7. 1. ***B. subtilis*** **spores' viability following GHz and THz exposure.** Viability of the spores were not affected following GHz exposure. The 12h THz treated sample and the untreated control did not exhibit a reduction in the viable counts. A statistically significant reduction was exhibited after 36 h of THz exposure in comparison to the control ($p = 0.041$).

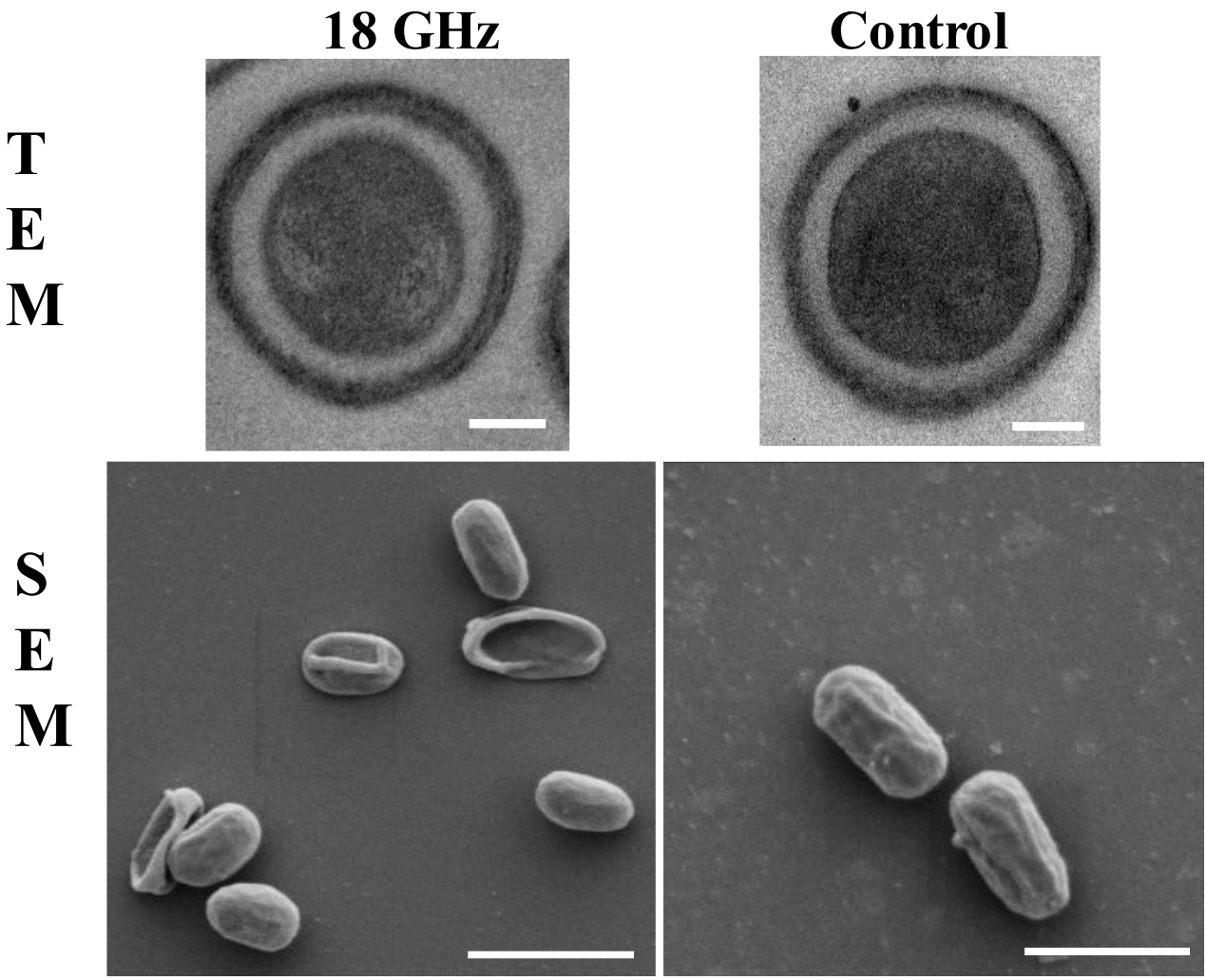

Figure 7. 2. *B. subtilis* spores' morphology following exposure to 18 GHz. TEM micrographs revealed no changes in the internal structure of the spores after exposure to 18 GHz. Scale bar 200 nm. The morphology of the GHz treated spores appears to be different to the untreated control. Spore morphology changes following GHz exposures of 30 s, spores appear dehydrated but no changes in spore viability detected. Scale bar 2 μm.

Following exposure to long term THz radiation of 36 h, the internal structure of the spores appeared to be affected as shown in Figure 734. Apart from internal damage to the spore core and the external layers, SEM micrographs displayed altered spores' morphology in the THz treated samples (**Figure 7.3; SEM**). The affected spores are highlighted in the red insets. It seems the spore core containing the DNA might be damaged (Plomp et al., 2005, Moeller et al., 2009) as observed in the TEM micrographs. For survival, bacterial spores must maintain integrity of their DNA for long periods, failure to do so will lead to the accumulation of DNA damage in their genomes as spores are metabolically inactive during dormancy whereas vegetative cells are capable of constantly repairing their DNA. After 36 h prolonged exposure to THz radiation, a four times reduction in germination of the spores was found **(Figure 7.1),** which could be due to dormant spores' inability to repair the cumulative damage on genomic DNA before transcription and beginning of replication (Moeller et al., 2009). In a study conducted by (Dittmann et al., 2015) it was reported that dormant *Bacillus* spores retain a highly ordered crystalline core structure that contains the genetic material, *i.e*., DNA, but only in the presence of small acid soluble proteins (SASPs) which are capable of protecting spore DNA (Moeller et al., 2009). Genomic instability due to long exposures to THz radiation was also reported by (Korenstein-Ilan et al., 2008) in lymphocytes and the authors suggested that THz radiation at a frequency of 0.1 THz was able to excite low-frequency collective vibrational modes of biomolecules (Korenstein-Ilan et al., 2008). Moeller et al. conducted the experiment with *B. subtilis* spores using EMFs in the range of UV light with a wavelength of 254 nm and have demonstrated that the spores of *B. subtilis* exhibited a higher degree of resistance (10 to 50 times) in comparison to vegetative cells (Moeller et al., 2009). It was reported that α/β-type SASP play a major role in spore resistance to 254 nm, dry heat, wet heat and oxidizing agents but not SASP-γ (Moeller et al., 2009). Interestingly, the spore water content was reported to affect the extent of resistance to hydrogen peroxide, moist heat but not EMFs in the range of UV radiation (Moeller et al., 2009). It was also suggested by Kaieda et al that bacterial spores possess an internal water content of about 10% but the mobility of core water remains controversial (Kaieda et al., 2013, Beaman et al., 1982). It has been proposed that the entire bacterial core exists in a glass state or an amorphous solid-like state (Alblett et al., 1999, Kaieda et al., 2013).

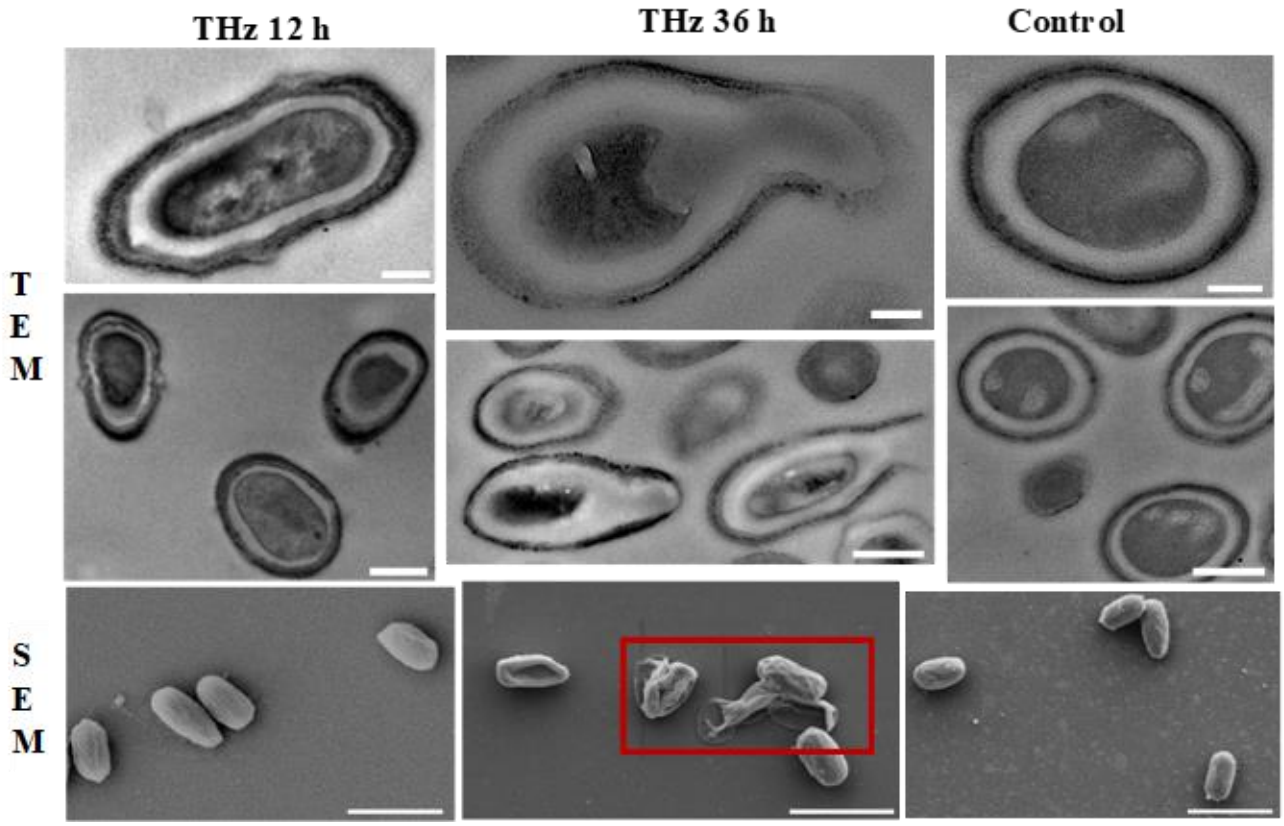

Figure 7. 3. *B. subtilis* spores' morphology following exposure to synchrotron THz radiation after 12 and 36 h. TEM Slicing of the 12 h THz treated spores did not exhibit any changes in comparison to the untreated control, whereas the spores were disintegrated after 36 h in the presence of synchrotron THz radiation. The spore core and the layers forming the spore capsule appear to be affected in 36 h exposed sample. Scale bar 200 nm (top row) 0.5 µm (middle row). The SEM micrographs illustrate no changes in the morphology of the spores after 12 h of THz exposure, however the spores following 36 h treatment appears to be damaged in comparison to the untreated control group. Scale bar 2 µm.

Upon interaction with EMFs in the range of THz radiation, the reduction in spore germination after 36 h of exposure due to disintegration of the spore core is not likely to originate from bulk heating due to negligible or no increase in temperature. Previous exposures of PC 12 cells to THz radiation and different bacterial strains to 18 GHz (Nguyen et al., 2015a, Nguyen et al., 2016, Shamis et al., 2012d) induced reversible cells' permeability, which was not detected in the untreated cells and the Peltier heat treated samples (Perera et al., 2018, Perera et al., 2019). In light of these results, it was suggested that observed effect is likely to be electro-kinetic in nature due to the increased conductivity and mobility of ions across the cell membrane, with potential contribution from microthermal changes that cannot be easily captured at the macro level, as well as from the direct interaction of the EMF with cell membranes and/or their structural and functional components (*e.g.*, phospholipids) (Nguyen et al., 2015a, Nguyen et al., 2016, Shamis et al., 2012c). It is known that non-ionizing EM oscillation on encountering a polar or a charged molecule transfers a fraction of its energy to the molecule which in turn starts to oscillate. The degree of thus-induced oscillation is greatest for unbound electrically charged particles, such as free ions that abound human tissues (Panagopoulos et al., 2013). Of most interest is the additional energy absorbed by water dipoles. It was reported that water molecules in the hydration shell and a biomolecule, *i.e.*, lactose, oscillate coherently relative to one another, where the coherent oscillation of water in the hydration shell absorbs more strongly in the THz region (Heugen et al., 2006) in comparison to as it does in bulk form. It can be assumed that the effects from THz exposure could be due to the strong absorption of THz radiation by the water molecules present in the core and the cortex of the spores and their driven oscillations which may agitate large biomolecules; however, the magnitude of such energy absorption or oscillation is more difficult to estimate due to the bound nature of many such molecules.

7.4. Conclusion

In conclusion, the spores of *B. subtilis* were unable to withstand long exposures of THz radiation and resulted in a decrease of spore germination in comparison to the untreated controls. For survival, bacterial spores must maintain integrity of their DNA for long periods, failure to do so will lead to the accumulation of DNA damage in their genomes as spores are metabolically inactive during dormancy whereas vegetative cells are capable of constantly repairing their DNA. It is likely that as a result of prolonged exposure (36 h) to THz radiation, a reduction in germination of the spores could be due to their inability to repair the cumulative damage on genomic DNA (Moeller et al., 2009). However, further in-depth investigations are required in order to understand the mechanism of the spore damage resulting from prolonged continued exposures to THz radiation.

Chapter 8. Translocation of silica nanospheres through giant unilamellar vesicles (GUVs) induced by EMFs of 18 GHz

8.1. Overview

Membrane model systems capable of mimicking live cell membranes were used for the first time in studying the effects arising from electromagnetic fields (EMFs) of 18 GHz where membrane permeability was observed following exposure. Present lack of understanding of the mechanisms that drive such a rapid change in membrane permeabilisation and the nature of biomolecules affected by high-frequency electromagnetic irradiation limit the use of 18 GHz EMFs in biomedical applications. A simple phospoholipid, DOPC (1,2-dioleoyl-*sn*-glycero-3-phosphocholine) labelled with a fluorescent marker 1,2-dioleoyl-sn-glycero-3-phosphoethanolamine-N-(lissamine rhodamine B sulfonyl) (rhodamine-DOPE) was used in constructing the Giant Unilamellar Vesicles (GUVs). The size of the constructed liposomes ranged from 5 to 20 µm with 39.8 % of the GUVs having a diameter of 10 µm, followed by 17.6 % with a size of 5 µm. The suspension of GUVs was then subjected to 18 GHz EMF at a heating rate of 20°C for 1 min, which will increase the temperature to 40°C with cooling time of 2 min following each exposure. After three cycles of exposure, enhanced membrane permeability was observed by the internalisation of hydrophilic silica nanospheres of 23.5 nm and their clusters. The untreated control did not exhibit any uptake of silica nanospheres. It is believed that the EMF-induced oscillations, *i.e.*, vibrations of water molecules (dipoles) have the potential to induce bilayer permeability of liposomes without affecting their integrity, as demonstrated in this study which will be ideal in the use of delivering foreign materials across live cell membranes.

8.2. Background

A highly controlled exposure of living organisms to high frequency electromagnetic fields (EMF) have emerged as a promising technique to efficiently induce temporary permeability with high level of post-treatment viability in a wide variety of cells. To this effect, a wide range of EMFs have been trialed, with EMF of 18 GHz showing a highly favorable combination of treatment efficiency, cell viability and induced biochemical changes. First demonstrated in *Escherichia coli* as a model organism with the help of dextran probes (15.9 nm) (Shamis et al., 2012b, Shamis et al., 2011b, Shamis et al., 2012c), the ability of brief 18 GHz treatment to trigger reversible permeabilisation in cellular membranes was later demonstrated in a large range of morphologically and structurally distinct microorganisms, including Gram positive cocci (Nguyen et al., 2015a), *Planococcus maritimus* KMM 3738, *Staphylococcus aureus* CIP65.8^{T}, *S. aureus* ATCC 25923 and *S. epidermidis* ATCC 14990^{T}, as well as eukaryotic cells, such as *Saccharomyces cerevisiae* ATCC 287 and pheochromocytoma cells (Nguyen et al., 2016). Transmission electron microscopy (TEM) results revealed that the EMF-treated cells were able to internalise nanospheres of 23.5 and 46.5 nm. Even though the degree of internalisation was found to be variable, most likely due to differences in cell wall structure of exposed organisms (Nguyen et al., 2015a). Successful induction of permeabilisation across all types of prokaryotic and eukaryotic cells irradiated with 18 GHz EMFs suggests certain universal processes that take place in water and/or at the interface under these irradiation conditions.

Present lack of understanding of the mechanisms that drive such a rapid change in membrane permeabilisation, and the nature of biomolecules affected by high-frequency electromagnetic irradiation limits the use of 18 GHz EMFs in biomedical applications. Indeed, the complexity of prokaryotic and eukaryotic cells and biologically systems makes identification of individual physical, chemical and biological events challenging. To aid with such investigation, a wide range of in vitro models that mimic specific cellular components or processes have been designed to understand how they are affected as a result of exposure to a specific stimulus, in our case, polarising electromagnetic oscillations. Among available systems, the resemblance of liposomes to biological membranes makes them an excellent tool for the study of processes that take place at the cellular membrane.

Discovered in the 1960s by Alec D Bangham, liposomes and cell-size giant unilamellar vesicles (GUVs) have established their position as simple membrane systems of choice for the investigation of function of complex biological membranes, and how these functions are affected by stimuli-induced changes in chemical composition, distribution and conformation of membrane building blocks (Bhatia

et al., 2015). In addition to fundamental biological studies, liposomes have been used extensively as successful drug carriers due to a favorable combination of biological properties, such as biocompatibility and biodegradability, and low toxicity and immunogenicity (Bozzuto and Molinari, 2015, Lewandowska-Lancucka et al., 2016). Liposomes are typically composed of phospholipids that rapidly self-assemble into a spherical lipid bilayer with an aqueous core (Pattni et al., 2015, Paini et al., 2015, Kubiak et al., 2011). Due to the presence of a hydrophilic core and hydrophobic bilayer, liposomes can incorporate active molecules, *i.e*., drugs, imaging agents and biomolecules, that are hydrophilic as well as lipophilic (Pattni et al., 2015, Paini et al., 2015). The therapeutic efficacy of liposomal drug delivery systems is inherently linked to their ability to deliver and release their cargo in controlled spatio-temporal manner (Bibi et al., 2012). This can be attained by designing liposomes to respond to local stimuli (e.g. pH or enzymes specific to the target site) or remote physical triggers (e.g. application of external heat, ultrasound, or light) (Dicheva et al., 2013, Guo and Szoka, 2003), with the latter considered a more attractive approach (Sercombe et al., 2015).

Therefore, the aim of this investigation was to using a model lipid bilayer system, study the effects of 18 GHz EMF exposure on lipid bilayer.

8.3. Results and Discussion

High frequency (18 GHz) EMF radiation treatment offers a promising means for inducing transient permeability in a wide range of cells, and as such can be used in drug delivery and gene therapy applications in medicine and biotechnology, and for the study of fundamental biochemical processes within cells. 18 GHz EMF treatment can potentially be integrated into lab-on-chip devices as a means for in-depth investigation of transport of exogenous molecules into the cells (for *e.g.*, study of molecular interactions with intracellular components) or efficient extraction of biomolecular components out of cells (Schmidt et al., 2017). However, for practical realisation of these applications, it is important to understand the mechanisms by which EMF induces permeabilisation, which is not a trivial task due to the multitude of interrelated biological, chemical and physical responses that EMF could trigger within cells. For this purpose, in this study, a well-defined model membrane system made up of DOPC–RhodPE was chosen to visualise the potential physico-chemical response of the lipid bilayer to EMFs of high frequency. The main advantages of this single layer lipid vesicle membrane system include ease of preparation and handling and close resemblance to the basic compartment structure of biological cells (Micheletto et al., 2016, Walde et al., 2010). The unilamellar vesicles (GUVs) used in this study are composed of conventional phospholipids with one hydrophilic head group attached to two lipophilic chains (Walde et al., 2010), with hydrophilic polar heads of DOPC directed towards the aqueous media and hydrophobic fatty acid chains forming the interior layer of the bilayer (Bozzuto and Molinari, 2015, Walde et al., 2010). The formation of liposomes occurred in less than 5 min after the aqueous sugar solution was added to the partially ordered stack of lipids due to spontaneous swelling of the dry lipid films, with the hydration process left undisturbed throughout the procedure.

The size of thus-prepared liposomes ranged from 5 to 20 µm. The highest fraction (39.8 %) of the GUVs had a diameter of 10 µm, followed by liposomes with a size of 5 µm (17.6 %). Presence of liposomes with a size of 10 – 20 µm varied in accordance with the size distribution curve **(Figure 8.1A)**. Time-lapse confocal microscopy over a period of 30 min confirmed excellent stability of thus-constructed liposomes. Examination of the images captured at 5 min intervals show that the liposomes preserved their structural integrity and remain in solution without bursting **(Figure 8.1B)**.

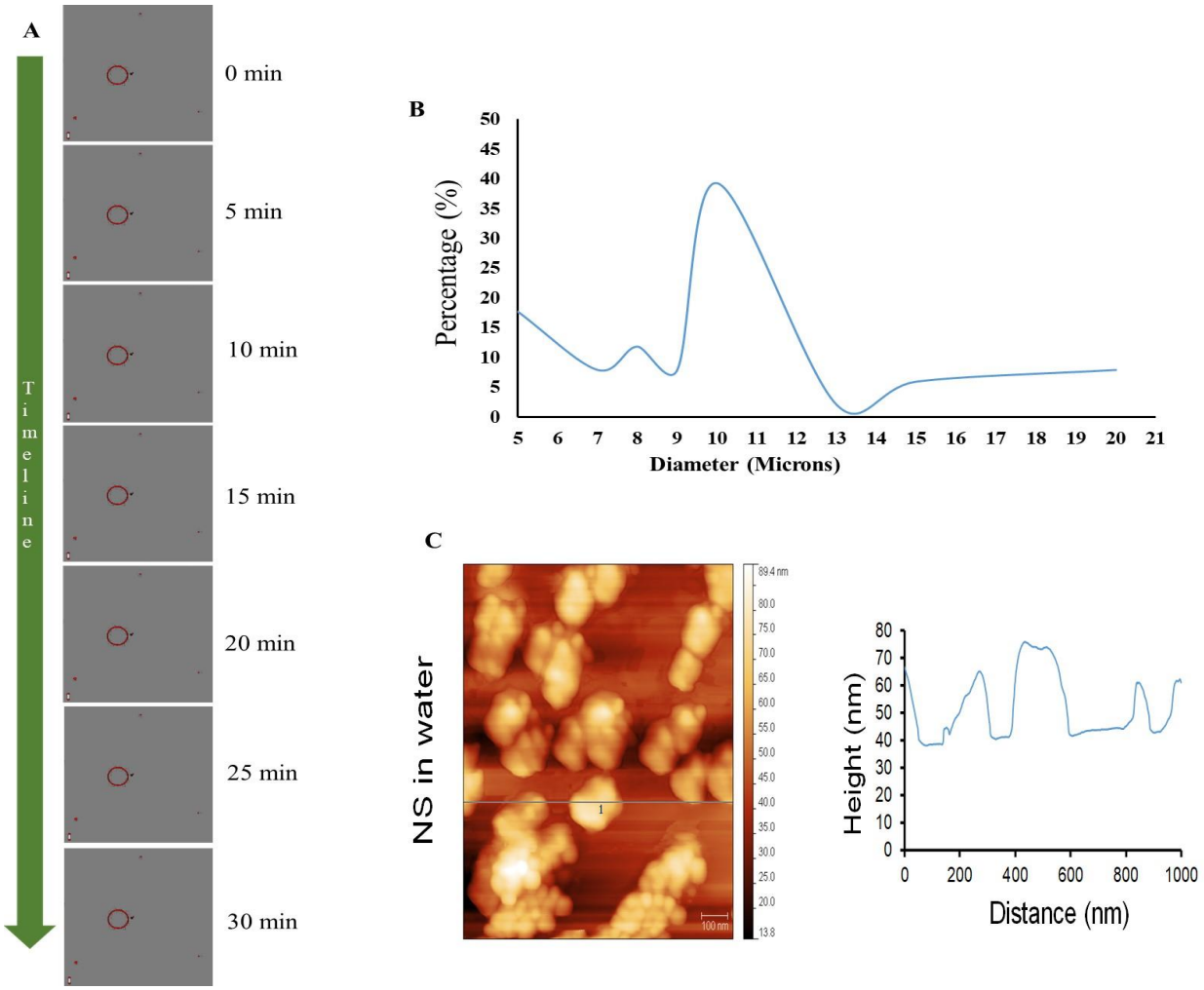

Figure 8. 1. The stability and size distribution of the GUVs and the size distribution of the nanospheres' clusters. (A) Time lapse images of GUVs in suspension. Images were captured continuously for a period of 30 min at 0, 5, 10, 15, 20, 25, 30 min. The GUVs remained stable in solution before exposure to EMF radiation. Scale bar 5 µm. (B) The size distribution of GUVs. The diameter of the liposomes synthesised using the gel assisted method ranged from 5 – 20 µm. (C) Atomic force microscopy of the nanosphere clusters and water and corresponding cross-sectional profile (right) indicating the height and width of the nanosphere cluster. The nanospheres were vortexed for one min in order to keep the experimental conditions consistent. The nanospheres tend to exist in clusters of 10 or more nanospheres (200 – 1000 nm).

In a manner similar to that observed in microbial and mammalian cells, treatment of liposomes with EMFs of 18 GHz induced membrane permeabilisation in the lipid bilayer. The membrane permeability was demonstrated by treatment-induced internalisation of hydrophilic silica nanospheres of 23.5 nm in diameter and their clusters **(Figure 8.**2**).** This type of nanospheres was purposefully selected for this study since their hydrophilic nature renders their passive transport across the hydrophobic lipid bilayer challenging. Prior to their addition to EMF-treated GUVs, the nanospheres were either sonicated and/or vortexed in order to re-disperse the particles and prevent their aggregation. The internalisation of the nanospheres and their clusters by the liposomes was then visualised using confocal laser scanning microscopy, with the typical images shown in (**Figure 8.2)**.

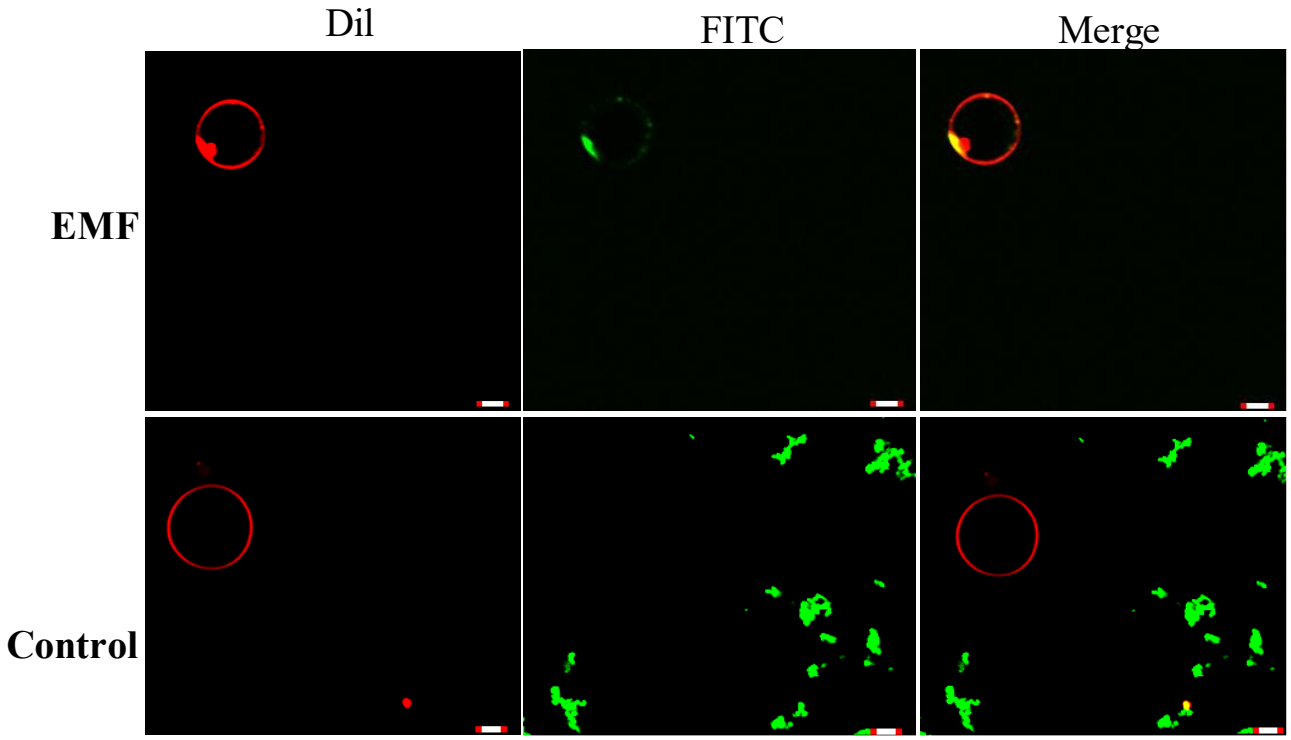

Figure 8. 2. EMF induced membrane permeability of GUVs. Confocal laser scanning micrographs showing the GUVs internalising nanospheres following EMF exposure. The original solution containing the nanospheres were sonicated before addition GUVs. The non - treated GUVs were used as the control, no nanosphere uptake was visualised, while the EMF treated GUVs (top row) were able to internalise nanospheres (existing as clumps). The presence of the green signal (FITC) overlapping with the red signal (Dil) when merged confirms that the nanospheres are present bound to the GUVs. Membrane permeability was not detected in the untreated GUVs as there was no overlapping of the FITC and Dil channels.

The incorporation of hydrophilic nanospheres into the lipid membrane was clearly visible: the overlapping of the red and green signals confirmed the presence of nanospheres bound to the lipid membrane and inside the GUVs (**Figure 8.2**), with the images suggesting a high affinity of nanospheres towards the lipid membrane after EMF exposure. This is in direct contrast to control samples, where no internalisation of nanospheres was detected. It should be noted that according to the results obtained by confocal microscopy, the most of the nanospheres appear to exist in clusters, rather than individual spheres of diameter 23.5 nm. Similar to most nanoparticles in suspension, hydrophilic silica nanospheres have a propensity to agglomerate, which may affect the mechanism by which they are internalised by cells (Halamoda-Kenzaoui et al., 2017).

To determine whether agglomeration indeed took place, atomic force microscopy was used to determine the size of the nanosphere clusters in solution. The AFM images obtained from vortexed (1 min) nanosphere samples in water indicate that the average height of a cluster was approximately 30 nm whereas the diameter ranged from 200 to 1000 nm. Considering the silicon particles used in this study are spherical, the cross-sectional profile confirmed that the nanoparticles largely exist as clusters, the average size of which is similar to that incorporated into the lipid membranes as visualised by confocal microscopy. Dynamic light scattering results of the sonicated solution of nanospheres reveal that they are mostly present in smaller clusters of ~ 63 nm (**Figure 4.1B)**.

In order to understand the mechanism by which EMF exposure induced translocation of nanospheres across lipid bilayers, the likely events that take place under microwave were considered. The length of the wave produced by 18 GHz electromagnetic field is comparable to the typical diameter of bacterial cells (Shamis et al., 2011b, Shamis et al., 2012c, Nguyen et al., 2015a). This means that the oscillation induced as a result of a transfer of energy from a polarized electromagnetic oscillation to molecules in ground state with cell suspensions will be most pronounced for small molecules, such as electrically charges ions and polar water molecules (Panagopoulos et al., 2013). Larger, bound molecules, such as those of the lipid bilayer, will also absorb some of the electromagnetic radiation, yet the magnitude of oscillations induced by such a transfer of energy may be significantly smaller and difficult to quantify. The EMF-induced oscillations, *i.e.*, vibrations, of water molecules have the potential to induce bilayer permeability of liposomes without affecting their integrity, as demonstrated in this experiment.

Indeed, the mechanical vibration of water dipoles during EMF exposure couple with partial reorientation of alignment of water molecules under the effect of electric field may lead to bending and/or breakage of hydrogen bonds. In turn, the vibrational motion-induced breakage of hydrogen molecules in water molecules may lead to changes in physicochemical properties of EMF-irradiated water, particularly with

respect to gas solubility (by affecting the interface between liquid and gas, *e.g.*, dissolved CO_2, phases) and hydration level of water ions. As such, EMF irradiation can lead to formation of submicro- and nanometer sized (~100 nm) bubbles filled with several hundred or less gas molecules (Attard, 2003).

The hydration shells surrounding thus-formed bubbles can prompt ordering of water, with the latter becoming a potentially prominent perturbation mechanism in solution, as shown in material synthesis applications (Katsir et al., 2007). These bubbles are relatively stable, and may interact with other molecules to form large complexes or supramolecular structures in colloidal suspensions (Jin et al., 2007). It has been suggested that the inherent presence of such bubbles and their subsequent bridging on the surfaces of hydrophobic materials in suspensions may be responsible for their long-ranged attraction (Attard, 2003). EMF exposure is thought to facilitate bubble nucleation by decreasing gas solubility, with the concentration of bubbles increasing as a function of increasing treatment time, working power and the initial dissolved oxygen concentration (Wang et al., 2016). The collapse of thus-formed bubbles may also lead to localised sharp increase in temperature (Asakuma et al., 2016), with the latter having capacity to catalyse chemical reactions, such as hydrolysis of molecules comprising lipid bilayers (Changi et al., 2012).

An EMF-induced change in the hydration of H_3O^+ and OH^- typically present in water, specifically the removal of the hydration shell, may increase their chemical activity (Dziuban, 2000, Walczak and Dziuban, 2004), leading to solution structuring, *e.g.*, cluster formation, and reactive species production (Ayrapetyan et al., 2009), as demonstrated by retained activity of the solution after EMF is removed (Colic and Morse, 1999). It has been shown that the size of the clusters detected in ENF-treated water was smaller than that of control, at 5–6 versus 10–13 molecules, respectively, resulting in a higher rate of dissolution of silica nanoparticles in the former (Walczak and Dziuban, 2004). The effect of magnetic field on adsorption and desorption of water molecules has also been shown to be affected by their location, with water molecules condensed in pores, in multilayers, and in clusters surrounding hydrophobic functional groups on surfaces responding to magnetic fields more that molecules in the first layer on hydrophilic surfaces (Ozeki et al., 1996, Higashitani et al., 1996).

The vibration-induced formation of biochemically reactive species may include the following reactions:

$$(H_2O)_n(H_2O \leftarrow H\text{–}OH \rightarrow OH_2)(H_2O)_m \rightarrow (H_2O)_n(H_2O + H\cdot + \cdot OH + OH_2)(H_2O)_m$$

$$2\ \cdot OH \rightarrow H_2O_2$$

$^3O_2 + \cdot H \rightarrow HO_2\cdot$

$HO_2\cdot + \cdot H \rightarrow H_2O_2$

$\cdot OH + H_2O_2 \rightarrow HO_2\cdot + H_2O$

$HO_2\cdot + HO_2\cdot \rightarrow H_2O_2 + {}^1O_2$

$h\nu + H_2O_2 \rightarrow 2\ \cdot OH$

Thus-generated reactive oxygen species may engage into chemical reactions with macromolecules comprising the lipid bilayer of the GUVs. Therefore, in addition to enhanced poration due to molecular vibrations, EMF exposure has the potential to induce chemical and thus conformational changes in phospholipids comprising the bilayer. Conformational changes in the hydrocarbon acyl chains and in acyl chain packing have been previously reported for egg lecithin multilamellar vesicles exposed to 900 MHz EMF (SAR 12 ± 1 W/kg) (Gaber et al., 2005).

The changes were in part attributed to hydrolysis of carboxylic and phosphoric esters of the lipids by hydrogen peroxide formed in water during EMF treatment. An EMF-induced change in lipid chemistry and packing affected the curvature of the lipid planes (Marsh, 2007) and membrane hydration (Tielrooij et al., 2009), with thus-formed curved lipid planes responsible for lateral diffusion of the lipids in the intermediate motional regime, which in turn increased the permeability of the lipid bilayer (Gaber et al., 2005, El Jastimi et al., 1999). The membrane curvature has also been shown to affect the manner in which other molecules bind to its surface (Lewis and Cafiso, 1999)

In our study, the increased affinity of hydrophilic nanospheres towards surfaces of liposomes potentially suggests that chemical modification may take place. However, considering that the chemical reactivity of microwave-irradiated water is retained for some time, the modification of nanoparticle surfaces should also be considered.

Another EMF effect on matter than warrants discussion is the possibility that the EMF induces a local mechanical change, i.e. a local elastic tension in the lipid bilayer through Maxwell's tensor, which can prompt the liposome to elongate or flatten from its spherical shape (Portet et al., 2012, Goldberg et al., 2018, Aranda et al., 2008). The interaction between a polarised electromagnetic oscillation and matter results in both energy and momentum transfer. Here, the momentum exchange

involves both the induction of a mechanical wave through the medium (due to pulling by the field on the medium), and partial transfer of the electromagnetic momentum to the medium, to which the medium responds by adjusting the internal stress components, with the resulting perturbation having zero total momentum [https://arxiv.org/pdf/1703.02109.pdf]. However, in the case of liposomes treated with 18 GHz, no visible change in the shape of the liposome was taken place. Therefore, prolation or oblation are unlikely to be responsible for the observed increase in membrane permeability in this study.

8.4. Conclusion

Exposures of EMFs of 18 GHz led to the incorporation of hydrophilic nanospheres into the lipid membrane, the overlapping (yellow) of the red and green signals confirmed the presence of nanospheres bound to the lipid membrane and inside the GUVs. The untreated control did not exhibit any uptake of silica nanospheres. It is believed that the EMF-induced oscillations, *i.e.*, vibrations of water molecules (dipoles) have the potential to induce bilayer permeability of liposomes without affecting their integrity.

Chapter 9. General Discussion

9.1 Overview

This chapter will emphasize the reversible permeabilization of bacterial membranes following 18 GHz EMF exposures and synchrotron source THz radiation on pheochromocytoma PC 12 neuron-like cells **(Chapter 4 and 5)**. This discussion will suggest a reason why *Bacillus subtilis* spores, which are remarkably resistant to extreme environmental conditions including UV radiation, exhibit deformities upon exposure to low power THz radiation for long periods **(Chapter 7)**. The proposed simple lipid membrane model, showing that Giant Unilamellar Vesicles (GUVs) composed of 1,2-dioleoyl-sn-glycero-3-phosphocholine (DOPC) were constructed **(Chapter 8)** to eliminate certain targets of the EMF exposures, including voltage gated channels. At these high frequencies, the electric and magnetic fields were tightly coupled and their effects could not be separately evaluated (Artacho-Cordon et al., 2013). Given the complexity in understanding as to how EMF exposures can induce the process of membrane permeabilization, possible mechanisms as to how this occurs is discussed. The importance of this research and possible future research directions are also included.

9.2. EMF induced reversible permeabilization in PC 12 cells

This study confirmed that 18 GHz EMF doses can induce the reversible permeabilization of PC 12 cell membranes. Membrane permeability was not observed in Peltier heat treatment and untreated control sample trials. Other techniques that can cause membrane changes include mechanical stress, sonoporation, electroporation and photoporation (Hansen et al., 2015, Zu et al., 2015, Sadiq et al., 2015). 18 GHz EMF doses may act as external stimulus, which can initiate membrane depolarization leading to permeability. EMF doses at this frequency produce a wavelength comparable in magnitude to that of the bacterial cell diameter, and therefore influenced the cell kinetics (Shamis et al., 2011b, Nguyen et al., 2015a, Shamis et al., 2012b). Reversible membrane permeability was detected following short 18 GHz EMF exposures to cells without causing any detrimental effect to their viability or metabolism, thereby providing a potential alternative to conventional poration techniques in drug delivery applications. The advantages of this technique is that the EMF exposures are for 30 s, and no harmful effects were detected. As a result, if this process is employed as a future drug delivery technique, the length of exposure may be of importance.

A thorough review of the literature has shown that voltage-gated calcium channels may be activated upon exposure to EMFs, with downstream responses mediated through the Ca^{2+}/calmodulin stimulation of nitric oxide synthesis and subsequent stimulation of the NO-cGMP-protein kinase G and NO-$ONOO^-$-oxidative stress pathways, where the former can have therapeutic and the latter can have pathophysiological bioeffects, as well as responses mediated by other processes regulated by Ca^{2+} .The EMF-induced formation of reactive oxygen species, such as peroxynitrite, may result in lipid peroxidation and oxidation of proteins within the cellular membrane, thereby changing the membrane fluidity, and affecting pore formation and resealing, cell metabolism and viability (Bruno and Justin, 1994). However, in the present study, the viability, metabolic activity and membrane functional integrity of cells exposed to short doses of 18 GHz EMF were not affected. There appears to be no direct interaction between the EMF doses with the cell DNA because the energy present in the EMF is insufficient to break the chemical bonds within the DNA molecules (Simk et al., 2001). The indirect link between EMF exposures and the DNA is via the formation of free radicals, which then can interact with the DNA and other cellular components, leading to free radical mediated effects (Simk et al., 2001). The absence of detrimental effects on cellular metabolism, genetic makeup, cellular viability

and morphology increases the potential of EMF exposures being utilized in the delivery of chemotherapeutic drugs for cancer treatment (Geng and Lu, 2013, Hansen et al., 2015) and gene therapy.

Furthermore, previous studies have been reported where 18 GHz EMF doses induced a reversible increase in the cell membrane permeability of different Gram-negative and Gram-positive bacterial species, including *Planococcusmaritimus* KMM 3738, *Staphylococcus aureus* CIP65.8^{T}, *S. aureus* ATCC 25923,*S. epidermidis* ATCC 14990^{T}, *Escherichia coli*; and yeast and red blood cells (Nguyen et al., 2015a, Shamis et al., 2011b). A similar nature of pore formation across multiple cell types that contain different levels of voltage-gated channels exposed to 18 GHz EMFs indicates that in this case, the formation of pores may have taken place at the level of the lipid bilayer, independently of the voltage-gated channels. Interestingly, the GUVs constructed in this study lacked any voltage gated channels. As a result, the GUVs exhibited membrane permeability in response to 18 GHz EMF doses, eliminating voltage-gated channels as being the target of exposure.

Taking these results into consideration, it can be concluded that the EMF field induced cell membrane permeability most likely did not to originate as a result of bulk heating. The use of Peltier heat treatment studies produced samples similar to those produced after EMF exposure (in the absence of microwave radiation). Cell permeabilization was not observed in the heat- treated samples. As hypothesized, the results obtained in this study allowed the conclusion to be made that the observed effects are likely to be electro-kinetic in nature due to the increased conductivity and mobility of ions across the cell membrane, with a potential contribution being made through microthermal changes that cannot be easily captured at the macro level, as well as from the direct interaction of the EMF with cell membranes and/or their structural and functional components (*e.g.*, phospholipids) (Nguyen et al., 2015a, Nguyen et al., 2016, Shamis et al., 2012c).

A possible target of the EMF exposures is water dipoles. It is well known that when a polarized, non-ionizing electromagnetic oscillation encounters a polar or charged molecule, it transfers a fraction of its energy to this molecule, driving it to oscillate. The degree of thus-induced oscillation is greatest for unbound electrically charged particles, such as free ions that abound in human tissues (Panagopoulos et al., 2013). Additional energy will be absorbed by the water dipoles, as well as by larger polar or charged molecules, including such biological

macromolecules as nucleic acids, lipids, and proteins. These interactions will also result in oscillations due to the applied EMFs, however the magnitude of such energy absorption or

oscillation is more difficult to estimate due to the bound nature of many such molecules. Yet, they may play an important role in the development of EMF-induced membrane permeability.

Like EMFs in the microwave range, exposure of bacterial cells to EMFs in the THz range triggered an increase in the observed cell membrane permeability of PC 12 cells. Increased permeability was evidenced by an increased internalization of silica nanospheres (d = 23.5 nm) and their clusters (d = 63.9 nm) by the THz treated PC 12 cells, as compared to the untreated control cells. It is evident that the permeabilisation of the PC 12 cells following exposure to THz radiation did not come about through to thermal effects, since the increase in temperature was negligible with the low power THz beam. The heat factor can be eliminated given the insignificant rise in temperature in the presence of synchrotron sourced THz radiation.

There is a strong interest in the development of effective, yet safe permeabilisation strategies, with currently used techniques including electroporation using an electrical field pulse (Sadiq et al., 2015), sonoporation with ultrasound waves (Yu and Xu, 2014, Ohta et al., 2008), and photoporation using laser pulses (Banavath et al., 2018).Our findings suggest that EMF doses in the THz range could be used as a powerful and a promising tool to enable a more efficient delivery of genes, nanoparticles and therapeutic drugs, where THz radiation could act as an external stimulus for rapid permeabilisation of the cell membrane while exhibiting non- significant changes to cell metabolism, viability and PC 12 cell differentiation. Another important property of the THz induced nanosphere delivery is that the technique allows the delivery of single nanospheres, as well as clusters, to the cells, which is critical in the process of metastasis (Schroeder et al., 2011).

The results obtained in this study are in general agreement with those obtained by Fröhlich (Fröhlich, 1968), who concluded that the interactions of THz radiation with cells may arise as mediated by the excitation of biological macromolecules or nonlinear/linear resonance mechanisms (Bogomazova et al., 2015). Furthermore, the existing body of literature suggests that the main targets of super high frequency EMF waves in cells are likely to be water molecules, membrane-associated proteins, *e.g.* the proton F_0F_1-ATPase bioenergetic enzyme in bacterial cells, and genetic material (Soghomonyan et al., 2016).

As mentioned earlier, water is the main constituent in all biological systems, the energy absorbed can initiate water cluster structuring and subsequent changes (increased or decreased) in chemical

activity or the level of hydration in intracellular structures and components, such as membrane-associated proteins (Soghomonyan et al., 2016, Weightman, 2012). The water cluster structuring and the energy absorption of water dipoles may influence the excitation of biological macromolecules, including proteins and phospholipids. Fröhlich also predicted that biological systems can support coherent excitations that fall in the range $10^9 – 10^{12}$ Hz (Weightman, 2012, Fröhlich, 1968), the synchrotron-sourced THz radiation has a frequency of 10^{12} Hz. The ability of vibrational modes within protein molecules to order and condense into a lowest-frequency vibrational mode in a process similar to Bose-Einstein condensation was demonstrated experimentally using egg white-derived lysozyme, where exposure to 0.4 THz electromagnetic radiation resulted in a local increase of electron density in a long α-helix motif linked to a slight longitudinal compression of the protein helix (Lundholm et al., 2015).

9.3. Response of spores to EMFs of 18 GHz and 0.3 to 19.5 THz

When exposed to short 18 GHz EMF doses, *B. subtilis* spore appear to be unaffected, with no changes being detected during their subsequent germination. Slight changes in spore morphology were detected, which were negligible, given that no changes were detected in spore germination in comparison to the untreated control. Exposure to long 18 GHz EMF doses was not performed in order to avoid the increase in temperature of the microwave chamber at a fixed frequency of 17 W in contrast to the low power of the synchrotron-sourced THz radiation. Short 18 GHz EMFs doses did not seem to influence the behavior, activity or morphology of *B. subtilis* spores.

In contrast, prolonged 0.3 – 19.5 THz EMF exposures reduced the germination of spores, leading to their destruction, whereas *Bacillus* spores have been reported to be extremely resistant (1075 times) to inactivation through this type of EMF exposure compared to that of their vegetative cells (Blatchley et al., 2005). Previous studies were conducted by exposing *B. subtilis, Bacillus cereus* and *Bacillus anthracis* spores to ultraviolet and gamma radiation (Blatchley et al., 2005). It was found that UV radiation at a wavelength of 254 nm appeared to have a pronounced effect on the *B. cereus* and *B. anthracis* spores compared to that of the *B. subtilis* spores.

Given these results, long EMF THz range exposures can be employed as a sterilization technique for the inactivation and destruction of spores. The heat load necessary to inactivate certain microorganisms depends on the degree of their heat resistance and the level of reduction required to deactivate the microbe (den Besten et al., 2018). Inactivation of bacterial spores requires higher heat loads than that required by the vegetative cells (den Besten et al., 2018), whereas THz EMF radiation with low power could be used as an alternative sterilization technique. Given the complexity of the structure of the *Bacillus* spore coating, and with water dipoles being the target of EM radiation together with the spore core possessing a low water content (~ 25 – 50% of the wet weight along with spore's DNA, ribosomes and its enzymes) (Zheng et al., 2016), EMF radiation is therefore less effective at sterilizing bacterial spores. As hypothesized earlier, the results obtained in this study allowed the postulation that the observed effects of EMF exposure are likely to be electro-kinetic in nature due to the increased conductivity and mobility of ions across the cell membrane, with a potential contribution being from the microthermal changes that cannot be easily captured at the macro level, as well as from the direct interaction of the EMF with cell membranes and/or their structural and functional components (Nguyen et al., 2015a, Nguyen et al., 2016,

Shamis et al., 2012c). The additional energy will be absorbed by the water dipoles, as well as by larger polar or charged molecules, including such biological macromolecules as nucleic acids, lipids, and proteins in the spore core, which may have led to the irreversible damage of the spore core.

For survival, bacterial spores must maintain the integrity of their DNA for long periods. Failure to do so will lead to the accumulation of DNA damage in their genomes, as spores are metabolically inactive during dormancy, whereas vegetative cells are capable of constantly repairing their DNA. After 36 h exposures to THz radiation, spores exhibited a reduction in their rates of germination, which could be due to their inability to repair the cumulative damage of the genomic DNA before transcription and the beginning of the replication process (Moeller et al., 2009).

9.4. Significant outcomes of the research and future directions

A significant outcome of the research is the conclusion that exposure of bacterial cells to EMF doses has the ability can induce membrane permeability over a wide range of frequencies. Membrane permeabilization was achieved using 18 GHz and 0.3 – 19.5 THz EMF doses in PC 12 cells and GUVs, which led to the ability to internalize silica nanospheres and their clusters. The ability to deliver foreign material into cells following EMF exposures, without any detrimental effects on cell viability, metabolism and growth, highlights the applicability of this technique for drug delivery. Membrane permeabilization was achieved upon short term exposures of 30 s (3 cycles) and 10 min of 18 GHz and 0.3 – 19.5 THz EMF doses, respectively. The varying exposure times were due to the low power beam of the synchrotron sourced THz radiation in comparison to that of the GHz EMF. Following GHz exposures, PC 12 cells remained viable for 9 min longer than that of the untreated control sample. The viability of the cells was not affected after being exposed to 18 GHz EMF doses, which increases the potential applicability of this technique in drug delivery applications. The mechanism of induced permeability has been suggested to arise from the water dipoles absorbing the energy, which leads to increased dipole vibrations, which in turn influences the behavior of the large macromolecules within the cell, such as lipids and proteins. This leads to changes in the lipid bilayer, and hence the ability to

form pores in the membrane. The mechanisms of prolonged exposures of THz radiation on spores, leading to their destruction, remains unclear and requires further experimental work. It can be assumed that the water content in the spore cortex is affected in a similar manner when being exposed to EMFs, leading to increase vibration with the accumulation of energy leading to the disruption of the cortex hence disintegration of the spore core and the other layers, causing irreversible damage.

10.References

ADAMS, D. S., MASI, A. & LEVIN, M. 2007. H+ pump-dependent changes in membrane voltage are an early mechanism necessary and sufficient to induce Xenopus tail regeneration. *Development,* 134**,** 1323-35.

AKESON, R. & WARREN, S. L. 1986a. PC12 Adhesion and Neurite Formation on Selected Substrates Are inhibited by some Glycosaminoglycans and a Fibronetion-derived Tetrapeptide. *Experimental Cell Research,* 162**,** 347-362.

AKESON, R. & WARREN, S. L. 1986b. PC12 Adhesion and Neurite Formation on Selected Substrates Are inhibited by some Glycosaminoglycans and a Fibronetion-derived Tetrapeptide. *Exp. Cell. Res.,* 162**,** 347-362.

ALAVI, M., KARIMI, N. & SAFAEI, M. 2017. Application of Various Types of Liposomes in Drug Delivery Systems. *Advanced Pharmaceutical Bulletin,* 7**,** 3-9.

ALBLETT, S., DARKE, A. H., LILLFORD, P. J. & MARTIN, D. R. 1999. Glass formation and dormancy in bacterial spores. *International journal of Food Science and Technology,* 34**,** 59-69.

ALEXANDROV, B. S., GELEV, V., BISHOP, A. R., USHEVA, A. & RASMUSSEN, K. Ø. 2010. DNA Breathing Dynamics in the Presence of a Terahertz Field. *Physics letters. A,* 374**,** 1214-1214.

ALEXANDROV, B. S., PHIPPS, M. L., ALEXANDROV, L. B., BOOSHEHRI, L. G., ERAT, A., ZABOLOTNY, J., MIELKE, C. H., CHEN, H. T., RODRIGUEZ, G., RASMUSSEN, K. O., MARTINEZ, J. S., BISHOP, A. R. & USHEVA, A. 2013. Specificity and heterogeneity of terahertz radiation effect on gene expression in mouse mesenchymal stem cells. *Sci Rep,* 3**,** 1184.

AM, O. B., AMIT, T. & YOUDIM, M. B. H. 2004. Contrasting neuroprotective and neurotoxic actions of respective metabolites of anti-Parkinson drugs rasagiline and selegiline. *Neuroscience Letters,* 355**,** 169-172.

ANGELOVA, M. & DIMITROV, D. S. 1988. A mechanism of liposome electroformation. *Trends in Colloid and Interface Science II.*

ANTON, E., ROTARU, A., COVATARIU, D., CIOBICA, A., TIMOFTE, D., POPESCU, R. & ANTON, C. 2015. Links between extremely high frequency electromagnetic waves and their biological manifestations. *Archives of Biological Sciences,* 67**,** 895-897.

ANTONIO, C. & DEAM, R. T. 2007. Can "microwave effects" be explained by enhanced diffusion? *Phys Chem Chem Phys,* 9**,** 2976-82.

ANTONOPOULOS, A., EISENBRANDT, H. & OBE, G. 1997. Effects of high frequency electromagentic fields on human lymphocytes in vitro. *Mutation research,* 395**,** 209-214.

ARANDA, S., RISKE, K. A., LIPOWSKY, R. & DIMOVA, R. 2008. Morphological Transitions of Vesicles Induced by Alternating Electric Fields. *Biophysical Journal,* 95**,** L19-L21.

ARIGA, T., MACALA, L. J., SAITO, M., MARGOLIS, R. K., GREENE, L. A., MARGOLIS, R. U. & YU, R. K. 1988. Lipid Composition of PC 12 Pheochromocytoma cells: Characterization of Globoside as a major neutral glycolipid. *American Chemical Society,* 27**,** 53-57.

ARTACHO-CORDON, F., SALINAS-ASENSIO MDEL, M., CALVENTE, I., RIOS-ARRABAL, S., LEON, J., ROMAN-MARINETTO, E., OLEA, N. & NUNEZ, M. I. 2013. Could radiotherapy effectiveness be enhanced by electromagnetic field treatment? *International Journal of Molecular Sciences,* 14**,** 14974-95.

ASAKUMA, Y., NAKATA, R., MATSUMURA, S. & SAPTORO, A. 2016. Mechanism of Microwave Heating through Molecular Orbital Method and Bubble Size Profiles. *Procedia Engineering,* 157**,** 13-18.

ASHWORTH, P. C., PICKWELL-MACPHERSON, E., PROVENZANO, E., PINDER, S. E., PURUSHOTHAM, A. D., PEPPER, M. & WALLACE, V. P. 2009. Terahertz pulsed spectroscopy of freshly excised human breast cancer. *Optics Express,* 17.

ATTARD, P. 2003. Nanobubbles and the hydrophobic attraction. *Advances in Colloid and Interface Science,* 104**,** 75-91.

ATTIAH, D. G., KOPHER, R. A. & DESAI, T. A. 2003a. Characterization of PC12 cell proliferation and differentiation-stimulated by ECM adhesion proteins and neurotrophic factors. *J. Mater. Sci. Mater. Med.,* 14**,** 1005-1009.

ATTIAH, D. G., KOPHER, R. A. & DESAI, T. A. 2003b. Characterization of PC 12 cell proliferation and differentiation-stimulated by ECM adhesion proteins and neurotrophic factors. *Journal of Materials Science: Materials In Medicine,* 14**,** 1005-1009.

AVEDISIAN, C. T., CAVICCHI, R. E., MCEUEN, P. L. & ZHOU, X. 2009. Nanoparticles for cancer treatment: role of heat transfer. *Annals of the New York Academy of Sciences,* 1161**,** 62-73.

AYRAPETYAN, G., HAYRAPETYAN, H., DADASYAN, E., BARSEGHYAN, S., BAGHDASARYAN, N., MIKAYELYAN, E. & AYRAPETYAN, S. 2009. The Non Thermal Effect of Weak Intensity Millimeter Waves on Physicochemical Properties of Water and Water Solutions. *Electromagnetic Biology and Medicine,* 28**,** 331-341.

BAGATOLLI, L. A., PARASASSI, T. & GRATTON, E. 2000. Giant phospholipid vesicles: comparison among the whole lipid sample characteristics using different preparation methods. A two photon flourescence microscopy study. *Chemistry and Physics of Lipids,* 105**,** 135-147.

BANAVATH, H. N., ALLAM, S. R., VALATHATI, S. S., SHARAN, A. & RAJASEKARAN, B. 2018. Femtosecond laser pulse assisted photoporation for drug delivery in Chronic myelogenous leukemia cells. *Journal of Photochemistry & Photobiology B: Biology,* 187**,** 35-40.

BANIK, S., BANDYOPADHYAY, S. & GANGULY, S. 2003. Bioeffects of microwave - a brief review. *Bioresource Technology,* 87**,** 155-159.

BERENDSEN, E. M., BOEKHORST, J., KUIPERS, O. P. & WELLS-BENNIK, M. H. 2016. A mobile genetic element profoundly increases heat resistance of bacterial spores. *ISME Journal,* 10**,** 2633-2642.

BERRIDGE, M. V. & TAN, A. S. 1993. Characterization of the cellular reduction of 3-(4,5-dimethylthiazol-2-yl)-2,5-diphenyltetrazolium bromide (MTT): subcellular localization, substrate dependence, and involvement of mitochondrial electron transport in MTT reduction. *Archives of Biochemistry and Biophysics,* 303**,** 474-82.

BHATIA, T., HUSEN, P., BREWER, J., BAGATOLLI, L. A., HANSEN, P. L., IPSEN, J. H. & MOURITSEN, O. G. 2015. Preparing giant unilamellar vesicles (GUVs) of complex lipid mixtures on demand: Mixing small unilamellar vesicles of compositionally heterogeneous mixtures. *Biochimica et Biophysica Acta (BBA) - Biomembranes,* 1848**,** 3175-3180.

BIBI, S., LATTMANN, E., MOHAMMED, A. R. & PERRIE, Y. 2012. Trigger release liposome systems: local and remote controlled delivery? *Journal of Microencapsulation,* 29**,** 262-276.

BLOISE, N., PETECCHIA, L., CECCARELLI, G., FASSINA, L., USAI, C., BERTOGLIO, F., BALLI, M., VASSALLI, M., CUSELLA DE ANGELIS, M. G., GAVAZZO, P., IMBRIANI, M. & VISAI, L. 2018. The effect of pulsed electromagnetic field exposure on osteoinduction of human mesenchymal stem cells cultured on nano-TiO2 surfaces. *PLoS One,* 13**,** e0199046.

BOBER, K., GILES, R. & WALDMAN, J. 1997. Tailoring the Microwave Permittivity and Permeability of Composite Materials. *Int. J. Infrared Millimeter Waves,* 18**,** 101-123.

BOCK, J., FUKUYO, Y., KANG, S., PHIPPS, M. L., ALEXANDROV, L. B., RASMUSSEN, K. Ø., BISHOP, A. R., ROSEN, E. D., MARTINEZ, J. S., CHEN, H.-T., RODRIGUEZ, G., ALEXANDROV, B. S. & USHEVA, A. 2011. Mammalian Stem Cells Reprogramming in Response to Terahertz Radiation. *PLOS ONE,* 5**,** e15806.

BOCZEK, T., KOZACZUK, A., FERENC, B., KOSIOREK, M., PIKULA, S. & ZYLINSKA, L. 2012a. Gene expression pattern in PC12 cells with reduced PMCA2 or PMCA3 isoform: selective up-regulation of calmodulin and neuromodulin. *Mol. Cell. Biochem.,* 360**,** 89-102.

BOCZEK, T., KOZACZUK, A., FERENC, B., KOSIOREK, M., PIKULA, S. & ZYLINSKA, L. 2012b. Gene expression pattern in PC12 cells with reduced PMCA2 or PMCA3 isoform: selective up-regulation of calmodulin and neuromodulin. *Mol Cell Biochem,* 360**,** 89-102.

BOGOMAZOVA, A. N., VASSINA, E. M., GORYACHKOVSKAYA, T. N., POPIK, V. M., SOKOLOV, A. S., KOLCHANOV, N. A., LAGARKOVA, M. A., KISELEV, S. L. & PELTEK, S. E. 2015. No DNA damage response and negligible genome-wide transcriptional changes in human embryonic stem cells exposed to terahertz radiation. *Scientific Reports,* 5**,** 7749.

BONETTA, L. 2005. The inside scoop - evaluating gene delivery methods. *Nature Methods,* 2**,** 875-883.

BOWMAN, T., EL-SHENAWEE, M. & CAMPBELL, L. K. 2016. Terahertz transmission vs reflection imaging and model-based characterization for excised breast carcinomas. *Biomedical optics express,* 7**,** 3756-3783.

BOZZUTO, G. & MOLINARI, A. 2015. Liposomes as nanomedical devices. *Int J Nanomedicine,* 10**,** 975-99.

BRUNO, G. & JUSTIN, T. 1994. Generation of reactive-oxygen species induced by electropermeabilization of Chinese hamster ovary cells and their consequence on cell viability. *European Journal of Biochemistry,* 223**,** 25-33.

BUBOLTZ, J. T. & FEIGENSON, G. W. 1999. A novel strategy for the preparation of liposomes: rapid solvent exchange. *Biochimica et Biophysica Acta,* 1417**,** 232-245.

BUNKER, A., MAGARKAR, A. & VIITALA, T. 2016. Rational design of liposomal drug delivery systems, a review: Combined experimental and computational studies of lipid membranes, liposomes and their PEGylation. *Biochim Biophys Acta*.

ÇAĞDAŞ, M., SEZER, A. D. & BUCAK, S. 2014. *Liposomes as Potential Drug Carrier Systems for Drug Delivery*.

CAGNI, E., REMONDINI, D., MESIRCA, P., CASTELLANI, G. C., VERONDINI, E. & BERSANI, F. 2007. Effects of exogenous electromagnetic fields on a simplified ion channel model. *J Biol Phys,* 33**,** 183-94.

CHALLIS, L. J. 2005. Mechanisms for interaction between RF fields and biological tissue. *Bioelectromagnetics,* Suppl 7**,** S98-S106.

CHANGI, S., MATZGER, A. J. & SAVAGE, P. E. 2012. Kinetics and pathways for an algal phospholipid (1,2-dioleoyl-sn-glycero-3-phosphocholine) in high-temperature (175–350 °C) water. *Green Chemistry,* 14**,** 2856-2867.

CHAO, M. V. & HEMPSTEAD, B. L. 1995. p75 and Trk: a two receptor system. *Trends in Neurosciences,* 18**,** 321-326.

CHEN, T., CHIU, H. W., PAN, Y. C., HSU, A. T., LIN, J. H. & YANG, K. T. 2014a. Intermittent hypoxia-induced protein phosphatase 2A activation reduces PC12 cell proliferation and differentiation. *J. Biomed. Sci.,* 21**,** 1-11.

CHEN, T., CHIU, H. W., PAN, Y. C., HSU, A. T., LIN, J. H. & YANG, K. T. 2014b. Intermittent hypoxia-induced protein phosphatase 2A activation reduces PC 12 cell proliferation and differentiation. *Journal of Biomedical Science,* 21**,** 1-11.

CHILLER, K., SELKIN, B. A. & MURAKAWA, G. J. 2001. Skin microflora and bacterial infections of the skin. *J Investig Dermatol Symp Proc,* 6**,** 170-4.

CHO, Y. 2003. The effect of extremely low frequency electromagnetic fields (ELF-EMF) on the frequency of micronuclei and sister chromatid exchange in human lymphocytes induced by benzo(a)pyrene. *Toxicology Letters,* 143**,** 37-44.

CHOUDHURY, A. K. R. 2014. Characteristics of light sources. *Principles of Colour and Appearance Measurement.*

CHUNG, J., KUBOTA, H., OZAKI, Y., UDA, S. & KURODA, S. 2010. Timing-dependent actions of NGF required for cell differentiation. *PLoS One,* 5**,** e9011.

CLOTHIER, R. H. & BOURNE, N. 2003. Effects of THz Exposure on Human Primary Keratinocyte Differentiation and Viability. *Journal of Biological Physics,* 29**,** 179-185.

COGEN, A. L., NIZET, V. & GALLO, R. L. 2008. Skin microbiota: a source of disease or defence? *Br J Dermatol,* 158**,** 442-55.

COLIC, M. & MORSE, D. 1999. The elusive mechanism of the magnetic 'memory' of water. *Colloids and Surfaces A: Physicochemical and Engineering Aspects,* 154**,** 167-174.

CONNOLLY, J. L., GREEN, S. A. & GREENE, L. A. 1984a. Comparison of Rapid Changes in Surface Morphology and coated Pit Formation of PC12 cells in Response to Nerve Growth Factor Epidermal Growth Factor and Dibutyryl Cyclicl AMP. *The Journal of Cell Biology*

98**,** 457-465.

CONNOLLY, J. L., GREEN, S. A. & GREENE, L. A. 1984b. Comparison of Rapid Changes in Surface Morphology and coated Pit Formation of PC12

cells in Response to Nerve Growth Factor Epidermal Growth Factor and Dibutyryl Cyclicl AMP. *J. Cell Biol.,* 98**,** 457-465.
COWAN, A. E., KOPPEL, D. E., SETLOW, B. & SETLOW, P. 2003. A soluble protein is immobile in dormant spores of *Bacillus subtilis* but is mobile in germinated spores: Implications for spore dormancy. *Proceedings of the National Academy of Sciences,* 100**,** 4209-4214.
COWAN, A. E., OLIVASTRO, E. M., KOPPEL, D. E., LOSHON, C. A., SETLOW, B. & SETLOW, P. 2004. Lipids in the inner membrane of dormant spores of *Bacillus* species are largely immobile. *Proceedings of the National Academy of Sciences,* 101**,** 7733-7738.
COWLEY, S., PATERSON, H., KEMP, P. & MARSHALL, J. 1994. Activation of MAP Kinase is Necessary and Sufficient for PC12 Differentiation and for Transformation of NIH 3T3 cells. *Cell* 77**,** 841-852.
CRAWLEY, D., LONGBOTTOM, C., WALLACE, V. P., COLE, B., ARNONE, D. & PEPPER, M. 2003. Three-dimensional terahertz pulse imaging of dental tissue. *Journal of Biomedical Optics,* 8**,** 303-7.
D'AGOSTINO, S., DELLA MONICA, C., PALIZZI, E., DI PIETRANTONIO, F., BENETTI, M., CANNATÀ, D., CAVAGNARO, M., SARDARI, D., STANO, P. & RAMUNDO-ORLANDO, A. 2018. Extremely High Frequency Electromagnetic Fields Facilitate Electrical Signal Propagation by Increasing Transmembrane Potassium Efflux in an Artificial Axon Model. *Scientific Reports,* 8**,** 9299.
DAS, A. K., GUPTA, P. & CHAKRABORTY, D. 2015. Physical methods of gene transfer: Kinetics of gene delivery into cells: A Review. *Agricultural Reviews,* 36**,** 61.
DAS, K. P., FREUDENRICH, T. M. & MUNDY, W. R. 2004. Assessment of PC12 cell differentiation and neurite growth: a comparison of morphological and neurochemical measures. *Neurotoxicol Teratol,* 26**,** 397-406.
DEEPIK, M., HARSHAVARDHAN, T., VIJAYALAXMI, N., KUMBAKONAM, A. & JAYAKRISHNA, B. 2014. Sonoporation-Invigorating Sound in Dentistry : A Review. *IJSS Case Reports & Reviews,* 1**,** 25-28.
DELALANDE, A., KOTOPOULIS, S., POSTEMA, M., MIDOUX, P. & PICHON, C. 2013. Sonoporation: mechanistic insights and ongoing challenges for gene transfer. *Gene,* 525**,** 191-9.
DEN BESTEN, H. M. W., WELLS-BENNIK, M. H. J. & ZWIETERING, M. H. 2018. Natural Diversity in Heat Resistance of Bacteria and Bacterial Spores: Impact on Food Safety and Quality. *Annual Review of Food Science and Technology,* 9**,** 383-410.
DERMOL-ČERNE, J., MIKLAVČIČ, D., REBERŠEK, M., MEKUČ, P., BARDET, S. M., BURKE, R., ARNAUD-CORMOS, D., LEVEQUE, P. &

O'CONNOR, R. 2018. Plasma membrane depolarization and permeabilization due to electric pulses in cell lines of different excitability. *Bioelectrochemistry,* 122**,** 103-114.
DESHMUKH, P. S., MEGHA, K., NASARE, N., BANERJEE, B. D., AHMED, R. S., ABEGAONKAR, M. P., TRIPATHI, A. K. & MEDIRATTA, P. K. 2016. Effect of low level subchronic microwave radiation on at Brain. *Biomedical and Environmental Sciences,* 29**,** 858-867.
DESPA, S. 1995. The influence of membrane permeability for ions on cell behaviour in an electric alternating field. *Phys. Med. Biol.,* 40**,** 1399-1409.
DICHEVA, B. M., HAGEN, T. L. M. T., LI, L., SCHIPPER, D., SEYNHAEVE, A. L. B., RHOON, G. C. V., EGGERMONT, A. M. M., LINDNER, L. H. & KONING, G. A. 2013. Cationic Thermosensitive Liposomes: A Novel Dual Targeted Heat-Triggered Drug Delivery Approach for Endothelial and Tumor Cells. *Nano Letters,* 13**,** 2324-2331.
DIMOVA, R., ARANDA, S., BEZLYEPKINA, N., NIKOLOV, V., RISKE, K. A. & LIPOWSKY, R. 2006. A practical guide to giant vesicles. Probing the membrane nanoregime via optical microscopy. *Journal of Physics Condensed Matter,* 18**,** S1151-76.
DITTMANN, C., HAN, H. M., GRABENBAUER, M. & LAUE, M. 2015. Dormant Bacillus spores protect their DNA in crystalline nucleoids against environmental stress. *Journal of Structural Biology,* 191**,** 156-64.
DORSETT, Y. & TUSCHL, T. 2004. siRNAs: applications in functional genomics and potential as therapeutics. *Nat Rev Drug Discov,* 3**,** 318-29.
DREFUSS, M. S. & CHIPLEY, J. R. 1980. Comparison of Effects of Sublethal Microwave Radiation and Conventional Heating on the Metabolic Activity of S*taphylococcus aureus*. *Applied and Environmental Microbiology,* 39**,** 13-16.
DREHER, D. & A.F., J. 1996. Role of Oxygen Free Radicals in Cancer Development. *European Journal of Cancer,* 32A**,** 30-38.
DRIKS, A. 1999. Bacillus subtilis Spore Coat. *Microbiology and Molecular Biology Reviews,* 63**,** 1-20.
DRIKS, A. 2002. Overview: development in bacteria: spore formation in Bacillus subtilis. *Cellular and Molecular Life Sciences,* 59**,** 389-391.
DUSCHER, D., BARRERA, J., WONG, V. W., MAAN, Z. N., WHITTAM, A. J., JANUSZYK, M. & GURTNER, G. C. 2016. Stem Cells in Wound Healing: The Future of Regenerative Medicine? A Mini-Review. *Gerontology,* 62**,** 216-25.
DZIUBAN, J. A. 2000. Microwave enhanced fast anisotropic etching of monocrystalline silicon. *Sensors and Actuators A: Physical,* 85**,** 133-138.

EDWARDS, K. A. & BAEUMNER, A. J. 2006. Analysis of liposomes. *Talanta,* 68**,** 1432-41.
EL JASTIMI, R., EDWARDS, K. & LAFLEUR, M. 1999. Characterization of Permeability and Morphological Perturbations Induced by Nisin on Phosphatidylcholine Membranes. *Biophysical Journal,* 77**,** 842-852.
ERGIN, V., ERDOGAN, M. & MENEVSE, A. 2015. Regulation of Shootin1 Gene Expression Involves NGF-induced Alternative Splicing during Neuronal Differentiation of PC12 Cells. *Sci. Rep.,* 5**,** 17931.
ERRINGTON, J. 2003. Regulation of endospore formation in Bacillus subtilis. *Nature Reviews/ Microbiology,* 1**,** 117-26.
FALONE, S., SANNINO, A., ROMEO, S., ZENI, O., SANTINI, S. J., RISPOLI, R., AMICARELLI, F. & SCARFI, M. R. 2018. Protective effect of 1950 MHz electromagnetic field in human neuroblastoma cells challenged with menadione. *Scientific Reports,* 8**,** 13234.
FAN, S., HE, Y., UNG, B. S. & PICKWELL-MACPHERSON, E. 2014. The growth of biomedical terahertz research. *Journal of Physics D: Applied Physics,* 47**,** 374009.
FENG, B., QIU, L., YE, C., CHEN, L., FU, Y. & SUN, W. 2016. Exposure to a 50-Hz magnetic field induced mitochondrial permeability transition through the ROS/GSK-3beta signaling pathway. *International Journal of Radiation Biology,* 92**,** 148-55.
FISCHER, B. M., WALTHER, M. & JEPSEN, P. U. 2002. Far-infrared vibrational modes of DNA components studied by terahertz time-domain spectroscopy. *Physics in Medicine & Biology,* 47**,** 3807.
FITZGERALD, A. J., WALLACE, V. P., JIMENEZ-LINAN, M., BOBROW, L., PYE, R. J., PURUSHOTHAM, A. D. & ARNONE, D. D. 2006. Terahertz pulsed imaging of human breast tumors. *Radiology,* 239**,** 533-40.
FIXLER, D., NICOLAU, D. V., CARTWRIGHT, A. N., REN, J., ZHAO, J., COOKS, T., BHAT, A. & LU, Q. 2018. Dark-field microscopic study of the interactions between gold/silver nanoparticles and giant unilamellar vesicles. *Nanoscale Imaging, Sensing, and Actuation for Biomedical Applications XV.*
FREIRE, E., GOMES, F. C. A., LINDEN, R. & NETO, V. M. 2002. Structure of laminin substrate modulates cellular signalling for neuritogenesis. *J. Cell Sci.,* 115**,** 4867-4876.
FRÖHLICH, H. 1968. Long-range coherence and energy storage in biological systems. *International Journal of Quantum Chemistry,* 2**,** 641-649.
FUJI, D. K., MASSOGLIA, S. L., SAVION, N. & GOSPODAROWICZ, D. 1982a. Neurite outgrowth and protein synthesis by PC12 cells as a function of substratum and nerve growth factor. *J. Neurosci.,* 2**,** 1157-1175.

FUJI, D. K., MASSOGLIA, S. L., SAVION, N. & GOSPODAROWICZ, D. 1982b. Neurite outgrowth and protein synthesis by PC 12 cells as a function of substratum and nerve growth factor. *The Journal of Neuroscience,* 2**,** 1157-1175.

FUNK, R. H., MONSEES, T. & OZKUCUR, N. 2009. Electromagnetic effects - From cell biology to medicine. *Prog Histochem Cytochem,* 43**,** 177-264.

GABER, M. H., ABD EL HALIM, N. & KHALIL, W. A. 2005. Effect of microwave radiation on the biophysical properties of liposomes. *Bioelectromagnetics,* 26**,** 194-200.

GARAJ-VRHOVAC, V., GAJSKI, G., PAŽANIN, S., ŠAROLIĆ, A., DOMIJAN, A.-M., FLAJS, D. & PERAICA, M. 2011. Assessment of cytogenetic damage and oxidative stress in personnel occupationally exposed to the pulsed microwave radiation of marine radar equipment. *International Journal of Hygiene and Environmental Health,* 214**,** 59-65.

GARCIA-PARRA, P., CAVALIERE, F., MAROTO, M., BILBAO, L., OBIETA, I., LOPEZ DE MUNAIN, A., ALAVA, J. I. & IZETA, A. 2012. Modeling neural differentiation on micropatterned substrates coated with neural matrix components. *Frontiers in Cell Neuroscience,* 6**,** 10.

GARCIA, P. A., DAVALOS, R. V. & MIKLAVCIC, D. 2014. A numerical investigation of the electric and thermal cell kill distributions in electroporation-based therapies in tissue. *PLoS One,* 9**,** e103083.

GARCIA, P. A., GE, Z., MORAN, J. L. & BUIE, C. R. 2016. Microfluidic Screening of Electric Fields for Electroporation. *Sci Rep,* 6**,** 21238.

GENG, T. & LU, C. 2013. Microfluidic electroporation for cellular analysis and delivery. *Lab Chip,* 13**,** 3803-21.

GLOBUS, T., MOYER, M. A., GELMONT, B., KHROMOVA, T., LVOVSKA, M. I., SIZOV, I. & FERRANCE, J. 2013. Highly Resolved Sub-Terahertz Vibrational Spectroscopy of Biological Macromolecules and Cells. *IEEE SENSORS JOURNAL,* 13.

GOLDBERG, E., SUÁREZ, C., ALFONSO, M., MARCHESE, J., SOBA, A. & MARSHALL, G. 2018. Cell membrane electroporation modeling: A multiphysics approach. *Bioelectrochemistry,* 124**,** 28-39.

GORDON, J., AMINI, S. & WHITE, M. K. 2013a. General overview of neuronal cell culture. *Methods Mol Biol,* 1078**,** 1-8.

GORDON, J., AMINI, S. & WHITE, M. K. 2013b. General overview of neuronal cell culture. *Methods Mol. Biol.,* 1078**,** 1-8.

GORYACHUK, A., SIMONOVA, A., KHODZITSKY, M., BOROVKOVA, M. & KHAMID, A. Gastrointestinal cancer diagnostics by terahertz time domain spectroscopy. 2017 IEEE International Symposium on Medical Measurements and Applications (MeMeA), 7-10 May 2017 2017. 134-137.

GREENE, L. A. 1978. Nerve Growth Factor Prevents The Death And Stimulates The Neuronal Differentiation Of Clonal PC 12 Pheochromocytoma Cells In Serum-Free Medium. *The Journa of Cell Biology,* 78**,** 747-755.

GREENE, L. A. & TISCHLER, A. S. 1976a. Establishment of a noradrenergic clonal line of rat adrenal pheochromocytoma cells which respond to nerve growth factor. *Cell Biology,* 73**,** 2424-2428.

GREENE, L. A. & TISCHLER, A. S. 1976b. Establishment of a noradrenergic clonal line of rat adrenal pheochromocytoma cells which respond to nerve growth factor. *Proceedings of the National Academy of Sciences of the United States of America,* 73**,** 2424-2428.

GRICE, E. A., KONG, H. H., CONLAN, S., DEMING, C., DAVIS, J., YOUNG, A., PROGRAM., N. C. S., BOUFFARD, G., BLASKESLEY, R., MURRAY, P., GREEN, E. T., M. & SEGRE, J. A. 2009. Topographical and Temporal Diversity of the Human Skin Microbiome. *SCIENCE,* 324.

GRICE, E. A. & SEGRE, J. A. 2011. The skin microbiome. *Nat Rev Microbiol,* 9**,** 244-53.

GROSSMAN, A. D. & LOSICK, R. 1988. Extracellular control of spore formation in *Bacillus subtilis*. *Proceedings of the National Academy of Sciences of the United States of America,* 85**,** 4369-4373.

GRULL, H. & LANGEREIS, S. 2012. Hyperthermia-triggered drug delivery from temperature-sensitive liposomes using MRI-guided high intensity focused ultrasound. *Journal of Controlled Release,* 161**,** 317-27.

GUO, X. & SZOKA, F. C. 2003. Chemical Approaches to Triggerable Lipid Vesicles for Drug and Gene Delivery. *Accounts of Chemical Research,* 36**,** 335-341.

GUPTA, M., SARANGI, B. R., DESCHAMPS, J., NEMATBAKHSH, Y., CALLAN-JONES, A., MARGADANT, F., MEGE, R. M., LIM, C. T., VOITURIEZ, R. & LADOUX, B. 2015. Adaptive rheology and ordering of cell cytoskeleton govern matrix rigidity sensing. *Nat Commun,* 6**,** 7525.

HAEMMERICH, D., SCHUTT, D. J., SANTOS, I. D., WEBSTER, J. G. & MAHVI, D. M. 2005. Measurement of temperature-dependent specific heat of biological tissues. *Physiological Measurement,* 26**,** 59-67.

HALAMODA-KENZAOUI, B., CERIDONO, M., URBÁN, P., BOGNI, A., PONTI, J., GIORIA, S. & KINSNER-OVASKAINEN, A. 2017. The agglomeration state of nanoparticles can influence the mechanism of their cellular internalisation. *Journal of Nanobiotechnology,* 15**,** 48.

HAN, X., GELEIN, R., CORSON, N., WADE-MERCER, P., JIANG, J., BISWAS, P., FINKELSTEIN, J. N., ELDER, A. & OBERDORSTER, G. 2011. Validation of an LDH assay for assessing nanoparticle toxicity. *Toxicology,* 287**,** 99-104.

HANSEN, E. L., SOZER, E. B., ROMEO, S., FRANDSEN, S. K., VERNIER, P. T. & GEHL, J. 2015. Dose-dependent ATP depletion and cancer cell death following calcium electroporation, relative effect of calcium concentration and electric field strength. *PLoS One,* 10**,** e0122973.
HARRISON, R. G. 1910. The outgrowth of the nerve fiber as a mode of protoplasmic movement *Journal of Experimental Zoology,* 9**,** 787-846.
HELLER, A. 2005. Integrated medical feedback systems for drug delivery. *AIChE Journal,* 51**,** 1054-1066.
HENRIQUES, A. O. & MORAN, J. C. P. 2007. Structure, Assembly, and Function of the Spore Surface Layers. *Annual Review of Microbiology,* 61.
HEUGEN, U., SCHWAAB, G., BRUNDERMANN, E., HEYDEN, M., YU, X., LEITNER, D. M. & HAVENITH, M. 2006. Solute-induced retardation of water dynamics probed directly by terahertz spectroscopy. *Proceedings of the National Academy of Sciences of the United States of America,* 103**,** 12301-12306.
HIEBL, B., PETERS, S., GEMEINHARDT, O., NIEHUES, S. M. & JUNG, F. 2017. Impact of serum in cell culture media on in vitro lactate dehydrogenase (LDH) release determination. *Journal of Cellular Biotechnology,* 3**,** 9-13.
HIGASHITANI, K., OSHITANI, J. & OHMURA, N. 1996. Effects of magnetic field on water investigated with fluorescent probes. *Colloids and Surfaces A: Physicochemical and Engineering Aspects,* 109**,** 167-173.
HINTZSCHE, H., JASTROW, C., KLEINE-OSTMANN, T., STOPPER, H., SCHMID, E. & SCHRADER, T. 2011. Terahertz radiation induces spindle disturbances in human-hamster hybrid cells. *Radiation Research,* 175**,** 569-74.
HISHIDA, M., SETO, H. & K., Y. 2018. Smooth/rough layering in liquid-crystalline/gel state of dry phospholipid film, in relation to its ability to generate giant vesicles. *Chemical Physics Letters***,** 1-9.
HOOP, M., CHEN, X. Z., FERRARI, A., MUSHTAQ, F., GHAZARYAN, G., TERVOORT, T., POULIKAKOS, D., NELSON, B. & PANE, S. 2017. Ultrasound-mediated piezoelectric differentiation of neuron-like PC12 cells on PVDF membranes. *Scientifc Reports,* 7**,** 4028.
HUANG, S. L. 2008. Liposomes in ultrasonic drug and gene delivery. *Advanced Drug Delivery Reviews,* 60**,** 1167-76.
HUANG, Z., ZHANG, C., ZHANG, X.-C., DONG, L., CUI, G., CHANG, C., ZHAO, H., LIANG, J. & ZHAO, X. 2018. Research on terahertz properties of rat brain tissue sections during dehydration. *SPIE***,** 8.
HYNES, R. O. 1992. Integrins: Versatility, Modulation and Signalling in Cell Adhesion. *Cell,* 69**,** 11-25.

ICNIRP. 2020. *International Comission Non-Ionizing Radiation Protection* [Online]. [Accessed 05.06.2020 2020].
JESKY, R. & CHEN, H. 2016a. The neuritogenic and neuroprotective potential of senegenin against A β-induced neurotoxicity in PC12 cells. *BMC Complement. Altern. Med.,* 16**,** 26.
JESKY, R. & CHEN, H. 2016b. The neuritogenic and neuroprotective potential of senegenin against Abeta-induced neurotoxicity in PC 12 cells. *BMC Complementary and Alternative Medicine* 16-26.
JIN, F., YE, J., HONG, L., LAM, H. & WU, C. 2007. Slow Relaxation Mode in Mixtures of Water and Organic Molecules: Supramolecular Structures or Nanobubbles? *The Journal of Physical Chemistry B,* 111**,** 2255-2261.
JOERGENSEN, M., AGERHOLM-LARSEN, B., NIELSEN, P. E. & GEHL, J. 2011. Efficiency of cellular delivery of antisense peptide nucleic acid by electroporation depends on charge and electroporation geometry. *Oligonucleotides,* 21**,** 29-37.
JOUBERT, V., LEVEQUE, P., RAMETTI, A., COLLIN, A., BOURTHOUMIEU, S. & YARDIN, C. 2006. Microwave exposure of neuronal cells in vitro: Study of apoptosis. *International Journal of Radiation Biology,* 82**,** 267-75.
KAIEDA, S., SETLOW, B., SETLOW, P. & HALLE, B. 2013. Mobility of core water in Bacillus subtilis spores by 2H NMR. *Biophysical Journal,* 105**,** 2016-23.
KATSIR, Y., MILLER, L., AHARONOV, Y. & BEN JACOB, E. 2007. The Effect of rf-Irradiation on Electrochemical Deposition and Its Stabilization by Nanoparticle Doping. *Journal of The Electrochemical Society,* 154**,** D249-D259.
KIM, J. H., YU, D. H., HUH, Y. H., LEE, E. H., KIM, H. G. & KIM, H. R. 2017. Long-term exposure to 835 MHz RF-EMF induces hyperactivity, autophagy and demyelination in the cortical neurons of mice. *Scientific Reports,* 7**,** 41129.
KLEINMAN, H. K., LUCKENBILL-EDDS, L., CANNON, F. W. & SEPHEL, G. C. 1987. Use of Extracellular Matrix Components for Cell Culture. *Anal. Biochem.,* 166**,** 1-13.
KONERU, J., REDDY, R., YALAMANCHALI, S. & ALAPARTHI, R. 2012. Therapeutic ultrasound - The healing sound and its applications in oral diseases: The review of literature. *Journal of Orofacial Sciences,* 4**,** 3.
KORENSTEIN-ILAN, A., BARBULK, A., HASIN, P., ELIRAN, A., GOVER, A. & KORENSTEIN, R. 2008. Terahertz Radiation Increases Genomic Instability in Human Lymphocytes. *Radiation Research,* 170**,** 224-234.

KUBIAK, J., BREWER, J., HANSEN, S. & BAGATOLLI, L. A. 2011. Lipid lateral organization on giant unilamellar vesicles containing lipopolysaccharides. *Biophys J,* 100**,** 978-86.

KURIBAYASHI, K., TRESSET, G., COQUET, P., FUJITA, H. & TAKEUCHI, S. 2006. Electroformation of giant liposomes in microfluidic channels. *Measurement Science and Technology,* 17**,** 3121-3126.

LANGER, R. & PEPPAS, N. A. 2003. Advances in Biomaterials, Drug delivery, and Bionanotechnology. *AIChE Journal,* 49**,** 2990-3006.

LEMFACK, M. C., RAVELLA, S. R., LORENZ, N., KAI, M., JUNG, K., SCHULZ, S. & PIECHULLA, B. 2016. Novel volatiles of skin-borne bacteria inhibit the growth of Gram-positive bacteria and affect quorum-sensing controlled phenotypes of Gram-negative bacteria. *Syst Appl Microbiol,* 39**,** 503-515.

LENTACKER, I., DE COOK, I., DE SMEDT, S. C. & MOONEN, C. T. W. 2014. Understanding ultrasound induced sonoporation: definitions and underlying mechanisms. *Advanced Drug Delivery Reviews,* 72**,** 49-64.

LEWANDOWSKA-LANCUCKA, J., MYSTEK, K., GILARSKA, A., KAMINSKI, K., ROMEK, M., SULIKOWSKI, B. & NOWAKOWSKA, M. 2016. Silicone-stabilized liposomes as a possible novel nanostructural drug carrier. *Colloids Surf B Biointerfaces,* 143**,** 359-370.

LEWCZUK, B., REDLARSKI, G., ZAK, A., ZIOLKOWSKA, N., PRZYBYLSKA-GORNOWICZ, B. & KRAWCZUK, M. 2014. Influence of electric, magnetic, and electromagnetic fields on the circadian system: current stage of knowledge. *Biomedical Research International,* 2014**,** 169459.

LEWIS, J. R. & CAFISO, D. S. 1999. Correlation between the Free Energy of a Channel-Forming Voltage-Gated Peptide and the Spontaneous Curvature of Bilayer Lipids. *Biochemistry,* 38**,** 5932-5938.

LI, W. Z., HAO, X. L., ZHAO, N., HAN, W. X., ZHAI, X. F., ZHAO, Q., WANG, Y. E., ZHOU, Y. Q., CHENG, Y. C., YUE, Y. H., FU, L. N., ZHOU, J. L., WU, H. Y. & DONG, C. J. 2016. Propylene glycol-embodying deformable liposomes as a novel drug delivery carrier for vaginal fibrauretine delivery applications. *J Control Release,* 226**,** 107-14.

LIECHTY, W. B., KRYSCIO, D. R., SLAUGHTER, B. V. & PEPPAS, N. A. 2010. Polymers for drug delivery systems. *Annu Rev Chem Biomol Eng,* 1**,** 149-73.

LINDENBAUM, M. H., CARBONETTO, S., GROSVELD, F., FLAVELL, D. & MUSHYNSKI, W. E. 1988. Transcriptional and post-transcriptional effects of nerve growth factor on expression of the three neurofilament subunits in PC-12 cells. *Journal of Biological Chemistry,* 263**,** 5662-5667.

LOBNER, D. 2000. Comparison of the LDH and MTT assays for quantifying cell death: validity for neuronal apoptosis? *Journal of Neuroscience Methods,* 96**,** 147-152.

LUNDHOLM, I. V., RODILLA, H., WAHLGREN, W. Y., DUELLI, A., BOURENKOV, G., VUKUSIC, J., FRIEDMAN, R., STAKE, J., SCHNEIDER, T. & KATONA, G. 2015. Terahertz radiation induces non-thermal structural changes associated with Fröhlich condensation in a protein crystal. *Structural dynamics (Melville, N.Y.),* 2**,** 054702-054702.

MALICH, G., MARKOVIC, B. & WINDER, C. 1997. The sensitivity and specificity of the MTS tetrazolium assay for detecting the in vitro cytotoxicity of 20 chemicals using human cell lines. *Toxicology,* 124**,** 179-192.

MARINO, A., CIOFANI, G., FILIPPESCHI, C., PELLEGRINO, M., PELLEGRINI, M., ORSINI, P., PASQUALETTI, M., MATTOLI, V. & MAZZOLAI, B. 2013. Two-photon polymerization of sub-micrometric patterned surfaces: investigation of cell-substrate interactions and improved differentiation of neuron-like cells. *ACS Appl. Mater. Interfaces,* 5**,** 13012-13021.

MARSH, D. 2007. Lateral Pressure Profile, Spontaneous Curvature Frustration, and the Incorporation and Conformation of Proteins in Membranes. *Biophysical Journal,* 93**,** 3884-3899.

MAZIA, D., SCHATTEN, G. & SALE, W. 1975a. Adhesion of cells to surfaces coated with polylysine. *J. Cell Biol.,* 66**,** 198-200.

MAZIA, D., SCHATTEN, G. & SALE, W. 1975b. Adhesion of cells to surfaces coated with polylysine. *Journal of Cell Biology,* 66**,** 198-200.

MCKENNEY, P. T., DRIKS, A. & EICHENBERGER, P. 2013. The *Bacillus subtilis* endospore: assembly and functions of the multilayered coat. *Nature Reviews,* 11.

MICHAEL, W., WILHELM, K., PAMELA, B., KLAUS, R. & THOMAS, E. 2013. Ultrafast two-dimensional terahertz spectroscopy of elementary excitations in solids. *New Journal of Physics,* 15**,** 025039.

MICHELETTO, Y. M., MARQUES, C. M., SILVEIRA, N. P. & SCHRODER, A. P. 2016. Electroformation of Giant Unilamellar Vesicles: Investigating Vesicle Fusion versus Bulge Merging. *Langmuir,* 32**,** 8123-30.

MOELLER, R., SETLOW, P., REITZ, G. & NICHOLSON, W. L. 2009. Roles of small, acid-soluble spore proteins and core water content in survival of Bacillus subtilis spores exposed to environmental solar UV radiation. *Applied and Environmental Microbiology,* 75**,** 5202-8.

MOZAFARI, M. R. 2005. Liposomes: an overview of manufacturing techniques. *Cellular & Molecular Biology Letters,* 10.

MOZAFERI, M. R. 2005. Liposomes: an overview of manufacturing techniques. *Cellular & Molecular Biology Letters,* 10**,** 711-719.
MUELLER, P. & CHIEN, T. F. 1983. Formation and properties of cell-size lipid bilayer vesicles. *Biophysical journal,* 44**,** 375-381.
NAKAZAWA, K., INOUE, K., OHARA-IMAIZUMI, M., FUJIMORI, K. & TAKANAKA, A. 1991. Inhibition of Ca-Channels by diazepam compared with that by nicardipine in phechromocytoma PC 12 cells. *Brain Research,* 553

44-50.
NAPPINI, S., AL KAYAL, T., BERTI, D., NORDÈN, B. & BAGLIONI, P. 2011. Magnetically Triggered Release From Giant Unilamellar Vesicles: Visualization By Means Of Confocal Microscopy. *The Journal of Physical Chemistry Letters,* 2**,** 713-718.
NEČAS, D. & KLAPETEK, P. 2012. Gwyddion: An Open-Source Software for SPM Data Analysis. *Central European Journal of Physics,* 10**,** 181-188.
NESIN, O. M., PAKHOMOVA, O. N., XIAO, S. & PAKHOMOV, A. G. 2011. Manipulation of cell volume and membrane pore comparison following single cell permeabilization with 60- and 600-ns electric pulses. *Biochim Biophys Acta,* 1808**,** 792-801.
NGUYEN, T. H., PHAM, V. T., NGUYEN, S. H., BAULIN, V., CROFT, R. J., PHILLIPS, B., CRAWFORD, R. J. & IVANOVA, E. P. 2016. The bioeffects resulting from prokaryotic cells and yeast being exposed to an 18 GHz electromagnetic field. *PLoS One,* 11**,** e0158135.
NGUYEN, T. H., SHAMIS, Y., CROFT, R. J., WOOD, A., MCINTOSH, R. L., CRAWFORD, R. J. & IVANOVA, E. P. 2015a. 18 GHz electromagnetic field induces permeability of Gram-positive cocci. *Sci Rep,* 5**,** 10980.
NGUYEN, T. H., SHAMIS, Y., CROFT, R. J., WOOD, A., MCINTOSH, R. L., CRAWFORD, R. J. & IVANOVA, E. P. 2015b. 18 GHz electromagnetic field induces permeability of Gram-positive cocci. *Scientific Reports,* 5**,** 10980.
NICHOLSON, W. L., MUNAKATA, N., HORNECK, G., MELOSH, H. J. & SETLOW, P. 2000. Resistance of *Bacillus* Endospores to Extreme Terrestial and Extraterrestial Environments. *Microbiology and Molecular Biology Reviews,* 64**,** 548-572.
NICHOLSON, W. L., SCHUERGER, A. C. & SETLOW, P. 2005. The solar UV environment and bacterial spore UV resistance: considerations for Earth-to-Mars transport by natural processes and human spaceflight. *Mutation Research,* 571**,** 249-64.

NISHIKI, T., NARUMIYA, S., MORII, N., YAMAMOTO, M., FUJIWARA, M., KAMATA, Y., SAKAGUCHI, G. & KOZAKI, S. 1990. ADP-Ribosylation of the rho/rac proteins induces growth inhibition,neurite outgrowth and acetylcholine esterase in cultured PC 12 cells. *Biochemical and Biophysical Research Communications,* 167**,** 265-272.

OGRA, Y., TEJIMA, A., HATAKEYAMA, N., SHIRAIWA, M., WU, S., ISHIKAWA, T., YAWATA, A., ANAN, Y. & SUZUKI, N. 2016. Changes in intracellular copper concentration and copper-regulating gene expression after PC12 differentiation into neurons. *Sci. Rep.,* 6**,** 33007.

OHTA, S., SUZUKI, K., OGINO, Y., MIYAGAWA, S., MURASHIMA, A., MATSUMARU, D. & YAMADA, G. 2008. Gene transduction by sonoporation. *Dev Growth Differ,* 50**,** 517-20.

OL'SHEVSKAIA, I., KOZLOV, A. S., PETROV, A. K., ZAPARA, T. A. & RATUSHNIAK, A. S. 2009. [Influence of terahertz (submillimeter) laser radiation on neurons in vitro]. *Zhurnal vysshei nervnoi deiatelnosti imeni I P Pavlova,* 59**,** 353-359.

OLIVEIRA, E. & SANTOS, H. M. 2016. An overview on sensing materials depending on the electromagnetic spectra region applied. *Dyes and Pigments,* 135**,** 3-25.

ONG, S. G., MING, L. C., LEE, K. S. & YUEN, K. H. 2016. Influence of the Encapsulation Efficiency and Size of Liposome on the Oral Bioavailability of Griseofulvin-Loaded Liposomes. *Pharmaceutics,* 8.

ORLOWSKA, A., PERERA, P. T., AL KOBAISI, M., DIAS, A., NGUYEN, H. K. D., GHANAATI, S., BAULIN, V., CRAWFORD, R. J. & IVANOVA, E. P. 2017. The Effect of Coatings and Nerve Growth Factor on Attachment and Differentiation of Pheochromocytoma Cells. *Materials (Basel),* 11.

OZEKI, S., MIYAMOTO, J., ONO, S., WAKAI, C. & WATANABE, T. 1996. Water−Solid Interactions under Steady Magnetic Fields: Magnetic-Field-Induced Adsorption and Desorption of Water. *The Journal of Physical Chemistry,* 100**,** 4205-4212.

PAINI, M., DALY, S. R., ALIAKBARIAN, B., FATHI, A., TEHRANY, E. A., PEREGO, P., DEHGHANI, F. & VALTCHEV, P. 2015. An efficient liposome based method for antioxidants encapsulation. *Colloids Surf B Biointerfaces,* 136**,** 1067-72.

PAKHOMOVA, O. N., GREGORY, B. W., KHOROKHORINA, V. A., BOWMAN, A. M., XIAO, S. & PAKHOMOV, A. G. 2011. Electroporation-induced electrosensitization. *PLoS One,* 6**,** e17100.

PALL, M. L. 2013. Electromagnetic fields act via activation of voltage-gated calcium channels to produce beneficial or adverse effects. *Journal of Cellular and Molecular Medicine,* 17**,** 958-65.

PALUCH, E. K. & RAZ, E. 2013. The role and regulation of blebs in cell migration. *Current Opinion in Cell Biology,* 25**,** 582-590.
PANAGOPOULOS, D. J., JOHANSSON, O. & CARLO, G. L. 2013. Evaluation of specific absorption rate as a dosimetric quantity for electromagnetic fields bioeffects. *PLoS One,* 8**,** e62663.
PANDEY, A., SINGH, P., JAUHARI, A., SINGH, T., KHAN, F., PANT, A. B., PARMAR, D. & YADAV, S. 2015a. Critical role of the miR-200 family in regulating differentiation and proliferation of neurons. *J Neurochem,* 133**,** 640-52.
PANDEY, A., SINGH, P., JAUHARI, A., SINGH, T., KHAN, F., PANT, A. B., PARMAR, D. & YADAV, S. 2015b. Critical role of the miR-200 family in regulating differentiation and proliferation of neurons. *J. Neurochem.,* 133**,** 640-652.
PATERSON, L., AGATE, B., COMRIE, M., FERGUSON, R., LAKE, T. K., MORRIS, J. E., CARRUTHERS, A. E., BROWN, C. T. A., SIBBETT, W., P.E., B., GUNN-MOORE, F., RICHES, A. C. & DHOLAKIA, K. 2005. Photoporation and cell transfection using a violet diode laser. *Optics Express,* 13**,** 595-600.
PATTNI, B. S., CHUPIN, V. V. & TORCHILIN, V. P. 2015. New Developments in Liposomal Drug Delivery. *Chemical Reviews,* 115**,** 10938-66.
PAULRAJ, R. & BEHARI, J. 2006. Single strand DNA breaks in rat brain cells exposed to microwave radiation. *Mutation Research/Fundamental and Molecular Mechanisms of Mutagenesis,* 596**,** 76-80.
PAULSSON, M., DEUTZMANN, R., TIMPL, R., DALZOPPO, D., ODERMATT, E. & ENGEL, J. 1985. Evidence for coiled-coil α-helical regions in the long arm of laminin. *The European Molecular Biology Organization* 4**,** 309-316.
PENG, H., WU, Y. & ZHANG, Y. 2012. Efficient delivery of DNA and morpholinos into mouse preimplantation embryos by electroporation. *PLoS One,* 7**,** e43748.
PERERA, P. G. T., APPADOO, R. T., CHEESEMAN, S., WANDIYANTO, J. V., LINKLATER, D., DEKIWADIA, C., TRUONG, V. K., TOBIN, M. J., VONGSVIVUT, J., BAZAKA, O., BAZAKA, K., CROFT, R. J., CRAWFORD, R. J. & IVANOVA, E. P. 2019. PC 12 Pheochromocytoma Cell Response to Super High Frequency Terahertz Radiation from Synchrotron Source. *Cancers,* 11**,** 1-17.
PERERA, P. G. T., NGUYEN, T. H. P., DEKIWADIA, C., WANDIYANTO, J. V., SBARSKI, I., BAZAKA, O., BAZAKA, K., CRAWFORD, R. J., CROFT, R. J. & IVANOVA, E. P. 2018. Exposure to high-frequency electromagnetic field triggers rapid uptake of large nanosphere clusters by

pheochromocytoma cells. *International Journal of Nanomedicine,* 13**,** 8429-8442.
PIERSCHBACHER, M. D. & RUOSLAHTI, E. 1984. Cell attachment activity of fibronectin can be duplicated by small synthetic fragments of the molecule. *Nature,* 309**,** 30-33.
PLOMP, M., LEIGHTON, T. J., WHEELER, K. E. & MALKIN, A. J. 2005. Architecture and High-Resolution Structure of *Bacillus thuringiensis* and *Bacillus cereus* Spore Coat Surfaces. *Langmuir,* 21**,** 7892-7898.
PODARU, G., OGDEN, S., BAXTER, A., SHRESTHA, T., REN, S., THAPA, P., DANI, R. K., WANG, H., BASEL, M. T., PRAKASH, P., BOSSMANN, S. H. & CHIKAN, V. 2014. Pulsed magnetic field induced fast drug release from magneto liposomes via ultrasound generation. *J Phys Chem B,* 118**,** 11715-22.
POGODIN, S., WERNER, M., SOMMER, J. U. & BAULIN, V. 2012. Nanoparticle-Induced Permemability of Lipid Membranes. *ACSNANO,* 12**,** 10555-10561.
PORTET, T., MAUROY, C., DÉMERY, V., HOULES, T., ESCOFFRE, J.-M., DEAN, D. S. & ROLS, M.-P. 2012. Destabilizing Giant Vesicles with Electric Fields: An Overview of Current Applications. *The Journal of Membrane Biology,* 245**,** 555-564.
RADOICIC, J., LU, G. J. & OPELLA, S. J. 2014. NMR structures of membrane proteins in phospholipid bilayers. *Q Rev Biophys,* 47**,** 249-83.
RAMAMOORTH, M. & NARVEKAR, A. 2015. Non viral vectors in gene therapy- an overview. *J Clin Diagn Res,* 9**,** GE01-6.
RAO, L., ZHAO, F., WANG, Y., CHEN, F., HU, X. & LIAO, X. 2016. Investigating the Inactivation Mechanism of Bacillus subtilis Spores by High Pressure CO2. *Frontiers in Microbiology,* 7**,** 1411.
REDLARSKI, G., LEWCZUK, B., ZAK, A., KONCICKI, A., KRAWCZUK, M., PIECHOCKI, J., JAKUBIUK, K., TOJZA, P., JAWORSKI, J., AMBROZIAK, D., SKARBEK, L. & GRADOLEWSKI, D. 2015. The influence of electromagnetic pollution on living organisms: historical trends and forecasting changes. *Biomedical Research International,* 2015**,** 234098.
REFOLO, L. M., SALTON, S. R. J., ANDERSON, J. P., MEHTA, P. & ROBAKIS, N. K. 1989. Nerve and epidermal growth factors induce the release of the Alzheimer Amyloid precursor from PC 12 cell cultures. *Biochemical and Biophysical Research Communications,* 164**,** 664-670.
RODRIGUEZ, N., PINCET, F. & CRIBIER, S. 2005. Giant vesicles formed by gentle hydration and electroformation: a comparison by fluorescence microscopy. *Colloids and Surfaces B: Biointerfaces,* 42**,** 125-30.

ROGERS, S. L., LETOURNEAU, P. C., PALM, S. L., MCCARTHY, J. & FURCHT, L. T. 1983. Neurite Extension by Peripheral and Central Nervous System Neurons in Response to Substratum-Bound Fibronectin and Laminin. *Dev. Biol.,* 98**,** 212-220.

ROMEO, S., SANNINO, A., SCARFI, M. R., VERNIER, P. T., CADOSSI, R., GEHL, J. & ZENI, O. 2018. ESOPE-Equivalent Pulsing Protocols for Calcium Electroporation: An In Vitro Optimization Study on 2 Cancer Cell Models. *Technology in Cancer Research & Treatment,* 17**,** 1533033818788072.

ROUFA, D. G., JOHNSON, M. I. & BUNGE, M. B. 1983. Influence of Ganglion Age, Nonneuronal Cells and Substratum on Neurite Outgrowth in Culture. *Developmental Biology,* 99**,** 225-289.

RUDKIN, B. B., LAZAROVICI, P., LEVI, B. Z., ABE, Y., FUJITA, K. & GUROFF, G. 1989. Cell cycle-specific action of nerve growth factor in PC 12 cells: differentiation without proliferation. *The European Molecular Biology Organization Journal,* 8**,** 3319-3325.

SABIN, J., PRIETO, G., RUSO, J. M., HIDALGO-ALVAREZ, R. & SARMIENTO, F. 2006. Size and stability of liposomes: a possible role of hydration and osmotic forces. *Eur Phys J E Soft Matter,* 20**,** 401-8.

SADIQ, A. A., ZALTUM, M. A. M., MAMMAN, H. B., ADON, M. N., OTHMAN, N. B., DALIMIN, M. N. & JAMIL, M. M. A. 2015. An overview: investigation of electroporation and sonoporation Techniques. *Institute of Electrical and Electronics Engineers* 1-6.

SAFARI, J. & ZARNEGAR, Z. 2014. Advanced drug delivery systems: Nanotechnology of health design A review. *Journal of Saudi Chemical Society,* 18**,** 85-99.

SAGI, Y., BASSER, P. J. & ASSAF, Y. 2009. Estimation of Cell Size Using the Composite Hindered and Restricted Model of Diffusion. *Magnetic Resonance in Medicine,* 17**,** 1390.

SALFORD, L. G., BRUN, A. & PERSSON, B. R. R. 1997. Brain tumour development in rats exposed to electromagnetic fields used in wireless cellular communication. *Wireless Networks,* 3**,** 463-469.

SAMSON, L. & CAIRNS, J. 1977. A new pathway for DNA repair in *Escherichia coli*. *Nature*.

SANTINI, S. J., CORDONE, V., FALONE, S., MIJIT, M., TATONE, C., AMICARELLI, F. & DI EMIDIO, G. 2018. Role of Mitochondria in the Oxidative Stress Induced by Electromagnetic Fields: Focus on Reproductive Systems. *Oxidative Medicine and Cellular Longevity,* 2018**,** 5076271.

SANTORO, N., LISI, A., POZZI, D., PASQUALI, E., SERAFINO, A. & GRIMALDI, S. 1997. Effect of extremely low frequency (ELF) magnetic

field exposure on morphological and biophysical properties of human lymphoid cell line. *Biochimica et Biophysica Acta,* 1357**,** 281-290.
SCHMIDT, S., SCHÜßLER, M., LUO, Z., JAKOBY, R., HERCE, H. D. & CARDOSO, M. C. Compact dualmode microwave electroporation and dielectrometry tool. 2017 First IEEE MTT-S International Microwave Bio Conference (IMBIOC), 15-17 May 2017 2017. 1-3.
SCHROEDER, A., AVNIR, Y., WEISMAN, S., NAJAJREH, Y., GABIZON, A., TALMON, Y., KOST, J. & BARENHOLZ, Y. 2007. Controlling Liposomal Drug Release with Low Frequency Ultrasound: Mechanism and Feasibility. *Langmuir,* 23**,** 4019-4025.
SCHROEDER, A., HONEN, R., TURJEMAN, K., GABIZON, A., KOST, J. & BARENHOLZ, Y. 2009. Ultrasound triggered release of cisplatin from liposomes in murine tumors. *J Control Release,* 137**,** 63-8.
SELVI, B. R., JAGADEESAN, D., SUMA, B. S., NAGASHANKAR, G., ARIF, M., BALASUBRAMANYAM, K., ESWARAMOORTHY, M. & KUNDU, T. K. 2008. Intrinsically Flourescent Carbon Nanospheres as a Nuclear Targeting Vector: Delivery of Membrane-Impermeable Molecule to Modulate Gene Expression In Vivo. *Nano Letters,* 8**,** 3182-3188.
SERCOMBE, L., VEERATI, T., MOHEIMANI, F., WU, S. Y., SOOD, A. K. & HUA, S. 2015. Advances and Challenges of Liposome Assisted Drug Delivery. *Frontiers in Pharmacology,* 6**,** 286.
SETLOW, B., KORZA, G., BLATT, K. M., FEY, J. P. & SETLOW, P. 2016. Mechanism of Bacillus subtilis spore inactivation by and resistance to supercritical CO2 plus peracetic acid. *Journal of Applied Microbiology,* 120**,** 57-69.
SETLOW, P. 2003. Spore germination. *Current Opinion in Microbiology,* 6**,** 550-556.
SETLOW, P. 2006. Spores of Bacillus subtilis: their resistance to and killing by radiation, heat and chemicals. *Journal of Applied Microbiology,* 101**,** 514-25.
SHAFER, T. J. & ATCHISON, W. D. 1991a. Transmitter, Ion Channel and Receptor Properties of Pheochromocytoma (PC12) cells: A model for Neurotoxicological studies. *Neurotoxicology,* 12**,** 473-492.
SHAFER, T. J. & ATCHISON, W. D. 1991b. Transmitter, Ion Channel and Receptor Properties of Pheochromocytoma (PC 12) cells: A model for Neurotoxicological studies. *Neurotoxicology,* 12.
SHAMIS, Y., CROFT, R., TAUBE, A., CRAWFORD, R. J. & IVANOVA, E. P. 2012a. Review of the specific effects of microwave radiation on bacterial cells. *Applied Microbiology and Biotechnology,* 96**,** 319-325.

SHAMIS, Y., CROFT, R., TAUBE, A., CRAWFORD, R. J. & IVANOVA, E. P. 2012b. Review of the specific effects of microwave radiation on bacterial cells. *Appl Microbiol Biotech,* 96**,** 319-325.

SHAMIS, Y., PATEL, S., TAUBE, A., MORSI, Y., SHRAMKOV, Y., CROFT, R., CRAWFORD, R. J. & IVANOVA, E. P. 2009. A New Sterilization Technique of Bovine Pericardial Biomaterial Using Microwave Radiation. *Tissue Engineering,* 15.

SHAMIS, Y., TAUBE, A., MITIK-DINEVA, N., CROFT, R., CRAWFORD, R. J. & IVANOVA, E. P. 2011a. Specific electromagnetic effects of microwave radiation on *Escherichia coli*. *Applied and Environmental Microbiology,* 77**,** 3017-3023.

SHAMIS, Y., TAUBE, A., MITIK-DINEVA, N., CROFT, R., CRAWFORD, R. J. & IVANOVA, E. P. 2011b. Specific electromagnetic effects of microwave radiation on Escherichia coli. *Appl Environ Microbiol,* 77**,** 3017-22.

SHAMIS, Y., TAUBE, A., SHRAMKOV, Y., MITIK-DINEVA, N., VU, B. & IVANOVA, E. P. 2008. Development of a Microwave Treatment Technique for Bacterial Decontamination of Raw Meat. *International Journal of Food Engineering,* 4**,** 1-13.

SHAMIS, Y., TRAUB, A., CROFT, R., CRAWFORD, R. & IVANOVA, E. P. 2012c. Influence of 18GHz microwave radiation on the enzymatic activity of Escherichia coli lactate dehydrogenase and cytochrome c oxidase. *Journal of physical science and application,* 2**,** 143-151.

SHAMIS, Y., TRAUB, A., CROFT, R. C., R. & IVANOVA, E. P. 2012d. Influence of 18GHz microwave radiation on the enzymatic activity of Escherichia coli lactate dehydrogenase and cytochrome c oxidase. *Journal of physical science and application,* 2**,** 143-151.

SHARP, M. D. & POGLIANO, K. 1999. An *in vivo* membrane fusion assay implicates SpoIIIE in the final stages of engulfment during *Bacillus subtilis* sporulation. *Proceedings of the National Academy of Sciences of the United States of America,* 96.

SHEIKH, S., PALLAGATTI, S., SINGH, B., PURI, N., SINGH, R. & KALUCHA, A. 2011. Sonoporation, a redifined ultrasound modality as therapeutic aid: A review. *Journal of Clinical and Experimental Dentistry,* 3**,** e228-34.

SHERRARD, R. M., MORELLINI, N., JOURDAN, N., EL-ESAWI, M., ARTHAUT, L. D., NIESSNER, C., ROUYER, F., KLARSFELD, A., DOULAZMI, M., WITCZAK, J., D'HARLINGUE, A., MARIANI, J., MCLURE, I., MARTINO, C. F. & AHMAD, M. 2018. Low-intensity electromagnetic fields induce human cryptochrome to modulate intracellular reactive oxygen species. *PLoS Biology,* 16**,** e2006229.

SILVA, C. A., LOPES, C. M., LOBO, J. M. & AMARA, M. H. 2015. Nucleic Acids Delivery Systems: A challenge for Pharmaceutical Technologists. *Current Drug Metabolism,* 16**,** 3-16.
SILVERSTEIN, T. P. & WILLIAMSON, J. C. 2019. Liposome permeability probed by laser light scattering. *Biochemistry and Molecular Biology Education*.
SIMKO, M., DROSTE, S., KRIENHUBER, R. & WEISS, D. 2001. Stimulation of phagocytosis and free radical production in murin macropahges by 50 Hz electromagentic fields

European Journal of Cell Biology, 80**,** 562-566.
SITNIKOV, D. S., ILINA, I. V., PRONKIN, A. A., OVCHINNIKOV, A. V., CHEFONOV, O. V., ZURINA, I. M., GORKUN, A. A. & KOSHELEVA, N. V. 2019. Studying the effect of high-power coherent terahertz pulses on mesenchymal stem cells. *Journal of Physics: Conference Series,* 1147.
SMITH, P. K., KROHN, R. I., HERMANSON, G. T., MALLIA, A. K., GARTNER, F. H., PROVENZANO, M. D., FUJIMOTO, E. K., GOEKE, N. M., OLSON, B. J. & KLENK, D. C. 1985. Measurement of Protein Using Bicinchoninic Acid. *Analytical Biochemistry,* 150**,** 76-85.
SMYE, S. W., CHAMBERLAIN, J. M., FITZGERALD, A. J. & BERRY, E. 2001. The interaction between Terahertz radiation and biological tissue. *Physics In Medicine And Biology,* 46**,** 101-112.
SOGHOMONYAN, D., TRCHOUNIAN, K. & TRCHOUNIAN, A. 2016. Millimeter waves or extremely high frequency electromagnetic fields in the environment: what are their effects on bacteria? *Applied Microbiology and Biotechnology,* 100**,** 4761-71.
SOKOLOVIC, D., DJINDJIC, B., NIKOLIC, J., BJELAKOVIC, G., PAVLOVIC, D., KOCIC, G., KRSTIC, D., CVETKOVIC, T. & PAVLOVIC, V. 2008. Melatonin reduces oxidative stress induced by chronic exposure of microwave radiation from mobile phones in rat brain. *Journal of Radiation Research,* 49**,** 579-586.
SONG, K. M., CHOI, M. J., KWON, M. H., GHATAK, K., PARK, S. H., RYU, D. S., RYU, J. K. & SUH, J. K. 2015. Optimizing in vivo gene transfer into mouse corpus cavernosum by use of surface electroporation. *Korean J Urol,* 56**,** 197-204.
SPECTOR, A. A. & YOREK, M. A. 1985. Membrane lipid composition and cellular function. *Journal of Lipid Research,* 26.
SRINORAKUTARA, T. 1998. Determination of Yeast Cell Wall Thickness and Cell Diameter Using New Methods. *Journal of Fermentation and Bioengineering,* 86**,** 253-260.

STEGLE, O., TEICHMANN, S. A. & MARIONI, J. C. 2015. Computational and analytical challenges in single-cell transcriptomics. *Nat Rev Genet,* 16**,** 133-45.

STRASAK, L., BARTOVA, E., KREJCI, J., FOJT, L. & VETTERL, V. 2009. Effects of ELF-EMF on brain proteins in mice. *Electromagnetic Biology and Medicine,* 28**,** 96-104.

SUBRAMANIAN, T., EMERICH, D. F., BAKAY, R. A. E., HOFFMAN, J. M., GOODMAN, M. M., SHOUP, T. M., MILLER, G. W., LEVEY, A. I., HUBERT, G. W., BATCHELOR, S., WINN, S. R., SAYDOFF, J. A. & WATTS, R. L. 1997. Polymer-encapsulated PC-12 cells demonstrate high-affinity uptake of dopamine in vitro and 18F-dopa uptake and metabolism after intracerebral implantation in nonhuman primates. *Cell Transplantation,* 6**,** 469-477.

TAHER, L., PFEIFFER, M. J. & FUELLEN, G. 2015. Bioinformatics approaches to single-blastomere transcriptomics. *Mol Hum Reprod,* 21**,** 115-25.

TAN, I. S. & RAMAMURTHI, K. S. 2014. Spore formation in Bacillus subtilis. *Environmental Microbiology Reports,* 6**,** 212-25.

TIELROOIJ, K. J., PAPARO, D., PIATKOWSKI, L., BAKKER, H. J. & BONN, M. 2009. Dielectric Relaxation Dynamics of Water in Model Membranes Probed by Terahertz Spectroscopy. *Biophysical Journal,* 97**,** 2484-2492.

TINEVEZ, J. Y., SCHULZE, U., SALBREUX, G., ROENSCH, J., JOANNY, J. F. & PALUCH, E. 2009. Role of cortical tension in bleb growth. *Proceedings of the National Academy of Sciences of the United States of America,* 106**,** 18581-18586.

TOMASELLI, K. J., DAMSKY, C. H. & REICHARDT, L. F. 1988. Purification and Characterization of Mammalian Integrins Expressed by a Rat Neuronal Cell Line (PC12) Evidence That They Function as α/β Heterodimeric Receptors for Laminin and Type IV Collagen. *J. Cell Biol.,* 107**,** 1241-1252.

TONAZZINI, I., MEUCCI, S., FARACI, P., BELTRAM, F. & CECCHINI, M. 2013. Neuronal differentiation on anisotropic substrates and the influence of nanotopographical noise on neurite contact guidance. *Biomaterials,* 34**,** 6027-36.

TOWHIDI, L., KHODADADI, D., MAIMARI, N., PEDRIGI, R. M., IP, H., KIS, Z., KWAK, B. R., PETROVA, T. W., DELORENZI, M. & KRAMS, R. 2016. Comparison between direct and reverse electroporation of cells in situ: a simulation study. *Physiol Rep,* 4.

TRAVERSE, S., GOMEZ, N., PATERSON, H., MARSHALL, C. & COHEN, P. 1992. Sustained activation of the mitogen-activated protein (MAP) kinase cascade may be required for differentiation of PC 12 cells. *Research Communication,* 288**,** 351-355.

TSOY, A., SALIEV, T., ABZHANOVA, E., TURGAMBAYEVA, A., KAIYRLYKYZY, A., AKISHEV, M., SAPARBAYEV, S., UMBAYEV, B. & ASKAROVA, S. 2019. The Effects of Mobile Phone Radiofrequency Electromagnetic Fields on beta-Amyloid-Induced Oxidative Stress in Human and Rat Primary Astrocytes. *Neuroscience,* 408**,** 46-57.

VALBONESI, P., FRANZELLITTI, S., BERSANI, F., CONTIN, A. & FABBRI, E. 2016. Activity and expression of acetylcholinesterase in PC12 cells exposed to intermittent 1.8 GHz 217-GSM mobile phone signal. *International Journal of Radiation Biology,* 92**,** 1-10.

VARTIO, T. 1982. Characterization of the Binding Domains in the Fragments Cleaved by Cathepsin G from Human Plasma Fibronectin. *European Journal of Biochemistry,* 123**,** 223-233.

VAUDRY, D., STORK, P. J. S., LAZAROVICI, P. & EIDEN, L. E. 2002. Signalling Pathways for PC 12 Cell Differentiation: Making the Right Connections. *SCIENCE,* 296.

VERMA, A. & STELLACCI, F. 2010. Effect of surface properties on nanoparticle-cell interactions. *Small,* 6**,** 12-21.

VIJAYALAXMI, CAO, Y. & SCARFI, M. R. 2014. Adaptive response in mammalian cells exposed to non-ionizing radiofrequency fields: A review and gaps in knowledge. *Mutation Research/ Reviews in Mutation Research*.

WALCZAK, R. & DZIUBAN, J. A. 2004. Microwave enhanced wet anisotropic etching of silicon utilizing a memory effect of KOH activation—a remote E2MSi process. *Sensors and Actuators A: Physical,* 116**,** 161-170.

WALDE, P., COSENTINO, K., ENGEL, H. & STANO, P. 2010. Giant vesicles: preparations and applications. *Chembiochem,* 11**,** 848-65.

WALLACE, V. P., FITZGERALD, A. J., PICKWELL, E., PYE, R. J., TADAY, P. F., FLANAGAN, N. & HA, T. 2006. Terahertz pulsed spectroscopy of human Basal cell carcinoma. *Applied Spectroscopy,* 60**,** 1127-33.

WANDIYANTO, J. V., LINKLATER, D., THARUSHI PERERA, P. G., ORLOWSKA, A., TRUONG, V. K., THISSEN, H., GHANAATI, S., BAULIN, V., CRAWFORD, R. J., JUODKAZIS, S. & IVANOVA, E. P. 2018. Pheochromocytoma (PC12) Cell Response on Mechanobactericidal Titanium Surfaces. *Materials (Basel),* 11.

WANG, L., MIAO, X. & PAN, G. 2016. Microwave-Induced Interfacial Nanobubbles. *Langmuir,* 32**,** 11147-11154.

WEBER, S., FERNANDEZ-CACHON, M. L., NASCIMENTO, J. M., KNAUER, S., OFFERMANN, B., MURPHY, R. F., BOERRIES, M. & BUSCH, H. 2013. Label-free detection of neuronal differentiation in cell populations using high-throughput live-cell imaging of PC12 cells. *PLoS One,* 8**,** e56690.

WEIGHTMAN, P. 2012. Prospects for the study of biological systems with high power sources of terahertz radiation. *Physical Biology,* 9**,** 053001.
WEINBERGER, A., TSAI, F. C., KOENDERINK, G. H., SCHMIDT, T. F., ITRI, R., MEIER, W., SCHMATKO, T., SCHRODER, A. & MARQUES, C. 2013. Gel-assisted formation of giant unilamellar vesicles. *Biophys J,* 105**,** 154-64.
WELLS, P. N. T., HALLIWELL, M., TANG, J. & LIANG, H. D. 2010. Sonoporation, drug delivery, and gene therapy. *Proceedings of the Institution of Mechanical Engineers, Part H: Journal of Engineering in Medicine,* 224**,** 343-361.
WES, P. D., HOLTMAN, I. R., BODDEKE, E. W., MOLLER, T. & EGGEN, B. J. 2016. Next generation transcriptomics and genomics elucidate biological complexity of microglia in health and disease. *Glia,* 64**,** 197-213.
WESTERINK, R. H. & EWING, A. G. 2008a. The PC12 cell as model for neurosecretion. *Acta Physiologica,* 192**,** 273-85.
WESTERINK, R. H. & EWING, A. G. 2008b. The PC12 cell as model for neurosecretion. *Acta Physiol. (Oxf),* 192**,** 273-285.
WILMINK, G. J. & GRUNDT, J. E. 2011. Invited Review Article: Current State of Research on Biological Effects of Terahertz Radiation. *Journal of Infrared, Millimeter, and Terahertz Waves,* 32**,** 1074-1122.
WILMINK, G. J., RIVEST, B. D., ROTH, C. C., IBEY, B. L., PAYNE, J. A., CUNDIN, L. X., GRUNDT, J. E., PERALTA, X., MIXON, D. G. & ROACH, W. P. 2011. In vitro investigation of the biological effects associated with human dermal fibroblasts exposed to 2.52 THz radiation. *Lasers in Surgery and Medicine,* 43**,** 152-163.
WOO, I., RHEE, I. & PARK, H. 2000. Differential damage in bacterial cells by microwave radiation on the basis of cell wall structure. *Applied and Environmental Microbiology,* 66**,** 2243-2247.
WOODWARD, R. M., COLE, B. E., WALLACE, V. P., PYE, R. J., ARNONE, D. D., LINFIELD, E. H. & PEPPER, M. 2002. Terahertz pulse imaging in reflection geometry of human skin cancer and skin tissue. *PHYSICS IN MEDICINE AND BIOLOGY,* 47**,** 3853-3863.
WU, I. L., NARAYAN, K., CASTAING, J. P., TIAN, F., SUBRAMANIAN, S. & RAMAMURTHI, K. S. 2015. A versatile nano display platfrom from bacterial spore coat proteins. *Nature Communications,* 6**,** 1-8.
WU, Z. R., BAILEY, S. N. & SABATINI, M. D. 2002. Cell-biological applications of transfected cell-microarrays. *TRENDS in Cell Biology,* 12.
XIANG, C. C. & CHEN, Y. 2000. cDNA microarray technology and its applications. *Biotechnology Advances,* 18**,** 35-46.

YANG, K., JUNG, K., KO, E., KIM, J., PARK, K. I., KIM, J. & CHO, S. W. 2013. Nanotopographical manipulation of focal adhesion formation for enhanced differentiation of human neural stem cells. *ACS Appl Mater Interfaces,* 5**,** 10529-40.

YANG, Y., LIU, M., GU, Y., LIN, S., DING, F. & GU, X. 2009. Effect of chitooligosaccharide on neuronal differentiation of PC-12 cells. *Cell Biol Int,* 33**,** 352-6.

YEN SHIN, J., LOPEZ-GARRIDO, J., LEE, S. H., DIAZ-CELIS, C., FLEMING, T., BUSTAMANTE, C. & POGLIANO, K. 2015. Visualization and functional dissection of coaxial paired SpoIIIE channels across the sporulation septum. *Elife,* 4**,** e06474.

YU, H. & XU, L. 2014. Cell experimental studies on sonoporation: state of the art and remaining problems. *J Control Release,* 174**,** 151-60.

ZENI, O., CHIAVONI, A. S., SANNINO, A., ANTOLINI, A., FORIGO, D., BERSANI, F. & SCARFÌ, M. R. 2003. Lack of Genotoxic Effects (Micronucleus Induction) in Human Lymphocytes ExposedIn Vitroto 900 MHz Electromagnetic Fields. *Radiation Research,* 160**,** 152-158.

ZENI, O., GALLERANO, G. P., PERROTTA, A., ROMANO, M., SANNINO, A., SARTI, M., D'ARIENZO, M., DORIA, A., GIOVENALE, E., LAI, A., MESSINA, G. & SCARFI, M. R. 2007. Cytogenetic observations in human peripheral blood leukocytes following in vitro exposure to THz radiation: a pilot study. *Health Physics Society* 92**,** 349-57.

ZHANG, Y. N., YANG, Y. F. & YANG, X. W. 2018. Blood-brain barrier permeability and neuroprotective effects of three main alkaloids from the fruits of Euodia rutaecarpa with MDCK-pHaMDR cell monolayer and PC12 cell line. *Biomedicine & Pharmacotherapy,* 98**,** 82-87.

ZHAO, L., HAO, Y.-H. & PENG, R.-Y. 2014a. Advances in the biological effects of terahertz wave radiation.pdf. *Military Medical Research,* 1**,** 1-4.

ZHAO, L., HAO, Y. H. & PENG, R. Y. 2014b. Advances in the biological effects of terahertz wave radiation. *Military Medical Research,* 1**,** 26.

ZHOU, L., LIM, Q. E., WAN, G. & TOO, H. P. 2010. Normalization with genes encoding ribosomal proteins but not GAPDH provides an accurate quantification of gene expressions in neuronal differentiation of PC12 cells. *BMC Genomics,* 11**,** 75.

ZU, Y., HUANG, S., LIAO, W. C., LU, Y. & WANG, S. 2015. Gold nanoparticles enhanced electroporation for mammalian cell transfection. *Journal of Biomedical Nanotechnology,* 10**,** 982-992.

ZUO, H., LIN, T., WANG, D., PENG, R., WANG, S., GAO, Y., XU, X., LI, Y., WANG, S., ZHAO, L., WANG, L. & ZHOU, H. 2014. Neural cell apoptosis

induced by microwave exposure through mitochondria-dependent caspase-3 pathway. *International Journal of Medical Sciences,* 11**,** 426-35.